UNIVERSITY OF MICHIGAN
DEC 11 1950
ENGINEERING LIBRARY

JOURNAL OF THE AERONAUTICAL SCIENCES

VOLUME 17 DECEMBER, 1950 NUMBER 12

CONTENTS

Transonic Flow Past Wedge Sections.....H. W. LIEPMANN AND A. E. BRYSON, JR. 745

A Study of the Response of an Airplane Landing Gear Using the Differential Analyzer.....WALTER C. HURTY 756

Analytical and Experimental Studies on Dynamic Loads in Airplane Structures During Landing.....T. H. H. PIAN AND H. I. FLOMENHOFT 765

An Extension of the Theory of the One-Dimensional Shock-Wave Structure.....LEONARD MEYERHOFF 775

The Transient Temperature Distribution in a Wing Flying at Supersonic Speeds.....JOSEPH KAYE 787

Readers' Forum: "On the Speed of an Airplane in Steady Flight," by Angelo Miele; "An Analogy Between Open Soap Bubble and Compressible Flow," by V. G. Szebehely; "On the Plastic Buckling of Plates According to the Flow Theory," by P. P. Bijlaard; "Note on Desirability of Completely Expanded Nozzles," by C. B. Cohen and P. J. Evans, Jr.; "Note on Base Pressure Measurements," by Dean R. Chapman; "The Reflection of 'Rectilinear' Waves in One-Dimensional Gas Flows," by Lorenzo Poggi; "Determination of Deflections in Redundant Structures," by H. L. Cox and D. G. Sopwith; "On the Equations of Longitudinal Stability," by John W. Miles.....808–816

Index to Volume 17..... 817

Published by the

INSTITUTE OF THE AERONAUTICAL SCIENCES, INC.

JOURNAL OF THE AERONAUTICAL SCIENCES

Editor: HUGH L. DRYDEN, *Director, N.A.C.A.*

Associate Editor: ROBERT R. DEXTER *Managing Editor:* BERNEICE H. JARCK

Editorial Committee

Aerodynamics

Francis Clauser
Howard Emmons
R. Paul Harrington
R. T. Jones
Carl Kaplan
W. B. Klemperer
John G. Lee
H. W. Liepmann
C. C. Lin
H. F. Ludloff
John R. Markham
Clark B. Millikan
Shatswell Ober
W. Bailey Oswald
Allen E. Puckett
Elliott G. Reid
H. J. F. Reid
Russell Robinson
G. B. Schubauer
W. R. Sears
John Stack
Th. von Kármán
Richard von Mises

Flight Testing

W. K. Ebel
R. R. Gilruth
Melvin N. Gough
Robert Stanley
E. G. Stout

Meteorology

C. F. Brooks
D. M. Little
E. J. Minser
F. W. Reichelderfer
H. C. Willett

Structures and Materials

W. B. Bleakney
E. W. Conlon
J. P. Den Hartog
L. H. Donnell
E. C. Hartmann
N. J. Hoff
E. E. Lundquist
C. F. Nagel, Jr.
J. S. Newell
Alfred S. Niles
W. Ramberg
E. Reissner
F. R. Shanley
H. W. Sibert
C. R. Strang
S. Timoshenko
H. S. Tsien
Chi-Teh Wang

Rotating Wing Aircraft

Robert Coleman
K. H. Hohenemser
Bartram Kelley
Ralph McClarren
R. H. Miller
R. H. Prewitt
Igor I. Sikorsky

Physiologic Problems

H. G. Armstrong
Louis H. Bauer
Eugene Du Bois
W. Randolph Lovelace, II
Ross A. MacFarland
A. D. Tuttle

Flight Propulsion

George W. Brady
Frank W. Caldwell
L. S. Hobbs
E. E. Johnson
Joseph Keenan
R. P. Kroon
Arthur Nutt
Hans Reissner
Abe Silverstein
C. Fayette Taylor
E. S. Taylor
P. Taylor
E. S. Thompson
H. S. Tsien

Aircraft Design

W. E. Beall
W. K. Ebel
Hall L. Hibbard
Richard Hutton
C. L. Johnson
I. M. Laddon
C. J. McCarthy
Fred E. Weick
Robert J. Woods

Air Transport

Charles Froesch
J. A. Herlihy
R. D. Kelly
Otto E. Kirchner
Jerome Lederer
John C. Leslie
R. Dixon Speas

Instruments

Allan G. Binnie
W. G. Brombacher
Charles H. Colvin
B. M. Craig
B. Del Mar
C. S. Draper
O. E. Esval
W. L. Howland
J. E. Lindberg
David W. Moore
George H. Purcell
W. A. Reichel
C. F. Savage
O. Hugo Schuck
C. L. Seward, Jr.
R. Sylvander
D. K. Warner
P. F. Weber

Vibration and Flutter

Lee Arnold
M. A. Biot
William Bollay
Chieh-Chien Chang
Martin Goland
J. P. Den Hartog

Fuels and Oils

D. P. Barnard
J. H. Doolittle
Graham Edgar
R. T. Goodwin
S. D. Heron
A. M. Rothrock

SUBSCRIPTION RATES

JOURNAL OF THE AERONAUTICAL SCIENCES, Published Monthly.—United States and Possessions: 1 Year, $12.00; Single Copies, $1.50. Foreign Countries Including Canada (American Currency Rate): 1 Year, $13.00; Single Copies, $1.50.

AERONAUTICAL ENGINEERING REVIEW, Published Monthly.—United States and Possessions: 1 Year, $3.00; Single Copies, $0.50. Foreign Countries Including Canada (American Currency Rates): 1 Year, $3.50; Single Copies, $0.50.

Notices of change of address should be sent to the Institute at least 30 days prior to actual change of address.

Manuscripts for publication, proofs, and all correspondence should be addressed to the Editorial Office of the JOURNAL.

Correspondence regarding subscriptions may be addressed to Publication Office, 20th and Northampton Sts., Easton, Pa., or to the Editorial Office of the JOURNAL OF THE AERONAUTICAL SCIENCES, 2 East 64th Street, New York 21, New York.

Copyright, 1950, by the Institute of the Aeronautical Sciences, Inc.

Entered as Second Class Matter at the Post Office, Easton, Pa., May 1, 1937. Acceptance for mailing at a special rate of Postage provided for in the Act of August 24, 1912. Authorized April 29, 1937.

JOURNAL OF THE AERONAUTICAL SCIENCES

VOLUME 17 DECEMBER, 1950 NUMBER 12

Transonic Flow Past Wedge Sections

H. W. LIEPMANN* AND A. E. BRYSON, JR.†

California Institute of Technology

SUMMARY

The paper gives the results of an interferometric wind-tunnel study of transonic flow past wedge sections. Both subsonic flow with a local supersonic zone and supersonic flow with a detached shock wave have been investigated. The pressure distribution on these wedges and the drag coefficients as functions of the Mach Number have been obtained. The results are compared with general theoretical considerations and recent theoretical work of Guderley and especially of Vincenti and of Cole. Based on theory and experiment, the behavior of the drag curve from $M = 0$ through $M = 1$ to supersonic flow can be completely determined.

SYMBOLS

M	= free-stream Mach Number
m	= local Mach Number
U	= free-stream velocity
u, v	= components of the local velocity
a^*	= critical velocity
$u' = u - U$	= perturbation velocity component
M_A, M_B / m_A, m_B	= refers to specific characteristic values of the Mach Number
θ	= wedge angle (semiapex angle)
C	= wedge chord
C_P	= pressure coefficient
C_D	= drag coefficient based upon C, θ (i.e., pressure drag coefficient of the half wedge)
γ	= ratio of specific heats
$\bar{C}_P$	= $C_P(\gamma + 1)^{1/3}/\theta^{2/3}$, reduced pressure coefficient
$\bar{C}_D$	= $C_D(\gamma + 1)^{1/3}/\theta^{5/3}$, reduced drag coefficient
ξ	= $(M^2 - 1)/[(\gamma + 1)\theta]^{2/3}$, transonic similarity parameter
X	= distance along the axis of the wedge measured from the apex

(I) INTRODUCTION

THE PAPER GIVES THE RESULTS of a detailed experimental investigation of two-dimensional transonic flow past wedge sections—i.e., profiles consisting of a simple wedge at zero angle of attack followed by a straight section. The significance of the data and the comparison with theory are discussed.

Investigations of transonic-flow problems are inherently not easy. In theory, one has to deal with a problem that cannot be handled with linearized equations without losing its essential features. In experiment, one is faced with the well-known difficulties of investigating the flow field near Mach Number 1—i.e., flow with extremely large lateral extent of the perturbation field of a body. In the last few years, progress in transonic-flow theory has been steady. The investigations of von Kármán, Busemann, Guderley, and others have led to a general understanding of the main features of transonic flow. Similarly, the technique of wind-tunnel experiments, especially the development of variable Mach Number supersonic tunnels and of interferometric measuring techniques, etc., has advanced considerably in the last few years.

During the course of experimental research of viscous phenomena and of boundary-layer shock-wave interaction carried out at GALCIT, under N.A.C.A. sponsorship, an interferometer was built. Before applying the interferometric technique to a problem as involved as the boundary-layer shock-wave interaction problem, it was decided to try to investigate in detail an essentially nonviscous transonic-flow field of large dimensions. In view of the status of transonic theory and the lack of experimental results in this range, it was clear that a study of the simplest transonic-flow problem was of great theoretical and practical interest. Hence, an investigation of transonic flow past wedge sections was undertaken. The choice of the section, angles, etc., was based upon the following considerations:

(1) Two-dimensional flow is preferable, since a theoretical study of two-dimensional flow is easier than axially symmetric flow and since, furthermore, the evaluation of interferograms is more direct and faster. Obviously, setting up of two-dimensional flow past a

Presented under the title "Experiments in Transonic Flow" at the Aerodynamics Session, Annual Summer Meeting, I.A.S., Los Angeles, July 12–14, 1950. Received August 9, 1950.

* Professor of Aeronautics, Guggenheim Aeronautical Laboratory.

† Graduate Student.

body is not easy at all, but this difficulty has to be accepted.

(2) The extremely large lateral extent of the perturbation field of a body in the transonic region makes it necessary to reduce size—e.g., the chord of the model—relative to the wind-tunnel dimensions as much as possible. This, in turn, tends to reduce the Reynolds Number of the model and thus increase the importance of boundary-layer and, in general, viscous phenomena. Since this investigation was mainly concerned with a nonviscous-flow problem, it was obviously necessary to reduce the viscous effects as much as possible. The very nature of the flow does not permit the increase of size of the model with respect to a given wind tunnel. However, one can restrict the importance of viscous phenomena to a large extent by choosing the geometry of a model such that the boundary layer is in a region of favorable pressure gradient. Separation problems are thus avoided, and the importance of boundary-layer effects is reduced. Based on this consideration, it was decided to investigate a wedge followed by a straight section rather than a double-wedge section. This choice of the model does not greatly restrict the investigation because the important part of a double-wedge section in nonviscous transonic flow for $M > 1$ is actually the forebody. The flow over the afterbody is supersonic throughout and, hence, can be treated with fairly standard methods.

Clearly, viscous phenomena cannot be completely eliminated in this fashion. For example, there is still a slight change of the effective shape of the wedge by the existence of the boundary layer, as well as a "rounding off" of the shoulder corner, etc. However, these effects are comparatively slight compared with large effects such as separation.

(3) Both theoretical advantages and practical need focus the interest upon thin sections. The wedge angles chosen were, thus, 4.5°, 7.5°, and 10° semiangles. It was not considered feasible to measure wedges with angles less than 4.5° semiangle due to structural difficulties. On the other hand, for small apex angles the transonic similarity law should allow the extension of data without additional measurements.

Because of the precautions outlined in (2) and the use of interferometric measuring methods, it proved possible to measure the complete pressure distribution as a function of Mach Number on wedges of length not greater than $^1/_4$ in. and to obtain reliable pressure drag data in spite of the fact that the Reynolds Number of the sections was only about 6×10^4.

Curiously enough, there does not seem to exist much previous experimental work on wedge sections in the transonic régime. Interferometric investigations of transonic flow of this type, carried out at Braunschweig after the war and reported by Pack,[1] are not too extensive and reliable, since the wind-tunnel flow was nonuniform, since the tunnel seems to have been choked during at least some of the measurements, and since only one supersonic Mach Number was investigated. No other systematic experimental investigation of the problem seems to have been published so far.

Theoretical results consisted, at the beginning of the present research, essentially of von Kármán's general similarity considerations,[2] of Busemann's general discussion of flows with detached shock waves,[3] and of papers by Guderley and by Guderley and Yoshihara, respectively—one is a general discussion of transonic flow patterns,[4] the other is a detailed computation of flow past thin sections at a free-stream Mach Number of unity.[5] During the course of the present experiments, it was learned that Vincenti,[6] at the Ames Aeronautical Laboratory, had carried out a detailed computation of flow past double-wedge sections with detached shock wave. The cited theoretical papers have the following in common: that they deal with the problem in transonic approximation but are rigorous within this frame. That is, no further simplifying assumptions are introduced, and in Guderley's and especially Vincenti's work the Tricomi equation in the hodograph is actually solved under the prescribed boundary conditions. Hence, these papers differ considerably from others not cited here, where other simplifying assumptions have been made, such as an assumed shape of the shock, etc.

Vincenti's work has so far not been published. However, because of the cooperation of the N.A.C.A., it was possible to exchange information between the Ames Aeronautical Laboratory and GALCIT, and, hence, a partial comparison of the present results with Vincenti's theoretical work is included here. For further details with respect to the theory and comparison with experiment, reference is made to forthcoming N.A.C.A. publications.

In the last few weeks, J. D. Cole, of GALCIT,[7] succeeded in finding a solution of the transonic equations for a free-stream Mach Number less than unity, from which the drag of the wedge can be obtained. Hence, it proved possible to compare the measured drag coefficients with theory both in the high subsonic region (Cole) and in the low supersonic region (Vincenti). The cooperation of Vincenti and Cole in making it possible to use the unpublished results is gratefully acknowledged.

The authors would also like to acknowledge the cooperation of the other members of the Transonic Research Group at GALCIT. Especially the help of S. Dhawan and G. Solomon was essential.

(II) Apparatus and Methods

(1) *Wind Tunnel*

The measurements were carried out in the GALCIT 4- by 10-in. Transonic Wind Tunnel. For a description of the tunnel, and especially of the flexible nozzle employed, see reference 8.

(2) Interferometer

An interferometer of somewhat unusual construction was used in this investigation. The interferometer is described in detail in reference 9.

(3) Models

Accurate lapped steel wedges were used. The general geometry of these wedge sections is shown in Fig. 1. Two pressure orifices symmetrically located on the sides of the wedge were used both to set the angle of attack to zero and to identify one of the interferometer fringes. An orifice near the shoulder was used as a second check on the measured Mach Number and fringe identification.

(4) Two-Dimensional Flow

To obtain two-dimensional conditions in the wind tunnel as nearly as possible, the span of the wedge section has to be carefully chosen. If the span is too long and extends well into the boundary layer on the wall, strong shock-wave boundary-layer interaction on the sidewalls results. If, on the other hand, the span of the wedge is chosen too short, one is faced with three-dimensional tip effects. Between these two limits there exists an optimum ratio of span to tunnel width. The optimum was found by gradually shortening the span of a given wedge section until the shock wave had reached its best definition as judged by both schlieren and interferometer observation. For the present tunnel, this turned out to be a ratio of model span to tunnel width of 0.875. The Ames Aeronautical Laboratory has made shadow photographs of tips of wedge sections with detached shock waves near the boundary layer on a flat wall. These shadow photographs were taken at right angles to the flow direction and the span so that the plane of the sections and the wall boundary, as well as a section through the shock, became visible. These photographs, which thanks to the cooperation of the N.A.C.A. were made available to the authors, confirm the fact that there exists an optimum tip distance from the wall such that very nearly two-dimensional flow is obtained over the section. More details and further checks will be reported later in N.A.C.A. publications.†

(5) Wind-Tunnel-Wall Interference

For the measurements of flows with detached shock waves, the interference of the top and bottom walls is zero, since the subsonic zone was kept well away from the walls. In the measurements in subsonic flow reported here, some interference must exist. However, the ratio of the height of the tunnel to the chord of the airfoil is so large that the effect is minor and consists mainly in a slightly altered free-stream Mach Number. This latter effect was taken into account.

† It should be remembered that a profile that does not touch the sidewalls is not equivalent to a three-dimensional body with an aspect ratio given by its span chord ratio but is more nearly equivalent to an infinitely long profile with periodic gaps equal to twice the distance of the edges from the sidewalls.

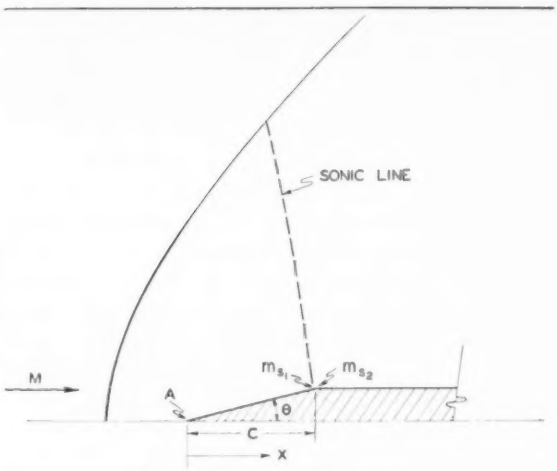

FIG. 1. Nomenclature diagram.

(III) CHARACTERISTIC FEATURES OF TRANSONIC FLOW PAST WEDGE SECTIONS

This is not the place to discuss the transonic problem in general; however, it appears useful and necessary to draw attention to some specific and important features of transonic flow past single-wedge sections. Some of these characteristics have been discussed before; some have, to the authors' knowledge, not been noticed or explicitly stated.

(1) Characteristic Values of the Free-Stream Mach Number

For a wedge section of half apex angle θ in uniform parallel flow, there exist the following characteristic Mach Numbers:

(a) M_A, the free-stream Mach Number at which the shock wave attaches.

(b) M_S, the Mach Number at which the flow behind the attached shock wave is exactly sonic.

(c) M_0, the Mach Number corresponding to the so-called Crocco point—i.e., the Mach Number at which a characteristic change in the curvature of the attached shock wave occurs.

M_0 is not too important for the present investigations. Reference is made to Guderley's paper[4] for a more detailed discussion of M_0.

(d) The critical Mach Number M_C—i.e., the free-stream Mach Number for which the local Mach Number first reaches unity—is zero for a wedge due to the sharp corner at the shoulder.

Hence, neglecting viscosity and boundary-layer effects, the transonic region for a wedge section extends from $M = 0$ to $M = M_S$.

(2) *Characteristic Values of the Local Mach Number*

The local Mach Number at the apex of the wedge and the Mach Number immediately before and behind the shoulder corner have characteristic values in transonic flow.

(a) The Mach Number at the apex of the wedge m_A, is always zero, since a stagnation point exists there.

(b) The Mach Number at the shoulder just before the turn, m_{S_1}, is always equal to unity.

(c) It is impossible to reach the free-stream Mach Number on the flat part of the wedge afterbody by an isentropic Prandtl-Meyer expansion around the corner. The flow around the corner overexpands first and recompresses through one or more shock waves.

Statement (a) is trivial; (b) and (c) follow directly from simple considerations: For supersonic flow with a detached shock wave, the sonic point must be at the shoulder of the wedge; if the sonic point lies between the apex and the shoulder, then the flow behind the sonic point would be supersonic and the shoulder could not influence the forebody and the shock wave. Since for a given wedge angle the distance of the shoulder from the apex—i.e., the chord C—is the only characteristic length of the problem, it must determine the distance of the detached shock wave, etc. Hence, the shoulder must influence the forebody, and the sonic point cannot lie ahead of the shoulder. Furthermore, subsonic compressible flow around a sharp corner is impossible. This statement is plausible, since, here, incompressible flow would reach infinite velocities and compressible flow at least supersonic velocities. Mathematically, this statement is shown to be true by observing that, if subsonic flow around a sharp corner were possible, the corner point would map into a line in the hogodraph plane. This requires that the Jacobian of the transformation vanish, which is impossible for subsonic flow (see, e.g., reference 10). In supersonic flow, this latter fact is possible and leads to the simple Prandtl-Meyer solution, in which the turning angle from a given Mach Number determines the flow uniquely. Statement (b) may be proved for subsonic flow by a comparatively simple argument.

It is also easy to show that the sonic line leaves the wedge shoulder normal to the direction of the flow—i.e., normal to the flanks of the wedge—and that the sonic line begins with infinite curvature.

Concerning (c), one may remark that, if completely isentropic recompression were possible, for transonic flow with a subsonic free-stream Mach Number the drag would be zero. However, this does not seem reasonable.

One can argue in more detail as follows: According to (b) the Mach Number ahead of the turn is equal to unity for the whole range of free-stream Mach Numbers from 0 up to M_S. The total angle of turn is always θ. However, Prandtl-Meyer flow starting from sonic velocity will lead to a Mach Number m_{S_2}, which is uniquely determined by θ. Clearly, in general, $m_{S_2} \neq M$; for example, in subsonic flow obviously $m_{S_2} > M$. Consequently, the boundary conditions can only be met by a combination of expansion and shock waves. It appears theoretically difficult to find the exact form of the shock waves. One may prove, though, that at least one wave has to originate obliquely from the corner and that an entropy integral extended over the shock or system of shocks must be equal to the total pressure drag over the forebody.[12]

Experimental observations of shock formations near the corner are strongly influenced by boundary-layer effects and are not easily evaluated.

(3) *Transonic Approximation and Transonic Similarity*

In the so-called transonic approximation, one considers the difference of any Mach Number in the field from unity as a small parameter. This implies that the wedge angle θ is also small, and one keeps in this approximation, in general, only the largest terms in θ and in $M^2 - 1$ or $m^2 - 1$.

Based upon this approximation the following results are easily obtained:

$$M_A{}^2 - 1 = (3/4^{2/3})\,[(\gamma + 1)\theta]^{2/3} \tag{1}$$

$$m_{S_2}{}^2 - 1 = (3/2)^{2/3}\,[(\gamma + 1)\theta]^{2/3} \tag{2}$$

$$M_S{}^2 - 1 = 2^{1/3}\,[(\gamma + 1)\theta]^{2/3} \tag{3}$$

Furthermore, the following relations obtained in the same approximation are useful for later applications. If M denotes the Mach Number ahead of a normal shock wave, m_1 the Mach Number behind, then

$$M^2 - 1 = 1 - m_1{}^2 \tag{4}$$

Furthermore, let M be the stream Mach Number and m the local Mach Number at a certain point, and assume again that

$$M^2 - 1 = \mu << 1$$

and

$$m^2 - 1 = \nu << 1$$

then, we have, for the pressure coefficient at this point,

$$\frac{p - p_\infty}{(1/2)\rho_\infty U_\infty{}^2} = C_P = \frac{2}{\gamma + 1}\,(\mu - \nu) \tag{5}$$

The transonic similarity rules are usually obtained from the differential equation of motion and the boundary conditions.[2] Eqs. (1) to (5) are consistent with similarity rules.

Eqs. (1), (2), (3), and (4) suggest the use of $(M^2 - 1) \div [(\gamma + 1)\theta]^{2/3}$ as independent variable and $(m^2 - 1) \div [(\gamma + 1)\theta]^{2/3}$ as dependent variable and, hence, suggest the existence of a functional relation of the form

$$\frac{m^2 - 1}{[(\gamma + 1)\theta]^{2/3}} = f\left\{\frac{M^2 - 1}{[(\gamma + 1)\theta]^{2/3}}\right\}$$

From Eq. (5) for C_P, it follows that

$$\frac{C_P(\gamma+1)^{1/3}}{\theta^{2/3}} = g\left\{\frac{M^2-1}{[(\gamma+1)\theta]^{2/3}}\right\} \tag{6}$$

Since C_D, the drag coefficient, is simply equal to the average pressure coefficient times the angle θ, we have

$$\frac{C_D(\gamma+1)^{1/3}}{\theta^{5/3}} = h\left\{\frac{M^2-1}{[(\gamma+1)\theta]^{2/3}}\right\} \tag{7}$$

Eqs. (6) and (7) are the well-known similarity laws of transonic flow.

In the following, $C_D(\gamma+1)^{1/3}/\theta^{5/3}$ will be denoted by $\bar{C}_D$ and $(M^2-1)/[(\gamma+1)\theta]^{2/3}$ by ξ. It is also possible to determine the form of the characteristic reference length l of the shock wave—e.g., the length from the centerline to the sonic point on the shock wave.

The drag coefficient C_D is related to the entropy change across a shock and, thus, to the Mach Number ahead of the shock wave through a relation of the form

$$C_D \sim [(M^2-1)^3/(\gamma+1)^2]\,(l/C) \tag{8}$$

valid for transonic flow (e.g., reference 12).

Thus, by comparing Eq. (8) with Eq. (7), we find

$$\frac{(M^2-1)^3}{(\gamma+1)^2}\frac{l}{C} \sim \frac{\theta^{5/3}}{(\gamma+1)^{1/3}}h\left\{\frac{M^2-1}{[(\gamma+1)\theta]^{2/3}}\right\}$$

or

$$(l/C) \sim [(\gamma+1)\theta]^{-1/3}\,(1/\xi^3)h\,(\xi)$$

or

$$\frac{l}{C}[(\gamma+1)\theta]^{1/3} = k\left\{\frac{M^2-1}{[(\gamma+1)\theta]^{2/3}}\right\} = k\,(\xi) \tag{9}$$

(4) *Slope of the Drag Curve at $M = 1$*

A simple and intuitive consideration enables one to determine the slope of the C_D versus M relation at $M = 1$. This slope will be found useful in joining Guderley's C_D value at $M = 1$ with Vincenti's drag curve for $M > 1$ and for a comparison with experiment. The reasoning is not restricted to this particular case but should apply to any profile for the part ahead of the sonic point.

Eq. (3) expresses the well-known fact that the Mach Number downstream of a weak, normal shock wave is as much below unity as the Mach Number upstream is above unity. That is, there exists a certain symmetry about $M = 1$. For M very near unity, the detached shock wave is far away from the wedge and is nearly normal; the Mach Number just downstream of the shock is slightly subsonic. For the pressure distribution on the wedge, it is thus irrelevant whether this subsonic Mach Number at large distances is due to the presence of a shock wave or due to the fact that the velocity at infinity is slightly below sonic. Consequently, the pressure or Mach Number distribution on the wedge should be independent of Mach Number in the neighborhood of $M = 1$. To find the slope of the drag curve, one has only to differentiate Eq. (4) with respect to $\mu = M^2 - 1$; thus,

$$\frac{dC_P}{d\mu} = \frac{2}{\gamma+1}\left[1 - \frac{d\nu}{d\mu}\right]$$

The above consideration implies that $\nu = m^2 - 1$ is independent of μ as $M \to 1$—i.e., if $\mu \to 0$—hence, at $M = 1$, we find

$$(dC_P/d\mu)_{\mu=0} = 2/(\gamma+1) \tag{10}$$

Transforming this into the proper transonic similarity form, we find, for the drag coefficient,

$$\frac{1}{\gamma+1}\left(\frac{d\,\dfrac{C_D(\gamma+1)^{1/3}}{\theta^{5/3}}}{d\,\dfrac{M^2-1}{[(\gamma+1)\theta]^{2/3}}}\right)_{\mu=0} = \left(\frac{dC_P}{d\mu}\right)_{\mu=0} = \frac{2}{\gamma+1}$$

and, consequently,

$$d\bar{C}_D/d\xi = 2 \tag{11}$$

Actually, the measurements at high subsonic and low supersonic velocities indicate that the Mach Number distribution over the forebody is independent of the free-stream Mach Number not only as $M \to 1$ but even for finite small differences from $M = 1$. The same result was also recently found by Bleakney and Griffith[11] using the Princeton shock tube. The recent theory of Cole furnishes essentially the same result analytically and leads to the correct slope [Eq. (11)] as $\theta \to 0$.†

(IV) General Remarks Concerning Comparison of Experimental Data with Approximate Theory

A short discussion is included here about a philosophy of comparing experimental data with approximate theories. Recently, extensive discussion has arisen in connection with the application of small perturbation theory of axial symmetric flow to experimental results. Especially, Van Dyke[13] has called attention to certain difficulties in choosing the proper parameters in an approximate theory. The following discussion is related to Van Dyke's arguments but differs slightly in the point of view. The transonic theory referred to here involves two different kinds of approximations. One is a physical approximation—the assumption of nonviscous flow. The second is a mathematical approximation that involves the use of the highest order terms in $M^2 - 1$—i.e., the difference of the Mach Number from unity—and in θ—i.e., the deflection angle.

It is the second type of approximation which will be discussed here. These approximations make certain functions of the flow field equivalent for the theory—i.e., within the approximation certain functions of the

† In Pack's report,[1] reference is made to an unpublished paper of Macoll and Codd, and it is indicated that similar considerations have been made there. However, the authors have so far been unable to obtain a copy of Macoll and Codd's work. G. Guderley has independently made similar considerations recently. Guderley's result differs from the one given here by a different definition for C_P.

FIG. 2. Subsonic infinite fringe interferogram. $M = 0.772$; $^1/_2$ angle of wedge = 10°.

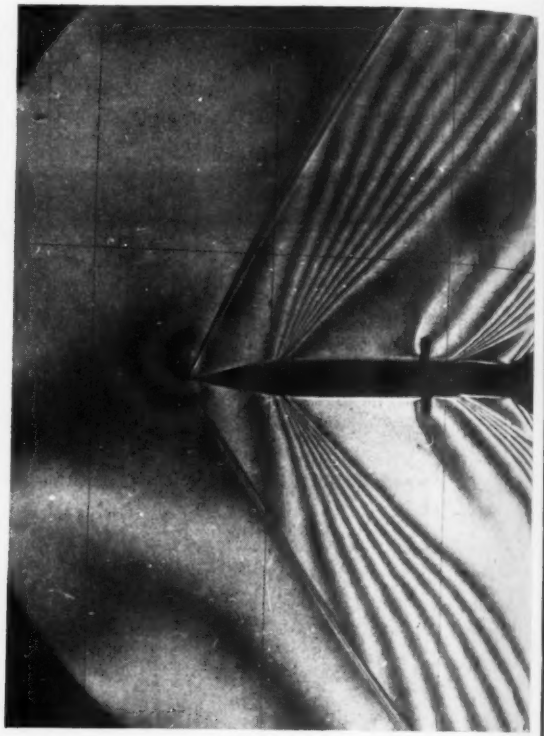

FIG. 4. Infinite fringe interferogram (attached shock). $M = 1.465$; $^1/_2$ angle of wedge = 10°.

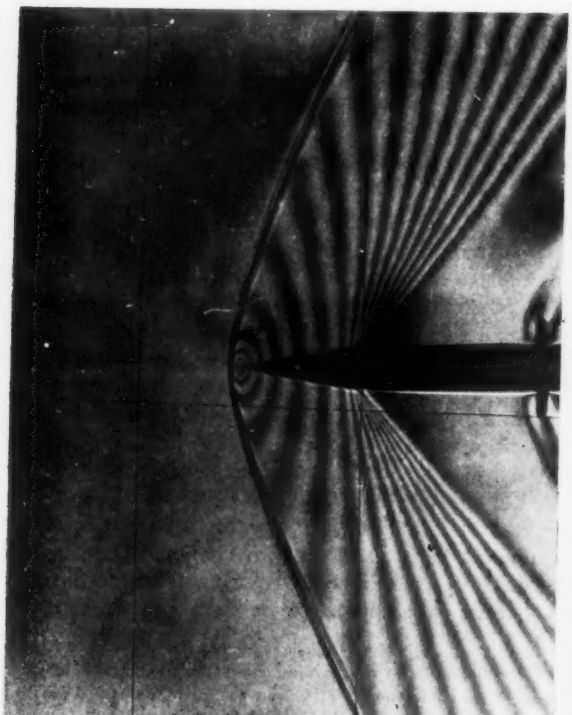

FIG. 3. Infinite fringe interferogram (detached shock). $M = 1.356$; $^1/_2$ angle of wedge = 10°.

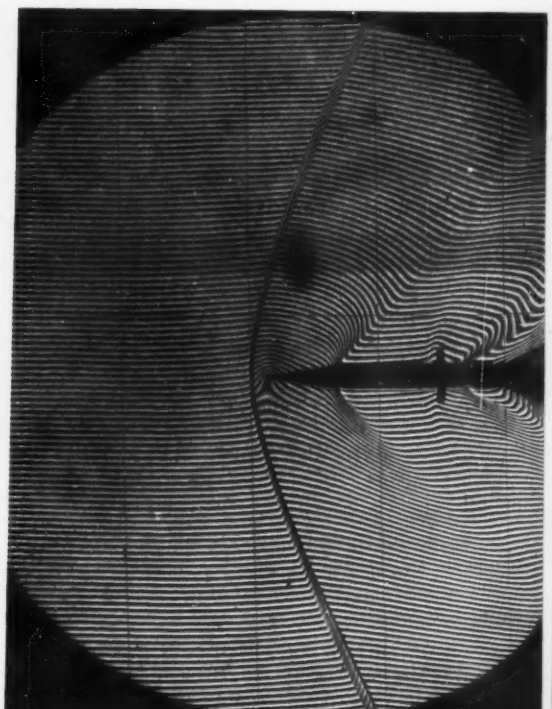

FIG. 5. Finite fringe interferogram. $M = 1.278$; $^1/_2$ angle of wedge = 10°.

velocity, etc., are identical. For example, $(P - P_\infty) \div (1/2)\rho_\infty U^2$, $-2(u'/a^*)$, $-2(u'/U)$ are equivalent within the approximation; hence, either of the last two expressions may be taken to define C_P. Similarly, $M^2 - 1$ and $2(M - 1)$ are equivalent, and, hence, the similarity parameter has the equivalent forms $(M^2 - 1)/\theta^{2/3}$ or $(M - 1)/\theta^{2/3}$. The experimental data of this study, and indeed practically all useful data, are obtained at values of θ and M for which the differences between equivalent expressions in the theory are not always negligible, and the question arises of how theory and experiment are to be evaluated.

(1) One may consider that the approximate theory is correct in the limit as $M \to 1$, $\theta \to 0$. This point of view is essentially implied if one uses mathematical order symbols as has been done extensively by the British school in linearized supersonic-flow theory. For the experimenter, this means that he should obtain data for a set of conditions for several θ and M and then establish the limiting law by extrapolating to $\theta \to 0$ and $M \to 1$. This latter result must then agree with the approximate theory.

(2) One may also look at the results of the theory as valid for small but finite values of $M^2 - 1$ and θ. Then the theory does not provide a definite result (as for example a drag curve) but rather a region, more or less narrow, of "equivalent" drag coefficients. It is not possible to distinguish between these within the framework of the theory. For example, such a region would be provided if C_P were alternatively defined by $-2(u'/a^*)$, $-2(u'/U)$, or $(P - P_\infty)/(1/2)\rho_\infty U^2$. The experiments should then fall within the limits of a band and can be used to decide which one of the equivalent expressions is the best in the sense that it extends the validity of the approximate theory over the widest possible range of the experimental parameters. In some cases a decision of this type can also be furnished by comparison with other theoretical results if the regions of validity overlap. Here, it can be seen, for example, that $M^2 - 1$ is a more reasonable choice than $2(M - 1)$, since with $M^2 - 1$ the transonic theory goes over smoothly into Ackeret's thin airfoil theory. This has already been shown by von Kármán.[2]

The above considerations led to the presentation chosen for the results of this investigation. It was found difficult to adopt the first point of view—i.e., to extrapolate the data to the limit $\theta \to 0$. This difficulty is essentially due to the nonlinear approach to this limit and to the experimental scatter.

The second point of view was accordingly adopted in presenting Fig. 13. Here, the theoretical indeterminacy is indicated by showing the range of C_P's between the limits defined by $-2(u'/a^*)$ and $-2(u'/U)$. It is clearly seen how the precision of the theory increases as $\theta \to 0$. The same convention for the presentation of supersonic theoretical results is adopted in Fig. 11. The same point of view can be adopted in presenting the slope at $M = 1$.† $dC_P/d\mu$ can, of course, be obtained also using the exact form of the pressure coefficient. In this case one has, instead of Eq. (10),

$$\left(\frac{dC_P}{d\mu}\right)_{\mu=0} = \frac{2}{\gamma}\left\{1 - \frac{1}{\gamma+1} \times \left[1 + \frac{\gamma-1}{\gamma+1}(m^2-1)\right]^{-\gamma/(\gamma-1)}\right\} \quad (12)$$

In first approximation with $m^2 - 1 = \nu << 1$, Eq. (10) results. Again, the approximate theory cannot distinguish between Eqs. (10), (11), or, for example,

$$\left(\frac{dC_P}{d\mu}\right)_{\mu=0} \doteq \frac{2}{\gamma+1}\left(1 + \frac{\nu}{\gamma+1}\right) \quad (13)$$

Similar results obviously hold for C_D. Thus, the slopes of C_D at $M = 1$ are presented as fans in Fig. 13, the larger slope corresponding to Eq. (10) and the smaller slope to Eq. (13). The difference is seen to be very small indeed for small θ.

(V) Results of the Measurements

(1) *General Character of the Flow Field*

Figs. 2 to 4 show typical interferograms of the flow phenomena using the so-called "infinite fringe" picture. The fringes shown correspond to lines of constant density and, thus, nearly to lines of constant Mach Number. The difference between successive fringes is approximately 0.05 Mach Number. For the actual evaluation it is more convenient to use the superposition method,[9] using a finite fringe picture such as Fig. 5 and a finite fringe picture of the undisturbed flow. The result is a picture as shown in Fig. 6. The lines of constant density appear here again. From photographs such as these, it is not difficult to evaluate the pressure field, determine the sonic lines, etc. In all these evaluations the increase in entropy through the shock wave was taken into account.

Fig. 7 shows typical tracings of the whole flow field about a wedge at different values of the free-stream Mach Number, obtained from superimposed finite fringe exposures.

(2) *Pressure Distributions*

The pressure distributions on one wedge section as functions of the free-stream Mach Number are shown in Figs. 8a and 8b. The slow and continuous variation from a typical subsonic to a typical supersonic distribution is clearly seen. For high subsonic free-stream Mach Numbers and for supersonic Mach Numbers with the bow wave detached, the sonic velocity is reached a little ahead of the corner. This is due to the boundary layer, which effectively rounds off the corner. After "attachment" of the shock wave, there exists a small subsonic zone around the very apex of the wedge. Clearly, the presence of the boundary layer distorts the

† This was pointed out to the authors by W. G. Vincenti.

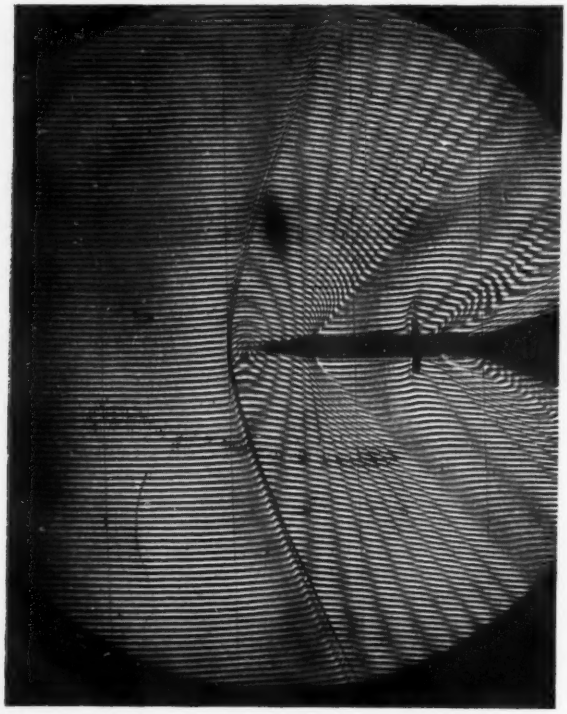

FIG. 6. Typical superimposed finite fringe interferogram. $M = 1.278$; $1/2$ angle of wedge $= 10°$.

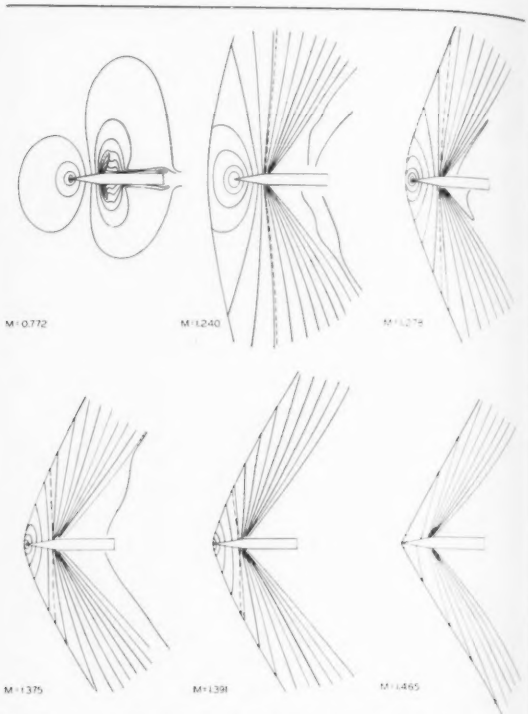

FIG. 7. ---indicates position of sonic line; $1/2$ angle of wedge = $10°$.

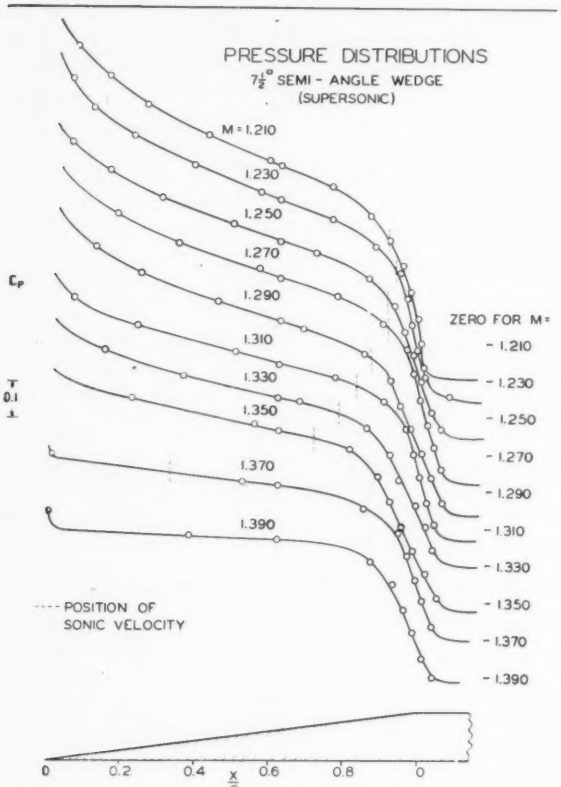

FIG. 8a.

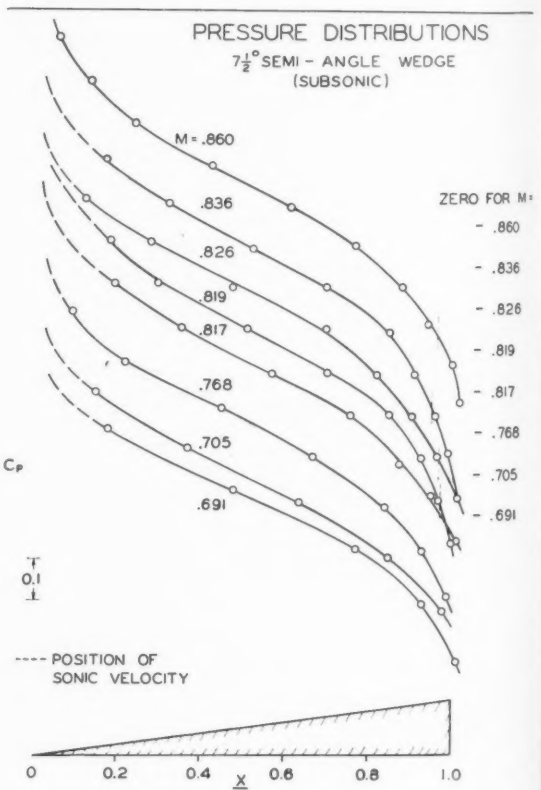

FIG. 8b.

measured pressure distribution. This is evident from the attached shock plots of Fig. 8a and also from a comparison of one of the measured pressure distributions with one computed by Vincenti, Fig. 9.† The order of magnitude of the change in pressure distribution and the qualitative behavior can be obtained from naive considerations of boundary-layer displacement. The layer is laminar, and, since the Reynolds Number based upon the chord is approximately 6×10^4, one can write for the displacement thickness δ^*/C at X/C approximately

$$\frac{\delta^*}{C} \sim \frac{1.7}{\sqrt{6 \times 10^4 \left(\frac{C}{X}\right)}} \sim 0.007 \sqrt{\frac{X}{C}}$$

The additional pressure change thus corresponds roughly to the change produced by a paraboloidal body with about 0.7 per cent maximum thickness at $X = C$. This turns out to be of the right order of magnitude as the observed deviations, and, hence, it seems reasonably certain that most of the deviations from the theoretical shape are due to boundary-layer influence. Since the additional pressure distribution is nearly antisymmetrical fore and aft, the drag is hardly influenced.

The influence of the expansion around the shoulder edge is felt upstream due to the boundary layer. Hence, sonic velocity is reached a little ahead of the corner. Experiments on shock-wave boundary-layer interaction have indicated that the distance of upstream influence of a compression in the laminar boundary layer is of the order of 20 to 40 times the boundary-layer thickness. For an expansion one expects less, since the boundary layer becomes thinner because of the gradient. In the present experiments,

$$\frac{\delta}{C} \sim \frac{5}{\sqrt{6 \times 10^4}} \sim 2 \times 10^{-2}$$

Hence, to find the sonic point 10 per cent ahead of the corner amounts to an influence through the boundary layer of roughly 5δ. Fig. 10 shows the movement of the sonic point with M as compared with the inviscid theory for a wedge with $\theta = 7.5°$.

Fig. 11 shows the local Mach Number m at the mid-chord point of a wedge with $\theta = 7.5°$ as function of the free-stream Mach Number M. The theoretical results of Vincenti and Guderley are shown, as well as the slope at $M = 1$, according to the general considerations outlined earlier. The local Mach Number appears to have a constant value over the range from about $M = 0.8$ to 1.2. Fig. 12 demonstrates the same effect by showing selected local Mach Number distributions for various M.

† The pressure distribution shown corresponds to the most unfavorable case, since the relative thickness of the boundary layer to the wedge is obviously largest for the smallest wedge angle.

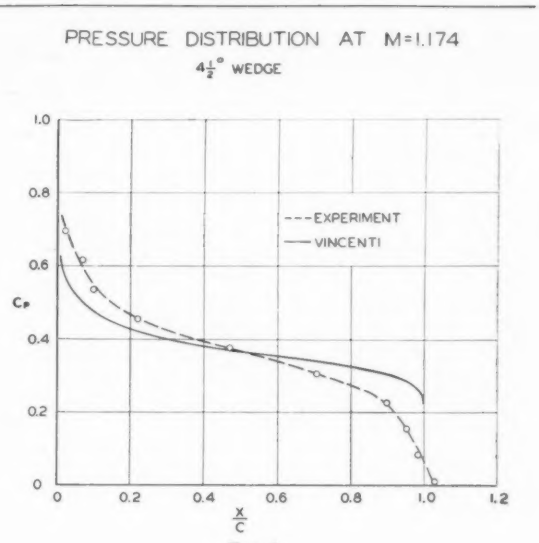

FIG. 9.

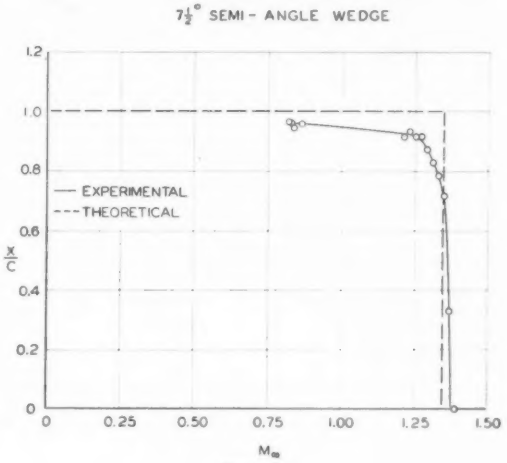

FIG. 10.

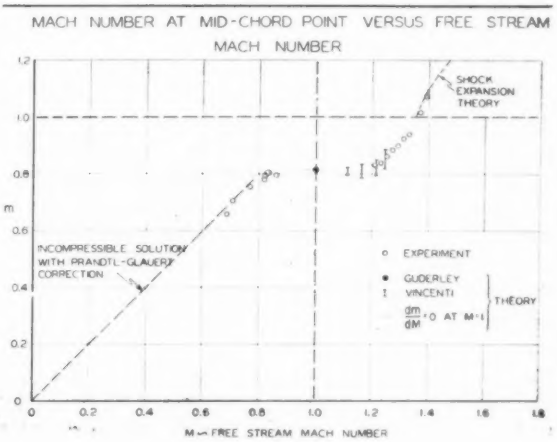

FIG. 11.

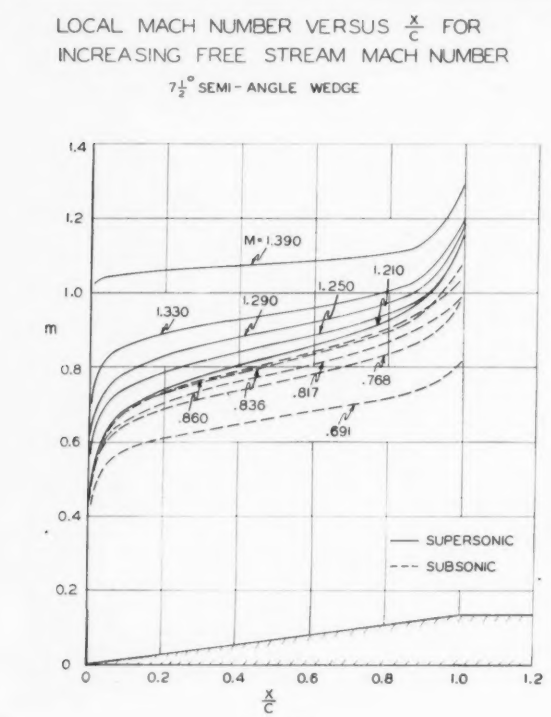

FIG. 12.

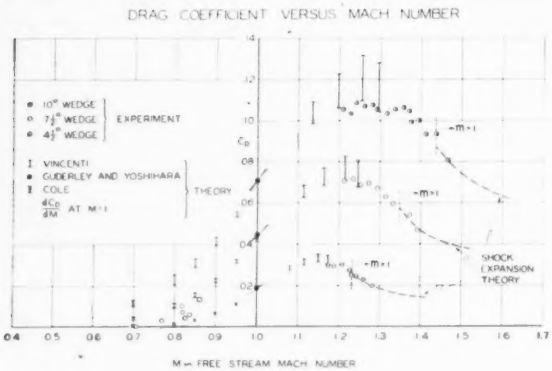

FIG. 13.

(3) *Drag Coefficient*

Fig. 13 presents the variation of the drag coefficient versus free-stream Mach Number for the three wedge angles. The theoretical values of Cole, Guderley, and Vincenti are shown. The results of Cole and Vincenti are presented as vertical lines rather than as points. For $M > 1$, the upper limit corresponds to evaluating C_D on the basis of taking $C_P = -2(u'/a^*)$; the lower limit of the lines corresponds to taking $C_P = -2(u'/U)$; the reverse is true for $M < 1$. For Guderley's value at $M = 1$, these two limits coincide. Plotting these results in this fashion shows clearly that the experiments and theory agree within the limits expected and that the theory becomes rapidly more precise for smaller wedge angles. The comparatively large scatter of the experimental drag measurements at subsonic speeds is due to the fact that the drag from the pressure distribution appears as the small difference between fairly large numbers.

Finally, Fig. 14 shows the drag coefficients plotted in the fashion of von Kármán's similarity rules. It is clearly seen that the measurements for the three wedges now lie much closer than before (Fig. 13) but that systematic deviations still exist. This is obviously due to the fairly large values of θ in these measurements. In cases such as these, the similarity rules can be expected to apply only approximately.

(VI) Concluding Remarks

The present measurements of pressure distribution and drag coefficient of simple wedge sections in transonic flow confirm, within the limits of accuracy of both theory and experiment, the theoretical results of von Kármán, Guderley, and especially the recent work of Vincenti and Cole.

The curve of pressure drag coefficient versus Mach Number for a simple wedge section rises rapidly at high subsonic Mach Numbers and reaches a maximum at a slightly supersonic Mach Number. Beyond this maximum the drag coefficient decreases as expected.

The pressure or Mach Number distribution on the wedge has a stationary value at $M = 1$, and, hence, the slope of the drag coefficient-Mach Number curve can easily be determined at $M = 1$. In transonic similarity parameters, $d\bar{C}_D/d\xi = 2$ at $M = 1$. It is found experimentally that the Mach Number distribution remains, in fact, practically constant through $M = 1$. The local Mach Number at a specific point on the wedge increases with M in subsonic flow, then remains constant through $M = 1$, and increases again in the supersonic régime. The range in which the local Mach Number remains constant is for thin wedges given approximately by

$$-1/2 < (M^2 - 1)/[(\gamma + 1)\theta]^{2/3} < 1/2$$

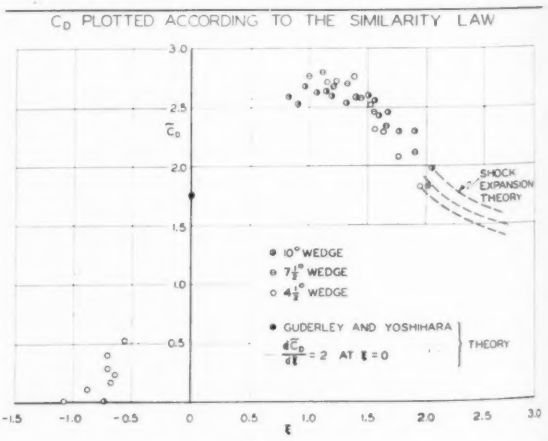

FIG. 14.

REFERENCES

[1] Pack, D. C., *Investigations of the Flow Past Finite Wedges of 20 Degree and 40 Degree Apex Angle at Subsonic and Supersonic Speeds, Using a Mach-Zehnder Interferometer*, British R. & M. No. 2321, 1949.

[2] von Kármán, Th., *The Similarity Law of Transonic Flow*, Journal of Mathematics & Physics, Vol. XXVI, p. 182, 1947.

[3] Busemann, A., *A Review of Analytical Methods for the Treatment of Flows with Detached Shock Waves*, N.A.C.A. T.N. No. 1858, 1949.

[4] Guderley, G., *Considerations of the Structure of Mixed Subsonic and Supersonic Flow Patterns*, AMC Wright Field Technical Report No. F-TR-2168-ND, October, 1947.

[5] Guderley, G., and Yoshihara, H., *The Flow over a Wedge Profile at a Mach Number One*, A. F. Technical Report No. 5783, 1949.

[6] Vincenti, W. G., unpublished, to appear shortly in an N.A.C.A. publication.

[7] Cole, J. D., unpublished, to appear shortly.

[8] Dhawan, S., and Roshko, A., *A Flexible Nozzle for a Small Supersonic Wind Tunnel*, unpublished, to appear shortly in the JOURNAL OF THE AERONAUTICAL SCIENCES.

[9] Ashkenas, H., and Bryson, A. E., Jr., *Design and Performance of a Simple Interferometer for Wind-Tunnel Measurements*, unpublished, to appear shortly in the JOURNAL OF THE AERONAUTICAL SCIENCES.

[10] Liepmann, H. W., and Puckett, A. E., *Introduction to Aerodynamics of a Compressible Fluid*, p. 190; John Wiley & Sons, Inc., New York, 1947.

[11] Bleakney, W., and Griffith, W., unpublished, private communication.

[12] Liepmann, H. W., *On the Relation Between Drag and Entropy*, Douglas Aircraft Report SM-13726, 1950.

[13] Van Dyke, M. D., *First- and Second-Order Theory of Supersonic Flow Past Inclined Bodies of Revolution*, presented at the I.A.S. Eighteenth Annual Meeting, January 23–26, 1950, to be published in the JOURNAL OF THE AERONAUTICAL SCIENCES.

First U. S. National Congress of Applied Mechanics

Plans have now been formulated to hold the First U.S. National Congress of Applied Mechanics on June 11–16, 1951, at Chicago, Ill. The Illinois Institute of Technology will be host to the Congress.

Members of the Institute, one of the sponsoring societies, are cordially invited to submit papers, which should constitute original research in applied mechanics. (Their length must not exceed 5,000 words or the equivalent in equations, tables, and diagrams.) Abstracts must be submitted to the Chairman of the Editorial Committee before April 14, 1951; complete papers must be submitted prior to June 11, 1951.

Additional information about the Congress may be obtained by writing to N. M. Newmark, Secretary of the Congress, University of Illinois, Urbana, Ill. All members are invited to attend.

A Study of the Response of an Airplane Landing Gear Using the Differential Analyzer*

WALTER C. HURTY†

University of California at Los Angeles

SUMMARY

The response of a conventional airplane landing gear is studied by deriving and solving the differential equations of motion for the system. The resistance of the air-oil shock strut depends upon an orifice damping coefficient and an exponent, γ, which determines the air pressure as a function of volume. A study of experimental "drop-test" results on similar systems is made to determine these constants. The nonlinear equations of motion are solved by means of the differential analyzer for (1) the landing condition as simulated by a drop test and (2) the taxiing condition in which a periodic ground contour function is assumed. The differential analyzer solutions for the landing condition are compared with drop-test results on the same system.

SYMBOLS

x, $\dot{x}$, $\ddot{x}$	= horizontal components of displacement, velocity, and acceleration, respectively; positive if directed in direction of motion of the airplane
z, $\dot{z}$, $\ddot{z}$	= vertical components of displacement, velocity, and acceleration, respectively; positive if directed up
φ	= angle included between the shock-strut centerline and the vertical
α	= angle included between a tangent to the ground contour at the point of contact and the horizontal
M	= one-half of total airplane mass less m
m	= mass of "unsprung system" including wheel, tire, axle, and shock-strut piston
F_s	= axial force applied to shock strut
$G(y_2)$	= normal ground force applied to tire
z_C', z_C''	= derivatives of the ground contour function taken with respect to x_C
L	= one-half of total aerodynamic lift on airplane
g	= acceleration of gravity
λ	= wave length of ground sinusoid
e	= amplitude of ground sinusoid
ω	= angular frequency of excitation
p_a	= air pressure in shock-strut cylinder
Δp_o	= pressure drop across orifice
p_f	= fluid pressure in shock strut below orifice
d_c, d_f, d_p	= diameters, respectively, of shock air chamber, fluid chamber at orifice, and piston
a_c, a_f, a_p	= cross-section areas corresponding to diameters d_c, d_f, and d_p
y_1	= displacement of shock-strut piston measured from fully extended position
y_2	= tire deflection
$F(y_1)$	= force due to air pressure; function of y_1
$R(\dot{y}_1)$	= damping function due to flow through orifice
V_a	= air volume in strut cylinder; function of y_1
V_o	= air volume when piston is fully extended
γ	= constant for polytropic compression and expansion of air
y_{1i}, y_{2i}	= initial values of y_1 and y_2 at beginning of motion
Q	= quantity of fluid flow through orifice
A_o	= orifice area
c_d	= orifice discharge coefficient
c_p	= orifice pressure coefficient
k_p	= shock-strut constant $= a_p/V_o$
h	= height of free drop in drop test

Subscripts A, B, and C refer, respectively, to the airplane center of gravity, the center of the wheel, and the point of contact of wheel with ground. Subscript so refers to snubber orifices.

INTRODUCTION

IN THE DESIGN OF AIRPLANE STRUCTURES, it is becoming increasingly important to take into consideration transient states of stress, as well as steady-state stresses resulting from periodic forces applied to the airplane. An example of the emphasis placed upon the determination of such dynamic stresses may be seen in the many efforts that have been made in recent years to determine stresses in the wings of an airplane resulting from the landing impact.[1, 2] The growing urgency of this problem has been brought about by two trends in airplane design: first, the use of thin wings demanded by aerodynamic considerations connected with high-speed flight; second, the disposition of items of considerable mass along the wing span outboard of the landing gear attachment points. Both factors reduce the natural frequencies of the wing in both bending and torsion and, hence, increase the likelihood of exciting large amplitude vibrations by means of ground forces.

The calculation of bending and torsional vibrations of an elastic wing can be made by well-established methods of analysis provided the forces applied by the landing gear are known as functions of time. It is the purpose of this paper to outline a method of determining such force functions in specific cases rather than to investigate the wing vibrations. Strictly speaking, the problem cannot thus be separated into two parts, since the motions of the shock-absorbing system and those of the vibrating wing are coupled. However, it has been shown[2] that the landing-gear forces can be determined with but a small error on the conservative

Received January 3, 1950.

* The author is indebted to Northrop Aircraft, Inc., and, in particular, to A. M. Schwartz and Dr. A. T. Zahorski of that company for the data used in this analysis. He also wishes to thank Prof. L. M. K. Boelter, Dean of the College of Engineering, University of California at Los Angeles, for making available the use of the differential analyzer for the solution of the equations.

† Assistant Professor, College of Engineering.

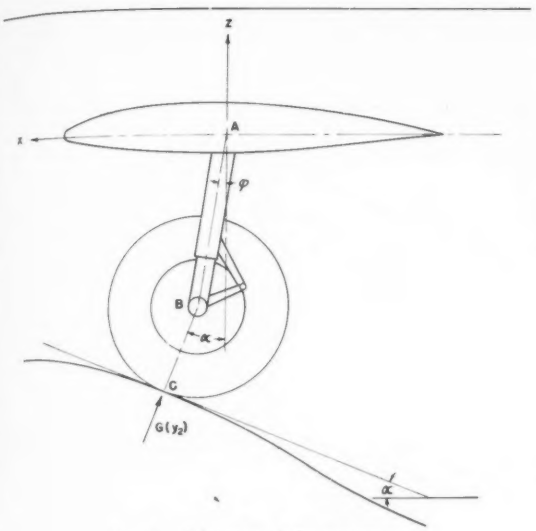

FIG. 1. Diagram of the system.

side by considering the airplane as a rigid body, and this procedure is followed in the present investigation.

The work reported here was carried out as part of a general analysis made in connection with the design of a particular airplane. In scope, the problem consisted of the determination, by analytical means, of the forces imposed on the wing by the landing-gear strut in landing and taxiing the airplane. Since the bending modes of vibration were of particular interest, only the vertical forces transmitted to the wing were found. The equations of motion derived for the two degree of freedom system are nonlinear and require for their solution the use of numerical analysis techniques or an analog computer. In this case, use was made of the mechanical differential analyzer located on the campus of the University of California at Los Angeles and operated by the College of Engineering. This machine is extremely versatile and well adapted to the solution of nonlinear differential equations.

EQUATIONS OF MOTION

The system, shown in Fig. 1, consists of a mass M, representing the airplane; a conventional air-oil shock strut; and a mass, m, representing the wheel, tire, axle, and shock-strut piston. Equations are derived for the motion of the system as the airplane rolls over an uneven ground surface at a constant velocity. From these equations we may write those pertinent to the landing case without difficulty. Energy dissipated by the tire is neglected, inasmuch as it will be small compared with that dissipated by the shock strut. Referring to Fig. 1, we may obtain the following velocity relationships useful in the derivation:

$$\left.\begin{aligned} \dot{x}_A &= \dot{x}_C + \dot{y}_1 \sin\varphi + \dot{y}_2 \sin\alpha \\ \dot{z}_A &= \dot{z}_C - \dot{y}_1 \cos\varphi - \dot{y}_2 \cos\alpha \\ \dot{x}_B &= \dot{x}_C + \dot{y}_2 \sin\alpha \\ \dot{z}_B &= \dot{z}_C - \dot{y}_2 \cos\alpha \end{aligned}\right\} \tag{1}$$

Differentiating with respect to time, the following acceleration equations are written:

$$\left.\begin{aligned} \ddot{x}_A &= \ddot{x}_C + \ddot{y}_1 \sin\varphi + \ddot{y}_2 \sin\alpha + \dot{y}_2\dot{\alpha}\cos\alpha \\ \ddot{z}_A &= \ddot{z}_C - \ddot{y}_1 \cos\varphi - \ddot{y}_2 \cos\alpha + \dot{y}_2\dot{\alpha}\sin\alpha \\ \ddot{x}_B &= \ddot{x}_C + \ddot{y}_2 \sin\alpha + \dot{y}_2\dot{\alpha}\cos\alpha \\ \ddot{z}_B &= \ddot{z}_C - \ddot{y}_2 \cos\alpha + \dot{y}_2\dot{\alpha}\sin\alpha \end{aligned}\right\} \tag{2}$$

The equations of equilibrium of the vertical components of the forces at points A and B are

$$-M\ddot{z}_A - Mg + L + F_s \cos\varphi = 0 \tag{3}$$

$$-m\ddot{z}_B - mg + G(y_2)\cos\alpha - F_s \cos\varphi = 0 \tag{4}$$

We substitute for $\ddot{z}_A$ and $\ddot{z}_B$ their equivalents given by equations and express the equilibrium equations in terms of the vertical components of the accelerations at the ground contact point C. This, in turn, may be calculated if we know the velocity of the airplane and the ground contour function.

$$\dot{z}_C = \dot{x}_C \tan\alpha \tag{5}$$

$$\ddot{z}_C = \ddot{x}_C \tan\alpha + \dot{x}_C\dot{\alpha}\sec^2\alpha \tag{6}$$

$$\left.\begin{aligned} \tan\alpha &= z_C', \quad \sec^2\alpha = 1 + z_C'^2 \\ \dot{\alpha} &= [z_C''/(1 + z_C'^2)]\dot{x}_C \end{aligned}\right\} \tag{7}$$

Finally, expressing $\dot{x}_C$ in terms of $\dot{x}_A$ from Eqs. (1) we can write the two equations of equilibrium as follows:

$$\ddot{y}_1(\cos\varphi + z_C'\sin\varphi) + \ddot{y}_2\sqrt{1 + z_C'^2} = \ddot{x}_A z_C' + z_C''\left(\dot{x}_A - \dot{y}_1\sin\varphi - \dot{y}_2\frac{z_C'}{\sqrt{1 + z_C'^2}}\right)^2 + g\left(1 - \frac{L}{Mg}\right) - \frac{F_s}{M}\cos\varphi \tag{8}$$

$$\ddot{y}_1 z_C'\sin\varphi + \ddot{y}_2\sqrt{1 + z_C'^2} = \ddot{x}_A z_C' + z_C''\left(\dot{x}_A - \dot{y}_1\sin\varphi - \dot{y}_2\frac{z_C'}{\sqrt{1 + z_C'^2}}\right)^2 + g - \frac{G(y_2)}{m\sqrt{1 + z_C'^2}} + \frac{F_s}{m}\cos\varphi \tag{9}$$

These equations are perfectly general in that they apply for any ground contour function we may choose as long as the tire is tangent to the ground at not more than one point. Although no fundamental difficulty is encountered in attempting to solve the equations by the differential analyzer, they may be simplified for most practical cases without appreciable loss of accuracy. In the present problem, the strut angle φ is small for the taxiing attitude of the airplane. Also, the ground slope z_C' is usually small compared with unity. Thus, Eqs. (8) and (9) may be simplified to the following form:

$$\ddot{y}_1 + \ddot{y}_2 = \ddot{x}_A z_C' + \dot{x}_A{}^2 z_C'' + g[1 - (L/Mg)] - (F_s/M) \quad (10)$$

$$\ddot{y}_2 = \ddot{x}_A z_C' + \dot{x}_A{}^2 z_C'' + g - \{[G(y_2) - F_s]/m\} \quad (11)$$

Considering the airplane velocity to be constant, the equations are finally arranged in the following dimensionless form:

$$\frac{\ddot{y}_1}{g} = \frac{G(y_2)}{mg} - \frac{F_s}{mg}\left(1 + \frac{m}{M}\right) - \frac{L}{Mg} \quad (12)$$

$$\frac{\ddot{y}_2}{g} = \frac{\dot{x}_A{}^2 z_C''}{g} - \frac{G(y_2)}{mg} + \frac{F_s}{mg} + 1 \quad (13)$$

It can easily be verified that Eqs. (12) and (13) apply to the landing condition on a level surface if we make z_C'' zero and apply the proper initial conditions.

It was of particular interest in this investigation to study the response of the system to excitation produced by a periodic ground function. Therefore, the simplest periodic function, the sinusoidal wave, was chosen.

$$z_C = (a/2)\,[1 - \cos(2\pi x_C/\lambda)] \quad (14)$$

This may be written as a function of time, and the dimensionless acceleration term may be expressed as

$$\dot{x}_A{}^2 z_C''/g = (a\omega^2/2g)\cos\omega t \quad (15)$$

It can be shown that the quantity $a\omega^2/2g$ is proportional to the ground reaction that would be developed if the system were rigid.

The Shock-Absorbing System

The shock-absorbing system consists of a conventional air-oil shock strut, such as used on most military and commercial airplanes, and a low-volume high load-capacity tire designed for airplanes having limited space for landing-gear retraction. The static and impact load-deflection characteristics are shown in Fig. 2. Fig. 3 shows the shock-strut design with the working parts essential to this discussion. The main orifice is metered as shown so that its area is a function of piston position. Snubber orifices are provided for rebound control and are effective only during the expansion stroke.

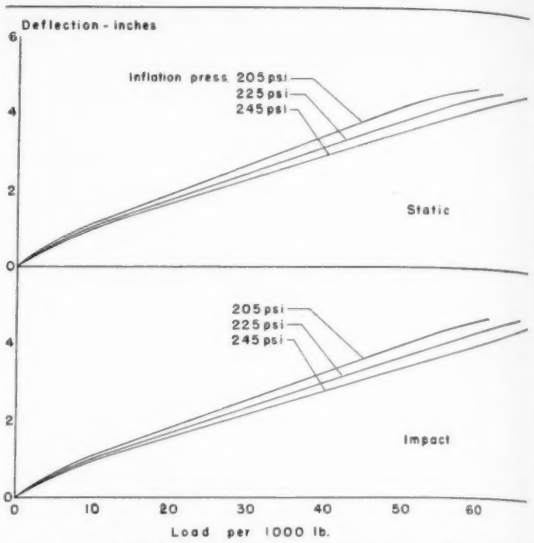

Fig. 2. Static and impact load-deflection characteristics of tire.

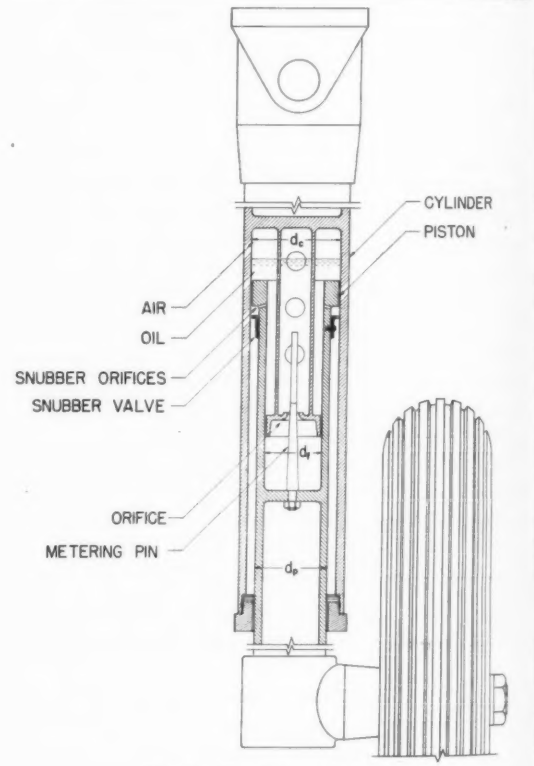

Fig. 3. Shock-strut design.

During the compression stroke, the fluid pressure below the orifice is equal to the pressure p_a and the pressure drop across the orifice Δp_o.

$$p_f = p_a + \Delta p_o \quad (16)$$

The compressive force on the piston is found by multiplying these pressures by corresponding piston areas.

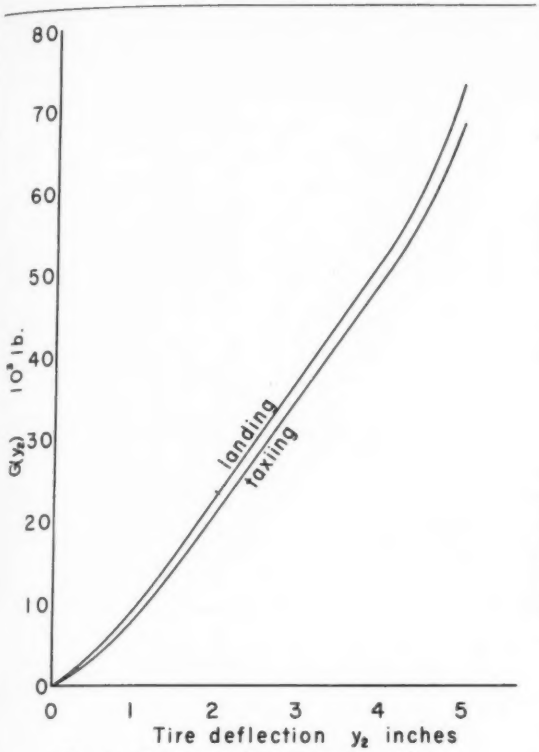

FIG. 4. Tire load-deflection function, $G(y_2)$.

$$F_s = p_a(a_c - a_f) + p_f a_f - p_a(a_c - a_p)$$
$$= p_a a_p + \Delta p_o a_f \tag{17}$$

The air pressure p_a is a function of piston position only while Δp_o is a function of both position and velocity. We may write

$$F_s = F(y_1) + R(y_1)\dot{y}_1^2 \tag{18}$$

To determine $F(y_1)$, it is assumed that the air pressure may be found from

$$p_a V_a^{\gamma} = \text{constant} \tag{19}$$

where γ is a suitably chosen constant. We may write V_a in terms of the air volume when the piston is fully extended.

$$V_a = V_o - a_p y_1 \tag{20}$$

Substituting in Eq. (19), the force $F(y_1)$ is obtained.

$$F(y_1) = \text{constant} \times [a_p/(V_o - a_p y_1)^{\gamma}] \tag{21}$$

The constant depends upon the position of the piston and the force applied to it at the beginning of the motion. Assuming that the air is initially at ambient temperature, we may consider the initial piston position to have been reached by an isothermal compression from the fully extended position. This permits us to express $F(y_1)$ in terms of the initial piston position and the force F_o which holds the piston against the stops when extended.

$$F(y_1) = (1 - k_p y_{1i})^{\gamma - 1} [F_o/(1 - K_p y_1)^{\gamma}] \tag{22}$$

To determine the orifice function $R(y_1)$, we use the equation for turbulent flow through orifices or other restrictions.

$$Q = C_d A_o \sqrt{2gh'} \tag{23}[6]$$

This equation may be used to give the pressure drop across the orifice in terms of orifice area and piston velocity.

$$\Delta p_o = (3.9 \times 10^{-5})/c_d^2)\ (a_f/A_o)^2 \dot{y}_1^2 \tag{24}$$

From this, $R(y_1)$ can be determined. For the compression stroke it is given by the equation

$$R(y_1) = (3.9 \times 10^{-5}/c_d^2)\ (a_f^3/A_o^2) \tag{25}$$

During the expansion stroke, the flow conditions are more complex because of the behavior of the return flow through the main orifice and flow through the snubber orifices. As the piston moves outward, oil in the chamber above the orifice is forced by air pressure to flow downward through the main orifice. The pressure conditions are

$$p_f = p_a - \Delta p_o$$
$$p_s = p_a + \Delta p_{so}$$

Under these conditions the force on the piston is given by

$$F_s = p_a(a_c - a_f) + p_f a_f - p_s(a_c - a_p)$$
$$= p_a a_p - \Delta p_o a_f - \Delta p_{so}(a_c - a_p) \tag{26}$$

and the expression for $R(y_1)$ is

$$R(y_1) = -\frac{3.9 \times 10^{-5}}{c_d^2}\frac{a_f^3}{A_o^2} - \frac{3.9 \times 10^{-5}}{c_{dso}^2}\frac{(a_c - a_p)^3}{A_{so}^2} \tag{27}$$

If the outward velocity of the piston becomes great enough, a critical velocity would be reached at which the resistance to flow through the main orifice would become equal to the pressure causing it. This condition would be characterized by the equation

$$\Delta p_o = p_a \tag{28}$$

At this velocity and beyond, the pressure p_f would drop to zero, and Eq. (26) would become

$$F_s = p_a(a_p - a_f) - \Delta p_{so}(a_c - a_p) \tag{29}$$

In this event we choose to continue to use Eq. (18), with suitable modification of R, which now becomes a function of velocity as well as displacement. We obtain it by letting $\Delta p_o = p_a$ in Eq. (26) and substituting p_a from Eq. (22).

$$R = -\frac{a_f}{a_p}\frac{(1 - k_p y_{1i})^{\gamma - 1}}{(1 - k_p y_1)^{\gamma}}\frac{F_o}{\dot{y}_1^2} - \frac{3.9 \times 10^{-5}}{c_{dso}^2}\frac{(a_c - a_p)^3}{A_{so}^2} \tag{30}$$

Numerical Data

Because Eqs. (12), (13), and (18), which make up the system of equations to be solved, are nonlinear, their solution is sought in numerical form. Therefore, it is necessary to introduce the numerical data to be used in the specific example to be considered.

The tire function $G(y_2)$ is obtained from the tire manufacturer's data shown in Fig. 2. The impact characteristics are used in the analysis. However, the static characteristics are used to establish initial conditions; hence, a rigorous treatment would require the use of a different load curve for each initial tire deflection considered. These, in turn, depend upon the weight of the airplane and the aerodynamic lift. Actually, the differences involved are small and are accounted for by using two curves—one for the landing condition and one for the taxiing conditions. These curves are plotted in Fig. 4.

At the present time, it appears that the constants γ and c_d can only be obtained by direct experiment. As a part of this general investigation, a number of landing-gear drop-test oscillograph records were analyzed in an attempt to determine them. These records were obtained from drop tests on shock struts similar in size and design to the one considered in this problem. Although many such drop tests have been made, not many include the direct measurement of air pressures throughout the compression and expansion strokes. Eight records in which air-pressure records were made were available for study, and the values of γ and c_d were based on results of the analysis of these records. Pressure-volume points from one of the records are plotted on logarithmic coordinates in Fig. 5. It is seen that these points group fairly closely about the straight line representing $\gamma = 1.1$, although in some of the records the scatter is somewhat greater than in the one shown. In all cases, the compression stroke begins with a γ close to the adiabatic constant for air, decreasing in value as the compression stroke progresses and then dropping still further at the end of the stroke and during the expansion stroke. The loop thus formed probably represents the heat loss through the walls of the strut during the process. From the records studied, it is concluded that γ is not a constant but that the heat transfer characteristics should be included in a rigorous study of such a system. However, from an energy standpoint, the error involved in taking γ as a constant is not great, and this simplification of the problem seems to be justified. For the solution of the present problem, a value of 1.1 was chosen.

The determination of c_d from the records is more difficult, and the values found show considerable scatter when plotted. It was found convenient to use an orifice pressure coefficient, c_p, defined by

$$\Delta p_o = c_p V_o^2 \tag{31}$$

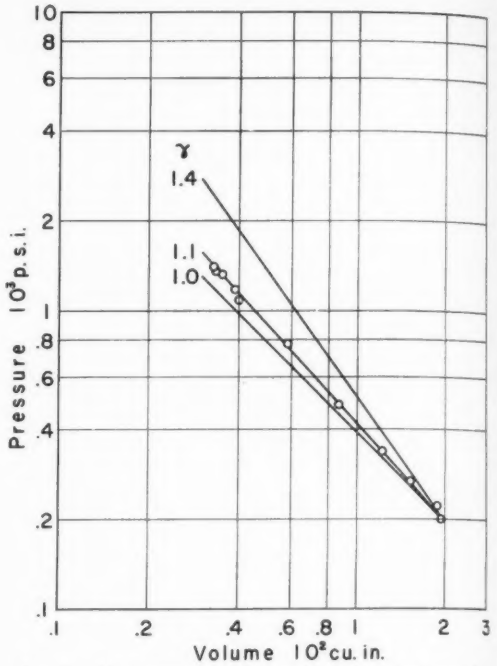

FIG. 5. Air pressure vs. volume from drop-test record.

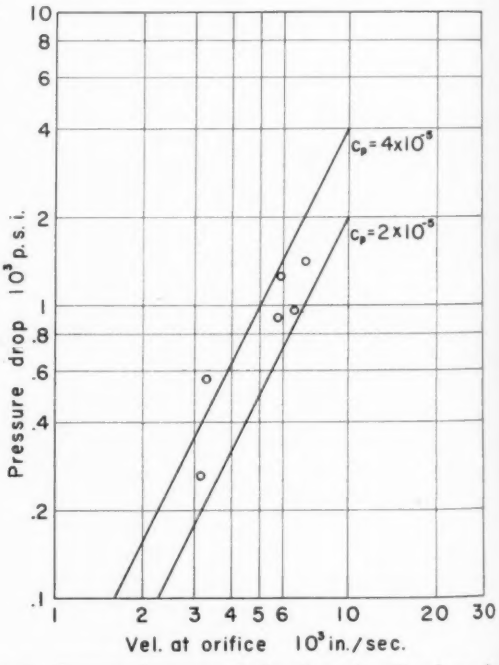

FIG. 6. Pressure drop vs. velocity through orifice from drop-test record.

The relationship between the two coefficients is

$$c_p = 3.9 \times 10^{-5}/c_d^2 \tag{32}$$

The velocity of flow through the orifice is dependent upon piston velocity and net orifice area, both of which

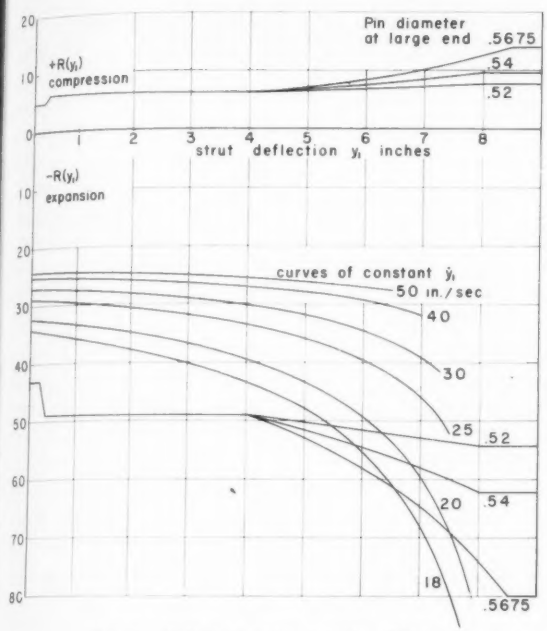

FIG. 7. Orifice damping function $R(y_1)$.

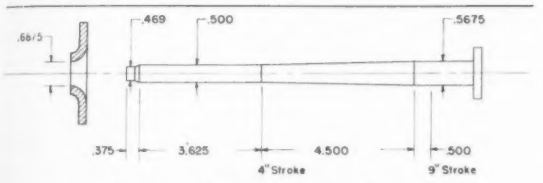

FIG. 8. Metering pin and orifice.

may be determined from the piston displacement trace and metering-pin dimensions.

$$V_o = (a_f/A_o)\dot{y}_1 \tag{33}$$

The pressure drop may be found if we know the damping force. In analyzing the records, this force was assumed to be the difference between the total compressive force on the piston and that due to the air pressure already determined. This neglects the effects of friction, which should be taken into account at this point. Attempts to evaluate the frictional force were not successful because the test data were not sufficiently complete for this purpose. However, near the end of the compression stroke where the damping force approaches zero, friction was found to be unimportant, as indicated by the fact that the measured force due to air pressure was nearly equal, in all cases, to the total force. Computed pressure drops were plotted against orifice velocity. A typical plot is shown in Fig. 6. The points are widely scattered but fall between $c_p = 2 \times 10^{-5}$ and $c_p = 5 \times 10^{-5}$. An average value of 3.5×10^{-5} is used in the majority of the differential analyzer solutions, although for comparison partial solutions of the drop-test condition were made using values ranging between 2.5×10^{-5} and 4.6×10^{-5}. For reverse flow through the main orifice, c_d is taken as 0.52, which is the value generally used for re-entrant tubes. The snubber orifices are small drilled holes with square edges, for which the coefficient is 0.61. The remaining data required to determine $F(y_1)$ and $R(y_1)$ depend on the dimensions of the shock strut and are listed in Table 1. Curves of $R(y_1)$ as used on the differential analyzer input table are shown in Fig. 7 and represent the function as derived for the metering pin shown in Fig. 8, as well as for pins having slightly smaller diameters at the large end. The latter curves were included to study the effect of metering-pin taper.

TABLE 1
Numerical Data

Total stroke of shock strut	9.00	in.
Static to fully compressed	1.66	in.
Air piston diameter, d_p	5.5	in.
Air volumes: Compressed	19.67	cu.in.
Static	59.02	cu.in.
Extended	233.49	cu.in.
Fluid piston diameter, d_f	4.75	in.
Main orifice diameter	0.6875	in.
Rebound check: Inside diameter of cylinder, d_c	5.75	in.
Number of snubber orifices	2	
Diameter of snubber orifices	0.0625	in.
Specific gravity of fluid	0.834	
Airplane gross weight	46,460	lbs.
Weight on main wheels in static position	40,580	lbs.
Weight of unsprung mass, per wheel	420	lbs.

DIFFERENTIAL ANALYZER SOLUTIONS

Inasmuch as several excellent papers[3-5] are available which describe machines of the type used in the solution of the present problem, no further description is included here. A schematic diagram of the machine circuit is shown in Fig. 9. Equipment used included eleven integrators; two input tables for introducing the functions $G(y_2)$ and $R(y_1)$; and three output tables on which were plotted y_1, y_2, $\dot{y}_1$, $\dot{y}_2$, and F_s/Mg as functions of time. The function $F(y_1)$ was generated in the machine by using two integrators—one with inverted input and output connections for generating the logarithm of $(1 - k_p y_1)$.

In order to begin the solutions on the differential analyzer, the initial conditions to be imposed must be known. These conditions determine the initial displacements of the integrators and the input and output tables. In the landing conditions, the motion consists of two phases: the first beginning at the instant of contact between the tire and the ground and consisting of tire deflection only. The shock-strut piston does not move relative to the cylinder during this phase because the initial force F_o is greater than the external force applied to the strut. The solution in this case may be found by making minor modifications to the machine circuit such that $\ddot{y}_1 = \dot{y}_1 = y_1 = 0$ during this period. The initial conditions, then, for the landing conditions are those that exist at the instant of ground contact.

$$\dot{y}_1 = y_1 = 0, \quad y_2 = 0, \quad \dot{y}_2 = \sqrt{2gh}$$

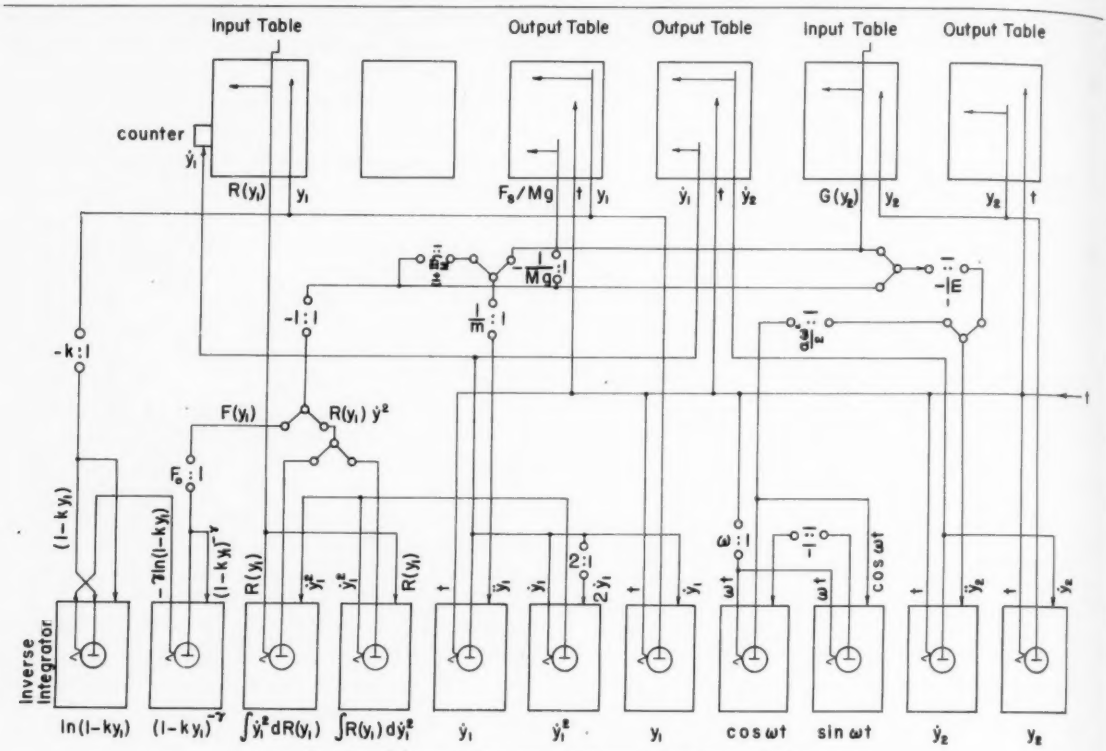

FIG. 9. Schematic diagram of differential analyzer circuit.

In the taxiing cases, the initial conditions were determined by considering the airplane to roll into the sinusoidal ground surface from a smooth horizontal plane. The system was considered to be in static equilibrium initially, and the deflections y_1 and y_2 were found as follows. The tire deflection was taken from the static load-deflection curve of Fig. 4 for the condition

$$G(y_2) = (M + m)g - L$$

The initial piston deflection was determined by considering the air to have undergone an isothermal compression from the extended position. This permits expressing y_1 in terms of the equilibrium force on the piston which, in turn, is equal to $Mg - L$. Thus, we write

$$y_{1_i} = \frac{1}{k_p}\left[1 - \frac{F_o/Mg}{1 - (L/Mg)}\right]$$

The remaining arbitrary initial values are $\dot{y}_1 = \dot{y}_2 = 0$. These four initial values, together with those for $\ddot{y}_1$ and $\ddot{y}_2$ which may be determined from Eqs. (12) and (13), are sufficient to set all the initial displacements in the machine. The solutions are obtained by setting the machine in motion and by allowing it to continue until the desired information is obtained. In the drop-test solutions, curves were plotted through the compression and subsequent expansion strokes to the point at which the tire left the ground on rebound. Beyond this point, the equations are no longer valid. In the taxiing solutions, the objective was to obtain steady-state oscillations of the system. Therefore, the solutions were continued until the transients were damped out and the motion during one oscillation was reproduced, or nearly reproduced, in the next.

RESULTS

The drop-test solutions were carried out in anticipation of an experimental drop-test program on the same system. Accordingly, the data used in the solutions were chosen to agree with the anticipated experimental conditions. It is unfortunate for the purpose of comparison that the experimental tests, which were conducted nearly a year after the numerical solutions were obtained, were carried out under somewhat different conditions so that exact comparisons cannot be made. However, some conclusions can be drawn which indicate that the analytical approach using the equations derived in this paper can be used with good results.

Differential analyzer solutions were obtained for the metering pin shown in Fig. 8, as well as for the variations in this pin indicated on the $R(y_1)$ curves of Fig. 7. Curves for a representative solution are shown in Fig. 10. In addition, partial solutions were made for a slightly different pin, not shown, which was subsequently used in the experimental tests and to which we shall refer as the "test pin." Solutions for this pin were not completed because they indicated that, for the gross weight considered and for the 27-in. free

drop, the tire would completely bottom, producing a peak load in excess of that permitted in the design specification. However, the "test pin" was used in the experimental tests with a lower gross weight, which permitted it to be used without causing the tire to bottom. Our comparison, then, must be made for different gross weights and only over that interval of time for which the differential solution was carried out. Curves A and B of Fig. 11 show, respectively, the experimental and analytical results for the "test pin" and show close agreement up to the point at which the tire bottoms. The weight difference does not nullify the comparison, inasmuch as experiments show that weight is a secondary factor in determining the load-factor curve provided given static tire and piston deflections are maintained. Curve C in the same figure is the analytical solution for the metering pin shown in Fig. 8. This pin is 0.1 in. larger in diameter at the end, which causes the load to increase more rapidly at the beginning of the stroke and gives the higher efficiency necessary to absorb the energy without bottoming the system. This curve is included to show the correspondence with the experimental curve during the expansion stroke. Reasonable agreement may be expected here, inasmuch as the expansion stroke is controlled largely by the snubber orifices, which were the same for both curves. In Fig. 12, the same three curves are shown plotted against piston position.

The primary objective in carrying out the solutions for the taxiing case was to determine the maximum response amplitudes corresponding to a state of resonance. Calculations carried out for a linearized system in which damping was neglected indicated that the lower natural frequency was near $\omega = 10$ rad. per sec.; therefore, a frequency range of $5 \leqq \omega \leqq 20$ was investigated. It was found that a value of 0.25 for $a\omega^2/2g$ represented the maximum excitation that could be permitted without bottoming the system or causing the tire to rebound. The response curves for this value of $a\omega^2/2g$ plotted over the above frequency range are shown in Fig. 13. A maximum response at $\omega = 10$ rad. per sec. is clearly shown. A representative solution as plotted by the differential analyzer is shown in Fig. 14. The amplitude of the ground sinusoid corresponding with the maximum excitation at resonance may be calculated.

$$a = \frac{2g}{\omega^2}\left(\frac{a\omega^2}{2g}\right) = \frac{2(386)}{100}(0.25) = 1.93 \text{ in.}$$

It is of some interest to compare the natural frequencies of the system as obtained from the differential analyzer solutions with those calculated using an idealized system in which no damping is present and linear tire and shock-strut spring characteristics are assumed. In this linear system, the actual tire load-deflection curve is replaced by a straight line tangent to the curve at the point of equilibrium. The shock-strut function $F(y_1)$ is replaced by a linear function whose slope is obtained

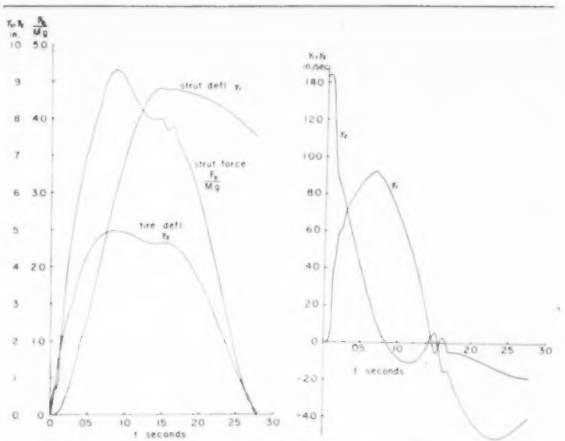

FIG. 10. Solution for drop-test case. (a) Left. (b) Right.

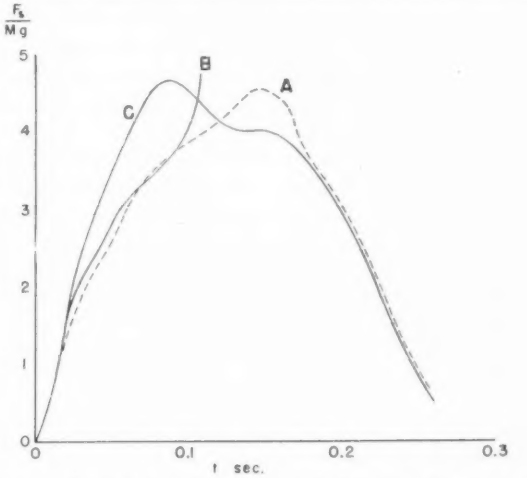

FIG. 11. Calculated and experimental drop-test load factors plotted as functions of time.

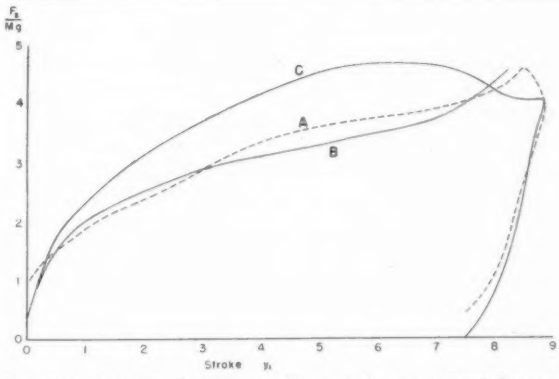

FIG. 12. Calculated and experimental drop-test load factors plotted as functions of piston position.

by substituting the equilibrium value of y_1 in the first derivative of Eq. (22). The differential equations obtained for such a system are linear, and their solution yields, for this example, angular frequencies of 10 and 157 rad. per sec. The lower frequency may be verified by measuring the period of oscillation from Fig. 14. In this mode, the motions of the piston and tire are essentially in phase. The higher frequency oscillation can be detected during the first 0.2 sec. of motion, particularly on the velocity curves. The measured period is approximately 0.04 sec., which agrees well with the calculated frequency. It is seen that in this mode the tire deflection and piston deflection are 180° out of phase.

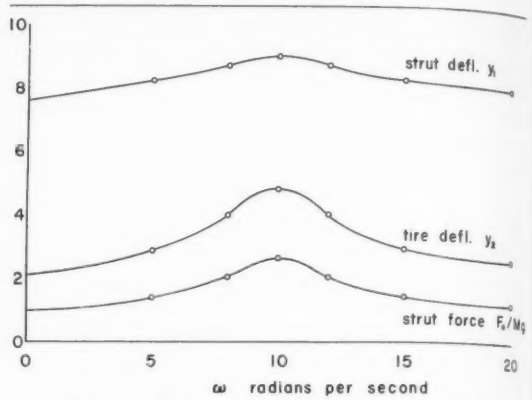

FIG. 13. Response curve for taxiing conditions.

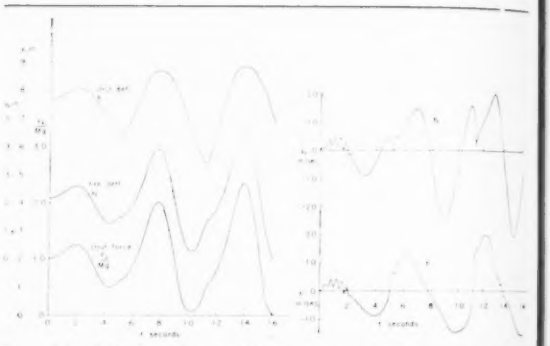

FIG. 14. Solution for taxiing case. (a) Left. (b) Right.

CONCLUSIONS

By means of the equations and methods given in this paper, the response of, and loads on, a conventional airplane landing gear in landing and taxiing may be found.

Comparison of the differential analyzer solutions for the landing condition with experimental drop-test results show good correlation for the example treated. More extensive and exact comparisons should be made for further verification of the method and numerical data used. In this connection, the use of more complete instrumentation in drop-test programs to aid in the evaluation of strut air pressures, temperatures, and frictional forces would be extremely valuable. On the basis of present available data, values of 1.1 and 3.5 $\times$ 10^{-5}, respectively, were chosen for γ and c_p.

The natural frequencies of the landing-gear system can be calculated with good accuracy by considering an idealized system with no damping and linear spring characteristics.

REFERENCES

[1] Biot, M. A., and Bisplinghoff, R. L., *Dynamic Loads on Airplane Structures During Landing*, N.A.C.A. A.R.R. 4H10, October, 1944.

[2] Stowell, E. Z., *Evaluation of Some Approximate Methods of Computing Landing Stresses in Aircraft*, N.A.C.A. T.N. No. 1584 May, 1948.

[3] Bush, V., and Caldwell, S. H., *A New Type of Differential Analyzer*, Journal of Franklin Institute, Vol. 240, No. 4, October, 1945.

[4] *The Differential Analyzer of the University of California*, published by University of California at Los Angeles, 1947.

[5] Crank, J., *The Differential Analyzer*, Longmans, Green and Company, New York, 1947.

[6] Marks, Lionel S., Mechanical Engineer's Handbook, 4th Ed., p. 253; McGraw-Hill Book Company, Inc., New York, 1941.

Analytical and Experimental Studies on Dynamic Loads in Airplane Structures During Landing

T. H. H. PIAN* AND H. I. FLOMENHOFT†

Massachusetts Institute of Technology

SUMMARY

Two assumptions are made in the analytical method for determining the transient stresses in airplane structures during landing. The first assumption, that the landing impact forces are independent of the response of the structure, is justified by a simple analytical study. The second assumption, that the damping and aerodynamic forces can be neglected, is verified by comparing the results of wind-on and wind-off drop tests of a model wing in a wind tunnel. The total transient stress is considered to be the sum of the stresses that would result if the system were restrained against vibrating and the additional stresses that result from the vibratory motion. This method has been made more suitable for practical application by the use of a transient analyzer. The drop tests also provide an experimental check on the analytical method.

INTRODUCTION

IN DETERMINING THE TRANSIENT STRESSES in the airplane structure during landing, it is desirable, for convenience in practical application, to make the simplifying assumptions that the landing impact force is independent of the response of the structure and that the damping and aerodynamic forces may be neglected. One purpose of the present paper is to summarize the analytical and experimental studies that justify the above two assumptions.

A general approach of the analyses of transient stresses in elastic structures has been outlined in reference 1. When the two assumptions described in the previous paragraph have been incorporated, the problem of analyzing the dynamic landing stresses reduces to the determination of the response of an undamped elastic structure subjected to an external load of prescribed time history. It has been shown in reference 1, that the response of an undamped structure can be represented by a superposition of the responses of the natural modes of vibration and that the response of each mode can be considered as that of an equivalent single degree of freedom system, excited by a prescribed generalized force.

Two methods of approach in determining the transient stresses have been given in reference 1. In the first method, the total stresses are obtained by the superposition of the stresses corresponding to the displacements in the normal modes of vibration. In the second method of approach, separate calculations are made for the stresses that would result if the system were restrained against vibrating and for the additional stresses resulting from the vibratory motion.

In applying the first method of approach, Biot and Bisplinghoff[2] have proposed the following method for estimating the dynamic stresses in an airplane structure during landing—adding, without regard to phase differences, the stresses corresponding to the maximum displacements in a few of the lower modes. The maximum amplitude of stress in each mode is estimated from an envelope of "dynamic response factors," determined from a statistical survey, which indicates the response to any force-time history that may be expected in the landing.

Drop tests of an airplane model at the National Bureau of Standards[3] were conducted to verify experimentally the method of approach of reference 2. The results indicate that the use of the envelope of dynamic response factors may be too conservative for design purposes. The experimental results also show that the neglect of phase relations and higher modes will cause negligible error in the determination of bending moment near the wing root. However, this may not be justified in a general case. For example, in the evaluation of the inertia forces at the wing tip during landing, both of these factors must be included in order to obtain an accurate solution.

The method proposed in the present paper for the transient landing stress analysis has been based on the second method of approach, in which the effects of static application of external forces and those due to vibratory inertia forces have been separated. Although the same method of approach has been followed by others,[4–6] it has been made more suitable for practical application by the use of a mechanical-analogy-type analyzer, which has been described in a separate paper.[7] By means of this analyzer, the static stresses and the vibratory stresses due to the first three modes can be superposed, with proper regard taken of their phase relations. The accuracy of this method has been checked by drop tests of a model wing that was designed to simulate an airplane with overhanging engines.

Received February 19, 1950.

* Senior Engineer, Aero-Elastic and Structures Research Laboratory, Department of Aeronautical Engineering.

† Now Aeronautical Engineer, Bureau of Aeronautics, Navy Department.

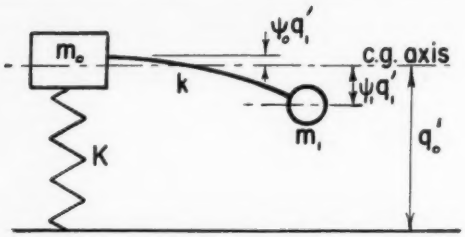

FIG. 1. Simple two-mass system representing an elastic wing with landing gear.

This paper presents the summary of a research program consisting of analytical and experimental studies of dynamic loads on airplanes during landing. This work was part of a project, sponsored by the Bureau of Aeronautics, Department of the Navy, on the investigation of stresses in aircraft structures under dynamic loading.

(I) Coupling Effect of the Flexibility of the Structure on Landing Impact Force

It has been pointed out that the problem of determining dynamic stresses in an airplane structure during landing can be simplified by assuming the landing impact force to be independent of the airplane structural flexibility. The validity of this assumption is examined by the analytical study that follows.

To simplify the problem, the following two assumptions are introduced: (1) The landing gear struts are massless springs and can be treated as a single spring of an equivalent stiffness K; (2) during impact, the structure assumes the same deflected position as its first symmetrical mode of vibration.

The deformation of the structure is defined by the normal function ϕ of the first symmetrical mode, which is so normalized that the generalized mass of the system is equal to the total mass, M, of the airplane. The mode coefficient corresponding to the point where the landing gear is attached is ϕ_L. The motion of the airplane is completely defined by specifying the displacement of the vibration mode, q_1, and the position of the center of gravity of the structure, q_0. Thus, under these assumptions, the airplane structure can be considered as a two degree of freedom system represented by a simple two-mass system, as shown in Fig. 1. The masses m_0 and m_1 are connected by a spring of stiffness k, and a spring of stiffness K is attached to m_0.

The motion of the equivalent system is defined by q_0', the position of the center of gravity of the system, and by $\psi_0 q_1'$ and $\psi_1 q_1'$, the displacements of the masses m_0 and m_1, respectively, from the c.g. axis. It can be seen that $\psi_1 = -(m_0/m_1)\psi_0$.

The conditions necessary for the two-mass system to be equivalent to the actual airplane structure are as follows:

(1) The total masses in both systems are equal—i.e.,

$$m_0 + m_1 = M \tag{1}$$

(2) The generalized masses corresponding to the vibration modes in both systems are equal—i.e.,

$$\left.\begin{aligned} &\psi_0^2 m_0 + \psi_1^2 m_1 = M \\ \text{or} \\ &\psi_0^2 m_0 \left[1 + (m_0/m_1)\right] = M \end{aligned}\right\} \tag{2}$$

(3) The mode coefficient corresponding to the mass m_0 for the two-mass system should be the same as that corresponding to the point on the actual structure where the landing gear is attached—i.e.,

$$\psi_0 = \phi_L \tag{3}$$

(4) The natural frequency of the two-mass system must be the same as the frequency of the first symmetrical mode of airplane vibration. The natural frequency of the free two-mass system can be expressed as

$$\omega = \sqrt{(m_0 + m_1)k/m_0 m_1}$$

Thus, it can be written that

$$\sqrt{(m_0 + m_1)k/m_0 m_1} = \omega_1 \tag{4}$$

where ω_1 is the natural frequency of the first symmetrical mode of the actual structure.

Combining Eqs. (1), (2), and (3), we obtain

$$m_1/m_0 = \phi_L^2 \tag{5}$$

From Eqs. (1), (4), and (5), we can see that, if M, ϕ_L, and ω_1 of the actual structure are given, m_0, m_1, and k can be determined.

In order to determine the effect of the flexibility of the structure on the impact load, we consider two systems as shown in Figs. 2a, and 2b. Fig. 2a represents a rigid body; Fig. 2b, a two-mass elastic system. Both of these systems are assumed to be descending at constant velocity, v, when the "landing spring" touches the ground. It is desired to find the time variation of the ground reaction $F(t)$ in each case. By using x_0 to

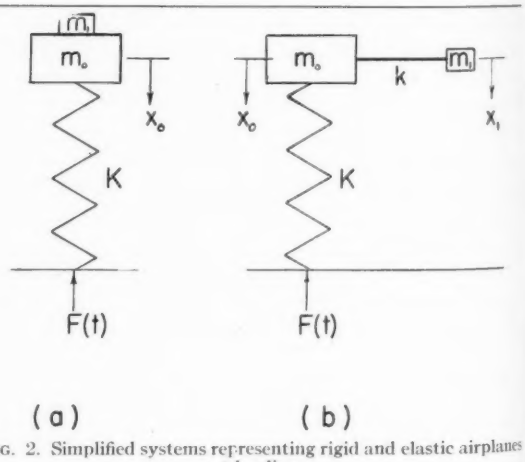

FIG. 2. Simplified systems representing rigid and elastic airplanes at landing.

indicate the displacement of the mass m_0, it can be seen that, at the initial condition when the spring begins to touch the ground, $x_0(0) = 0$ and $\dot{x}_0(0) = v$.

(a) *Rigid Body*

The differential equation of motion is

$$(m_0 + m_1)\ddot{x}_0 + Kx_0 = 0 \tag{6}$$

Its solution is

$$x_0 = (v/\omega_L) \sin \omega_L t \tag{7}$$

where $\omega_L = \sqrt{K/(m_0 + m_1)}$ equals the natural frequency of the landing-gear strut.

The time-history of the ground reaction can be written as

$$\left.\begin{aligned} F(t) &= Kx_0 \\ \text{or} \qquad & \\ F(t) &= (vK/\omega_L) \sin \omega_L t \end{aligned}\right\} \tag{8}$$

(b) *Two-Mass Elastic System*

The motion of the mass m_1 is represented by the relative displacement x_1 with respect to the mass m_0. The differential equations of motion are

$$\begin{aligned} (m_0 + m_1)\ddot{x}_0 + m_1\ddot{x}_1 + Kx_0 &= 0 \\ m_1(\ddot{x}_0 + \ddot{x}_1) + kx_1 &= 0 \end{aligned}$$

The initial conditions are: at $t = 0$,

$$\begin{aligned} x_0 &= 0, \quad \dot{x}_0 = v \\ x_1 &= 0, \quad \dot{x}_1 = 0 \end{aligned}$$

The solutions of these equations are

$$\left.\begin{aligned} x_0 &= \frac{v(1+\mu)}{\omega_L(\alpha_1^2 - \alpha_2^2)} \left\{\left[\frac{\beta^2}{(1+\mu)\,\alpha_2^2} - 1\right]\frac{1}{\alpha_2} \sin \alpha_2\omega_L t - \left[\frac{\beta^2}{(1+\mu)\,\alpha_1^2} - 1\right]\frac{1}{\alpha_1} \sin \alpha_1\omega_L t\right\}\right) \\ x_1 &= \frac{v(1+\mu)}{\omega_L(\alpha_1^2 - \alpha_2^2)} \left(\frac{1}{\alpha_2} \sin \alpha_2\omega_L t - \frac{1}{\alpha_1} \sin \alpha_1\omega_L t\right) \end{aligned}\right\} \tag{9}$$

where

$$\mu = m_1/m_0$$

$$\beta = \frac{\text{free-free frequency of the two-mass system}}{\text{frequency of the landing gear strut}} = \frac{\omega_f}{\omega_L} = \sqrt{\frac{k(m_0 + m_1)}{m_0 m_1}} \Big/ \sqrt{\frac{K}{m_0 + m_1}}$$

$$\alpha_1 = \sqrt{[(1 + \mu + \beta^2)/2] + \sqrt{[(1 + \mu + \beta^2)/2]^2 - \beta^2}}$$

$$\alpha_2 = \sqrt{[(1 + \mu + \beta^2)/2] - \sqrt{[(1 + \mu + \beta^2)/2]^2 - \beta^2}}$$

The time-history of the ground reaction for the case of elastic body is, then,

$$F(t) = \frac{vK}{\omega_L}\left(\frac{1+\mu}{\alpha_1^2 - \alpha_2^2}\left\{\left[\frac{\beta^2}{(1+\mu)\alpha_2^2} - 1\right]\frac{1}{\alpha_2} \sin \alpha_2\omega_L t - \left[\frac{\beta^2}{(1+\mu)\,\alpha_1^2} - 1\right]\frac{1}{\alpha_1} \sin \alpha_1\omega_L t\right\}\right) \tag{10}$$

We wish to compare the maximum value of impact force for the case of the elastic body with that for the case of the rigid body. By examining Eqs. (8) and (10), we conclude that the ratio between the maximum impact force for the elastic body and that for the rigid body is equal to the maximum value of the expression within the parentheses of Eq. (10). The impact force ratios for various values of μ and β have been calculated and plotted as in Fig. 3.

The result can also be represented in terms of the following two parameters:

(1) $\dfrac{T_I}{T_N}$ = duration of impact/natural period of the considered mode of airplane vibration

(2) ϕ_L = the mode coefficient in the considered mode at the point where the landing gear is attached. (The mode has been so normalized that the generalized mass is the same as the mass of the airplane)

The ratio of T_I/T_N is equal to $1/2\beta$, and the mode coefficient ϕ_L is equal to $\sqrt{\mu}$ Fig. 3 also indicates the variation of the ratio of impact force for a flexible airplane to that for a rigid airplane for different ratios of T_I/T_N and different values of ϕ_L.

This figure shows that, for $0.25 < T_I/T_N < 2.5$ and $0 < \phi_L < 1$, the impact force for the flexible structure is 0.71 to one times that for the rigid structure. For current design of large landplanes with $T_I/T_N \approx 1$ and $0 < \phi_L < 0.5$, the impact force for the flexible structure would show a reduction of less than 10 per cent as compared with that for a rigid structure.

Both experimental and analytical investigations of the effect of wing flexibility on the force-time relation in the shock strut during landing impact have been conducted at the National Bureau of Standards.[8] In

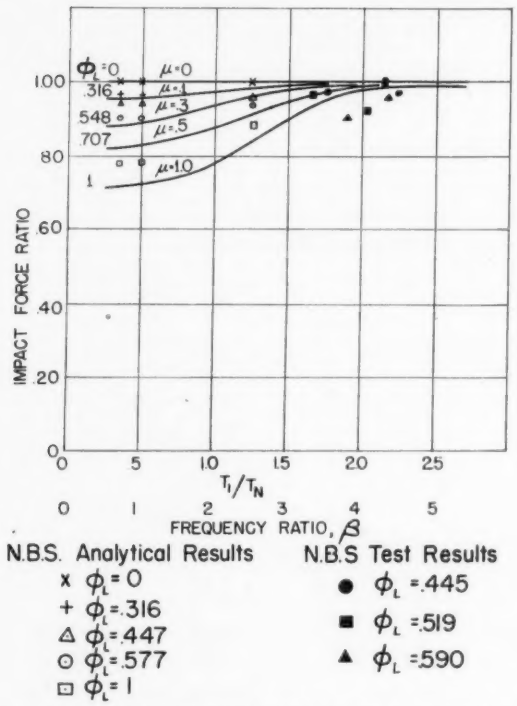

FIG. 3. Effect of frequency and mass distribution on magnitude of impact force.

these investigations a simple two degree of freedom dynamic model, having a landing gear with both elastic and damping characteristics, were used. Since the analysis of the problem becomes much more complicated, only a few cases have been considered. The result of the test program indicated that for a duration of impact greater than one and one-half times the natural period of the wing, the force-time relation in the shock structure was substantially the same as though the flexible structure had been replaced by a rigid body having the same net weight. The peak force for $1.5 < T_I/T_N < 2.5$ showed a reduction of up to 10 per cent due to flexibility. The analysis conducted at the National Bureau of Standards showed that, for $0.231 < T_I/T_N < 2.47$ and for $1 > \phi_L > 0$, the impact force for the flexible wing was from 0.775 to one times that for the rigid wing. These results are also shown in Fig. 3.

In conclusion, it may be stated that the effect of wing flexibility is to cause such a slight reduction in the shock-strut force that it may be neglected in the design of conventional airplanes.

(II) Determination of Transient Stresses During Landing When the Damping and Aerodynamic Forces Are Neglected

In the present treatment we assume that the airplane is making a landing approach with a constant sinking speed, so that prior to landing it is in a state of equilibrium under the gravity forces and the aerodynamic forces. During impact, the landing forces, assumed to be predetermined, are applied directly to the structure. It is desirable to determine the stresses corresponding to the transient motion and to superpose those stresses upon those corresponding to the initial steady condition.

We consider a general case in which the airplane is subjected to a number of impact loads $F_1(t)$, $F_2(t)$, ..., $F_n(t)$. These may be, for example, the normal and drag loads at the landing gears at right- and left-hand sides of the airplane. The airplane is assumed to have the rigid body motions of the vertical, pitching, and rolling degrees of freedom. The rigid body rotations are assumed to be small.

The deformation of the structure is represented by the superposition of the displacements in the normal modes of vibration of the unrestrained airplane. The transient displacement of each of the vibration modes, say the rth mode, is indicated by $q^{(r)}(t)$. The corresponding mode shape is described by a deflection function $\phi^{(r)}$, which is so normalized that the generalized mass, M_r, is equal to the total mass, M, of the airplane. The generalized mass is defined as

$$M_r = \int [\phi^{(r)}]^2 \, dm \tag{11}$$

where the integration is carried over the entire airplane.

If the damping and aerodynamic forces are neglected, the normal modes are uncoupled. Consequently, the equation of motion for the rth vibration mode is

$$M\ddot{q}_r + M\omega_r^2 q_r = Q_r(t) \tag{12}$$

where ω_r is the rth circular frequency of natural oscillation and $Q_r(t)$ is the generalized force corresponding to the rth generalized coordinate. In the present case,

$$Q_r(t) = \sum_i^n \phi_{F_i}{}^{(r)} F_i(t) \tag{13}$$

where $\phi_{F_i}{}^{(r)}$ is the normalized mode displacement, in the same direction as the external load F_i, corresponding to the point of the structure at which F_i is applied.

Since the problem is linear, the responses in the vibration modes of the airplane and, hence, the transient stresses in the structure can be obtained by considering each external load separately. Corresponding to the load $F_i(t)$, the differential equation of motion in the rth mode is

$$M\ddot{q}_r + M\omega_r^2 q_r = \phi_{F_i}{}^{(r)} F_i(t) \tag{14}$$

The displacement q_r and the acceleration $\ddot{q}_r$ can then be determined by applying the method given in reference 1,

$$q_r = \frac{\phi_{F_i}{}^{(r)}}{M\omega_r} \int_0^t F_i(t) \sin \omega_r(t - \tau) d\tau \tag{15}$$

$$\ddot{q}_r = \frac{\phi_{F_i}{}^{(r)}}{M} \int_0^t \cos \omega_r(t - \tau) \frac{d}{d\tau} F_i(\tau) d\tau \tag{16}$$

It is desired to determine the stress due to the transient motion by separating the part that would be obtained if the structure were restrained against vibrating from the stress due to the vibrating motion of the system. The first part is the stress that the engineer ordinarily computes when the structure is assumed rigid. This stress is a result of the external force $F_i(t)$ and the reaction forces that are caused by the rigid body accelerations in the vertical, pitching, and rolling degrees of freedom; hence, this stress is proportional to $F_i(t)$. The second part of the transient stress is due to the inertia forces corresponding to the accelerations in the various vibration modes. The transient stress corresponding to the acceleration in the rth mode is proportional to $\ddot{q}_r(t)$. For convenience in computation, we express $F_i(t)$ as

$$F_i(t) = (F_i)_{max.} f_i(t) \tag{17}$$

where $f_i(t)$ is a nondimensional function with a maximum amplitude of unity. We see that the stress at a particular point P can be written in the following form:

$$\sigma_P = \sum_i^n B_{0i} f_i(t) + \sum_r \sum_i^n B_{ri} K_{ri}(t) \tag{18}$$

where

$$K_{ri}(t) = \int_0^t \cos \omega_r(t - \tau) \frac{d}{d\tau} f_i(\tau) d\tau \tag{19}$$

As an illustration, we consider an airplane in the two-wheel symmetrical landing condition (Fig. 4). The problem is one of determining the time-histories of the bending moments, torsional moments, and shears along the wing structure due to a vertical landing reaction $^1/_2F(t)$ at each landing gear. We assume that the elastic axis of the wing is a straight line perpendicular to the plane of symmetry of the airplane and that the wing section is rigid in the chordwise direction. We employ the following notation and sign convention:

- M = total mass of the airplane
- I_z = pitching moment of inertia of the entire airplane
- $m(x)$ = mass of wing per unit wing span
- $I(x)$ = moment of inertia about the elastic axis per unit wing span
- $S(x)$ = unbalanced moment about the elastic axis per unit wing span, positive when c.g. is behind the elastic axis
- $h^{(r)}(x)$ = normal function describing the mode shape of bending of the elastic axis on the rth symmetrical mode
- $\alpha^{(r)}(x)$ = normal function describing the mode shape of twisting about the elastic axis in the rth symmetrical mode
- M_r = generalized mass in the rth mode, defined by

$$M_r = \int_{-b/2}^{b/2} (mh^2 + I\alpha^2 + 2Sh\alpha) dx$$

Mode function is normalized so that $M_r = M$

- $\phi_F^{(r)}$ = mode coefficient of the rth symmetrical mode corresponding to the point in the wing structure where the landing gear is located

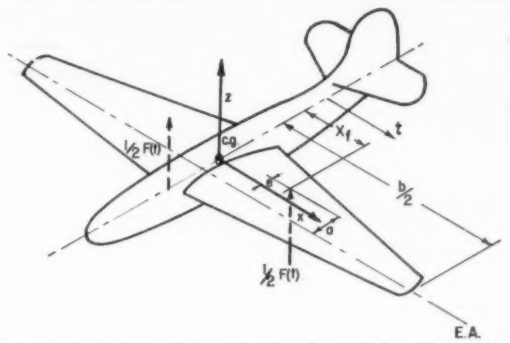

FIG. 4. Airplane under symmetrical vertical landing load.

- e = moment arm of the vertical reaction about the c.g. of the airplane, positive when the load is behind the c.g.
- a = moment arm of the vertical reaction about the elastic axis of the wing, positive when the load is behind the elastic axis
- x_F = location of the landing gear from the centerline of the airplane
- z = rigid body vertical displacement, positive upward
- θ = rigid body pitching displacement, positive nose down
- V = shear distribution, positive downward
- B.M. = bending moment distribution, positive when bottom surface is in compression
- T.M. = torsional moment distribution, stalling moment positive

The rigid body acceleration of the airplane consists of a vertical translation, $\ddot{z}$, and a pitching motion, $\ddot{\theta}$. These can be expressed in terms of the landing impact force $F(t)$:

$$\ddot{z} = F(t)/M \tag{20}$$

$$\ddot{\theta} = eF(t)/I \tag{21}$$

Again, for simplicity, we write

$$F(t) = n_{max.} Mgf(t) \tag{22}$$

and

$$K_r(t) = \int_0^t \cos \omega_r(t - \tau) \frac{d}{d\tau} f(\tau) d\tau \tag{23}$$

where $n_{max.}$ is the landing load factor used in the conventional stress analysis.

The time-histories of the stresses in the wing structure can be written in the form of

$$\sigma = B_0 f(t) + \sum_1^n B_r K_r(t) \tag{24}$$

The coefficients B_0 and B_r can be expressed as follows:

(1) *Shear Distribution, V:*

$$B_0 = n_{max.} g \int_x^{b/2} \left(m + \frac{eMS}{I_z} \right) dx, \quad x > x_F$$

$$B_0 = n_{max.} g \left[\int_x^{b/2} \left(m + \frac{eMS}{I_z} \right) dx - \frac{1}{2} M \right], \quad x < x_F$$

$$B_r = n_{max.} g \phi_F^{(r)} \int^{b/2} [mh^{(r)} + S\alpha^{(r)}] dx \tag{25}$$

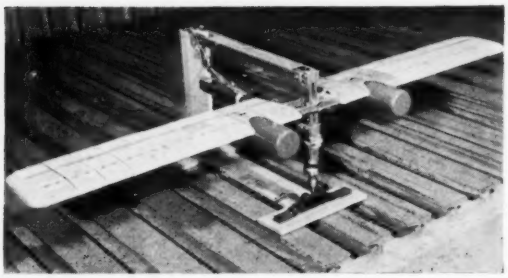

FIG. 5. Photograph of the drop test model wing.

(2) *Bending Moment Distribution, B.M.:*

$$B_0 = n_{max.} g \int_{b/2}^{x} \int_{b/2}^{x} \left(m + \frac{eMS}{I_x} \right) dxdx, \quad x > x_F$$

$$B_0 = n_{max.} g \left[\int_{b/2}^{x} \int_{b/2}^{x} \left(m + \frac{eMS}{I_x} \right) dxdx - \frac{1}{2} M(x_F - x) \right], \quad x < x_F$$

$$B_r = n_{max.} g \phi_F^{(r)} \int_{b/2}^{x} \int_{b/2}^{x} [mh^{(r)} + S\alpha^{(r)}] \, dxdx \qquad (26)$$

(3) *Torsional Moment Distribution, T.M.:*

$$B_0 = n_{max.} g \int_{x}^{b/2} \left(\frac{eMI}{I_x} + S \right) dx, \quad x > x_F$$

$$B_0 = n_{max.} g \left[\int_{x}^{b/2} \left(\frac{eMI}{I_x} + S \right) dx - \frac{1}{2} Ma \right], \quad x < x_F$$

$$B_r = n_{max.} g \phi_F^{(r)} \int_{x}^{b/2} [I\alpha^{(r)} + Sh^{(r)}] \, dx \qquad (27)$$

It can be seen that the problem of determining the transient stresses in the airplane structure during landing is reduced to the solution of equations of the same form as that of Eq. (24). The solution may be accomplished by numerical or analytical integration. However, both processes are tedious and are often impractical for the designer. A mechanical-analogy-type analyzer, which may be used to determine the time-histories of the stresses in an undamped elastic structure, has been developed at the Massachusetts Institute of Technology.[7] The two main functions of the analyzer are: (1) to evaluate the integrals $K_1(t)$, $K_2(t)$, . . . , etc.; (2) to superpose the various terms of Eq. (24) with proper regard taken of their phase relations. The first function is accomplished by the use of torsional pendulum simulators; the second function, by the proper design of the electronic pickup and recording circuit.

(III) Experimental Verifications of Methods of Analysis

Experimental verifications of Biot and Bisplinghoff's method of determining transient stresses in the airplane structures have been made in the National Bureau of Standards.[3] The experimental investigation described in this paper was extended to (1) the verification of the method of analysis proposed in the previous part and (2) the determination of the effects of the aerodynamic forces on the transient stresses in the airplane structure during landing.

Description of the Model

A model was constructed which is dynamically similar to a large twin-engined airplane. It consists essentially of an elastic wing with two overhanging engines, a rigid fuselage, and a single-strut landing gear mounted at the centerline.

The wing is rectangular in plan form, with structural strength provided by two magnesium spars connected by Duralumin torque tubes. The airfoil shape is maintained by wood covering, made in sections so that it would not contribute stiffness to the primary structure. Large concentrated masses attached to the wing structure comprised the nacelle section.

The shock strut consists of a cylinder containing a piston and piston rod, at the bottom of which dual model airplane wheels are attached. Movement of the piston deflects a coil spring and forces oil through an orifice. The shape of the impact force-time curve was varied by changing the grade of oil and the stiffness of spring and by using different combinations of rubber pads on which the wheels landed at impact.

The wing and the shock strut were attached to a parallelogram linkage that was connected to a steel channel fixed to the floor and could thus undergo only translation during the drop. Fig. 5 illustrates the general arrangement of the model wing.

Instrumentation

Instrumentation for the test was required for measuring the bending and torsional moments at a wing root station, $1^1/_4$ in. from the center of the model, the bending moment outboard of the engine section at a station $8^3/_4$ in. from the center, the acceleration at a point near the wing tip, the acceleration at the fuselage, and the impact force in the shock strut.

All quantities except acceleration were measured by means of wire-resistance strain gages. Each pickup for bending or torsional moment consisted of four gages, one at the top and bottom of each wing spar. For measuring bending moment, the gages on the top and on the bottom were connected in series to form a pair. For measuring torsional moments, the gage on the top of one spar was connected in series with the gage on the bottom of the other spar to form a pair. Each of these pairs of strain gages was connected to a Consolidated bridge balance channel.

The load in the shock strut was determined by measuring the strain in a fixed-ended steel beam on which the wheels landed. A pair of strain gages were attached to the top and bottom surface near the root of the beam

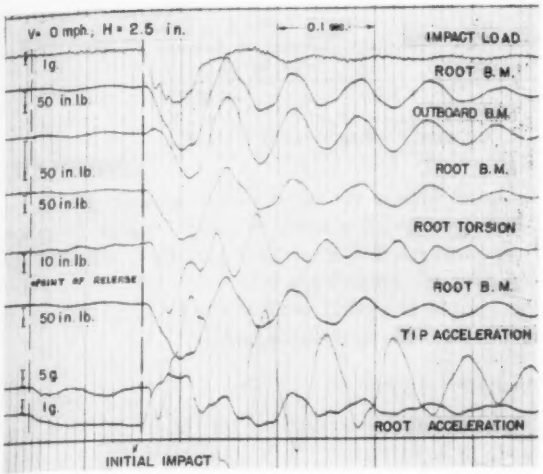

FIG. 6. Oscillograph record for 2.5-in. drop at 0 m.p.h. air speed.

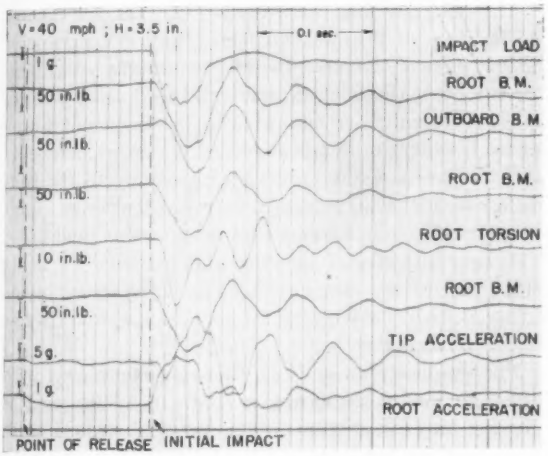

FIG. 7. Oscillograph record for 3.5-in. drop at 40 m.p.h. air speed.

and were also connected to a Consolidated bridge balance channel. The signals from the bridge circuits were amplified and recorded by an oscillograph.

Accelerations were measured with a vacuum tube "transducer" accelerometer developed at M.I.T. The signals from the accelerometers were also fed into the recording oscillograph.

Description of Test

An important requirement in dropping the model is that the wing be in a strain-free condition before release in order to minimize the vibrations excited by the sudden removal of the supporting forces. Consequently, the model was supported by seven strings, connected to a dural beam by means of adjustable screws. The model was released through a single wire that held the dural bar.

Drop tests were made in a wind tunnel for air speeds of 0, 20, 40, and 60 m.p.h. At each speed, drops were made starting at a height of 1 in., and increasing in $^1/_2$-in. steps until a load factor of approximately 5 was attained.

Test Results

Oscillograph records showing the results of the drop tests from different heights and at different air speeds were obtained. Typical records are shown in Figs. 6 and 7. It was found that the impact force-time curves corresponding to different values of maximum impact were not exactly similar. However, the curves corresponding to the same values of maximum impact but to different air speeds were similar. This latter fact facilitated the investigation of the effects of aerodynamic forces on the transient stresses in the structure under the application of the same external impact force.

The test results are presented in the form of plots of maximum moment and maximum acceleration against maximum strut force at the four different air speeds,

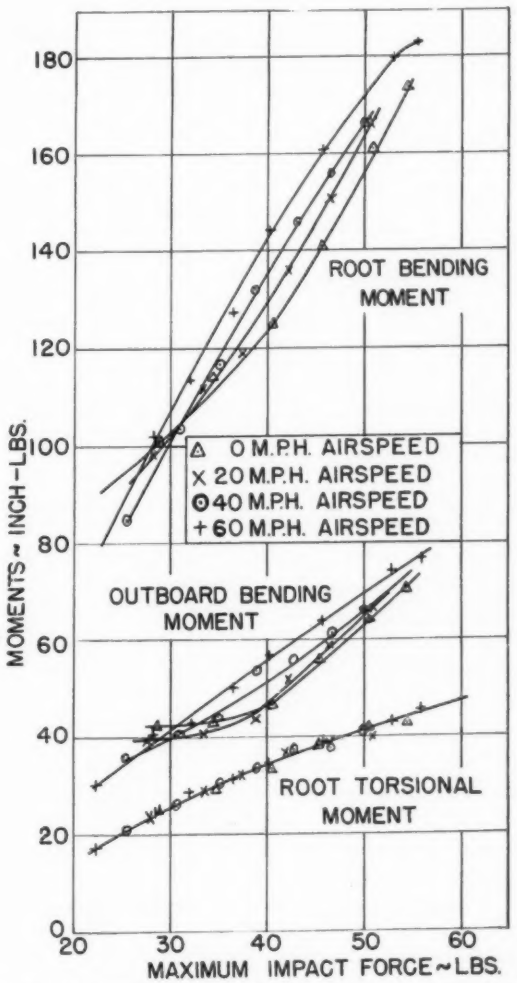

FIG. 8. Maximum bending and torsional moments vs. maximum landing impact force at different air speeds.

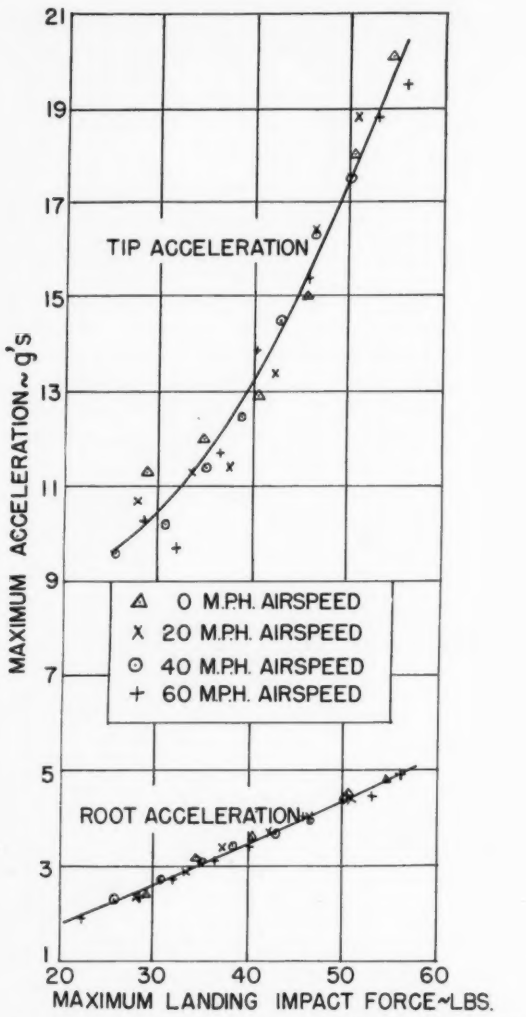

FIG. 9. Maximum accelerations vs. maximum landing impact force at different air speeds.

shown in Figs. 8 and 9. These results indicate that the aerodynamic forces tend to raise the maximum bending moments in the wing structure when subjected to the same impact force. This is due mainly to the decrease in effective wing angle of attack during the landing impact. The decrease in angle of attack causes a decrease in lift force, which, in turn, corresponds to an increase in bending moment.

The maximum percentage increases in bending moments due to 40- and 60-m.p.h. wing speed are shown in Table 1. These two wind-tunnel tests are equivalent to full-scale landings of 107 and 160 m.p.h., respectively. In general, the test results indicate that, for the usual landing speeds of less than 100 m.p.h., the effect of aerodynamic forces on the transient bending and torsional stresses is small. It can also be concluded, from Fig. 9, that the aerodynamic force has no noticeable effect on the accelerations at the wing root and the wing tips.

TABLE 1
Maximum Percentage Increase in Bending Moments Due to Air Speed

Item	40 M.P.H.	60 M.P.H.
Root Bending Moment	9.9%	13.9%
Out-board Bending Moment	11.3%	18.6%

Comparison of the records for still-air drop tests and for drop tests with wind on (Figs. 6 and 7, respectively) reveals the important fact that, although the aerodynamic forces have little effect on the maximum transient stresses that occur at the first peak, they tend to damp out the oscillations rapidly.

Analysis

The following calculations on the model wing were made in order to test the practicability and the accuracy of the methods outlined in Section (II) for determining the transient stresses in airplane structures during landing.

The computations were carried out for the case of 2.5-in. drop at 0 m.p.h. air speed, giving a maximum impact force of 45.5 lbs. In order to obtain a better form for the comparison of experimental and analytical results, the results are presented in terms of nondimensional quantities. The calculated maximum moments and maximum accelerations corresponding to the condition that the structure is restrained against vibratory motion were chosen as the reference quantities. The time-histories of bending and torsional moments and accelerations were expressed in terms of the quantities $(B.M.)/(B.M.)_{ref.}$, $(T.M.)/(T.M.)_{ref.}$, and $(Acc.)/(Acc.)_{ref.}$, respectively.

For simplicity in analysis, the wing is replaced by a dynamic model as shown in Fig. 10. The wing is divided into five sections. The mass of each of these sections was considered to be concentrated in the spanwise direction at its center of gravity except for the center-section mass, which is included with that of the fuselage. In the chordwise direction, each section

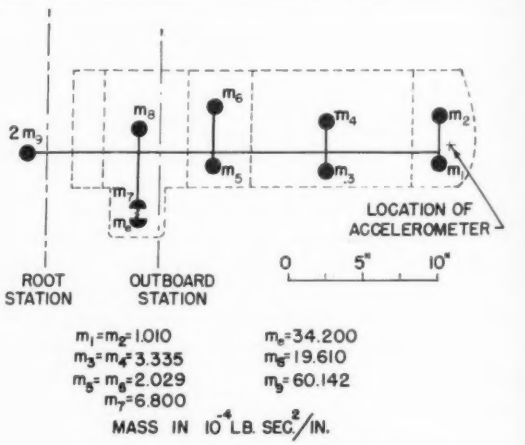

FIG. 10. Dynamic model of the model wing.

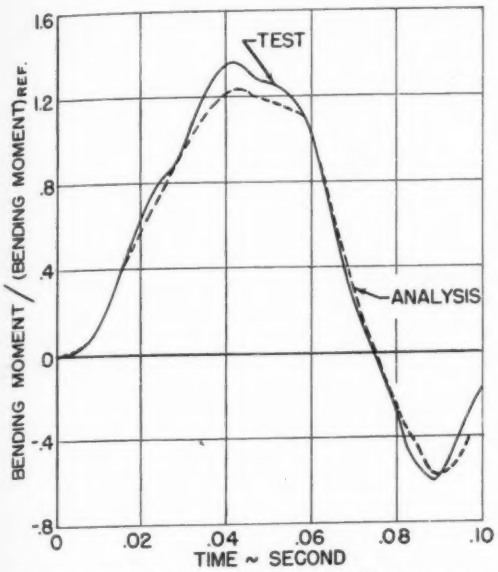

FIG. 11. Time-history of wing root bending moment.

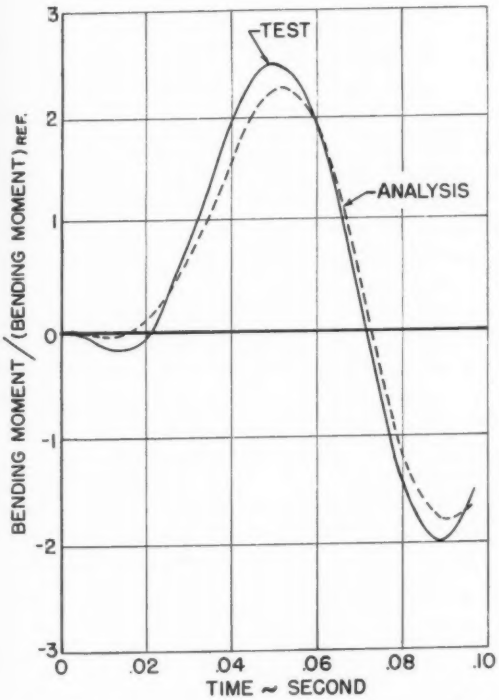

FIG. 12. Time-history of outboard bending moment.

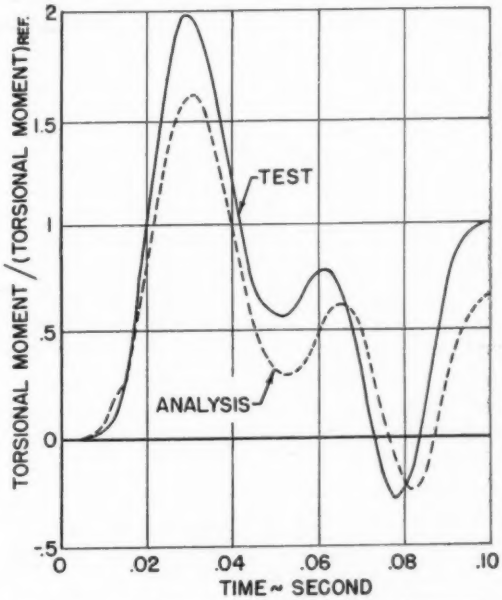

FIG. 13. Time-history of wing root torsional moment.

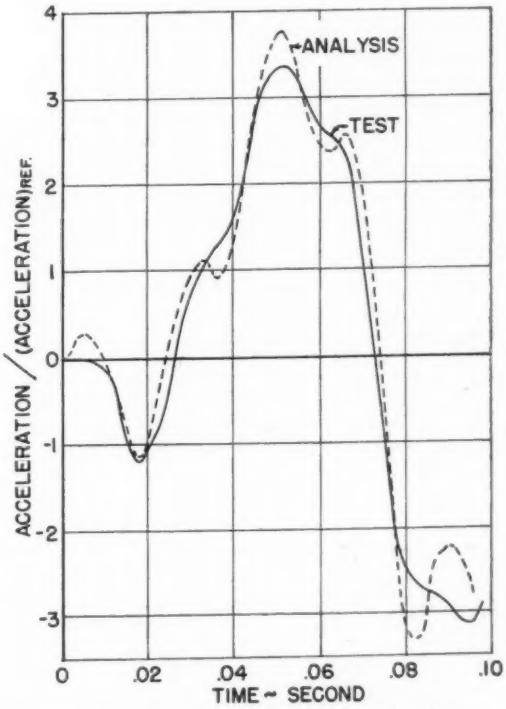

FIG. 14. Time-history of wing tip acceleration.

TABLE 2
Comparison of Results of Tests and Analysis

Item	Positive Maximum			Negative Maximum		
	Measured	Computed	Per cent error	Measured	Computed	Per cent error
$(B.M.)_R/(B.M.)_{R_{ref.}}$	1.36	1.23	−9.5	−0.59	−0.580	1.7
$(B.M.)_O/(B.M.)_{O_{ref.}}$	2.50	2.30	−8	−2.00	−1.78	11
$(T.M.)/(T.M.)_{ref.}$	1.98	1.605	−18.9	...	...	...
$(Acc.)_{tip}/(Acc.)_{ref.}$	3.40	3.80	11.8	−3.17	−3.30	−4.1
$(Acc.)_{fus.}/(Acc.)_{ref.}$	0.908	0.892	−1.8	...	...	...

is replaced by a pair of concentrated masses. The masses in each pair are made equal in the three outboard sections and are located at equal distances from the chordwise c.g. location. In the engine section the masses are distributed so that the location of the front mass is coincided with that of the center of gravity of the lead weight that was used for simulating the overhanging engine. The front mass of the engine section is divided into two elastically connected masses, m_1 and m_e, because the support of the lead weight is flexible.

The first three coupled mode shapes and frequencies for the free-free wing with the fuselage restrained against pitching motion are computed by a process of matrix iteration.[9,10] The flexibility influence coefficients of the dynamic model, required in this computation, were experimentally determined.

The transient stress in the airplane structure is given by

$$\sigma(t) = B_0 f(t) + B_1 K_1(t) + B_2 K_2(t) + B_3 K_3(t) \quad (28)$$

where $f(t)$ is the forcing function in nondimensional form and $K_r(t)$ is the time integral defined previously. The constants B_0, B_1, B_2, and B_3 corresponding to the bending and torsional moments in the wing are obtained by formulas similar to Eqs. (26) and (27). In the present case, since the lumped masses are used, the integral expression of Eqs. (26) and (27) are replaced by summations. For the determination of the accelerations at the point P in the airplane structure, the expressions for B_0 and B_r are

$$B_0 = n_{max.}g$$
$$B_r = n_{max.}g\phi_F^{(r)}\ \phi_P^{(r)} \quad (29)$$

where $\phi_P^{(r)}$ is the mode coefficient corresponding to the point P.

When the results are presented in terms of nondimensional quantities, the following equation results:

$$\frac{\sigma(t)}{\sigma_{ref.}} = \frac{\sigma(t)}{B_0} = f(t) + \frac{B_1}{B_0} K_1(t) + \frac{B_2}{B_0} K_2(t) + \frac{B_3}{B_0} K_3(t) \quad (30)$$

The impact force-time curve used in the analysis was taken from the shock-strut load record for the 2.5-in. drop at zero wing speed (Fig. 6). The curve is rough in the first part of the drop as a result of the higher frequency oscillations in the shock strut and in the impact beam used for measuring the load. In the analysis, a faired curve was used because rigid body acceleration records indicated that this "hash" was not transmitted through the shock strut.

The time-histories of the bending moment at the wing root, the bending moment just outboard of the engine station, the torsional moment at the wing root, and the accelerations at the wing tip and at the fuselage were evaluated by means of the transient analyzer and are plotted in Figs. 11 through 15. For comparison, the results obtained from the drop-test records are also plotted on each of these figures. A tabular comparison of the measured and computed results is given in Table 2.

It can be seen that, except for the torsional moment, agreement between the test and analytical results is fairly good. The error in the computation of the torsional moment is believed to be the result of inaccuracy in the estimation of the basic torsional properties of the wing structure.

Inspection of the curves of Figs. 11 through 15 indicates that the stress-time curve obtained from the analysis has the same general shape as that obtained in the tests. This is a good indication that the effect of normal modes higher than the third is not significant.

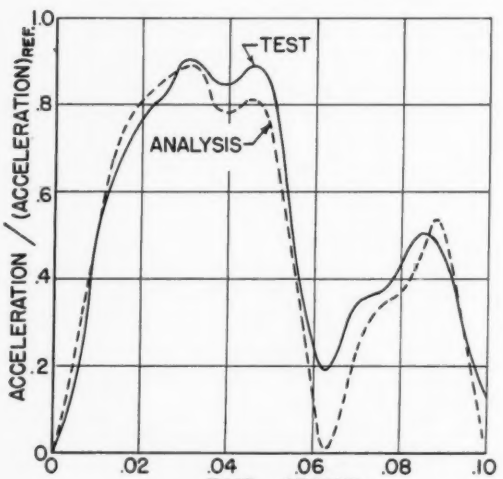

FIG. 15. Time-history of wing root acceleration.

REFERENCES

[1] Bisplinghoff, R. L., Isakson, G., and Pian, T. H. H., *Methods in Transient Stress Analysis*, Journal of the Aeronautical Sciences, Vol. 17, No. 5, p. 259, May, 1950.

(*Continued on page 786*)

An Extension of the Theory of the One-Dimensional Shock-Wave Structure*

LEONARD MEYERHOFF†
Polytechnic Institute of Brooklyn

SUMMARY

This paper presents the method and results of an analytical investigation of the flow inside a shock wave in a steady one-dimensional flow. Two categories are treated: The first considers the problem for constant gas properties, while the second is concerned with the influence of specific heat, conductivity, and viscosity, dependent on temperature.

For the problem with constant gas properties, numerical solutions are given which show that there must be an infinite number of shock-wave type solutions. Only one of these solutions terminates in a region of uniform flow with the values of Rankine-Hugoniot. These solutions, obtained partly by differential analyzer and partly by hand, are given for initial Prandtl Numbers, $P_r \equiv c_p\mu/k$, of 0.75 (T = 0°C.) and 0.657 (T = 500°C.). A comparison shows that the shock-wave thickness for an initial Mach Number of 2.0 is about three times greater for $P_r = 0.657$ than for $P_r = 0.75$.

For the problem with temperature-dependent gas properties, the method and results are shown in detail for the case of uniform exit flow. It was necessary to calculate the change in the limit values of Rankine-Hugoniot because of variable gas properties in order to perform the required numerical integrations. The temperature variations used for c_p, μ, and k correspond to experimental data. A numerical example, given for an initial Mach Number of 4.0, shows that the shock-wave thickness is approximately two and one-half times greater than that for constant gas properties; it is about two and one-half times greater than the mean free molecular path.

INTRODUCTION

THE TERM "STRUCTURE OF THE SHOCK WAVE" is used here to mean the continuous variation of the flow variables of velocity, pressure, temperature, density, etc., inside that small region that is called a shock wave. A shock-wave type of flow variation is characterized by a rapid (and continuous) change in the flow quantities across a transition region (which is the shock wave), whose length, based on mathematical studies,‡ is known to be some multiple of 10^{-5} cm. The greater the initial Mach Number, the smaller the transition length. These analytical investigations also show that in this transition region the curve of any flow quantity exhibits an inflection point. In this paper, the inflection point, which seems to be necessary analytically for the existence of a shock wave, is referred to as the center of the shock wave. It is known that the rate of change of the flow variables is greatest at the shock-wave center. For example, there the velocity and temperature gradients are, in general, some multiples of -10^{10} (cm./sec.)/cm. and $+10^{8}$ °C./cm., respectively.**

Because of the mathematical difficulties involved in using the Navier-Stokes equations, all known studies of this problem have been restricted to one-dimensional flow and, until recently,[3,10,15] with the assumption of constant gas properties. With these simplifications, the flow variation through the shock wave is fairly well established by these studies.

One question that has always been raised is whether it is valid to use a continuum approach to such a phenomenon that occurs in so small a region. Several papers have been written,[13, 14] which treat the gas as a discontinuous medium by means of molecular theories. While these studies have not changed the known phenomenologic aspect of the problem, they have added important knowledge to questions about statistical equilibrium, heat capacity lag, etc., of the gas. The results of one of the molecular studies[13] have led the authors of reference12 to conclude, in their paper on the shock-wave thickness, that the Navier-Stokes equations are valid for this problem within certain obvious limits—that is, as long as disassociation and condensation effects are not present or that the gas is not highly rarefied or has a high stagnation temperature.

In the present paper, the one-dimensional Navier-Stokes equations are applied for shock-wave flows to show the following:

(a) The influence on the shock-wave solutions due to the initial temperature—i.e., due to initial Prandtl Number, $c_p\mu/k$.

(b) The relation of the classical shock-wave solution, which terminates in the limit values of Rankine-Hugoniot, to other shock-wave type solutions contained in the Navier-Stokes equations.

Presented at the Aerodynamics Session, Eighteenth Annual Meeting, I.A.S., New York, January 23–26, 1950.

* This paper, based on work done for the Office of Naval Research of the U.S. Navy on Contract No. N6ori-206, Task Order I, is an extension of a series of reports written in collaboration with Dr. H. J. Reissner. The paper is also part of a dissertation submitted in partial fulfillment of the requirements for the Ph.D. degree in Applied Mechanics at the Polytechnic Institute of Brooklyn. The problem was suggested by Dr. H. J. Reissner, of the Polytechnic Institute of Brooklyn, to whom the author is indebted for criticism and advice.

† Research Associate, Department of Aeronautical Engineering and Applied Mechanics.

‡ See list of references.

** For the example given in Section (IV) of this paper for temperature-dependent gas properties and an initial Mach Number of 4.0, it is found that $du/dx = -10^{10}$ (cm./sec.)/cm. and $dT/dx = +3.64 \times 10^{8}$ °C./cm.

(c) The method and results for temperature-variable viscosity, conductivity, and specific heat, of which the variations follow the existing experimental data for these gas characteristics.

SYMBOLS

x = positional coordinate
u = velocity
ρ = mass density
p = pressure
T = absolute temperature
a = speed of sound
m = mass flow, $u\rho$
M = Mach Number, u/a
U = velocity ratio, u/u_0
Π = temperature ratio, T/T_0
μ = viscosity coefficient
k = thermal conductivity
c_v = specific heat at constant volume
c_p = specific heat at constant pressure
γ = ratio of specific heats, c_p/c_v
P_r = Prandtl Number, $c_p\mu/k$
R = gas constant expressed in physical system of units, $c_p - c_v$
E = intrinsic energy, $\int c_v\,dT$
$(\,)' \equiv d/dx$
0 = subscript denoting a flow value at $x = -\infty$
c = subscript denoting a flow value at the shock-wave center
1 = subscript denoting a flow value at $x = +\infty$

(I) THE SYSTEM OF EQUATIONS OF A STEADY ONE-DIMENSIONAL VISCOUS HEAT-CONDUCTING FLOW

The system of equations defining the special case of *steady* one-dimensional flow is a special case of the general system of the three-dimensional equations. These one-dimensional equations are given below for (a) constant physical gas properties and (b) variable physical gas properties, where the subscript 0 denotes initial flow conditions.

(a) Constant Gas Properties[1]	(b) Variable Gas Properties[2]

The equation of continuity is:

$$(d/dx)(\rho u) = 0 \tag{1}$$

The integral of Eq. (1) is

$$\rho u = \rho_0 u_0 = m \tag{1a}$$

where m is an integration constant.

The Navier-Stokes equation of motion is:

$$m\frac{du}{dx} = -\frac{dp}{dx} + \frac{4}{3}\mu_0\frac{d^2u}{dx^2} \tag{2}$$

$$m\frac{du}{dx} = -\frac{dp}{dx} + \frac{4}{3}\frac{d}{dx}\left(\mu\frac{du}{dx}\right) \tag{3}$$

Each of these equations has a first integral with a second integration constant mC—namely,

$$mu - mC = -p + \frac{4}{3}\mu_0\frac{du}{dx} \tag{2a}$$

$$mu - mC = -p + \frac{4}{3}\mu\frac{du}{dx} \tag{3a}$$

In this paper mC is derived from initial *uniform* flow conditions, denoted by the subscript 0; therefore

$$p_0 + mu_0 = mC \tag{2b, 3b}$$

The equation of state for a perfect gas is:

$$p = RT\rho \tag{4}$$

The equation for the thermodynamic balance of heat flow is:

$$\frac{4}{3}\mu_0\left(\frac{du}{dx}\right)^2 + k_0\frac{d^2T}{dx^2} - c_{v_0}m\frac{dT}{dx} - p\frac{du}{dx} = 0 \tag{5}$$

$$\frac{4}{3}\mu\left(\frac{du}{dx}\right)^2 + \frac{d}{dx}\left(k\frac{dT}{dx}\right) - mc_v\frac{dT}{dx} - p\frac{du}{dx} = 0 \tag{6}$$

The system of equations for variable gas properties can be combined to form a third-order, nonlinear ordinary differential equation with variable coefficients, where the velocity u is the dependent variable and the abscissa x is the independent variable. This equation is derived as follows:

First, the pressure, p, in the heat flow Eq. (6) is replaced by its value in terms of the velocity given by Eq. (3a), so that Eq. (6) changes into

$$\frac{d}{dx}\left(k\frac{dT}{dx}\right) - mc_v\frac{dT}{dx} - mC\frac{du}{dx} + m\frac{d}{dx}\left(\frac{u^2}{2}\right) = 0 \tag{6a}$$

After the temperature T and its gradient* T' are replaced in Eq. (6a), in terms of the velocity, the desired velocity equation will follow; this required temperature relation, obtained by a combination of Eqs. (3a) and (4), is of the following form:

$$T = \frac{1}{R}\left[u(C-u) + \frac{2\mu}{3m}(u^2)'\right] \tag{3b}$$

From Eq. (3b), the temperature gradient is

$$T' = \frac{1}{R}\left[u'C - (u^2)' + \frac{2\mu}{3m}(u^2)'' + \frac{2}{3}\frac{u'}{m}(u^2)'\right] \tag{3c}$$

Eq. (6a), with this value of T', assumes the following form in terms of the velocity u—namely:

$$[b(u^2)'']' + [(b_2 - mk)(u^2)'] - \frac{2}{3}\mu c_v m(u^2)'' + \left[h - \frac{2}{3}mc_v\mu'\right](u^2)' + [lu']' - qu' = 0 \tag{7}$$

where the coefficients of Eq. (7) are variable and have the values shown below:

$$\left.\begin{aligned} b &= (2/3)\mu k \\ b_2 &= (2/3)\mu' k, \qquad l = mkC \\ h &= m^2[(c_p + c_v)/2], \qquad q = m^2Cc_p \end{aligned}\right\} \tag{a}$$

Eq. (7) is treated by a perturbation procedure in reference 3 by Reissner and Meyerhoff, in which the gas properties μ, c_v, and k are expressed as functions of the temperature T. Because the form of Eq. (7) is rather complicated, it was found preferable to treat this problem with variable gas properties in another way. This treatment is presented in a later section of the paper. First, however, certain results will be derived for the case of constant gas properties.

If all the gas characteristics are assumed to be constant, then Eq. (7) reverts to the differential equation derived in reference 4. This latter equation is a *second*-order, nonlinear ordinary differential equation with constant coefficients—namely,

$$(u^2)''b_0 - (u^2)'f_0 + u'l_0 + u^2h_0 - uq_0 = D \tag{8}$$

where the constant coefficients here are

$$\left.\begin{aligned} b_0 &= \frac{2}{3}\mu_0 k_0, \qquad h_0 = m^2c_{p_0}\frac{\gamma_0+1}{2} \\ f_0 &= m\left(k_0 + \frac{2}{3}c_{v_0}\mu_0\right), \qquad q_0 = m^2Cc_{p_0} \\ l_0 &= mCk_0, \qquad D, \text{ integration constant} \end{aligned}\right\} \tag{b}$$

* $' \equiv d/dx$.

It can easily be shown that Eq. (8) is identical to those equations developed for this same problem in different forms by Rayleigh[5] and Taylor.[6]

Only one exact closed form solution of Eq. (8) is known which exhibits a *continuous flow variation* through the shock wave. This solution, first developed by Becker,[7] exists if the nondimensional ratio of the gas characteristics, $P_r \equiv c_p\mu/k$, has the special value of 0.75.† The velocity versus x curve obtained from this exact solution begins and ends in regions of uniform flow, where, at the flow exit, the Rankine-Hugoniot limit values appear.

These limit values are another exact result that can be derived from Eq. (8) (for the trivial solution u = constant). If this value of u is inserted into Eq. (8), the following quadratic relation appears:

$$u^2h_0 - uq_0 = D \tag{8a}$$

The result can be interpreted in two ways: either that there are two constant velocities possible all along the flow or, if the velocity is variable along the flow, they can appear only asymptotically at $x = \pm\infty$. This is because, at the location of these constant solutions, all derivatives become zero. The latter possibility leads to the Rankine-Hugoniot limit values—namely,

$$u_1^2h_0 - u_1q_0 = D = u_0^2h_0 - u_0q_0$$

or

$$(U_1 - 1)\left(U_1 - 2\frac{\gamma_0}{\gamma_0+1}C_0 + 1\right) = 0; \quad U \equiv \frac{u}{u_0} \tag{8b}$$

where the subscript 1 denotes the limit value at the exit; also,

$$C_0 = 1 + (1/\gamma_0 M_0^2)$$

and

$$U_1 = 2[\gamma_0/(\gamma_0+1)]C_0 - 1$$

is the exit limit ratio value expressed in terms of the initial flow conditions.

The derivation of the corresponding limit values for variable gas properties from the differential Eq. (7) is more complicated. The reason is that, contrary to Eq. (8), in Eq. (7) only derivatives of u are present. In Section (III) of this paper it is shown how these limit values for variable gas properties can be derived from the individual equations leading to Eq. (7).

Before going on to the material in Sections (III) and (IV) derived for variable gas properties, some new results will be presented in Section (II) which are obtained for the case of constant gas properties.

It was decided to examine Eq. (8) for other possible shock-wave solutions besides that given by Becker.[7]

† According to the data in references 8 and 9, the value of P_r = 0.75 would seem to appear at a temperature below 0°C. However, within the experimental accuracy, it may be considered as the value at 0°C.

It was further decided to determine the influence of an initial Prandtl Number different from 0.75. In Section (II), the procedure and the subsequent results of numerical investigations are presented (for an initial Mach Number $M_0 = 2.0$) as obtained partly by the use of the M.I.T. Differential Analyzer* and partly by hand computation.

* The suggestion to use the analyzer machine was made by Dr. Hans Reissner.

(II) The Numerical Investigation of Eq. (8) (Constant Gas Properties)

It seemed advisable to rearrange the differential Eq. (8) in terms of the velocity ratio $u/u_0 \equiv U$. Eq. (8) then assumes the form:

$$(U^2)''b_1 - (U^2)'f_1 + U'l_1 + U^2h_1 - Uq_1 + U_1h = 0 \tag{8c}$$

where

$$\left.\begin{aligned}
&U \equiv u/u_0 && ()' \equiv d/dx \\
&b_1 \equiv \frac{b_0}{u_0} = \frac{1}{u_0}\left(\frac{2}{3}\mu_0 k_0\right) && h_1 \equiv \frac{h_0}{u_0} = \frac{m^2}{u_0} c_{r_0} \frac{\gamma_0 + 1}{2} \\
&f_1 \equiv \frac{f_0}{u_0} = \frac{m}{u_0}\left(k_0 + \frac{2}{3} c_{r_0}\mu_0\right) && q_1 \equiv \frac{q_0}{u_0^2} = \frac{m^2}{u_0} C_0 c_{p_0} \\
&l_1 \equiv l_0/u_0^2 = (m/u_0)C_0 k_0 && D_1 \equiv D/u_0^3 = -h_1 U_1 \\
&C_0 = C/u_0 = 1 + (1/\gamma_0 M_0^2) && U_1 = 2\frac{\gamma_0}{\gamma_0 + 1} C_0 - 1; \text{ the Rankine-Hugoniot limit ratio value}
\end{aligned}\right\} \tag{c}$$

The Boundary Conditions

There are *five* conditions to be satisfied by the solution of the differential Eq. (8c).

Three entrance conditions are assumed to be located as in previous reports, at so great a distance from the shock wave (expressed by $x \to -\infty$) that the flow in this region can be considered as uniform with prescribed values of *velocity*, *temperature*, and *pressure*. These three prescribed values are sufficient to determine the three integration constants appearing in Eq. (8c)—viz.,

$$\left.\begin{aligned}
&\text{(a)} \quad m = \rho_0 u_0 \\
&\text{(b)} \quad C_0 = \frac{p_0}{m} + u_0 = 1 + \frac{1}{\gamma_0 M_0^2} \\
&\text{(c)} \quad D_1 = h_1 U_1
\end{aligned}\right\} \tag{8d}$$

Two more conditions must be chosen at some point along the flow in order to determine the flow downstream of the shock wave. The only clearly definable point is the inflection point (called the center of the shock wave) on the transition curve across the shock wave between the higher and lower velocity. This point, *essential for the existence of a shock wave*, is chosen at the origin of the coordinate system, so that one more boundary condition is

$$U'' = 0, \quad \text{at } x = 0 \tag{8e}$$

The final condition to be chosen before the numerical solution is started, can be either U or U' at $x = 0$. If one of these values is assumed, in addition to $U'' = 0$, the other value (and also all successive derivatives at $x = 0$) can be determined from the differential Eq. (8c). That is, for $U'' = 0$ (at $x = 0$), Eq. (8c) shows that the values of U and U' are connected by the quadratic relation

$$U_c' = \frac{3m}{4\mu_0}\left[\eta_1\left(U_c - \frac{C_0}{2\eta_1}\right) \pm \sqrt{\eta_1^2\left(U_c - \frac{C_0}{2\eta_1}\right)^2 - n_2\,(U_c - 1)(U_c - U_1)}\right] \tag{9}$$

where the subscript c denotes the center (inflection) point of the shock wave and

$$\left.\begin{aligned}
&\eta_1 \equiv 1 + \frac{2}{3\gamma_0} P_{r_0}; \qquad P_{r_0} \equiv \frac{c_{p_0}\mu_0}{k_0}, \text{ the Prandtl Number} \\
&\eta_2 \equiv (2/3)\,[(\gamma_0 + 1)/\gamma_0]P_{r_0}
\end{aligned}\right\} \tag{d}$$

The choice of the velocity ratio $U_c \equiv u_c/u_0$ at $x = 0$ must be interpreted, as stated above, as the equivalent of an exit condition for the flow downstream of the shock wave (usually denoted by $x \to +\infty$). Since no rigorous procedure seems to exist to determine a general relation between U at $x \to +\infty$ and U_c (at $x = 0$), a certain special guide has been used for the selection of a value of U_c where $U_c'' = 0$. This guide is taken from the known closed form solution of Eq. (8c) given by Becker[7] for $P_{r_0} = 0.75$. From Becker's solution, a simple formula relating U_c and $(U_1)_{x \to +\infty}$ can

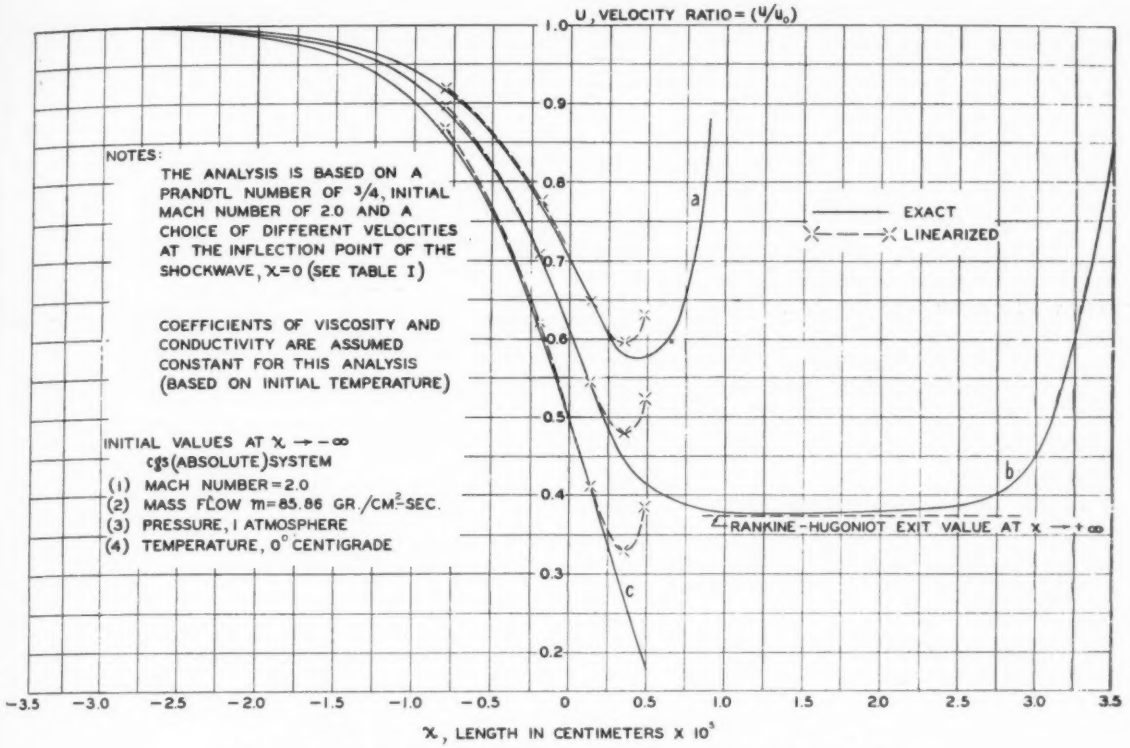
U, VELOCITY RATIO = (u/u₀)
1.0
0.9
0.8
0.7
0.6
0.5
0.4
0.3
0.2
NOTES:
THE ANALYSIS IS BASED ON A PRANDTL NUMBER OF 3/4, INITIAL MACH NUMBER OF 2.0 AND A CHOICE OF DIFFERENT VELOCITIES AT THE INFLECTION POINT OF THE SHOCKWAVE, X=0 (SEE TABLE I)
COEFFICIENTS OF VISCOSITY AND CONDUCTIVITY ARE ASSUMED CONSTANT FOR THIS ANALYSIS (BASED ON INITIAL TEMPERATURE)
INITIAL VALUES AT X → −∞
CGS (ABSOLUTE) SYSTEM
(1) MACH NUMBER = 2.0
(2) MASS FLOW m = 85.86 GR./CM²-SEC.
(3) PRESSURE, 1 ATMOSPHERE
(4) TEMPERATURE, 0° CENTIGRADE
EXACT
LINEARIZED
a
b
c
RANKINE-HUGONIOT EXIT VALUE AT X → +∞
−3.5 −3.0 −2.5 −2.0 −1.5 −1.0 −0.5 0 0.5 1.0 1.5 2.0 2.5 3.0 3.5
X, LENGTH IN CENTIMETERS X 10⁵

FIG. 1. One-dimensional shock-wave solutions for a Prandtl Number of 0.75.

be derived—namely,

$$U_e = \sqrt{U_1} \tag{10}$$

Two general cases, based on two values of the Prandtl Number, are chosen for the numerical solution of Eq. (8c)—i.e., $P_{r_0} = 0.75$, $T_0 \doteq 0°C$. and $P_{r_0} = 0.657$, $T_0 = 500°C$.[8] Furthermore, three velocity ratios, which are the same for the two general cases, are chosen at the inflection point. One velocity is based on relation (10) given above; two other values are also selected, one slightly larger and the other slightly smaller than that from Eq. (10). The initial Mach Number for all solutions is $M_0 = 2.0$.

The Influence of the Boundary Conditions

Three velocity curves are shown on Fig. 1. These curves, are based on a Prandtl Number of $^3/_4$ and three chosen velocity ratios U_e at the inflection point—namely, (a) 0.70000, (b) 0.61237, and (c) 0.60000. The velocity ratio (b) is computed from Eq. (10), which is derived from the exact particular integral of Becker;[7] it will be recalled that this integral of Becker *does not* contain any *non*uniform solutions at plus infinity for the velocity and the other variables.

It will be noticed that *none* of the three curves on Fig. 2 shows the characteristic uniform velocity downstream of the shock wave of Becker's solution. This fact is not surprising for curves (a) and (c) because they are derived from boundary values at the inflection point for which exact solutions in closed form are not known and probably do not exist. However, the velocity curve (b) *should* have approached uniformity downstream, because curve (b) is Becker's case since the boundary values used at the inflection point are calculated directly from Becker's exact solution.

When this surprising feature of curve (b) first appeared in the results found by the M.I.T. Differential Analyzer, the Computing Group initially considered machine errors as a possibility of its cause. However, after the work was investigated by an extremely accurate hand computational method, it was found that an instability was inherent to the problem and could not be avoided by any method of computation. The use of the term "instability" here means that there exists an extreme sensitivity against minute changes of boundary values (for example, at a deviation less than 10^{-4} per cent).

It is natural to ask what causes the velocity curve (b) on Fig. 1 to agree with Becker's solution up to a certain positive abscissa value and then become instable? The answer, as it will now be shown, is directly related to the accuracy or number of significant figures to which the velocity ratio U and velocity gradient U_e' for curve (b) were computed for the numerical analysis.

The explanation is seen clearest from the more straightforward derivation of Becker's solution presented by Morduchow and Libby.[10] One sees from an inspection of this solution that, if $P_{r_0} = 0.75$, then the

order of the nonlinear Eq. (8c) can be reduced to the following first-order equation:

$$UU' - \frac{3}{8}\frac{m}{\mu_0}\frac{\gamma_0 + 1}{\gamma_0}(U - U_1) = \frac{3}{4}\frac{m}{\mu_0}\frac{\gamma_0 + 1}{\gamma_0} N \exp.\left(\frac{c_{p_0} m}{k_0} x\right) \quad (11)$$

If the value of the integration constant N in Eq. (11) is taken as zero, then the resulting differential equation leads to the *particular* solution of Becker. *Only from this particular result* does one obtain a flow with a uniform velocity at plus infinity. For any other real value of the integration constant, N, the solutions of Eq. (11) will show nonuniform flows downstream of the inflection point; such solutions, moreover, cannot be obtained in a closed form in terms of elementary functions.

Now, when the boundary values U_e and U_e' (calculated from Becker's solution for N equal to zero) to be used by the differential analyzer to derive curve (b) on Fig. 1 are inserted into Eq. (11), the left side of Eq. (11) should reduce to zero. This did not occur *exactly* for the numerical solution of Becker's case reported here on Fig. 1. The reason, therefore, that even a highly accurate numerical solution [derived from Eq. (8)] will not, in general, reduce this left side of Eq. (11) to zero is the existence of an exponential, exact complementary integral with an exponent of extremely high value. The order of magnitude of this exponential term is 3×10^5.

The conclusions from this discussion and from the results shown on Fig. 1 are that (a) there are an infinite number of shock-wave type solutions possible from Eq. (8) and (b) that only one shock-wave solution, however, terminates in a state of uniform flow. The solution for uniform exit flow is the one that yields, at the exit, the limit values of Rankine-Hugoniot. These limit values, located theoretically at plus infinity, show, as is well known, that the limit pressure is greater than the pressure at the flow entrance. This flow, while predicted theoretically and satisfying the conservation conditions of mass and momentum, could not be produced experimentally. It is to be anticipated that, when a two-dimensional solution is obtained for this problem, a flow will appear, as shown by experiments, with *finitely located* limit values of higher pressure and lower velocity, for which, however, the final downstream pressure is lower than the entrance pressure.

The discussion above is concerned with the numerical solutions derived for a flow with a Prandtl Number of 0.75. Attention will now be called to the solutions obtained by numerical integrations for a Prandtl Number of 0.657. These latter solutions are plotted on Fig. 2. Here, the boundary velocity ratios, U_e, at the inflection point are the same as those on Fig. 1. The initial Mach Number is still 2.0.

When the Prandtl Number is not 0.75, there is no exact relation available to calculate a velocity ratio U_e for which uniform flow appears as $x \to +\infty$. However, by the assumption of continuity of solutions for the case of $P_{r_0} = 0.657$, shown on Fig. 2, it can be expected that there will be a solution that becomes asymptotically uniform as $x \to +\infty$. (In fact such a solution could be derived from the general procedure developed in the last section of this paper.)

An inspection of Fig. 2 shows that these numerical solutions are similar in form to those on Fig. 1—i.e., nonuniform velocity variations downstream of the shock wave. A significant characteristic of the curves for lower Prandtl Number, shown on Fig. 2, may be seen in the smaller velocity gradients across the shock wave.*

The dotted line curves shown on Figs. 1 and 2 were calculated from the perturbation solution developed in reference 4.

For the purpose of comparison, the Becker solution is plotted on Fig. 3, together with the corresponding solution for $P_{r_0} = 0.657$. This comparison is based on the same initial Mach Number and mass flow and the same (boundary) velocity at $x = 0$. The curve for $P_{r_0} = 0.657$, a replot of curve (b) on Fig. 2, before it rises downstream of the shock wave is probably a good approximation to the solution with uniform flow as $x \to +\infty$. From this comparison, the smaller velocity gradient across the shock wave is apparent for the lower Prandtl Number. It should be noted that, whereas the curves on Fig. 3 are obtained for equal initial values of Mach Number (but unequal initial pressures), the curves on Figs. 1 and 2 are calculated for equal initial values of Mach Number and pressure (but unequal mass flows). Because of the interdependence of initial temperature, Mach Number, and mass flow, it is not possible to make the comparison for exactly the same initial conditions.

The approximate solution developed by Taylor[6] is shown on Fig. 3 for comparison.

This completes the section on the shock-wave structure for constant gas properties. In the sections to follow, an analysis is given for the case of the temperature-dependency of the gas properties μ, k, and c_p.

(III) The Determination of Rankine-Hugoniot Limit Values for Temperature-Dependent Gas Properties

In Section (IV) of this paper a method to determine the shock-wave structure is developed for the realistic case of temperature-dependent gas properties. Needed

* The velocity gradients at the shock-wave center ($x = 0$) are about one-third smaller for $P_{r_0} = 0.657$. This means that the shock-wave thickness, as defined by Prandtl,[11] is therefore three times greater. This thickness is defined as $\Delta u/u_c'$, where Δu = difference between velocities at $x = \pm\infty$ (i.e., $u_0 - u_1$) and u_c' = velocity gradient at the shock-wave center.

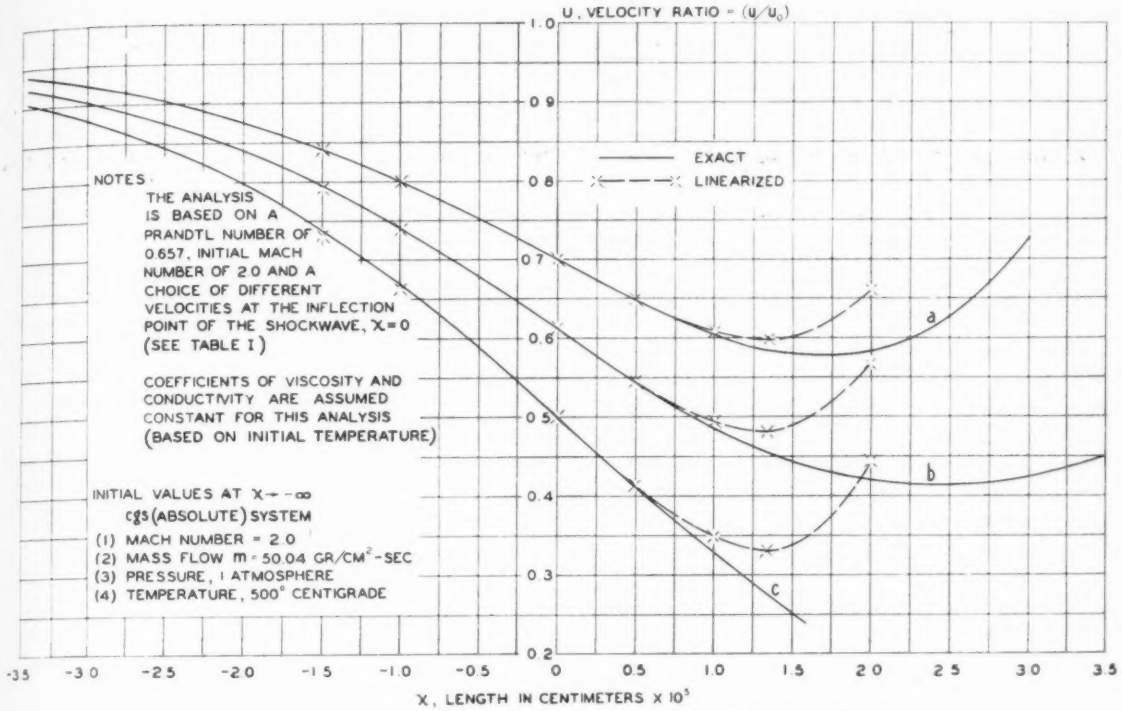
U, VELOCITY RATIO = (u/u₀)
EXACT
LINEARIZED
NOTES
THE ANALYSIS IS BASED ON A PRANDTL NUMBER OF 0.657, INITIAL MACH NUMBER OF 2.0 AND A CHOICE OF DIFFERENT VELOCITIES AT THE INFLECTION POINT OF THE SHOCKWAVE, X = 0 (SEE TABLE I)
COEFFICIENTS OF VISCOSITY AND CONDUCTIVITY ARE ASSUMED CONSTANT FOR THIS ANALYSIS (BASED ON INITIAL TEMPERATURE)
INITIAL VALUES AT X → −∞
cgs (ABSOLUTE) SYSTEM
(1) MACH NUMBER = 2.0
(2) MASS FLOW m = 50.04 GR/CM²-SEC
(3) PRESSURE, 1 ATMOSPHERE
(4) TEMPERATURE, 500° CENTIGRADE
a
b
c
X, LENGTH IN CENTIMETERS X 10⁵

FIG. 2. One-dimensional shock-wave solutions for a Prandtl Number of 0.657.

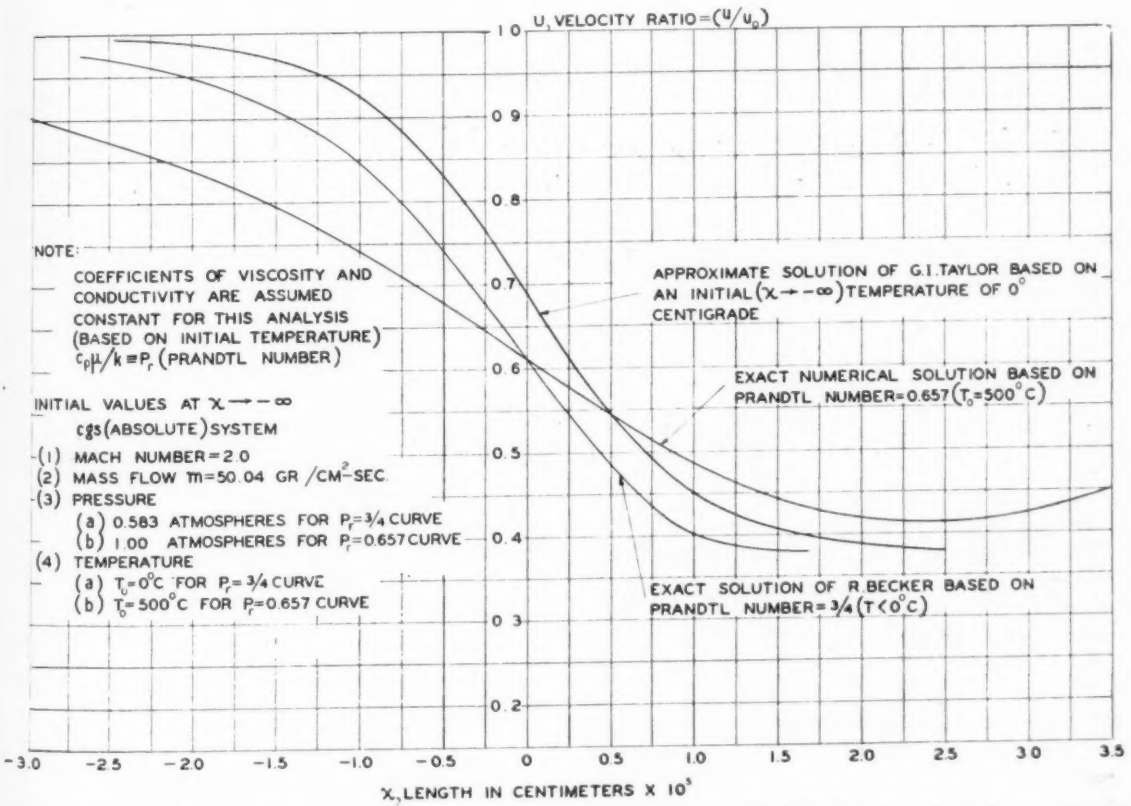
U, VELOCITY RATIO = (u/u₀)
NOTE:
COEFFICIENTS OF VISCOSITY AND CONDUCTIVITY ARE ASSUMED CONSTANT FOR THIS ANALYSIS (BASED ON INITIAL TEMPERATURE)
cpμ/k ≡ Pr (PRANDTL NUMBER)
INITIAL VALUES AT X → −∞
cgs (ABSOLUTE) SYSTEM
(1) MACH NUMBER = 2.0
(2) MASS FLOW m = 50.04 GR/CM²-SEC
(3) PRESSURE
(a) 0.583 ATMOSPHERES FOR Pr = 3/4 CURVE
(b) 1.00 ATMOSPHERES FOR Pr = 0.657 CURVE
(4) TEMPERATURE
(a) T₀ = 0°C FOR Pr = 3/4 CURVE
(b) T₀ = 500°C FOR Pr = 0.657 CURVE
APPROXIMATE SOLUTION OF G.I. TAYLOR BASED ON AN INITIAL (X → −∞) TEMPERATURE OF 0° CENTIGRADE
EXACT NUMERICAL SOLUTION BASED ON PRANDTL NUMBER = 0.657 (T₀ = 500°C)
EXACT SOLUTION OF R. BECKER BASED ON PRANDTL NUMBER = 3/4 (T < 0°C)
X, LENGTH IN CENTIMETERS X 10⁵

FIG. 3. The effect of Prandtl Number on the velocity gradient across a one-dimensional shock wave in a viscous heat-conducting compressible fluid.

for that work are the Rankine-Hugoniot limit values for temperature-dependent gas properties. These values will now be derived.

The differential Eq. (7) of velocity is shown to follow from the system of one-dimensional flow equations in which μ, k, and c_v are assumed to vary along the flow with the temperature. A trivial solution of Eq. (7), it was shown, is u = constant. This trivial solution, does not lead to a quadratic equation for the velocity (the Rankine-Hugoniot limit values) similar to Eq. (8a), since Eq. (7) contains terms that are only derivatives of the velocity. Therefore, in order to derive the analogy to the limit values of Rankine-Hugoniot for the temperature-dependency of all the gas properties, the individual equations of the system must be applied directly.

The heat balance Eq. (6a) is the first to be used. If use is made of the ideal gas relation for the intrinsic energy—namely,

$$c_v dT = dE \tag{12}$$

then it is possible to integrate Eq. (6a) once. The result of this integration is

$$k\frac{dT}{dx} - mE - mCu + \frac{mu^2}{2} = \text{constant} \tag{13}$$

We are interested in determining the relations between the flow variables that will be found in the uniform flow regions on both sides of the shock wave; in these regions the term $k(dT/dx)$ must vanish. Eq. (13) can then be written as follows:

$$(E_1 - E_0) + Cu_1 - \frac{u_1^2}{2} = Cu_0 - \frac{u_0^2}{2} = \text{constant} \tag{13a}$$

where the subscript 1 denotes the flow at $x \to +\infty$, and

$$(E_1 - E_0) = \int_{T_0}^{T_1} c_v\, dT \tag{12a}$$

Hence, Eq. (13a) can be written in the form

$$\int_{T_0}^{T_1} c_v\, dT + Cu_1 - \frac{u_1^2}{2} = Cu_0 - \frac{u_0^2}{2} \tag{13b}$$

and is a first relation between T_1, u_1, and the initial conditions denoted by the subscript 0.

A second required relation in terms of T_1 and u_1 is given by Eq. (3b). Considering, as before, only the two regions of uniform flow, then from Eq. (3b) this second necessary relation follows:

$$T_1 = (u_1/R)(C - u_1) \tag{14}$$

Eqs. (13b) and (14) are the two equations in T_1 and u_1 from which the limit values of Rankine-Hugoniot can be calculated for temperature-dependent gas properties. The value of the intrinsic energy term given by Eq. (12) can be simply obtained by a graphical integration of a curve of c_v vs. T as given, for example, in reference 9. Such an integration made from the data in reference 9 is shown on Fig. 7 ($\int_{T_0}^{T} c_v\, dT$ vs. temperature).

It is interesting to note from Eqs. (13b) and (14) that the variable specific heat c_v is the only gas property on which the new limit values depend, despite the fact that all the physical characteristics of the gas are taken as temperature-varying.

It is convenient to express Eqs. (13b) and (14) in their nondimensional forms before carrying out the solution by graphical means. These nondimensional forms are

$$\frac{E_1}{u_0^2} + C_0U_1 - \frac{1}{2}U_1^2 = C_0 - \frac{1}{2} \tag{13c}$$

and

$$T_1/T_0 = \gamma_0 M_0^2 U_1(C_0 - U_1) \tag{14a}$$

where

$$U_1 \equiv u_1/u_0$$
$$C_0 \equiv C/u_0$$

C is defined by Eq. (2b, 3b). A simple form for C_0 follows from Eq. (2b, 3b)—viz.,

$$C_0 \equiv \frac{C}{u_0} = \frac{p_0}{mu_0} + 1 = \frac{p_0}{\rho_0 u_0^2} + 1 \tag{e}$$

Combining Eq. (e) with the well-known sonic speed relation—namely,

$$a_0^2 = \gamma_0(p_0/\rho_0) \tag{f}$$

the value of C_0, in terms of the initial Mach Number M_0, becomes

$$C_0 = 1 + (1/\gamma_0 M_0^2) \tag{g}$$

After the velocity ratio U is calculated, the corresponding pressure ratio follows from the momentum relation (3a), which, if written in the form appropriate for the present example, becomes

$$p_1 = mC - mu_1 \tag{15}$$

If this equation is divided by p_0 and the initial Mach Number M_0 is introduced, then Eq. (15) can be written in the following nondimensional form:

$$p_1/p_0 = \gamma_0 M_0^2(C - U_1) \tag{15a}$$

The density ratio ρ_1/ρ_0 follows from the continuity Eq. (1a)—namely,

$$\rho_1/\rho_0 = 1/U_1 \tag{16}$$

Finally, the asymptotic Mach Number M_1 beyond the shock wave can be calculated from the ratio

$$M_1/M_0 = (u_1/a_1)/u_0/a_0$$

or

$$M_1 = M_0U_1[(\gamma_0/\gamma_1)/(T_1/T_0)]^{1/2} \tag{17}$$

where $\gamma_1 = c_{p_1}/c_{v_1}$ corresponds to the temperature T_1.

On Fig. 4, these new asymptotic limit values,* as calculated from the above procedure, are plotted for a range of initial Mach Numbers 1.0 to 7.0. These limit values are computed for an initial free-stream temperature of 0°C. and an initial pressure of one atmosphere. Also plotted on Fig. 4 for comparison are the corresponding Rankine-Hugoniot values based on the assumption of constant specific heat.

An inspection of this comparison shows that the influence on the limit values due to variable specific heat begins at a Mach Number of 2.0 and that the changes increase with the Mach Number. It is surprising to note that the influence of the c_v variation produces an increase in the pressure and density but a decrease in the temperature. Other conclusions based on this comparison are that the influence of c_v variable is (a) the greatest on the temperature and density ratios and (b) the least for the pressure ratio.

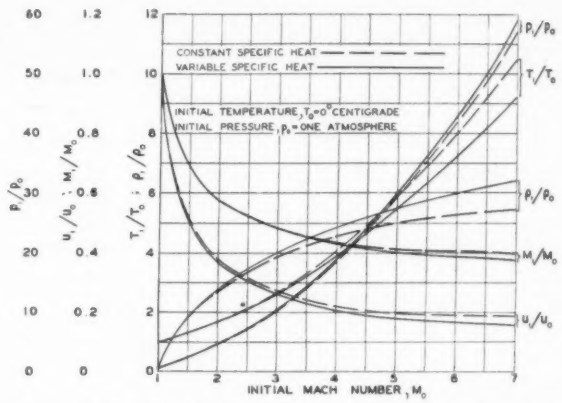

FIG. 4. The Rankine-Hugoniot limit values based on the temperature-dependent specific heats in comparison with the Rankine-Hugoniot values under the assumption of constant specific heats.

(IV) THE SHOCK-WAVE STRUCTURE FOR TEMPERATURE-DEPENDENT VISCOSITY, CONDUCTION, AND SPECIFIC HEAT†

Fairly accurate numerical solutions of the one-dimensional flow equations can be derived by the step-by-step method described below. This method is general insofar that it can be applied for both variable and constant gas properties and for both uniform and nonuniform exit flows. An example is given here of a numerical solution for an initial Mach Number $M_0 = 4.0$, variable μ, k, and c_v, and uniform exit flow.

Four equations, given previously in Sections (I) and (III) are required for this analysis. These are Eqs. (13), (3a), (4), and (1a).

Eqs. (13) and (3a) can, by a simple transformation, be written as one equation—namely,

$$\frac{dT}{du} = \frac{4\mu}{3k}\,\frac{C_1 + mE + mCu - (mu^2/2)}{mu - mC + p} \tag{18}$$

After replacing p and ρ, respectively, in Eq. (18) by their values in Eqs. (4) and (1a), the following equation appears:

$$\frac{dT}{du} = \frac{4\mu}{3k}\,\frac{C_2u + uE + Cu^2 - (u^3/2)}{u - C + RT} \tag{18a}$$

where

$$C_2 \equiv C_1/m = -E_0 - Cu_0 + (u_0^2/2)$$

$$E = \int_{T_{e\,(\text{exit})}}^{T} c_v\,dt \tag{12}$$

μ, k, and c_v are temperature-dependent.

The integration of Eq. (18a) leads to‡

$$T = \frac{4}{3}\int_{u=u_{e\,(\text{exit})}}^{u} \frac{u}{k}\,\frac{C_2u + uE + Cu^2 - (u^3/2)}{u - C + RT} \times du + C_3 \tag{18b}$$

For the problem treated here, the boundary conditions are prescribed as uniform at both ends of the flow. This procedure of integrating from exit to the entrance then assures that the exit condition is satisfied. Therefore, the integrals above use as the lower limit the values of $T = T_{\text{exit}}$ and $u = u_{\text{exit}}$ at the end of the flow. The reason for this will be seen shortly. As stated at the beginning of this section, an example will be given only for the case of uniform exit flow. For this case the boundary values of the integral (18b) are then taken as the Rankine-Hugoniot limit ratios T_1 and u_1 given on Fig. 4. If this is done and if Eq. (18b) is rearranged to the more convenient nondimensional form, one obtains

$$\Pi = \frac{4}{3}\,\frac{c_{v_0}\mu_0}{k_0}\int_{U=U_1}^{U}\left(\frac{\mu/\mu_0}{k/k_0}\right)\frac{U\left\{\dfrac{E}{E_0} - 1 + (\gamma_0 - 1)(U-1)\left[1 + \gamma_0 M_0^2\left(1 - \dfrac{U+1}{2}\right)\right]\right\}}{(\Pi/\gamma_0 M_0^2) - U(C_0 - U)}\,dU + \Pi_1 \tag{18c}$$

where $\Pi \equiv T/T_0$ and $U \equiv u/u_0$.

* Rankine-Hugoniot values for variable specific heat, which are obtained with Berthelot's equation of state, were given in reference 16. The limit values of reference 16 agree well with those given in this paper. This agreement would seem to show that the difference of equation of state has a small influence.

† The procedure for this analysis follows in some points the work of Becker.[7] See page 32 of that reference. In references 10 and 15, the value of μ/k is permitted to vary with the local flow temperature in such a way that P_r remains constant at 0.75. In Section (IV), the local flow temperature determines the local P_r as given by the experimental data of reference 9.

‡ The exit values here are characterized by the velocity and temperature at the exit and not by the abscissa x.

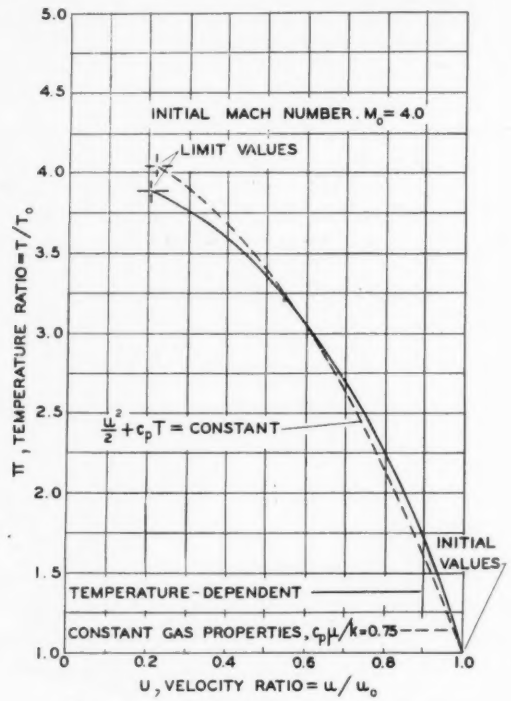

FIG. 5. T/T_0 vs. U/U_0 across shock wave.

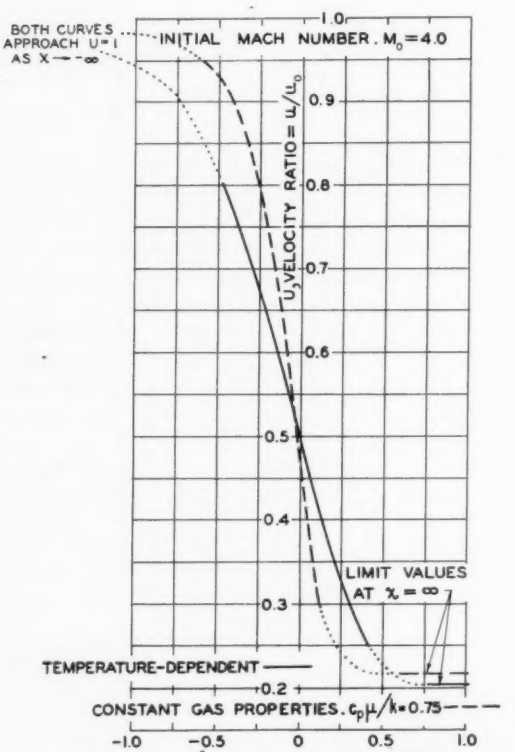

FIG. 6. Velocity variation through shock wave.

The solution of Eq. (18c) is achieved by a simple graphical iteration procedure. *A first approximation to this solution* can be obtained by drawing a curve of temperature ratio vs. velocity ratio through the two sets of coordinate values (U_1, Π_1) (1, 1) corresponding to the flow conditions at the exit and entrance, respectively. Here it must be remembered that the above exit values must be the Rankine-Hugoniot values for c_v variable.

As an aid in drawing the first approximation curve, the T vs. u relation can be used which follows from the exact one-dimensional solution of Becker.[7] This relation is for a parabola and has the form

$$(u^2/2) + c_{p_0}T = (u_0^2/2) + c_{p_0}T_0 = \text{constant}$$

or, in the ratio form,

$$\frac{U^2}{2} + \frac{\Pi}{(\gamma_0 - 1)M_0^2} = 0.5 + \frac{1}{(\gamma_0 - 1)M_0^2} \tag{19}$$

The values of μ and k required* to solve Eq. (18c) must correspond to the local temperature (which corresponds to the chosen velocity), while a value of E at this same temperature can be obtained as described in Section (III). Fig. 7 shows a plot of E vs. T for c_v variable.

A plot of Π vs. U is shown on Fig. 5. This curve gives the curve calculated for $M_0 = 4.0$ from the Becker relation (19) and the corresponding curve calculated by successive approximations from Eq. (18c). It is seen from this figure that Eq. (19) is a good approximation for developing the integration of Eq. (18c).

After the correct temperature-velocity curve is calculated, the x-coordinates to which these values belong can be obtained from a direct graphical integration of Eq. (3a), which first must be changed to the following form:

$$x = \frac{4}{3m}\int_{u_c}^{u} \mu u\,[RT - u(C - u)]^{-1}\,du + \text{constant} \tag{20}$$

or, in terms of nondimensional ratios,

$$x = \frac{4\mu_0}{3m}\int_{U_c}^{U}\left(\frac{\mu}{\mu_0}\right)\left[\frac{\Pi}{\gamma_0 M_0^2 U} - (C_0 - U)\right]^{-1} dU + \text{constant} \tag{20a}$$

The lower limit U_c is the value of the velocity at the shock-wave center (where $U'' = 0$). If it is prescribed that $U = U_c$ at $x = 0$, then the integration constant in Eq. (20a) is zero. The integration of Eq. (20a) is then performed to the right and left of $U = U_c$. Finally, a word about determining U_c.

Eq. (3a), from which Eq. (20a) followed, can also be written in the form

* The values of variables μ, k, and c_v used to derive the results of this paper are taken from reference 9.

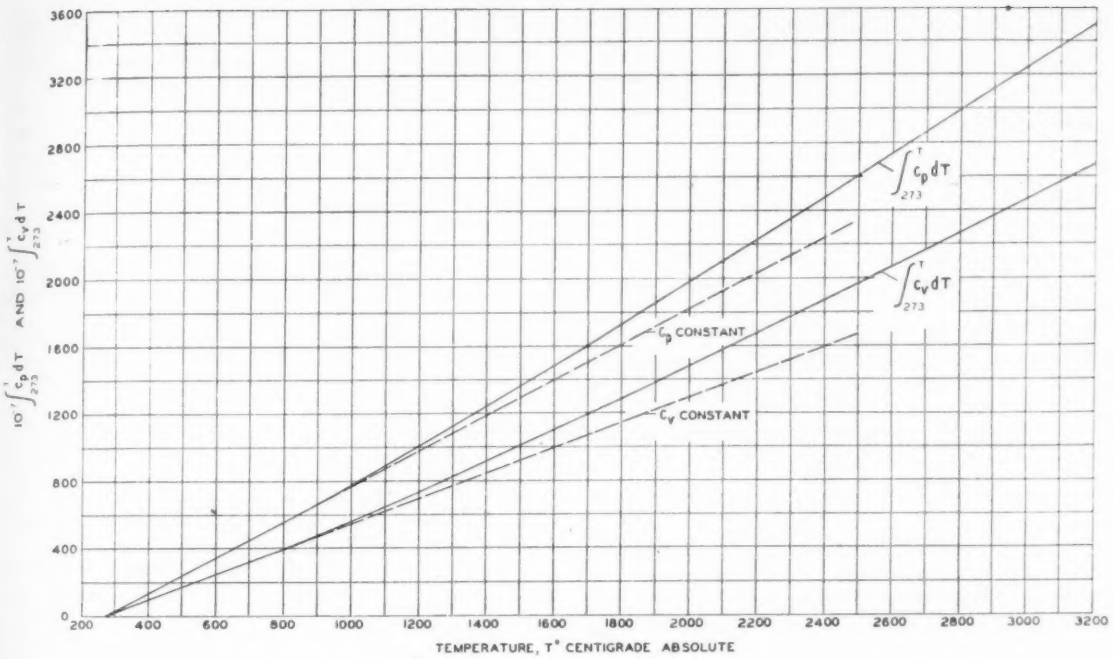

FIG. 7. The variation of integrals $\int_{T_0 = 273^\circ \text{ Abs. C.}}^{T} c_p\,dt$ and $\int_{T_0 = 273^\circ \text{ Abs. C.}}^{T} c_v\,dt$ with temperature.

$$\frac{dU}{dx} = \frac{3m}{4\mu}\left[\frac{(\gamma_0 M_0^2)^{-1}\,\Pi - U(C_0 - U)}{U}\right] \qquad (21)$$

A plot of dU/dx vs. U is made from Eq. (21) using the Π and U values calculated from Eq. (18c). On this plot it will be found that the velocity gradient has a maximum value; this maximum value corresponds to $U' = 0$, so that the velocity at this point of the dU/dx vs. U curve is U_c.

Following the procedure described above and using the Π vs. U values on Fig. 5, a plot of U vs. x was calculated and is shown on Fig. 6. Also shown on this figure is the corresponding shock-wave solution for constant gas properties which is given by the solution of Becker.

This comparison shows that, with variable gas properties, the influence of the shock wave extends further upstream and downstream; hence, the transition region is greater than that with constant gas properties. This "softening" of the shock wave is due to the large increase in μ and k in the region of the inflection point. The thickness of this shock wave is about two and one-half times greater than that for constant gas characteristics. It is also about two and one-half times greater than the mean free path of the molecules.

In closing, a word about the validity of the Navier-Stokes equations for this problem. The usually accepted criterion for such validation has been based on a comparison of the shock-wave thickness with the molecular mean free path. However, Puckett and Stewart[12] show that the shock-wave thickness is always several mean free-paths thick if the mean free path is based on the flow conditions at the shock-wave center. They further state, based on the work of Bethe and Teller,[13] that a better criterion of the validity of the Navier-Stokes equations is the number of molecular collisions required for statistical equilibrium to occur in the shock wave. It may be concluded from this that, as long as dissociation, condensation, etc., effects do not occur or the gas is not highly rarefied, the Navier-Stokes equations will adequately describe the shock-wave phenomenon.

It would seem that the Navier-Stokes relations are valid for viscous shock-wave problems within certain obvious limits. A difficulty in this work, not previously mentioned, is the formidable problem of obtaining reliable experimental data for comparison with the analytical studies.

REFERENCES

[1] Lamb, H., *Hydrodynamics;* Dover Publications, 1945.

[2] Meyerhoff, L., *On the Theory of the Steady, One-Dimensional Shock Waves, Including the Temperature Dependency of the Viscosity, Heat Conduction and Specific Heat,* Dissertation for the Degree of Doctor of Philosophy, Polytechnic Institute of Brooklyn, June, 1949.

[3] Meyerhoff, L., and Reissner, H. J., *The Standing, One-Dimensional Shock Wave Under the Influence of Temperature-Dependent Viscosity, Heat Conduction and Specific Heat,* PIBAL No. 150, Contract No. N6ori-206, T.O. I, June, 1949.

[4] Reissner, H. J., and Meyerhoff, L., *A Contribution to the Exact Solutions of the Problem of a One-Dimensional Shock Wave in a Viscous, Heat Conducting Fluid,* PIBAL No. 138, Contract No. N6ori-206, T.O. I, November, 1948.

(*Continued on next page*)

[5] Rayleigh, Lord, *Aerial Plane Waves of Finite Amplitude*, Scientific Papers, Vol. V; Cambridge, 1912.

[6] Taylor, G. I., *The Conditions Necessary for Discontinuous Motion in Gases*, Proc. Roy. Soc., London, A 84, pp. 373–377, 1910.

[7] Becker, R., *Impact Waves and Detonation, Part I*, N.A.C.A. T.M. No. 505, 1929.

[8] Tribus, M., and Boelter, L. M. K., *An Investigation of Aircraft Heaters, Part II, Properties of Gases*, N.A.C.A. Wartime Report W-9, October, 1942.

[9] Keenan, J. H., and Kaye, J., *Thermodynamic Properties of Air Including Polytropic Functions;* John Wiley & Sons, Inc., New York, 1945.

[10] Morduchow, M., and Libby, P. A., *On a Complete Solution of the One-Dimensional Flow Equations of a Viscous Heat Conducting Compressible Gas*, Journal of the Aeronautical Sciences, Vol. 16, No. 11, p. 674, November, 1949.

[11] Prandtl, L., *Zür Theorie des Verdictungsstosses*, Zeitschrift für das gesamte Turbinenwesen, Vol. 3, p. 241, 1906.

[12] Puckett, A. E., and Stewart, H. J., *The Thickness of a Shock Wave in Air*, Quarterly of Applied Mathematics, January, 1950.

[13] Bethe, H. A., and Teller, E., *Deviations from Thermal Equilibrium in Shock Waves*, Ballistic Research Laboratories, Report No. X-117, Aberdeen Proving Ground, Md.

[14] Wang Chang, C. S., *On the Theory of the Thickness of Weak Shock Waves*, Department of Engineering Research, University of Michigan, APL/JHU CM-503, UMH-3-F, August, 1948.

[15] Thomas, L. H., *Note on Becker's Theory of the Shock Front*, Journal of Chem. Phy., Vol. 12, No. 11, November, 1944.

[16] Eggers, A. J., Jr., *One-Dimensional Flows of an Imperfect Diatomic Gas*, N.A.C.A. T.N. No. 1861, April, 1949.

Analytical and Experimental Studies on Dynamic Loads in Airplane Structures During Landing

(*Continued from page 774*)

[2] Biot, M. A., and Bisplinghoff, R. L., *Dynamic Loads on Airplane Structures During Landing*, N.A.C.A. Wartime Report No W-92 (A.R.R. 4410), October, 1944.

[3] Ramberg, W., and McPherson, A. E., *Experimental Verification of Theory of Landing Impact*, paper presented at the Sixth International Congress of Applied Mechanics, Paris, 1946.

[4] Williams, D., *Dynamic Loads in Aeroplanes Under Given Impulsive Loads with Particular Reference to Landing and Gust Loads on a Large Flying Boat*, A.R.C., R. and M. No. 2221, 1948 (submitted as R.A.E. Reports S.M.E. 3309 and 3316, 1945).

[5] Wasserman, L. S., *The Prediction of Dynamic Landing Loads*, paper presented at the Seventh International Congress of Applied Mechanics, London, 1948.

[6] Jenkins, E. S., and Pancu, C. D. P., *Dynamic Loads on Airplane Structures*, paper presented at the S.A.E. National Aeronautic and Air Transport Meeting, April, 1948.

[7] Bisplinghoff, R. L., Pian, T. H. H., and Levy, L. I., *A Mechanical Analyzer for Computing Transient Stresses in Airplane Structures*, paper presented at the A.S.M.E. Annual Meeting, New York, N.Y., November 27–December 2, 1949

[8] McPherson, A. E., Evans, J., Jr., and Levy, S., *Influence of Wing Flexibility on Force-Time Relation in Shock Strut Following Vertical Landing Impact*, N.A.C.A. T.N. No. 1995, November, 1949.

[9] Levy, S., *Computation of Influence Coefficients for Aircraft Structures with Discontinuities*, Journal of the Aeronautical Sciences, Vol. 14, No. 10, p. 547, October, 1947.

[10] Leal, O. N., Bisplinghoff, R. L., and Pian, T. H. H., *Studies of Transient Stresses in an Airplane Model Wing During Drop Tests*, Proceedings of Society for Experimental Stress Analysis, Vol. VI, No. 1, 1948.

The Transient Temperature Distribution in a Wing Flying at Supersonic Speeds*

JOSEPH KAYE†

Massachusetts Institute of Technology

SUMMARY

The motion of a vehicle at high supersonic speeds results in a large nonuniform temperature rise within the vehicle. Several new problems, such as the magnitudes of the thermal stresses and of the aerodynamic deflections caused by this nonuniform temperature distribution, must be solved by the designer. These problems depend, in turn, on accurate prediction of this transient temperature distribution.

The calculation of the transient temperature distribution is illustrated for the case of a thin wedge-shaped wing or airfoil subjected to constant acceleration from Mach Numbers of 1.4 to 6. The calculation depends strongly on the state of the art relative to heat transfer at supersonic speeds; as a result, the calculations may be systematically in error because of the lack of data in this art.

A long and laborious numerical method of solution of the differential equation for heat flow in two dimensions with boundary conditions dependent on time is presented, and the resultant temperature distributions in the wing are given in chart form. In this solution the spanwise heat flow is assumed to be negligible. The results indicated that the heat-flow problem could be reduced to one-dimensional heat flow in the direction normal to the chord without sacrifice of accuracy for a wing with a maximum thickness ratio of less than 10 per cent.

A shorter numerical method of solution of the differential equation for heat flow in one dimension—normal to the chord—is presented. It is shown that this method yields temperature distributions that are in excellent agreement with those calculated by the method for two-dimensional heat flow. This shorter method was used to investigate the effects of changes in the coefficients of heat transfer and in the values of the acceleration. It is shown that this shorter numerical method of solution is applicable to the general case of a thin airfoil, provided the variation of the local coefficient of heat transfer with time is available.

SYMBOLS

A = heat transfer area
a = velocity of sound
c_p = specific heat at constant pressure
G = flow per unit area or mass velocity = ρV
g = acceleration given to unit mass by unit force = 32.174 ft. per sec.^{2}
h = coefficient of heat transfer
k = thermal conductivity
l = half thickness of wing
M = Mach Number = V/a
Nu = Nusselt Number = hx/k
p = static pressure
Pr = Prandtl Number = $c_p\mu/k$
Q = heat transfer
q = rate of heat transfer
R = gas constant
r = recovery factor = $(t_{aw} - t_m)/(t_s - t_m)$
Re = Reynolds Number = $\rho Vx/\mu$
T = temperature, °F. absolute
t = temperature, °F.
V = velocity
v = specific volume
w = mass rate of flow
x = position coordinate normal to chord
y = position along chord from leading edge
α = thermal diffusivity = $k/\rho\, c_p$
α' = angle between shock and incident flow
β = angle of attack
ϵ = turning angle in expansion
μ = viscosity
ρ = density
θ = time
ω = vector angle of characteristic curve in hodograph plane
ω' = wedge angle for shock

Subscripts

aw = adiabatic wall
m = mean stream condition
0 = initial condition
s = stagnation condition
w = wall or surface condition

INTRODUCTION

ATTEMPTS to make air-borne devices move at ever increasing speeds have resulted in the discovery of new problems that must be solved for successful flight. Such is the case of the aircraft or missile that is required to move at high supersonic speeds—that is, speeds of the order of several times the velocity of sound in air. In this case, in addition to new aerodynamic problems that confront the designer, he must investigate the effects of the large temperature rise of the surface of the moving object and of the resultant temperature distribution within the object. For example, if the object is required to fly steadily at an altitude of 50,000 ft. and at a speed of 5,500 m.p.h. (or a Mach Number of 8), then the temperature of the surface of the object will be of the order of 4,000°F.

If the surface temperature of an air-borne supersonic vehicle can become so large, it is evident that the designer will be faced with a host of new problems that depend on the transient temperature distribution in the vehicle. Investigation of this transient tempera-

Presented at the Aerodynamics Session, Eighteenth Annual Meeting, I.A.S., New York, January 23–26, 1950.

* This paper represents a portion of the work carried out for the U.S. Air Force under Contract No. W33-038 ac-17239; this paper is an advance release of a portion of U.S.A.F. Technical Report 5786. The following students assisted in the portion of the program described here: G. H. McLafferty, Jr., J. C. Stamper, Jr., and Victor C. Yeh. In addition, the assistance of R. H. Shoulberg and Miss Barbara M. Healy is gratefully acknowledged.

† Associate Professor of Mechanical Engineering.

ture distribution within the vehicle has led to results that are of great value to the designer.

Consider an object moving relative to a fluid, such as an aircraft or a missile moving through air. The velocity of the fluid relative to the object is reduced from a finite value at a large distance to zero at the surface of the object. The temperature of the fluid rises from its value at a large distance to almost the stagnation temperature (the temperature corresponding to zero velocity of the fluid) at the surface of the object. If we limit our discussion to a gas that has an equation of state of the form

$$pv = RT \tag{1}$$

then the stagnation temperature is the same whether the reduction to zero velocity is accomplished at constant pressure by an irreversible mechanism, such as shear forces in the boundary layer, or by a reversible process such as diffusion to higher pressure.

If the temperature of the object is uniform and identical with the temperature of the air at the surface of the object, there will be no heat transfer between air stream and object. Then the temperature of the fluid at the surface of the object is called the "adiabatic wall temperature." The relation between the adiabatic wall temperature and the temperature of the fluid at a large distance—the free-stream temperature—is given simply in terms of the recovery factor, defined as follows:

$$r = \frac{T_{aw} - T_m}{T_s - T_m} = \frac{T_{aw} - T_m}{V_m^2/2gc_p} \tag{2}$$

It is seen that the recovery factor r is the ratio of the excess of the adiabatic wall temperature over the free-stream temperature to the excess of the stagnation temperature over the free-stream temperature. Values of the recovery factor are based at present on relatively few analytical and experimental studies. These values will be discussed more fully later in this paper.

For subsonic speeds, the adiabatic wall temperature of the fluid is not appreciably greater than the free-stream temperature. For supersonic speeds, however, the adiabatic wall temperature increases rapidly with increasing Mach Number, until at Mach Numbers greater than about 5 it becomes one of the most important variables to be considered in the design of high-speed vehicles. This increase in adiabatic wall temperature with increasing Mach Number is shown in Figs. 1 and 2 for flight at sea level and at the isothermal atmosphere at altitudes from 35,000 to about 100,000 ft. (labeled 50,000 ft.), respectively. The two uppermost curves in each of these figures represent the adiabatic wall temperatures for air for a recovery factor of unity and, hence, also the stagnation temperatures; the lower curves are for recovery factors of 0.9 and 0.8. The uppermost curve is calculated with a constant specific heat of air, while the other three are based on a variable specific heat, using values of enthalpy from *Gas Tables*.[1]

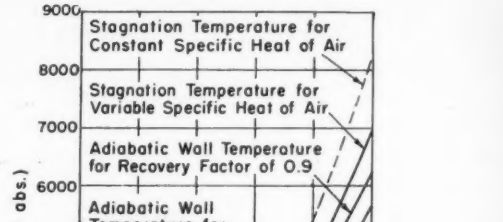

Stagnation and Adiabatic Wall Temperatures for Flight at Constant Speed in Air at 50,000 Feet.

FIG. 1.

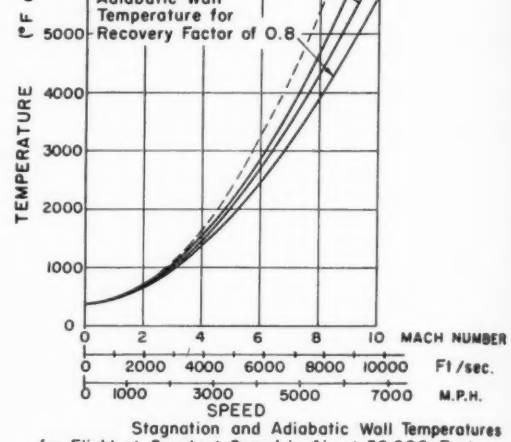

Stagnation and Adiabatic Wall Temperatures for Flight at Constant Speed in Air at Sea Level.

FIG. 2.

The striking feature in Figs. 1 and 2 is the extremely large value of the adiabatic wall temperature at the higher Mach Numbers. Since the adiabatic wall temperature is usually higher than the temperature

of the object, except in steady flight, the serious nature of the "aerodynamic heating" of the object, as it is often called, at Mach Numbers above approximately 4 to 5 becomes immediately apparent.

The effects of these large adiabatic wall temperatures are alleviated to some extent in a supersonic vehicle by the finite rate of heat transfer to the object and by the radiation from its surface. Both of these effects will reduce the surface temperature of the vehicle below the adiabatic wall temperature. It is apparent, however, that flight at high Mach Numbers will raise many questions such as the following:

(a) What is the surface temperature of the vehicle for flight under accelerating conditions and under steady conditions?

(b) What is the temperature distribution within the structure of the object?

(c) Is it possible to estimate rapidly the temperature distribution for flight under conditions of constant acceleration?

(d) What are the effects of the nonuniform temperature distribution? Or, what are the thermal stresses?

(e) What is the effect of temperature distribution on the aerodynamic characteristics of the wing, such as angle of attack, deflections, etc.?

(f) What metals will be satisfactory for use in high-speed vehicles?

(g) What are the cooling requirements for safe operation of these vehicles?

The purpose of the present paper is to present some answers to questions (a), (b), and (c), not for the general case of any object but for the special case of a solid, homogeneous, thin wedge-shaped wing. It was apparent that a detailed examination of a single shape would help in discovering the basic problems of aerodynamic heating and would help in pointing out the basic data needed for future investigations. The results obtained in this study have justified this approach to the problem.

Review of Previous Work on Temperature Distribution in an Object Moving at Supersonic Speeds

A careful search of the unclassified literature did not disclose any previous work on the temperature distribution in a body moving at supersonic speeds. On the other hand, several recent papers were found on the skin temperature of a body moving at high speeds.

Wood[2] calculated the surface temperatures of a symmetrical double-wedge airfoil for steady supersonic flight at Mach Numbers from 2 to 10, for emissivities from 0 to 1, and for altitudes from 50,000 to 200,000 ft. He attempted to include the effects of solar radiation. He did not investigate the surface temperatures for flight at variable speed—i.e., for an accelerating vehicle. He emphasized the large number of problems that must be solved before his assumptions or extrapolations could be considered satisfactory.

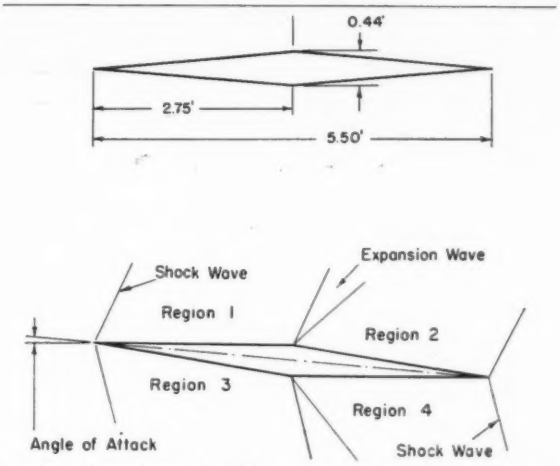

FIG. 3. Dimensions and airflow pattern of a wedge-shaped wing.

Scherrer[3] presented an approximate method for calculating the cooling requirements of a body of revolution in steady supersonic flight based on the assumption of a laminar boundary layer around the entire body.

Stalder and Jukoff[1] presented "a general method, using the methods of kinetic theory, whereby the surface temperatures of bodies can be calculated for steady flight at any speed in a rarefied gas." The study, because of its method, was limited mainly to extremely high altitudes. The effects of solar radiation were also included, and some effects of internal cooling were mentioned.

Huston, Warfield, and Stone[5] compared "the time history of the skin temperature measured on the nose of a V-2 missile with the time history of the temperature computed by use of Eber's experimental relation for heat-transfer coefficients for conical bodies under supersonic conditions." They developed a general numerical method for computing the time history of the skin temperature of a cone, taking into account the effects of solar heating and radiation to the atmosphere.

Lo[6] presented a numerical method for the calculation of the transient skin temperature of conical bodies during high-speed flight. He included the effect of emission from the skin but neglected the absorption of solar radiation by the skin.

Johnson and coworkers[7] reviewed the literature and summarized the data available for recovery factors and heat-transfer coefficients for supersonic velocities. In this report they use several examples to illustrate the calculation of skin temperatures of an object in high-speed flight.

Finally, the measurements of skin temperatures on the nose of a V-2 rocket by Fischer and Norris[8] should be mentioned here. Measurements made during the transient period of variable acceleration were analyzed to yield some data on heat-transfer coefficients for laminar and turbulent boundary layers.

Statement of the Problem

Consider a solid, homogeneous, thin wedge-shaped wing, such as that shown in Fig. 3, which is flying steadily at a low supersonic velocity, such as a Mach Number of 1.4. The wing is suddenly subjected to a constant acceleration until it attains a larger supersonic velocity, such as a Mach Number of 6, and then it is flown steadily at this Mach Number. What is the temperature distribution in the wing at any time after the start of the sudden acceleration? During the period of constant acceleration, the temperature of the wing is a function of both position and time. During the time period beginning with steady flight at a Mach Number of 6, the temperature of the wing is dependent on both position and time, but the adiabatic wall temperature and heat-transfer coefficient are now independent of time. When the final steady state is attained, the temperature will be, of course, independent of time but not of position in the wing, since the ambient temperatures in the four regions of the wing will have different values.

We are thus concerned with the solution of the differential equation governing the transfer of heat for two distinctly different types of boundary conditions. For the first, corresponding to the period of constant acceleration, the boundary conditions at any point on the wing surface are a function of time. For the second, starting with the transient heating process in steady flight at the higher velocity, the boundary conditions at any point on the wing surface are independent of time. Many solutions are available in the literature for the second type of constant boundary conditions, but only a few solutions of an extremely specialized form are known for the first type of variable boundary conditions. Examples of solutions of the second type of constant boundary conditions are available in reference 9 in the form of the Gurney-Lurie charts and the Hottel charts for a large slab. Examples of solutions in analytical form for the first type are available in reference 10, but none of these corresponds to the boundary conditions peculiar to the wedge-shaped wing undergoing acceleration.

Excellent solutions for engineering calculations are available in the form of the Gurney-Lurie and the Hottel charts for the case of boundary conditions independent of time. These charts may be used as fair approximations to obtain the transient temperature distribution in the wedge-shaped wing on a basis of one-dimensional heat flow for the period of time beginning with steady flight. The error introduced is caused by the fact that the initial condition used in the construction of the charts was one of uniform temperature, whereas the initial temperature in the wedge-shaped wing is the temperature distribution corresponding to the end of the period of constant acceleration. For large values of the acceleration, the error made in using these charts would be negligible. Hence, this phase of the transient heating problem was considered solved. The major effort in this work was directed toward obtaining solutions of the differential equation for flow of heat for the case of boundary conditions dependent on time.

Assumptions

The following assumptions, which tend to oversimplify the real problem, were made:

(1) The wing is a solid symmetrical double wedge without sweepback and with a constant chord, as shown in Fig. 3. The chord is 5 ft. 6 in., and the maximum thickness is 8 per cent of the chord.

(2) The supersonic flow of air by the wing is assumed to be two-dimensional, independent of the span. For supersonic speeds above Mach Number of 1.4, Fig. 3 shows the flow pattern around the wing with a pair of shock waves at the leading and the trailing edges and a pair of expansion waves at the mid-chord.

(3) The wing loading is fixed at 100 lbs. per sq.ft.

(4) The wing is made of steel with constant values of the thermal conductivity, specific heat, and density.

(5) The spanwise heat transfer is negligible.

(6) Heat transfer by radiation to or from the wing surface is negligible.

(7) Flight is at a fixed altitude of 50,000 ft.

(8) The flight of the wing begins with an almost uniform temperature distribution in the wing corresponding to steady flight at a Mach Number of 1.4.

These assumptions were made primarily to reduce the large number of laborious computations required for solution of the two-dimensional heat flow in the wing. It is believed that they do not affect seriously the final results on temperature distribution in the wing during the transient heating period. The effects of changing some of these assumptions were investigated later by the simpler solution based on one-dimensional heat flow. The maximum thickness of 8 per cent was selected to keep the drag low for the supersonic velocities studied here. The selection of steel as the material of the wing was recommended because of the large temperatures that would be encountered at the higher Mach Numbers. The effects of radiation could have been taken into account, but it was decided to neglect these in order to retain simplicity. Although the studies were made for flight at an altitude of 50,000 ft., they apply in fact, with slight modifications, to the isothermal atmosphere ranging from 35,000 to about 100,000 ft.; for simplicity, the figure legends show only 50,000 ft.

Sources of Data

Properties of Air

The properties of air were taken directly from *Gas Tables* by Keenan and Kaye.[1] Here, it is assumed that Eq. (1) is valid for air and that the specific heat of

air is a function of temperature. The thermal conductivity, viscosity, and Prandtl Number of air are tabulated on page 34 of *Gas Tables*.

Properties of Steel

As stated in assumption (4), the properties of the steel wing were assumed to be constant; this was done in order to simplify the laborious calculations required by the method of finite differences for solution of the two-dimensional heat flow in the wing. The following values were used:

k = 22 B.t.u. per hour ft. °F.
c_p = 0.118 B.t.u. per lb. °F.
ρ = 486 lbs. per cu.ft.

Properties of Two-Dimensional Supersonic Flow About Wing

By means of the assumptions (1), (2), (3), and (7), the supersonic flow conditions in the four regions around the wing, shown in Fig. 3, were determined. The angle of attack was first found at each Mach Number by means of the slope of the curve of lift coefficient versus Mach Number as given by Ivey.[11] With this angle of attack, either *Gas Tables* or reference 12 was used to obtain the flow conditions in each of the four regions around the wing. From the known velocities around the wing, the temperatures corresponding to the ambient conditions in the four regions, to stagnation, and to the adiabatic wall were easily computed for steady flight at a given speed. Detailed calculations are given in Appendix (I).

Fig. 4 presents the results of such calculations for the wedge-shaped wing shown in Fig. 3. The abscissa is the flight Mach Number corresponding to the speed of the wing and is based on the sound velocity in air at an altitude of 50,000 ft. Separate scales are also given showing the wing speed in units of feet per second and of miles per hour. The stagnation temperature is given as the uppermost curve. The ambient temperatures of the four regions corresponding to the flow pattern shown in Fig. 3 are shown as the four nearly flat curves at the bottom of Fig. 4. Since the differences in temperature are so small for these four regions, the adiabatic wall temperatures calculated from these four ambient temperatures and from the ambient Mach Number were so close together that a single line has been employed in place of four lines on Fig. 4 to represent the adiabatic wall temperature. A recovery factor of 0.9 was used in these calculations.

The curves in Fig. 4 start at a Mach Number of 1.4 mainly to be fairly certain that the flow pattern given in Fig. 3 would be valid. For Mach Numbers less than 1.4 it appears that the shock is detached from the leading edge and that this would result in somewhat different temperatures for the four regions of the wing. Since the effects of aerodynamic heating are small at Mach Numbers less than 1.4, the entire range from a

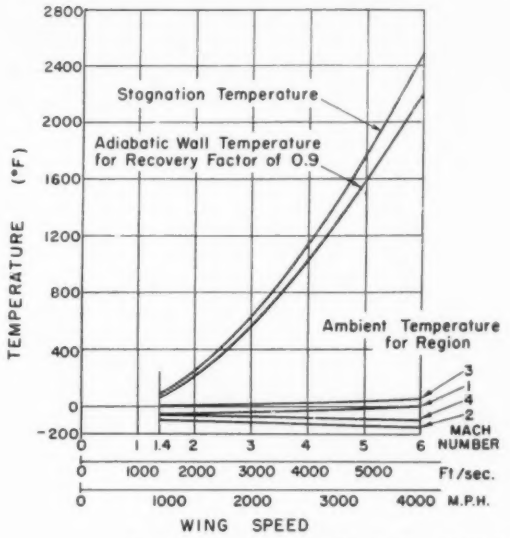

Temperatures Corresponding to Four Ambient Regions, to Stagnation, and to the Adiabatic Wall for Flight of a Wedge Shaped Wing at Constant Speed at 50,000 Feet.

FIG. 4.

Mach Number of 0 to 1.4 was not considered in this report.

Fig. 4 shows that the adiabatic wall temperature for a wedge-shaped wing is about 2,200°F. for steady flight at a Mach Number of 6. On the one hand, if one accelerates such a wing rapidly from a Mach Number of 1.4 to 6 and then flies steadily at 6, the temperature difference available for heat transfer into the wing will be considerable. On the other hand, if one accelerates the wing slowly, the temperature difference for heat transfer may be small. The temperature distributions in the wing resulting from these widely different accelerations for the same increase of Mach Number will be markedly dissimilar. It is evident, therefore, that the acceleration of the wing must be tied together with the data in Fig. 4 before one can establish either the rate of heat transfer into the wing or the temperature distribution at any time. This is the primary reason why much attention has been given to the acceleration of the wing in this study.

Values of the Recovery Factor

The recovery factor has been defined as the ratio of the excess of the adiabatic wall temperature over the free-stream temperature to the excess of the stagnation temperature over the free-stream temperature. It is given simply by Eq. (2).

The recovery factor can be measured in a stream of air by several methods. One method consists of placing a plate thermometer in the stream, waiting for steady-state conditions, and then noting the reading of the plate thermometer, T_{aw}; the free-stream temperature, T_m; and the free-stream velocity, V_m. The value

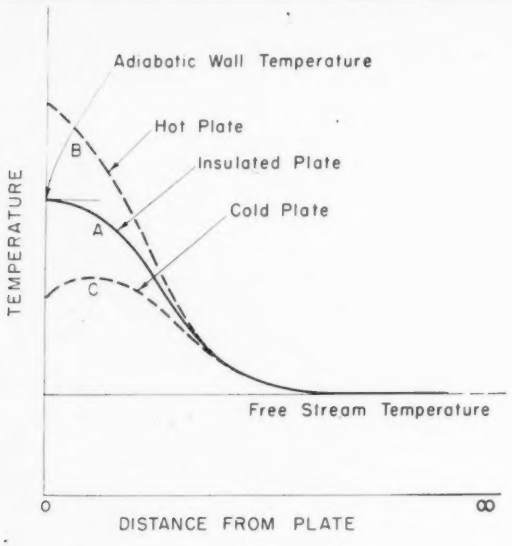

Distribution of Temperature in the Boundary Layer With Fixed Free Stream Conditions for Hot, Insulated, and Cold Plates

FIG. 5.

of the free-stream temperature is usually calculated from a pressure measurement. The temperature of the plate must be uniform—i.e., no temperature gradients should exist in the plate—either parallel or perpendicular to the direction of flow. A thin plate constructed from a metal of high conductivity or a well-insulated plate covered with a thin metallic coating are two approximations to this plate thermometer.

For a plate thermometer, the temperature distribution is given schematically in Fig. 5 as curve A for an insulated plate. It is seen that the plate temperature is the adiabatic wall temperature with zero temperature gradient at the surface of the plate. If the temperature of the plate is controlled at any desired value by extraneous devices, then curves B and C indicate schematically the temperature distributions in the boundary layer for plates that are hotter and colder, respectively, than the adiabatic wall temperature for the same fixed free-stream conditions. The importance of the concept of adiabatic wall temperature will be discussed in greater detail in the section on coefficients of heat transfer.

Other methods of measuring the recovery factor for flow over objects of different shapes are also known. In addition, recovery factors can be measured for flow of air through tubes of circular cross section; it appears probable that the most accurate measurements of recovery factor have been obtained by this method. Such measurements have been published recently by McAdams, Nicolai, and Keenan[13] for subsonic velocities and by Kaye, Keenan, and McAdams[14] for supersonic flow of air in a pipe.

Theoretical investigations have also been carried out to determine the adiabatic wall temperature, recovery factor, and distribution of temperature within the boundary layer for flow of compressible and incompressible fluids. Most of the results obtained analytically have been for a laminar boundary layer. Several summaries of these investigations are available; one of the latest can be found in reference 7. The reader is referred to this report for details of these studies; several of the theoretical temperature distributions in the boundary layer are also reproduced there.

Recovery factors have been measured for adiabatic flow of air over flat plates, cones, wedges, and cylinders and for flow of air inside tubes of circular cross section. The available data for recovery factors for flow over various objects are summarized in reference 7. For subsonic flow of air over a flat plate, this report states the situation as follows:

(a) The values of the recovery factor are independent of both Mach Number and Reynolds Number for both laminar and turbulent boundary layers.

(b) For a laminar boundary layer, the recovery factor is equal to the square root of the Prandtl Number—i.e.,

$$r = (Pr)^{1/2} \tag{3}$$

(c) For a turbulent boundary layer, the recovery factor is equal to the cube root of the Prandtl Number—i.e.,

$$r = (Pr)^{1/3} \tag{4}$$

For supersonic flow of air over objects, the amount of available data and theory is so small that the situation calls for some skillful guesswork. Johnson concludes in the above report that for supersonic flow past bodies one should use the values of the recovery factor for a flat plate with the same kind of boundary layer. This point of view is supported, in part, by the recently published work on recovery factors for supersonic flow of air through round tubes by Kaye, Keenan, and McAdams.[14] The recovery factors obtained for conditions where the laminar boundary layer prevailed agreed within one-half of 1 per cent with a curve representing the square root of the Prandtl Number; such values are in excellent agreement with those for subsonic velocities with a laminar boundary layer. On the other hand, the recovery factors obtained from a one-dimensional analysis for conditions where a turbulent boundary layer prevailed varied from about 0.9 at a Mach Number of 2.4 to about 0.8 at a Mach Number of 1.4 and neither resembled the corresponding experimental values for subsonic flow nor the rough analytical values for a turbulent boundary layer in supersonic flow.

It is evident from the above discussion that much more experimental and theoretical work on recovery factors is necessary before one can select accurate values for supersonic-flow conditions. In fact, it should be

noted that data for recovery factors are practically nonexistent above a Mach Number of 3. It was decided, therefore, to select a recovery factor of 0.9 for all calculations in the present paper for the following reasons:

(1) The Prandtl Number of the working fluid, air, is about 0.73 at temperatures corresponding to an altitude of 50,000 ft. The square root is 0.85 and the cube root is 0.90. For simplicity, a value of 0.9 was chosen.

(2) The selection of 0.9 implies that the temperature distribution curves calculated for this report tend to be in error on the conservative side, since the resultant surface temperatures, temperature gradients, and thermal stresses will tend to be somewhat higher than the values one would have calculated with a lower value of the recovery factor.

(3) The surface temperature of the wing is always nonuniform in flight, so that an unknown error is introduced by using a recovery factor corresponding to uniform temperature in the body.

(4) The effects of radiation at high surface temperatures on the value of the recovery factor are unknown at present.

The Coefficients of Heat Transfer for Supersonic Velocities

Numerous investigators have studied experimentally and theoretically the problem of the rate of heat transfer between a surface and a fluid that moves at subsonic velocities. The results of these studies are usually expressed in terms of an arbitrary coefficient of heat transfer and in terms of some simple means of evaluating of the properties of the fluid. In turn, the coefficients of heat transfer are correlated with the geometry, the properties of the fluid, and the type of flow that prevails, such as laminar or turbulent flow. For moderate subsonic velocities the state of the art is fairly well advanced.

In contrast to this picture, little is known about heat transfer for flows at high subsonic and supersonic speeds. Indeed, the amount of theoretical and experimental work which has been done on heat transfer at supersonic speeds is a small fraction of that done at moderate subsonic speeds during the past 60 years.

The following reasons may account for this great difference in work output in the two fields:

(1) The need for solution of practical heat-transfer problems involving supersonic velocities has arisen only recently.

(2) The need for knowledge of the behavior of supersonic flows has been emphasized only recently.

(3) The problem of predicting coefficients of heat transfer for supersonic flow of a compressible fluid is a much more complex one than that encountered at subsonic velocities.

(4) The experimental study of heat-transfer coefficients for supersonic flows has required a simultaneous determination of recovery factors for the same free-stream conditions. This difficulty will be discussed in greater detail in the section on "effective coefficient" of heat transfer.

Mean Coefficient of Heat Transfer

For low to moderate subsonic velocities it has been customary to use the following arbitrary definition of the coefficient of heat transfer between a fluid and a surface:

$$h_m = (q/A)/(t_w - t_m) \tag{5}$$

where h_m is the "mean coefficient," q/A is the heat flux, t_w is the temperature of the surface, and t_m is the average or bulk temperature of the fluid at a given cross section.

For high subsonic or for supersonic velocities of a compressible fluid, such as air, the temperature distribution in the boundary layer is shown in Fig. 5 for the cases of adiabatic flow, of heat transfer from a hot plate to air, and of heat transfer from air to a cold plate. If we apply the above arbitrary definition of the "mean coefficient" to this set of temperature distributions, we see that this mean coefficient is zero for the insulated plate, positive for the hot plate, and negative for the cold plate as long as the wall temperature is greater than the free-stream temperature. It is evident that the mean coefficient is of no value for high velocities.

Effective Coefficient of Heat Transfer

The situation described above can be remedied by using another arbitrary definition of the heat-transfer coefficient as follows:

$$h_e = (q/A)/(t_w - t_{aw}) \tag{6}$$

where h_e is the "effective coefficient," t_w is the surface temperature during heat transfer for given free-stream conditions, and t_{aw} is the surface temperature for adiabatic flow with the same free-stream conditions—i.e., the adiabatic wall temperature.

The advantages of this definition of effective coefficient are that the heat transfer must be zero for zero temperature difference and that the coefficient is always positive. In addition, some experimental data indicate that this coefficient is approximately independent of the size of the temperature difference ($t_w - t_{aw}$). A disadvantage of this effective coefficient is that its use requires a knowledge of the adiabatic wall temperature for the same free-stream conditions. The adiabatic wall temperature can be obtained from Eq. (2) as

$$t_{aw} = t_m + (rV_m^2/2gc_p)$$

This equation requires some knowledge of the recovery factor r before it can be used. In the section on recovery factors, however, we found that hardly any data are available on recovery factors for supersonic flows. The absence of such data implies, in turn, that the ex-

perimental data on effective coefficients of heat transfer are probably not suited for accurate calculations. Herein lies one of the weakest members of the structure used in this study. An additional question that introduces some uncertainty in the use of the effective coefficient is what temperature should be used to evaluate the properties of air in any correlation of the heat-transfer test results. The correct answer to this question is not known for large temperature differences. For these reasons, we have treated the effective coefficient in this report more in the nature of a parameter whose proper value can be assessed only through future experimental work.

The effective coefficient of heat transfer has been used throughout this report; in all that follows, the word "effective" will be omitted.

Experimental Data

The experimental data on local heat-transfer coefficients for supersonic flow have been summarized by Johnson, et al.[7] These data were obtained from experiments with supersonic flow of air over a cone and over a flat plate. In addition, a recent piece of test work by Fischer and Norris,[8] by means of analysis of skin-temperature measurements on the nose of a V-2 rocket, has provided more information on these coefficients. Finally, the recent experimental work with air flowing at supersonic velocities in a tube, by Kaye, Keenan, and McAdams,[14] has helped to clarify the situation to a greater degree.

The conclusions drawn from the available test data are summarized as follows:

(*1*) *Laminar Boundary Layer.*—For a laminar boundary layer in either a subsonic or a supersonic stream, the test data on local heat-transfer coefficients are in fair agreement with the theoretical work of Pohlhausen* for incompressible flow over a flat isothermal plate. The equation used for correlation of the local coefficient of heat transfer for subsonic and supersonic velocities does not differ greatly from that used by Johnson, et al.[7]—namely,

$$Nu = hx/k = 0.33Re_x^{1/2}Pr^{1/3} \tag{7}$$

or, in another form,

$$St = h/c_pG = 0.33Re_x^{-1/2}Pr^{-2/3} \tag{8}$$

where the Nusselt and Reynolds Numbers are to be evaluated in terms of the distance from the leading edge, x.

The choice of the temperature to be used in the evaluation of the fluid properties is arbitrary for supersonic flows; various experimenters have used the temperature corresponding to the surface, to ambient conditions just outside the boundary layer, and to diverse combinations of these two. In this paper, the properties of air were evaluated at a temperature corresponding to ambient conditions just outside the boundary layer around the wedge-shaped wing.

(*2*) *Turbulent Boundary Layer.*—For a fully developed turbulent boundary layer in either a subsonic or a supersonic stream, the test data on local coefficients of heat transfer are in fair agreement with the empirical correlation for turbulent subsonic flow over a flat plate—namely,

$$Nu = hx/k = 0.030Re_x^{0.8}Pr^{1/3} \tag{9}$$

or, in another form,

$$St = h/c_pG = 0.030Re_x^{-0.2}Pr^{-2/3} \tag{10}$$

The Nusselt and Reynolds Numbers are to be evaluated in terms of the distance from the leading edge, x. The experimental data for supersonic flow of air in tubes presented by Kaye, Keenan, and McAdams[14] also support the above relation, since these data for the fully developed turbulent boundary layer are well represented by the empirical correlation equation for pipe flow of McAdams;[9] this correlation equation, in turn, does not differ greatly from Eqs. (9) and (10) for turbulent flow of air over a flat plate.

For this paper, the temperature at which the properties of air were evaluated for use in Eqs. (9) and (10) was that corresponding to ambient conditions just outside the boundary layer around the wedge-shaped wing. This choice introduces an uncertainty in the calculations which can be removed only when additional experimental data become available.

(*3*) *Transition from the Laminar to the Turbulent Boundary Layer.*—The supersonic test data mentioned above indicate that an appreciable length of flow is required during the transition from a laminar to a fully developed turbulent boundary layer. Much uncertainty is thereby introduced in the choice of the proper values of the heat-transfer coefficient to be used for a given object such as the wedge-shaped wing. Indeed, the situation is not one inviting accuracy at all, since the "inception of the transition" process is not known with reasonable precision. In addition, the test data for transition were usually obtained under steady-state conditions with almost constant surface temperatures. For a wedge-shaped wing with a variable surface temperature in accelerating flight, it is extremely doubtful that one can do more than make a judicious guess as to the transition region, its inception, or the length of flow required to attain the fully developed turbulent boundary layer. Some theoretical work by Lees[16] on the stability of the laminar boundary layer in a compressible fluid indicates that the point where a small disturbance in the laminar boundary layer begins to grow to one with large amplitudes, and then causes breakdown or instability, is dependent mainly on the Mach Number and the temperature of the surface relative to that of the air. His results indicate that this point of incipient instability is displaced downstream in the

* Pohlhausen's work is summarized in English by Goldstein,[15] pp. 623–631.

flow if either the Mach Number is increased to that of a highly supersonic stream or if the temperature of the surface is reduced below that of the fluid; for these two cases he found that the Reynolds Number was not the important criterion for onset of the transition from laminar to turbulent flow. For the case of the wedge-shaped wing traveling at supersonic speeds, these considerations of stability introduce further uncertainties into the choice of the correct heat-transfer coefficient. If the laminar layer persists for a relatively long distance from the leading edge of this wing, then the coefficients of heat transfer will be reduced in magnitude and the solution of the transient heat-flow problem will be somewhat different from that presented in this paper.

In the absence of data and for the reasons mentioned above, it was assumed that the "point of transition" from a laminar to a turbulent boundary layer is the same for supersonic as for subsonic flow. The value of the critical Reynolds Number, based on distance from the leading edge, at transition was therefore selected as 500,000. This leads to a laminar boundary layer only for a few inches from the leading edge of the wing and to a turbulent boundary layer for the remainder of the wing. Such a selection results in using the much larger surface coefficients of heat transfer over most of the wing and in overestimating the magnitude of the temperature distributions and of the thermal stresses. If a higher value of the critical Reynolds Number had been selected, the results to be given later for the one-dimensional heat-flow problem would not have been affected, but those obtained for two-dimensional heat flow would have been changed slightly.

Calculated Values of the Heat-Transfer Coefficient

Fig. 6 provides a comparison of the calculated heat-transfer coefficients for a laminar and for a turbulent boundary layer on a flat plate for several Mach Numbers at the same free-stream conditions of temperature and density. The three curves marked laminar boundary layer were computed from Eq. (8), with the assumption that it is valid over the distance shown from the leading edge. The remaining three curves are for a turbulent boundary layer and computed from Eq. (10), with the assumption that it is valid from nearly the leading edge of the flat plate. It is evident that the coefficients for the turbulent boundary layer are roughly eight to ten times as large as those for the laminar boundary layer for the same distance from the leading edge and for the same free-stream conditions.

Inability to predict the type of boundary layer on the wedge-shaped wing can thus lead to serious errors in the prediction of the heat-transfer coefficients; the effects of this uncertainty on the final results will be discussed later in greater detail. The properties of air were evaluated at an altitude of 50,000 ft. for a tem-

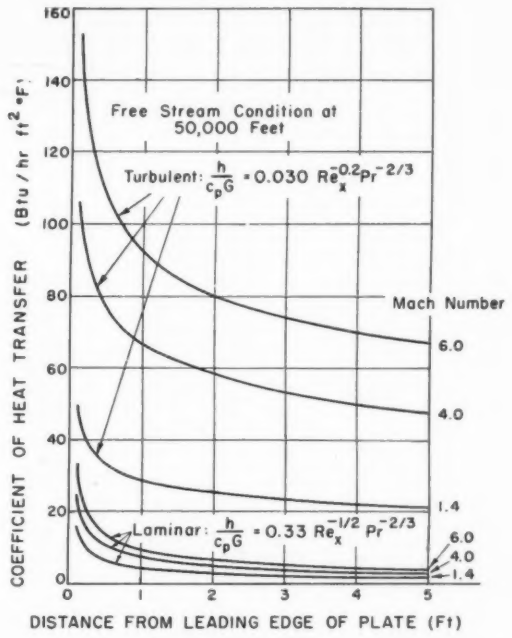

Comparison of Heat Transfer Coefficients for Steady Flow with Laminar and Turbulent Boundary Layers on a Flat Plate.

FIG. 6.

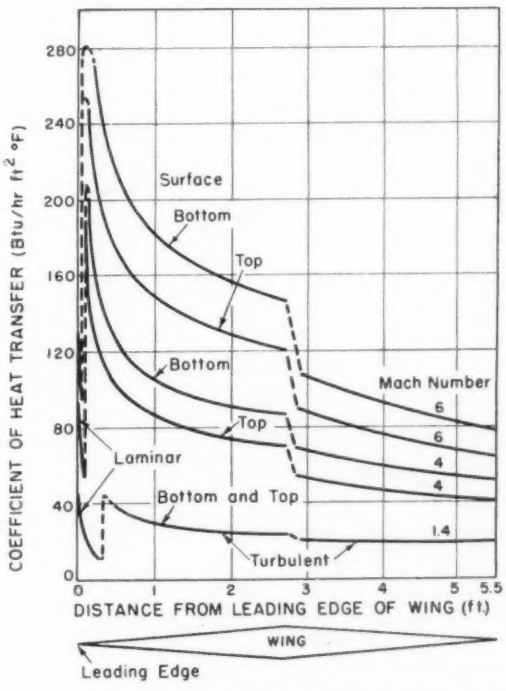

Calculated Values of Coefficients of Heat Transfer for Flight of Wedge Shaped Wing at Constant Mach Number at 50,000 Feet

FIG. 7.

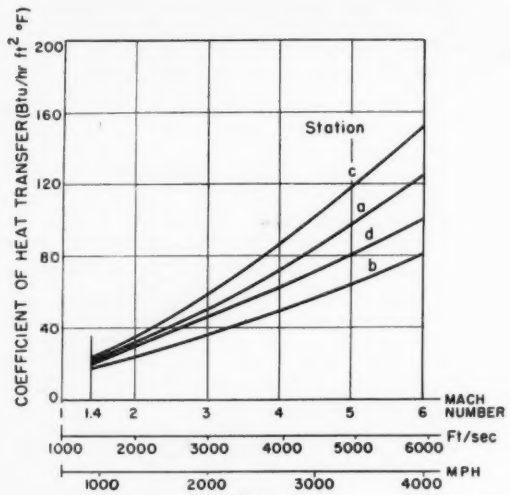

Calculated Values of Coefficients of Heat Transfer for Four Selected Stations on Wedge Shaped Wing for Flight at 50,000 Feet.

FIG. 8.

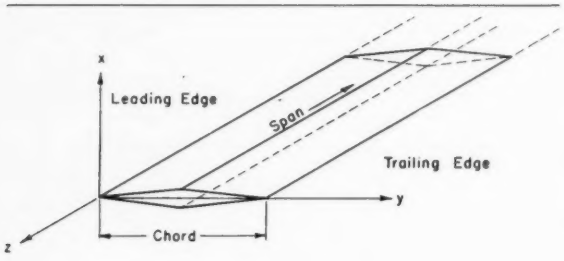

Isometric Sketch of Wedge Shaped Wing Showing Selection of Coordinate System.

FIG. 9.

perature of −67°F. and a density of 0.01161 lb. per cu.ft.

Fig. 7 presents the variations of coefficient of heat transfer actually used in the calculation of the temperature distribution of the wing. The lowest curve, representing the variation along both the top and bottom surfaces for flight at a constant Mach Number of 1.4 at an altitude of 50,000 ft., is actually the average of two curves lying close together. The other curves for Mach Numbers of 4 to 6 show the difference between the coefficients for the top and bottom surfaces of the wing. Each curve starts with a branch corresponding to the laminar boundary layer; this branch is followed by a dashed line that represents the transition region for a critical Reynolds Number of 500,000; finally, the almost discontinuous break at the mid-chord represents the effect of the expansion wave. The variation of the coefficient at the mid-chord is not known, but it is taken to be continuous since, in the absence of experimental data, it is assumed that the boundary layer is continuous in the vicinity of the expansion waves.

Fig. 8 shows the variations of the heat-transfer coefficient for four selected points on the wing for flight at several speeds at 50,000 ft. The relation between heat-transfer coefficient and Mach Number is nearly linear for these four selected points and for most points along the surface of the wing not too close to either the leading or trailing edges. In some of the calculations of this paper it has been assumed that this linear variation is valid; it has helped in reducing both the labor and time required for the solution of the problem. It is evident from the discussion of the experimental data on heat-transfer coefficients for supersonic velocities that this assumption of linear variation of coefficient with Mach Number will not seriously affect the accuracy of the calculated temperature distributions in the wedge-shaped wing.

In the computations of the coefficients of heat transfer in Figs. 7 and 8 for the wedge-shaped wing, Eqs. (8) and (10) were used for the laminar and turbulent boundary layers, respectively. For each of the four regions around the wedge, shown in Fig. 3, the ambient temperature, pressure density, and Mach Number were calculated from the wing loading, angle of attack, lift coefficient, etc. The details are given in Appendix (I). At any point along the surface of wing, the coefficient of heat transfer was then computed from the appropriate equation using the ambient properties of air and the ambient Mach Number. Since the ambient conditions change downstream of the shock waves at the leading edge and downstream of the expansion waves at the mid-chord, the values of the heat-transfer coefficients shown in Figs. 7 and 8 do not correspond exactly to those shown in Fig. 6 for flow over a flat plate with the same free-stream conditions at the several Mach Numbers.

Two-Dimensional Temperature Distribution in the Wing

Differential Equation

Employing the rectangular coordinate system shown in the isometric sketch of the wing in Fig. 9, the differential equation for heat flow in the solid wing is

$$\frac{\partial^2 T}{\partial x^2} + \frac{\partial^2 T}{\partial y^2} + \frac{\partial^2 T}{\partial z^2} = \frac{1}{\alpha}\frac{\partial T}{\partial \theta} \qquad (11)$$

Since we have assumed that the spanwise heat flow is zero, Eq. (11) reduces to the following one for the two-dimensional heat flow:

$$(\partial^2 T/\partial x^2) + (\partial^2 T/\partial y^2) = (1/\alpha)(\partial T/\partial \theta) \qquad (12)$$

In addition, the adiabatic wall temperature and the coefficient of heat transfer are functions of position along the surface of the wing and of time, so we have

$$T_{aw} = f_1(x, y, \theta) \quad (13)$$

$$h = f_2(x, y, \theta) \quad (14)$$

The boundary conditions required for the solution of Eq. (12) are so complex that an analytical solution is impractical. Hence, a long and laborious stepwise method was employed to obtain the transient temperature distribution in the wing.

Calculations

The stepwise numerical solution of Eq. (12) was patterned after the method described by Emmons.[17, 18] This method is the so-called "relaxation" method of Southwell[19] when applied to the case of steady-state problems. In the case of the wedge-shaped wing, it was divided into a set of 113 stations, connected by rods, along which the heat flow was concentrated. For this geometry, illustrated in Fig. 10, the adiabatic wall temperature and heat-transfer coefficients were computed at each of the surface stations for a series of time intervals for a constant acceleration of one Mach Number every 30 sec. (32.4 ft. per sec.^{2}), very nearly 1g. The details of these stepwise calculations are given in Appendix (I). It required a total of 32 time snapshots to cover the range from an initial Mach Number of 1.4 to one of 6.

Results of Calculations of Two-Dimensional Temperature Distribution in Wing

The results based on the numerical method of finite differences for solution of the heat-flow equation in two dimensions are shown quantitatively in Figs. 11 to 19. In order to keep the number of charts within reason, the transient temperature distribution is shown at selected Mach Numbers for several planes and surfaces and at selected planes or stations for all Mach Numbers.

One important feature is immediately visible in these charts: The maximum temperature occurs at the leading and trailing edges of the wing and is equal to the adiabatic wall temperature at a Mach Number of 6, or to about 2,220°F. Because of this high value of the temperature, the leading and trailing edges must be given special attention in the design of any thin sharp wings flying at high supersonic speeds. The transient temperature distribution within 1 or 2 in. from either

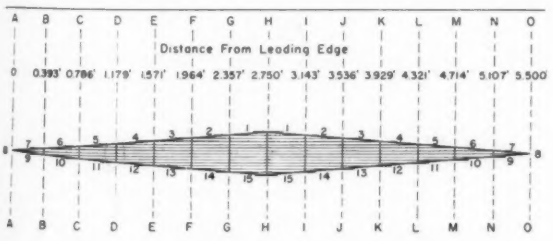

Wedge Shaped Wing Showing Network used for Numerical Solution of Heat Flow in Two Dimensions.

FIG. 10.

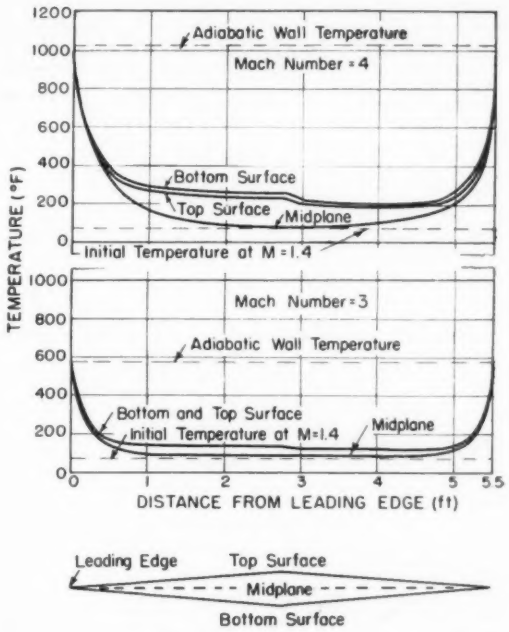

Chordwise Temperature Distribution in Wing from Calculations of Two Dimensional Heat Flow for Constant Acceleration of 1g from a Mach Number of 1.4 to 3 and 4 at 50,000 Feet.

FIG. 11.

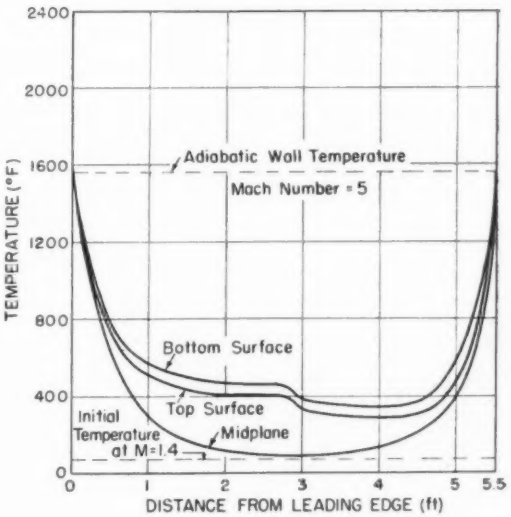

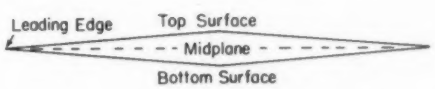

Chordwise Temperature Distribution in Wing from Calculations of Two Dimensional Heat Flow for Constant Acceleration of 1g from a Mach Number of 1.4 to 5 at 50,000 Feet.

FIG. 12.

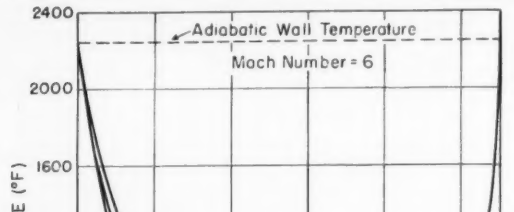

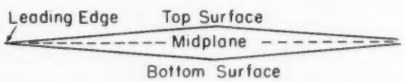

Chordwise Temperature Distribution in Wing from Calculations of Two Dimensional Heat Flow for Constant Acceleration of 1g from a Mach Number of 1.4 to 6 at 50,000 Feet.

FIG. 13.

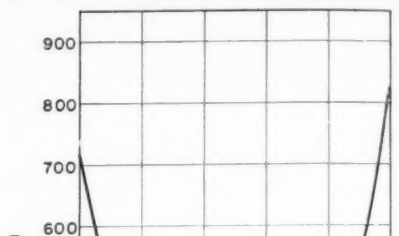

Vertical Temperature Distribution Along Plane F from Calculations of Two Dimensional Heat Flow for Constant Acceleration of 1g from a Mach Number of 1.4 to 2,3,4,5, and 6 at 50,000 Feet

FIG. 15.

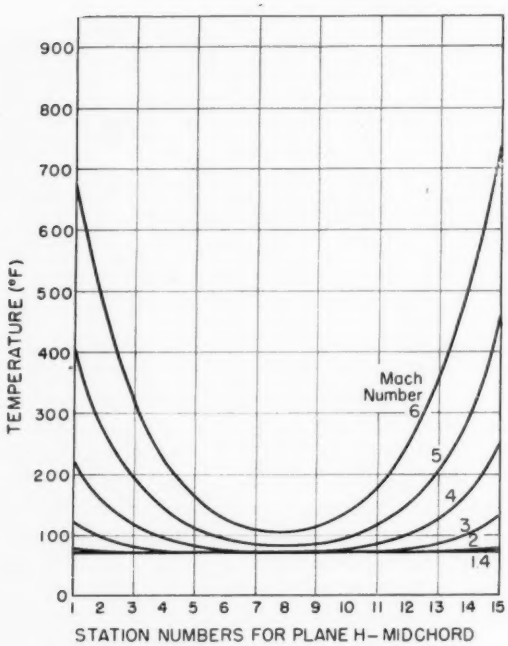

Vertical Temperature Distribution at Midchord from Calculations of Two Dimensional Heat Flow for Constant Acceleration of 1g from a Mach Number of 1.4 to 2,3, 4,5, and 6 at 50,000 Feet.

FIG. 14.

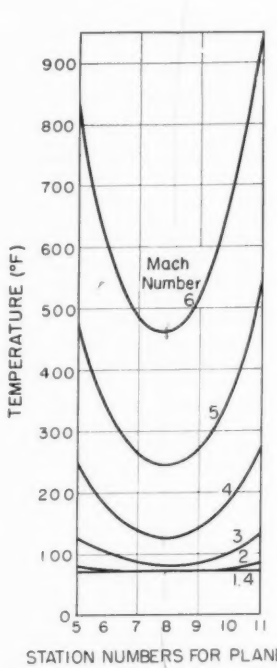

Vertical Temperature Distribution Along Plane D from Calculations of Two Dimensional Heat Flow for Constant Acceleration of 1g from a Mach Number of 1.4 to 2, 3, 4, 5 and 6 at 50, 000 Feet.

FIG. 16.

the leading edge or the trailing edge constitutes a special problem not treated here. If it is desired to use, for the leading and trailing edges, a metal other than steel (such as titanium) or a good thermal insulator (such as a ceramic), then the transient temperature distribution could be obtained in terms of the properties of these materials by numerical methods similar to those used here.

These charts also show that the temperature of the bottom surface of the wing is always larger than the temperature of the top surface. This difference in temperature is a result of the larger coefficients of heat transfer on the bottom surface of the wing as compared to those on the top surface. In addition, both surface temperatures are considerably larger than the mid-plane temperature; the maximum difference in these temperatures occurs near the mid-chord, where one would naturally expect to find the largest thermal lag of the wing.

These charts also illustrate the significant difference in chordwise and vertical temperature gradients in the wing. The calculations indicate that the temperature gradient perpendicular to the chord—the vertical direction—is several times as large as the chordwise temperature gradient, except perhaps in the immediate vicinity of the leading and trailing edges. This large difference in temperature gradient is important in this study, for it indicates that we would be amply justified in treating the heat flow as a one-dimensional rather than as a two-dimensional problem.

Figs. 11, 12, and 13 show the temperature distribution in the chordwise direction of the wing along the top and bottom surfaces and along the mid-plane or chord

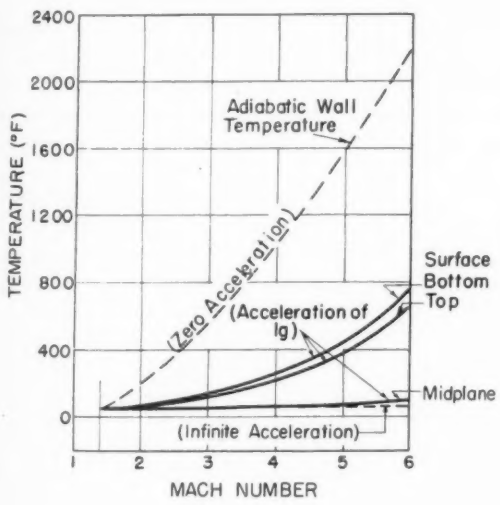

Temperature Distribution at Midchord from Calculations of Two Dimensional Heat Flow for Constant Acceleration of 1g from a Mach Number of 1.4 at 50,000 Feet.

FIG. 17.

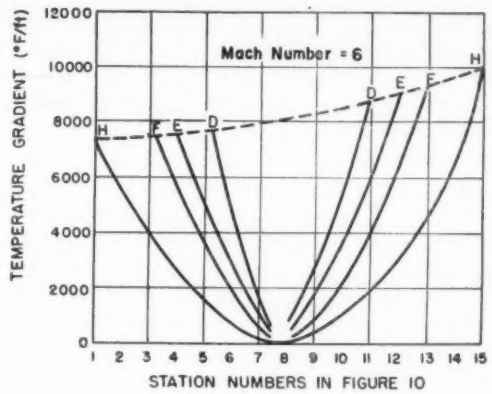

Temperature Gradients Along Vertical Planes in Wing from Calculations of Two Dimensional Heat Flow for Constant Acceleration of 1 g from Mach Number 1.4 to 6 at 50,000 Feet.

FIG. 18.

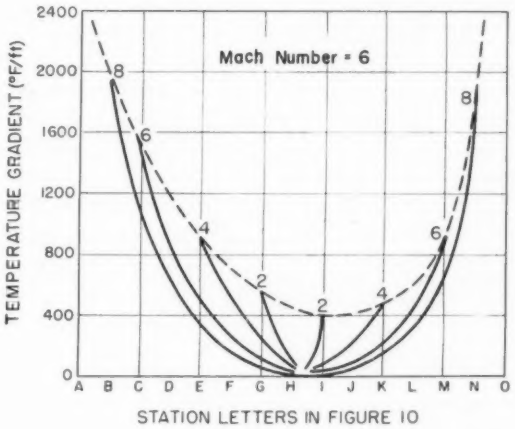

Temperature Gradients Along Horizontal Planes in Wing from Calculations of Two Dimensional Heat Flow for Constant Acceleration of 1g from a Mach Number of 1.4 to 6 at 50,000 Feet.

FIG. 19.

for selected Mach Numbers. In each chart, the dashed line at the bottom represents the initial uniform temperature of the wing for steady flight at a Mach Number of 1.4, and the dashed line at the top represents the maximum temperature available for heat flow at the given time, or the adiabatic wall temperature. Thus, a comparison can be quickly made of the rise in temperature at a given point of the wing at various times of flight and of the temperature difference that is causing heat flow at these Mach Numbers.

In Fig. 11, the temperatures are shown for Mach Numbers of 3 and 4, after constant acceleration of 1g from the initial Mach Number of 1.4. It is apparent that the surface temperatures are rising slowly, except in the immediate vicinity of the leading and trailing edges. In addition, there is a considerable lag in the temperature rise along the mid-plane except near the

leading and trailing edges. Figs. 12 and 13, for Mach Numbers of 5 and 6, respectively, illustrate this behavior even more clearly. The temperature distributions for the upper and lower surfaces show distinct dips in the vicinity of the mid-chord of the wing. These dips result from the sudden dips in the surface coefficients of heat transfer, shown in Fig. 7, which are caused by the change in ambient properties of the air in the rear half of the wing after passing through the expansion waves at the mid-chord. It will be noticed that there is no dip in the same region for the various curves of mid-plane temperature. The absence of the dips here is explained, in part, by the thermal lag of the mid-plane which would tend to smooth out such a dip and, in part, by the use of a "coarse" network of 113 points in the two-dimensional calculations of heat flow.

The two-dimensional temperature distributions could also be drawn at selected Mach Numbers along planes parallel to the four surfaces of the wing. This, however, was not attempted here because the number of charts would soon become unreasonably large. Hence, the temperature distributions were plotted for selected planes parallel and perpendicular to the chord. These planes correspond to the vertical planes labeled by letters A to O and to the horizontal planes labeled by numbers 1 to 15 in Fig. 10. It was again necessary to select only a few interesting charts from the total number available.

Figs. 14, 15, and 16 present the vertical temperature distributions for several Mach Numbers at planes H, F, and D, shown in Fig. 10, and corresponding to the mid-chord, to about 2 ft. and 1.2 ft. from the leading edge, respectively. Similar curves would be obtained if we plotted the temperature distributions for vertical planes corresponding to the same distances from the trailing edge. The scales used in Figs. 14, 15, and 16 are the same, but the decreasing width of the abscissa corresponds to the decreasing thickness of the wing as we move from the mid-chord to the leading edge. These curves illustrate again the thermal lag of the interior of the wing at all planes perpendicular to the chord except near the edges. Curves of temperature distribution along planes parallel to the chord are not included here, since they would be similar to those shown in Figs. 14, 15, and 16.

Fig. 17 shows the temperature distribution at the mid-chord as a function of Mach Number and of time. The temperature at the mid-plane rises slightly above the initial value. The difference between the adiabatic wall temperature and either top or bottom surface temperature is much larger than the temperature difference between either surface and the mid-plane. This effect is due to the much greater resistance to heat transfer along the air-to-metal path, as compared to the thermal resistance of the metal itself, and to the fairly large acceleration of 1g used in the calculations.

Effect of Variable Acceleration

Although the effect of variable acceleration was not studied by the numerical method used for two-dimensional heat flow, the limiting magnitudes of the acceleration are evident in Fig. 17 for finite values of the coefficient of heat transfer. If we consider the limit of an infinitesimal acceleration, then the temperature distribution in the wing is that for steady flight at the given Mach Number; this is nearly a uniform temperature that is equal to the adiabatic wall temperature. Hence, the curve so labeled in Fig. 17 represents very nearly the temperature distribution for zero acceleration with a finite heat-transfer coefficient. If we consider the other limit of an infinite acceleration, then the temperature distribution throughout the wing will be a straight line representing the initial temperature at a Mach Number of 1.4 as long as the heat-transfer coefficient is less than infinite. Therefore, it is evident that, as the acceleration decreases from infinity to zero, all the resultant temperature distributions must lie between the curve for the adiabatic wall temperature and the straight line representing the initial temperature. These curves are so labeled in Fig. 17.

Temperature Gradients in Wing

Figs. 18 and 19 show approximate values of the temperature gradients along vertical and horizontal planes in the wing, respectively, at a Mach Number of 6 after constant acceleration of 1g. The scales in Figs. 18 and 19 are different. Inspection shows that the temperature gradients in a vertical plane are larger by a considerable factor than those in the horizontal plane, with the exception of those near the leading and trailing edges. Since these calculations of two-dimensional heat flow are not valid at the edges because of the "coarse" network of points used, we feel that the edge problem should be treated separately. It should be noted that, in Fig. 18, the temperature gradients for the rear half of the wing are practically the same as those for the front half for the corresponding vertical planes and therefore are omitted from this figure. For the same reason, only the temperature gradients for horizontal planes in the top half of the wing are shown in Fig. 19. We note from Figs. 18 and 19 that the two families of curves representing the temperature gradients along vertical and horizontal planes are slightly asymmetrical about the mid-chord and the mid-plane, respectively. In addition, the positions of zero temperature gradients are displaced slightly from the centers of the mid-chord and of the mid-plane; the small displacements are caused by the slight degree of asymmetry of the two-dimensional heat flow in the wedge-shaped wing. In conclusion, it is evident from Figs. 18 and 19 that the two-dimensional heat flow can be successfully reduced to a one-dimensional problem without introducing serious errors in the resultant tem-

perature distributions; both the large ratios of temperature gradients and of areas normal to the direction of heat flow support this result.

One-Dimensional Heat Flow in Wing

The stepwise numerical method used in the calculation of the transient two-dimensional temperature distribution in the wing was a long and tedious process. It was natural, therefore, to seek shorter methods of calculation for the solution of the differential equation of heat flow with boundary conditions dependent on time. Several shorter methods were found and used; all were based on the assumption that the temperature distribution along a line perpendicular to the chord of the wing can be obtained from the one-dimensional heat flow along this line. In other words, the chordwise heat flow was neglected. The results from the previous calculations of the two-dimensional heat flow showed that this assumption would probably introduce negligible errors at all points in the wing except near the leading and trailing edges. This prediction has been verified from the calculations based on heat flow in one dimension for the thin wedge-shaped wing.

Many important advantages were obtained upon simplifying the problem to heat flow in one dimension. Both numerical and analytical solutions were found. The numerical solution required only a small fraction of the time input necessary in the two-dimensional case. In addition, the number of variables which could be studied by this shorter numerical solution was practically unlimited; these variables included the thickness, surface coefficient, acceleration, type of material, etc.

Analytical solutions of the one-dimensional heat flow were found based on special assumptions of the variation of coefficient of heat transfer with time. In order to keep the size of this paper within reasonable bounds, the presentation of the analytical solutions will be given at a later date.

Numerical Method of Solution of One-Dimensional Heat Flow

Consider first the special case of the wedge-shaped wing shown in the sketch in Fig. 9. This wing is flying steadily at a Mach Number of 1.4 at an altitude of 50,000 ft.; it is suddenly subjected to a constant acceleration of 1g until it reaches a Mach Number of 6; then it is flown steadily at a Mach Number of 6. For the transient heat flow during the period of constant acceleration, we will show how the temperature distribution can be estimated rapidly and quantitatively by the assumption of one-dimensional heat flow perpendicular to the chord. In addition, the resulting method can be easily generalized to apply to any thin wing, provided the variation of the local surface coefficient of heat transfer with the time of flight is known.

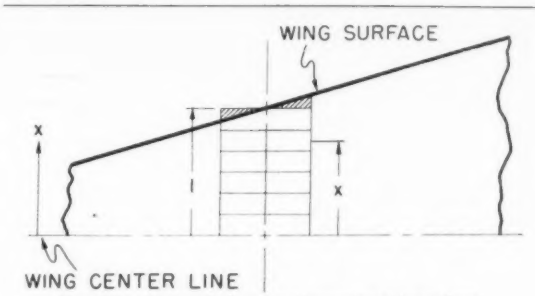

FIG. 20. Network for one-dimensional heat flow.

The mathematical problem is greatly simplified by the assumption of one-dimensional heat flow. Using the coordinate system of Fig. 9, the differential equation is

$$\partial^2 t/\partial x^2 = (1/\alpha)\,(\partial t/\partial \theta) \tag{15}$$

The heat flow is thus along a thin section normal to the chord, as shown in Fig. 20 where l is one-half the wing thickness at the given point along the chord. The three boundary conditions are then as follows:

$$\text{(1) At } \theta = 0,\ t = t_{aw} \tag{16}$$

$$\text{(2) At } x = 0,\ \partial t/\partial x = 0 \tag{17}$$

$$\text{(3) At } x = l,\ k\,(\partial t/\partial x) = h(t_{aw} - t_s) \tag{18}$$

We assume in condition (1) that the initial temperature throughout the thin section is uniform and equal to the adiabatic wall temperature for steady flight at a Mach Number of 1.4. In addition, since the local coefficient of heat transfer and the adiabatic wall temperature are functions of time, we can also write

$$h = f_3(\theta) \tag{19}$$

$$t_{aw} = f_4(\theta) \tag{20}$$

Since the position of this thin section from the leading edge is considered fixed, h and t_{aw} depend only on the time of flight. It is primarily for this reason that we can generalize this treatment to the case of any thin wing and solve for the temperature distribution, provided the functions in Eqs. (19) and (20) are available for a given point on the wing.

The numerical method of solution of Eq. (15) with the boundary conditions given in Eqs. (16), (17), and (18) was similar to that described by Emmons[17, 18] and McAdams.[9] The thin section normal to the chord was subdivided into a finite number of parts, and the temperature rise of each part was computed by a repetitious stepwise procedure covering the entire time period of constant acceleration. For large values of the acceleration, a small number of time snapshots was sufficient; the entire calculation then required a few man-hours. For small values of the acceleration, many more time snapshots were needed, and the time of calculation ran to as much as 3 man-days per temperature distribution.

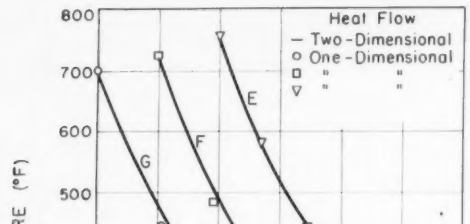

Comparison of Temperature Distributions Calculated from Heat Flow in One and Two Dimensions for Vertical Planes G, F, and E for Constant Acceleration of 1 g from a Mach Number of 1.4 to 6 at 50,000 Feet.

FIG. 21.

Results of Numerical Method of Solution of Heat Flow in One Dimension

The first objective of the numerical method of solution based on heat flow in one dimension was to discover the magnitude of the error that results from this simplification. This objective was accomplished by making a sufficiently large number of calculations with this shorter method so that comparisons could be made with the temperature distributions obtained from the time-consuming calculations based on two-dimensional heat flow for the same set of flight conditions and of variation of local coefficient of heat transfer with time. The second objective was to investigate the variation of a number of important variables, such as local coefficient of heat transfer, acceleration, thickness of the wing, size of the network in calculations, etc.

Fig. 21 presents a comparison of the temperature distributions calculated from the numerical methods of solution for heat flow in one and in two dimensions. The temperature distributions shown here are only for the top half of the wing for vertical planes G, F, and E shown in Fig. 10, so that the station numbers refer only to those in the top half of the wing. The solid curves in Fig. 21 represent the temperature based on two-dimensional heat flow and are identical with similar lines shown previously. The circles, squares, and triangles represent the temperatures based on the numerical method of solution for one-dimensional heat flow. The comparison of the temperatures is also made in the form of the deviation plot under the main chart in Fig. 21. Here the deviations of the temperatures calculated from one-dimensional heat flow from those based on two-dimensional heat flow are plotted against station number. This deviation plot was required in order to show the small differences in temperatures calculated from the two different methods.

The comparison, shown in Fig. 21, of the temperature distribution based on the two methods of calculation was made for identical conditions of flow, acceleration, wing geometry, coarseness of network, etc., and for the same variation of coefficient of heat transfer with time. The largest deviation is less than 10°F. Similar comparisons were made of the temperature distributions for Mach Numbers of 3, 4, and 5, but the maximum deviation occurred in the comparison shown in Fig. 21 for a Mach Number of 6. The deviations plotted in this figure show a small systematic trend that is most evident at the centerline station 8; the points deviate increasingly from the solid lines as we move toward the leading edge of the wing—i.e., from G to F to E—since heat flow from the hotter lower half of the wing was present in the two-dimensional calculations but not in the one-dimensional points. The erratic scattering in Fig. 21 is believed to be due to computational errors. The conclusion is that the simplification to heat flow in one dimension introduces a negligible error compared to the temperatures calculated from two-dimensional heat flow with the same coarseness of network of stations.

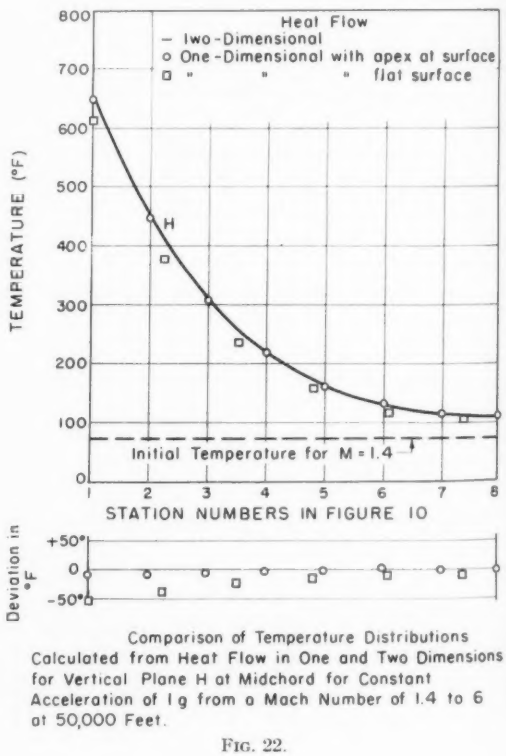

Comparison of Temperature Distributions Calculated from Heat Flow in One and Two Dimensions for Vertical Plane H at Midchord for Constant Acceleration of 1 g from a Mach Number of 1.4 to 6 at 50,000 Feet.

FIG. 22.

Fig. 22 presents a comparison of the temperature distributions, along vertical plane H at the mid-chord, calculated from the numerical methods of solution for heat flow in one and in two dimensions. The temperature deviations based on the two-dimensional method are also given. The comparisons were made for identical conditions of flow, acceleration, wing geometry, coarseness of network, etc., and for the same variation of coefficient of heat transfer with time. These comparisons are indicated by the solid curve for the two-dimensional case and by the circles for the one-dimensional case. In addition, another comparison has been added to this chart to illustrate the effect of replacing the triangular top of the section centered at plane H by a flat surface coincident with horizontal plane 1 for the method of one-dimensional heat transfer; this change in geometry results in a change of volume of the material assigned to the surface station; the temperatures calculated with this geometry are shown by the squares. Comparisons similar to those shown in Fig. 22 were made for Mach Numbers of 3, 4, and 5, but the extreme deviations were found to occur for a Mach Number of 6.

For the same conditions of geometry the deviations shown in Fig. 22 are less than 10°F. for a Mach Number of 6. If the surface geometry is changed by replacing the triangular top of the center of the wedge-shaped wing with a flat surface passing through the apex, then the surface temperature based on one-dimensional heat flow will be about 40°F. lower than that obtained from the two-dimensional calculations; for the stations inside the wing the deviation will be considerably less. The deviations found for this change in surface geometry are caused by the comparatively large change in volume of the material assigned to the surface station when the same coarseness of network is used.

The comparisons in Figs. 21 and 22 establish quantitatively that the complicated calculation of two-dimensional heat flow can be replaced by a number of simpler calculations based on heat flow in one dimension for the same local coefficients of heat transfer. This simpler calculation could be applied with success to the temperature distribution near the leading and trailing edges if the local heat-transfer coefficients were available.

Effect of Variable Coefficient of Heat Transfer

The simple numerical method of solution of heat flow in one dimension was used to investigate the effect of changes in several variables. Similar studies could not have been made in the time available if only the method based on two-dimensional heat flow had been used. In addition to providing results quickly, the simpler method proved to be a valuable aid in guiding the analytical studies that were carried on simultaneously. The first variable studied was the local coefficient of heat transfer; the comparison of surface temperatures for several variations of coefficient with time or Mach Number is given in Fig. 23 for an acceleration of $2g$. Similar charts were drawn for stations inside the wing, but the differences in temperature between the curves for the three variations of coefficient were less than those shown for the curves for the surface station.

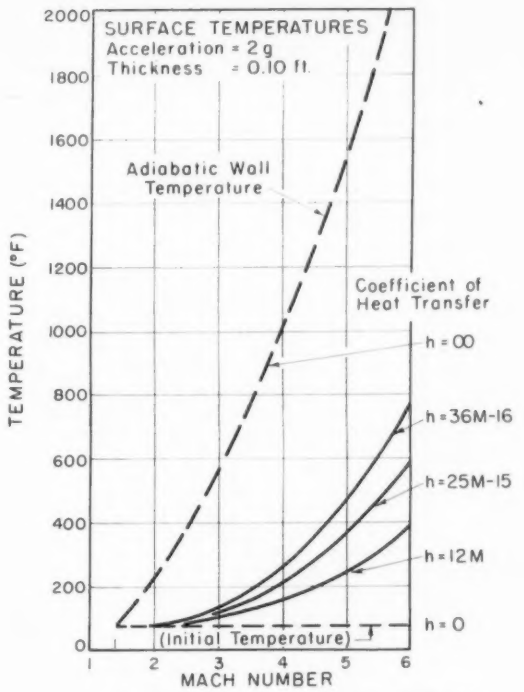

Comparison of Surface Temperatures for Several Variations of Heat Transfer Coefficient with Time Calculated from Heat Flow in One Dimension for Constant Acceleration of 2 g at 50,000 Feet.

FIG. 23.

All temperature curves for various values of the coefficient lie between the limits of curves for zero and for infinite coefficient; for the case of zero coefficient, the surface temperature is the initial temperature and, for infinite coefficient, is the same as the adiabatic wall temperature. The three linear relations between coefficient and Mach Number used in the calculations are good approximations for three different positions along the wedge-shaped wing to the actual variation of coefficient with time. It is evident that the temperature distributions cannot be calculated accurately unless the relation of coefficient of heat transfer with time is also given accurately.

Effect of Variable Acceleration

Fig. 24 presents a comparison of surface temperatures for the entire range of values of the acceleration calculated from the numerical method of solution of one-dimensional heat flow. Similar charts were constructed for the temperature at internal stations; on

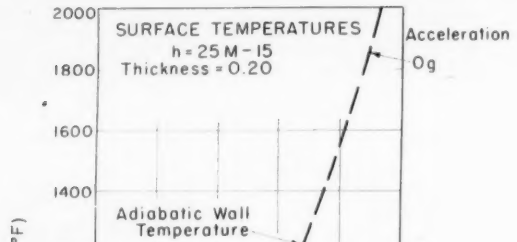

Comparison of Surface Temperatures for Several Accelerations Calculated from Heat Flow in One Dimension for Flight at 50,000 Feet.

FIG. 24.

these charts the curves for the various values of the acceleration tended to crowd together more than those on Fig. 24. For infinite acceleration the surface temperature remains equal to the initial temperature. For zero acceleration, the surface temperature equals the adiabatic wall temperature; hence, the temperature curves for finite acceleration lie between these two limits. It is seen from Fig. 24 that the selection of an acceleration of 1g for the calculation of the two-dimensional heat flow resulted in temperature values about halfway between the extreme values possible.

Effect of Size of Network

The effect of change of size of network was studied by means of the numerical method for heat flow in one dimension. It was found that halving the length of the rods connecting the stations shown in Fig. 10—or in other words, increasing the number of stations in the one-dimensional case from 6 to 12—resulted in a maximum difference of 17°F. in the temperature of the surface station for the extreme case of a Mach Number of 6. The error introduced by the uncertainty in the value of the coefficient of heat transfer alone would probably be larger than this figure. Hence, it is concluded that the numerical method of solution with the coarse network used in the one-dimensional heat flow is a satisfactory solution to the problem, with an error probably much less than that introduced by the basic data.

CONCLUSIONS

Calculations of heat flow in two dimensions for a wing flying at supersonic speeds, with boundary conditions dependent on time from a Mach Number of 1.4 to one of 6, have shown the following:

(1) The leading and trailing edges of the wing are the most severely affected by aerodynamic heating.

(2) The temperature distribution in the wing as a function of time of flight.

(3) The temperature gradients at a Mach Number of 6 are considerably larger in the vertical direction than in the chordwise direction.

(4) The flow of heat could be approximated with small error by one-dimensional flow.

Calculations of heat flow in one dimension with boundary conditions dependent on time—namely, perpendicular to the chord—have shown the following:

(1) The error made in assuming heat flow in one rather than in two dimensions is negligible for thin wings for practical purposes.

(2) The effects of variable coefficients of heat transfer, of variable acceleration, and of size of network have been examined.

These calculations are strongly dependent on the state of the art of heat transfer at supersonic speeds. Since the state of the art is poor, much experimental work is needed to verify the basis of these calculations.

Finally, these calculations of transient temperature distribution in the wing form the basis for the calculation of thermal stresses and aerodynamic deflections of the wing.

REFERENCES

[1] Keenan, J. H., and Kaye, J., *Gas Tables*, John Wiley & Sons, Inc., New York, 1948.

[2] Wood, G. P., *Calculation of Surface Temperatures in Steady Supersonic Flight*, N.A.C.A. T.N. No. 1114, 1946.

[3] Scherrer, R., *The Effects of Aerodynamic Heating and Heat Transfer on the Surface Temperature of a Body of Revolution in Steady Supersonic Flight*, N.A.C.A. T.N. No. 1300, 1947.

[4] Stalder, R. S., and Jukoff, D., *Heat Transfer to Bodies Travelling at High Speed in the Upper Atmosphere*, N.A.C.A. T.N. No. 1682, 1948.

[5] Huston, W. B., Warfield, C. N., and Stone, A. T., *A Study of Skin Temperatures of Conical Bodies in Supersonic Flight*, N.A.C.A. T.N. No. 1724, 1948.

[6] Lo, H., *Determination of Transient Skin Temperature of Conical Bodies During Short-Time, High-Speed Flight*, N.A.C.A. T.N. No. 1725, 1948.

[7] Johnson, H. A., Rubesin, M. W., Sauer, F. M., Slack, E. G., and Possner, L., *A Design Manual for Determining the Thermal Characteristics of High Speed Aircraft*, A.A.F. Technical Report 5632, 1947.

[8] Fischer, W. W., and Norris, R. H., *Supersonic Convective Heat-Transfer Correlation from Skin-Temperature Measurements on a V-2 Rocket in Flight*, Paper No. 48-A-54, presented at the Annual Meeting, 1948, A.S.M.E.

[9] McAdams, W. H., *Heat Transmission;* McGraw-Hill Book Company, Inc., New York, 1942.

[10] Carslaw, H. S., and Jaeger, J. C., *Conduction of Heat in Solids;* Oxford Press, 1947.

[11] Ivey, H. R., *Notes on the Theoretical Characteristics of Two-Dimensional Supersonic Airfoils*, N.A.C.A. T.N. No. 1179, 1947.

[12] Ivey, H. R., Stickle, G. W., and Schuettler, A., *Charts for Determining the Characteristics of Sharp-Nose Airfoils in Two-Dimensional Flow at Supersonic Speeds*, N.A.C.A. T.N. No. 1143, 1947.

[13] McAdams, W. H., Nicolai, L. A., and Keenan, J. H., *Measurements of Recovery Factors and Coefficients of Heat Transfer in a Tube for Subsonic Flow of Air*, Trans. A.I.C.E., Vol. 42, pp. 907–925, 1946.

[14] Kaye, J., Keenan, J. H., and McAdams, W. H., *Report of Progress on Measurements of Friction Coefficients, Recovery Factors, and Heat Transfer Coefficients for Supersonic Flow of Air in a Pipe*, presented at the Fluid Mechanics and Heat Transfer Institute, Berkeley, Calif., June, 1949.

[15] Goldstein, S., *Modern Developments in Fluid Mechanics;* Oxford University Press, 1938.

[16] Lees, L., *The Stability of the Laminar Boundary Layer in a Compressible Fluid*, N.A.C.A. T.N. No. 1360, 1947.

[17] Emmons, H. W., *The Numerical Solution of Heat-Conduction Problems*, Trans. A.S.M.E., Vol. 65, pp. 607–615, 1943.

[18] Emmons, H. W., *The Numerical Solution of Partial Differential Equations*, Quart. of Appl. Math., Vol. II, No. 3, pp. 173–195, 1944.

[19] Southwell, R. V., *Relaxation Methods in Engineering Science*, Oxford University Press, 1946.

JAS Dec. 1950

Appendix (I)—Calculations of Heat Flow in Two Dimensions

Supersonic Flow About Wedge-Shaped Wing

Consider the supersonic flow pattern shown in Fig. 25. There are four regions of the flow path wherein the properties of air are needed for the calculations of two-dimensional heat flow; these regions are indicated on this figure by subscripts 1, 2, 3, and 4. The symbols used, given in the beginning of this paper, are the same, in general, as those given on page 129 of reference 1. In the following sample calculations, the data in references 1 and 12 were used for the properties of supersonic flow.

Sample Calculations for Wing Flying at a Mach Number of 2

Assumptions: (1) Mach Number is 2; (2) steady flight at 50,000 ft.; (3) wing loading is 100 lbs. per sq.ft.

Calculations: From Table 60 of *Gas Tables*, for 50,000 ft. we get

$$T_0 = -67°\text{F.} = 393°\text{F. absolute}$$
$$\rho_0 = 0.0116 \text{ lb. per cu.ft.}$$
$$p_0 = 1.69 \text{ lbs. per sq.in. absolute}$$

From Table 2 of *Gas Tables*, the velocity of sound at 393°F. absolute is

$$a_0 = 971 \text{ ft. per sec.}$$

The velocity is then

$$V_0 = M_0 a_0 = 1{,}942 \text{ ft. per sec.}$$

From the definition of lift coefficient we get

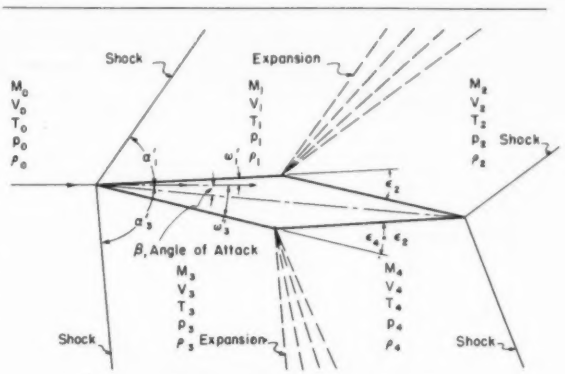

Sketch Showing Details of Supersonic Flow Pattern in Four Regions About Wedge Shaped Wing

FIG. 25.

$$C_L = \frac{W/S}{\rho V^2/2g} = \frac{100}{(0.0116)(1{,}942^2)/(2)(32.2)} = 0.147$$

From Fig. 6 of reference 11, we find, for a Mach Number of 2, that the slope of the curve of lift coefficient versus angle of attack is

$$dC_L/d\beta = 0.041$$

Hence, the angle of attack is

$$\beta = 0.147/0.041 = 3.58°$$

The symmetrical double-wedge wing has a maximum thickness of 8 per cent. This results in a half angle of 4.59°. The wedge angle for the shock at the upper leading edge of region 1 is then

$$\omega_1' = 4.59° - \beta = 1.01°$$

With this value of the wedge angle and the value of Mach Number upstream of the shock (M_0 here and M_x in *Gas Tables*), we enter Table 56 of *Gas Tables*, and, for the angle between the shock and the incident flow, we find

$$\alpha_1' = 30.8°$$

From Table 57 of *Gas Tables*, with ω' and α', we find the Mach Number downstream of the shock in region 1

$$M_1 = 1.97$$

From Table 58 of *Gas Tables*, we get the ratio of downstream to upstream pressure for the shock and therefore the pressure in region 1

$$p_1/p_0 = 1.06$$
$$p_1 = (1.06)\ (1.69) = 1.79 \text{ lbs. per sq.in. absolute}$$

From Table 59 of *Gas Tables*, we get the ratio of downstream to upstream density for the shock and therefore the density in region 1

$$\rho_1/\rho_0 = 1.04$$
$$\rho_1 = (1.04)(0.0116) = 0.0121 \text{ lb. per cu.ft.}$$

The temperature in region 1 is obtained by applying

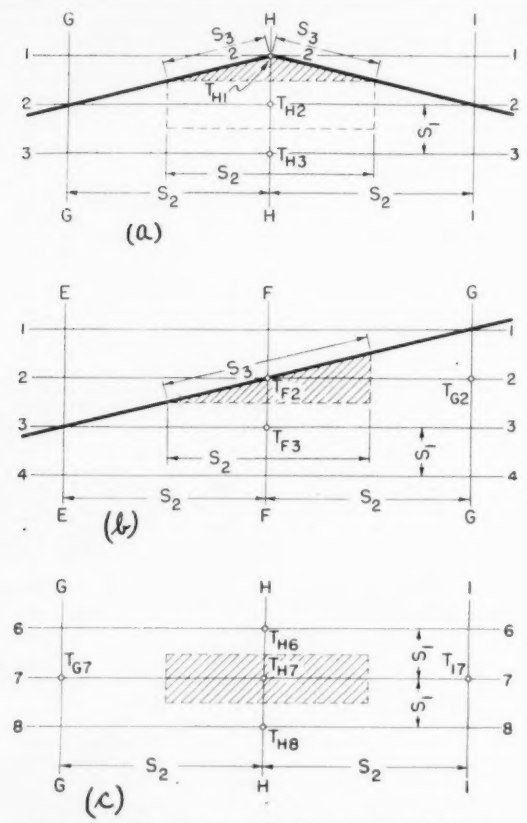

FIGS. 26a, 26b, and 26c. Details of network for two-dimensional heat flow.

the perfect gas relationship for air as follows:

$$T_1/T_0 = (p_1/p_0)\,(\rho_0/\rho_1)$$
$$\rho_1 = (1.06)/(1.04) = 1.02$$

and so

$$T_1 = (1.02)(393) = 399°\text{F. absolute}$$

The velocity is given by

$$V_1/V_0 = (M_1/M_0)\sqrt{T_1/T_0}$$

and so

$$V_1 = 1{,}942\left(\frac{1.97}{2.00}\right)\sqrt{\frac{399}{393}} = 1{,}920 \text{ ft. per sec.}$$

All ambient properties of air in region 1 are now known.

The air passes through an expansion wave in flowing from region 1 to 2. From Table 54 of *Gas Tables* and the Mach Number before the expansion, M_1, we find the vector angle of the characteristic curve in the hodograph plane

$$\omega_1 = 25.50°$$

Since the airflow changes its direction through the expansion, we get, for the vector angle of the characteristic curve in the hodograph plane for region 2,

$$\omega_2 = \omega_1 + \epsilon_2 = 25.5° + 9.18° = 34.7°$$

From Table 54,[1] the Mach Number downstream of the expansion in region 2, M_2, is found from this value of ω_2

$$M_2 = 2.32$$

From Table 54,[1] we get

$$M_1 = 1.97, \quad p_1/p_0 = 0.134, \quad \rho_1/\rho_0 = 0.238$$
$$M_2 = 2.32, \quad p_2/p_0 = 0.0795, \quad \rho_2/\rho_0 = 0.161$$

Hence, we find

p_2 = 1.06 lbs. per sq.in. absolute
ρ_2 = 0.0822 lb. per cu.ft.

$$T_2 = T_1\left(\frac{p_2}{p_1}\right)\left(\frac{\rho_1}{\rho_2}\right) = 348°\text{F. absolute}$$

$$V_2 = V_1\left(\frac{M_2}{M_1}\right)\sqrt{\frac{T_2}{T_1}} = 2{,}110 \text{ ft. per sec.}$$

The ambient properties of the air in region 2 are now known. The properties in regions 3 and 4 were calculated similarly.

The properties of air computed for the four regions of the wing are summarized in Table 1.

Numerical Method of Solution for Two- Dimensional Heat Flow

The preceding calculations show the method of obtaining the supersonic flow conditions about the wedge-shaped wing. The method of calculation of the two-dimensional heat flow is presented here. Consider the wedge-shaped wing subdivided into a network of 113 stations in a plane normal to the span, as shown in Fig. 10. We assume that the stations are connected by rods along which heat flow is concentrated between pairs of stations. Details of three typical stations and of the areas (or volume if the third dimension along the span is included) associated with these rods are shown in Fig. 26. Thus an internal station, H7, is shown in Fig. 26c and the area associated with it is represented by the shaded area centered on H7. A typical surface station, F2, is shown in Fig. 26b, and, finally, the mid-chord station is shown in Fig. 26a. The two-dimensional heat flow is then broken up into one-dimensional heat flow between any one station and its closest neighbors along the net of connecting rods. For any pair of stations we used the differential equation for heat flow in finite difference form, given by

$$Q = -kA\,(\Delta T/\Delta x)\,\Delta\theta \qquad \text{(A-1)}$$

Let us apply this to a typical internal station, to a typical surface station, and to the mid-chord station and use the symbols given in Fig. 26.

(*a*) *Typical Internal Station.*—The heat flow during a time interval $\Delta\theta$ into station H7 from station H8 is simply

$$Q = kS_2[(T_{H8} - T_{H7})/S_1]\,\Delta\theta$$

TABLE 1

Properties of Air in Regions Around Wedge-Shaped Wing Moving at Three Supersonic Speeds

Flight Mach Number, M_0	Angle of Attack, β (Deg.)	Region	Wedge Angle for Shock, ω'	Angle Between Shock and Incident Flow, α'	Turning Angle in Expansion, ϵ	Ambient Mach Number, M	Ambient Velocity, v (Ft. per Sec.)	Ambient Temperature, T (°F. Absolute)	Ambient Pressure, p (Lbs. per Sq.In. Absolute)	Ambient Density, ρ (Lbs. per Cu.Ft.)
2.00	3.58	1	1.01	30.8		1.97	1,920	399	1.79	0.0121
		2			9.18	2.32	2,110	348	1.06	0.00822
		3	8.17	37.4		1.70	1,760	445	2.63	0.0159
		4			9.18	2.03	1,940	384	1.59	0.0112
4.00	1.89	1	2.70	16.3		3.80	3,840	426	2.21	0.0140
		2			9.18	4.54	4,010	325	0.847	0.00705
		3	6.48	19.2		3.53	3,750	471	3.14	0.0180
		4			9.18	4.19	3,900	364	1.28	0.00950
6.00	1.21	1	3.38	11.9		5.59	5,820	452	2.75	0.0164
		2			9.18	6.95	6,020	308	0.682	0.00597
		3	5.80	13.8		5.20	5,720	505	3.78	0.0202
		4			9.18	6.46	5,970	358	1.01	0.00763

Upstream Conditions

Altitude = 50,000 ft.
Wing loading = 100 lbs. per sq.ft.
Maximum wing thickness = 8 per cent
Included wedge angle = 9.18°

Temperature, T_0 = 393°F. absolute
Pressure, p_0 = 1.69 lbs. per sq.in. absolute
Density, ρ_0 = 0.0116 lb. per cu.ft.
Sound velocity, a_0 = 971 ft. per sec.

where the spanwise length is taken as unity. The total heat flow in station H7 from all four surrounding stations is

$$Q = k\Delta\theta\left[\frac{S_2}{S_1}(T_{H8} - T_{H7}) + \frac{S_2}{S_1}(T_{H6} - T_{H7}) + \frac{S_1}{S_2}(T_{G7} - T_{H7}) + \frac{S_1}{S_2}(T_{I7} - T_{H7})\right] \quad \text{(A-2)}$$

The rise in temperature of the material associated with station H7 during the time interval $\Delta\theta$ is given by

$$T_{H7}' - T_{H7} = Q/\rho c S_1 S_2 \quad \text{(A-3)}$$

where T_{H7} and T_{H7}' denote the temperatures at the beginning and the end of the time interval $\Delta\theta$, respectively. We can eliminate T_{H7} by proper choice of the time interval, such as by

$$1 = \frac{2k\Delta\theta}{\rho c S_1^2}\left[1 + \left(\frac{S_1}{S_2}\right)^2\right] \quad \text{(A-4)}$$

By elimination of T_{H7} from Eqs. (A-2) and (A-3), we get for the temperature, at the end of the time interval,

$$T_{H7}' = (\lambda/2)\left[(T_{H6} + T_{H8}) + \tau^2(T_{G7} + T_{I7})\right] \quad \text{(A-5)}$$

where the thickness ratio, τ, is defined by

$$\tau = S_1/S_2 \quad \text{(A-6)}$$

and

$$\lambda = \frac{1}{1 + (S_1/S_2)^2} = \frac{1}{1 + \tau^2} \quad \text{(A-7)}$$

(*b*) *Typical Surface Station.*—The heat flow into a typical surface station in the time interval $\Delta\theta$ is

$$Q = \bar{h}A(\bar{T}_{aw} - \bar{T}_s)\Delta\theta \quad \text{(A-8)}$$

where the bars refer to an average value of the variable during this time interval. The total heat flow into station F2, in Fig. 26b, is

$$Q = \bar{h}S_3(\bar{T}_{aw} - \bar{T}_{F2})\Delta\theta + k\Delta\theta \times \left[\frac{S_2}{S_1}(T_{F3} - T_{F2}) + \frac{S_1}{S_2}(T_{G2} - T_{F3})\right] \quad \text{(A-9)}$$

The temperature rise of station F2 is given by

$$T_{F2}' - T_{F2} = 2Q/\rho c S_1 S_2 \quad \text{(A-10)}$$

where the factor of 2 is used because the surface station F2 contains only half as much metal as an internal station. Combining Eqs. (A-4), (A-9), and (A-10) and eliminating T_{F2}, we get

$$T_{F2}' = \lambda\left[\frac{\bar{h}}{k}\tau S_3(\bar{T}_{aw} - \bar{T}_{F2}) + T_{F3} + \tau^2 T_{G2}\right] + (1 - \lambda - \lambda^2)T_{F2} \quad \text{(A-11)}$$

(*c*) *Mid-Chord Station.*—The mid-chord surface station, shown in Fig. 26a, is treated similarly to surface station F2, except that the heat-transfer area was adjusted and the volume of material at station H1 is one-quarter that of an internal station. We get

$$Q = \bar{h}\Delta\theta S_3(\bar{T}_{aw} - \bar{T}_{H1}) + k\Delta\theta(S_2/S_1)(T_{H2} - T_{H1}) \quad \text{(A-12)}$$

$$T_{H1}' - T_{H1} = 4Q/\rho c S_1 S_2 \quad \text{(A-13)}$$

$$T_{H1}' = 2\lambda[(\bar{h}/k)\tau S_3(\bar{T}_{aw} - \bar{T}_{H1}) + T_{H2}] - (2\lambda - 1)T_{H1} \quad \text{(A-14)}$$

(*Continued on page 816*)

Readers' Forum

BRIEF REPORTS of investigations in the aeronautical sciences and discussions of papers published in the JOURNAL are presented in this special department. The publication will be completed approximately 8 weeks after receipt of the material. The Editorial Committee does not hold itself responsible for the opinions expressed by the correspondents. Contributions should not exceed 800 words in length.

On the Speed of an Airplane in Steady Flight

Angelo Miele
Professor of Mechanics, Escuela de Aviación Militar, Cordoba, Argentina; also, Assistant Professor, Aerodynamic Design, Escuela Superior de Aerotécnica, Córdoba, Argentina
September 8, 1950

I HAVE READ THE INTERESTING ARTICLE published by Freeman[1] about the velocity of an airplane in many conditions of unaccelerated flight, and I have observed that the equations that give the speed can also be deduced from a more general formula containing, as particular cases, those obtained by Mr. Freeman.

As a matter of fact, all the cases treated by the author (straight and circling level flight and climbing, descending, and vertical diving flight) can be studied under a general scheme, considering that the most general steady motion of an airplane is a helicoidal motion with vertical axis, constant velocity, and constant rotational speed.[2]

It is known that, for a given thrust and for an ideal ambient of constant air density, there is a triple infinity of possible helicoidal paths, each of which is determined if three independent parameters are given (within certain limits, of course).

The following symbols are used:

A.R. = wing aspect ratio
C_D = drag coefficient
C_{Dp} = parasite drag coefficient
C_L = lift coefficient
$C_{LE} = \sqrt{\pi \text{A.R.} e C_{Dp}}$ = lift coefficient maximum for lift/drag ratio
D = drag
e = airplane efficiency factor
$E = C_L/C_D$ = lift/drag ratio
$E_{max} = \sqrt{\pi \text{A.R.}}/4C_{Dp}$ = maximum lift/drag ratio
$F_c = (W/g)(V^2/r)$ = centrifugal force
$F_i = V/V_{MT}$ = induced drag factor
g = acceleration of gravity
L = lift
$n = L/W$ = lift/weight ratio
$r = R/\cos^2\theta$ = radius of curvature of the helicoidal path
R = radius of the cylinder to which the helix belongs
S = wing surface
T = thrust
$T_n = T \pm W \sin\theta$ = net thrust (± for descending or climbing flight)
V = velocity
V_{MT} = maximum theoretical speed ideally obtainable, for a given net thrust, without induced drags and without compressibility effects
W = weight
θ = absolute value of the path inclination with respect to a horizontal plane
ρ = air density
φ = absolute value of the angle of bank
$\omega = (V/R)\cos\theta$ = angular velocity

Discussing, for the sake of simplicity, a helicoidal uniform flight without sideslip and assuming that the resulting aerodynamic force lies in the plane of symmetry, the general vectorial condition of equilibrium of forces is

$$\boldsymbol{T} + \boldsymbol{D} + \boldsymbol{L} + \boldsymbol{W} + \boldsymbol{F}_c = 0 \tag{1}$$

Admitting the thrust, as usual, parallel to the velocity, the projection of all the forces on the axes of the principal trihedral of the path (tangent, principal normal, binormal) leads to the following scalar equations:*

$$T - (1/2)C_D \rho S V^2 \pm W \sin\theta = 0 \tag{2}$$

$$\frac{W}{g}\frac{V^2}{R}\cos^2\theta - \frac{1}{2}C_L \rho S V^2 \sin\varphi = 0 \tag{3}$$

$$(1/2)C_L \rho S V^2 \cos\varphi - W\cos\theta = 0 \tag{4}$$

in which the aerodynamic coefficients C_L, C_D are not independent but related (incompressible flow) by the parabolic formula

$$C_D = C_{Dp} + (C_L^2/\pi \text{A.R.} e) \tag{5}$$

Eqs. (2), (3), (4), and (5) form a system of four equations with six variables

$$C_D,\ C_L,\ V,\ \theta,\ \varphi, R \tag{6}$$

which is determined if two parameters are given—e.g., path inclination and angle of bank.

From Eqs. (2) and (4) the lift/drag ratio is obtained,

$$E = \frac{C_L}{C_D} = \frac{W\cos\theta}{T_n\cos\varphi} \tag{7}$$

and from Eqs. (5) and (7), the corresponding lift coefficient,

$$\frac{C_L}{C_{LE}} = \frac{E_{max.}}{E}\left[1 \pm \sqrt{1 - \left(\frac{E}{E_{max.}}\right)^2}\right] \tag{8}$$

Eqs. (4) and (8) give the expression of the speed

$$V = \sqrt{\frac{T_n}{C_{Dp}\rho S}\left[1 \mp \sqrt{1 - \left(\frac{E}{E_{max.}}\right)^2}\right]} \tag{9}$$

and Eqs. (3), (4), and (9) the radius of the cylinder to which the helicoidal path belongs

$$R = \frac{V^2}{g}\frac{\cos\theta}{\tan\varphi} = \frac{T_n\cos\theta}{gC_{Dp}\rho S\tan\varphi}\left[1 \mp \sqrt{1 - \left(\frac{E}{E_{max.}}\right)^2}\right] \tag{10}$$

Finally, angular velocity is deduced from Eqs. (3), (4), and (10)

$$\omega = \frac{g}{V}\tan\varphi = g\tan\varphi\sqrt{\frac{C_{Dp}\rho S}{T_n}}\left(\frac{E_{max.}}{E}\right)^2 \times \left[1 \pm \sqrt{1 - \left(\frac{E}{E_{max.}}\right)^2}\right] \tag{11}$$

and lift-weight ratio from Eq. (4)

$$n = L/W = \cos\theta/\cos\varphi \tag{12}$$

It is important to emphasize that:

(1) Two possible angles of attack and, therefore, two possible helicoidal paths exist for each couple of values θ, φ. The greater velocity, the greater radius, and the smaller rotational speed correspond to the smaller lift coefficient and vice versa.

(2) The exposed formulas contain explicitly the solution of the problem if thrust can be considered independent of speed; otherwise, they must be solved by trial.

* The sign preceding the third term of Eq. (2) must be considered positive for descending flight, negative for climbing flight.

TABLE 1
Net Thrust, Lift-Drag Ratio, and Lift-Weight Ratio for Many Flight Conditions

Flight Condition	T_n	$E = \frac{C_L}{C_D}$	$n = \frac{L}{W}$	Remarks
General helicoidal flight	$T \pm W \sin\theta$	$\frac{W\cos\theta}{\cos\varphi\,[T \pm W\sin\theta]}$	$\frac{\cos\theta}{\cos\varphi}$	+ Descending flight − Climbing flight
Straight level flight	T	$\frac{W}{T}$	1	$\varphi = 0$ $\theta = 0$
Straight climbing flight	$T - W\sin\theta$	$\frac{W\cos\theta}{T - W\sin\varphi}$	$\cos\theta$	$\varphi = 0$
Straight descending flight	$T + W\sin\theta$	$\frac{W\cos\theta}{T + W\sin\theta}$	$\cos\theta$	$\varphi = 0$
Vertical diving flight	$T + W$	0	0	$\varphi = 0$ $\theta = n/2$
Vertical dive—no thrust	W	0	0	$\varphi = 0$ $\theta = n/2$ $T = 0$
Level circling flight	T	$\frac{W}{T\cos\varphi}$	$\frac{1}{\cos\varphi}$	$\theta = 0$
Turning gliding flight	$W\sin\theta$	$\frac{\cot\theta}{\cos\varphi}$	$\frac{\cos\theta}{\cos\varphi}$	$T = 0$
Straight gliding flight	$W\sin\theta$	$\cot\theta$	$\cos\theta$	$\varphi = 0$ $T = 0$

(3) Results are closely subordinated to the validity of the basic hypothesis—namely, incompressible flow and flight lift coefficient lower than limit lift coefficient up to which parabolic and experimental polars are in agreement.

(4) Results could also be extended to the study of flight conditions in compressible airflow if the dependence of the parameters of the parabolic polar on Mach Number is known and if iterative methods are applied. But this does not seem to be useful from a practical standpoint.

In certain particular flight conditions, factors T_n, E, and n assume the expressions given in Table 1. Some of them, introduced in Eq. (9), lead, through simple algebraic transformations, to the formulas obtained by Mr. Freeman in his paper.

To conclude, when the assumption of independence of thrust from speed is correct (it is approximately the case of turbojet aircraft) Eq. (10) may be expressed as the product of two factors of physical significance[4, 5]

$$V = F_i V_{MT} \tag{13}$$

where

$$V_{MT} = \sqrt{2T_n/C_{Dp}\rho S} \tag{14}$$

is the maximum theoretical speed ideally obtainable, for a given net thrust, with no induced drags and no compressibility effects, and where

$$F_i = (1/\sqrt{2})\sqrt{1 \mp \sqrt{1 - (E/E_{max.})^2}} \tag{15}$$

is a reduction factor ($\leqslant 1$) synthetically containing the effect of induced drags on speed.

REFERENCES

[1] Freeman, H. B., *Simple Analytical Equations for the Velocity of an Airplane in Unaccelerated Level, Climbing, and Diving Flight*, Journal of the Aeronautical Sciences, Vol. 14, No. 3, pp. 185–189, March, 1947.

[2] von Mises, R., *Theory of Flight*, 1st Ed., p. 571; McGraw-Hill Book Company, Inc., New York, 1945.

[3] Page, R. K., *Performance Calculation for Jet-Propelled Aircraft*, The Journal of The Royal Aeronautical Society, Vol. 51, No. 437, pp. 440–450, May, 1947.

[4] Miele, A., *Il Calcolo della Velocità Orizzontale di Regime degli Aeroplani a Reazione in Corrente Incompressibile ed in Corrente Compressibile*, Rivista Aeronautica, Vol. XXV, No. 9, pp. 557–570, September, 1949.

[5] Miele, A., *Il Calcolo delle Caratteristiche di Salita e della Quota di Tangenza degli Aeroplani Azionati da Turboreattori*, L'Aerotecnica, Vol. XXX, No. 2, pp. 76–96, April, 1950.

An Analogy Between Open Soap Bubble and Compressible Flow

V. G. Szebehely

Associate Professor of Research, Department of Applied Mechanics, Virginia Polytechnic Institute, Blacksburg, Va.

September 8, 1950

THE WELL-KNOWN ANALOGY between torsion and a soap bubble assumes infinitesimal bubble height. If the exact equation of an open bubble is compared with the basic equation for compressible flow, another analogy can be shown. The governing differential equation of an unloaded open bubble is

$$\frac{\partial^2 z}{\partial x^2}\left[1 + \left(\frac{\partial z}{\partial y}\right)^2\right] + \frac{\partial^2 z}{\partial y^2}\left[1 + \left(\frac{\partial z}{\partial x}\right)^2\right] - 2\frac{\partial^2 z}{\partial x \partial y}\frac{\partial z}{\partial x}\frac{\partial z}{\partial y} = 0 \tag{1}$$

and the basic equation for the steady, potential flow of a compressible, inviscid fluid

$$\frac{\partial^2 \phi}{\partial x^2}\left[c^2 - \left(\frac{\partial \phi}{\partial x}\right)^2\right] + \frac{\partial^2 \phi}{\partial y^2}\left[c^2 - \left(\frac{\partial \phi}{\partial y}\right)^2\right] - 2\frac{\partial^2 \phi}{\partial x \partial y}\frac{\partial \phi}{\partial x}\frac{\partial \phi}{\partial y} = 0 \tag{2}$$

The latter can be transformed by the

$$\bar{v}^2 = (\partial\phi/\partial x)^2 + (\partial\phi/\partial y)^2$$

relation and using the $a^2 = c^2 - \bar{v}^2$ notation, into

$$\frac{\partial^2 \phi}{\partial x^2}\left[a^2 + \left(\frac{\partial \phi}{\partial y}\right)^2\right] + \frac{\partial^2 \phi}{\partial y^2}\left[a^2 + \left(\frac{\partial \phi}{\partial x}\right)^2\right] - 2\frac{\partial^2 \phi}{\partial x \partial y}\frac{\partial \phi}{\partial x}\frac{\partial \phi}{\partial y} = 0 \tag{3}$$

Eq. (2) was obtained by combining the Euler equation,

$$\rho \text{ grad } (\bar{v}^2/2) + \text{grad } p = 0$$

the continuity equation,

$$\text{div } (\rho \bar{v}) = 0$$

the definition of the velocity of sound,

$$c = \sqrt{dp/d\rho}$$

and introducing the velocity potential ϕ.

Here, p is pressure; $\bar{v}$, velocity vector (= grad ϕ); and ρ, density.

Eq. (3) shows complete analogy to Eq. (1) if $a^2 = 1$, which is the case of the "under transonic" flow, since the Mach Number for this case is $M = \sqrt{1 - (1/c^2)}$. A detailed analysis will be published at a later date.

On the Plastic Buckling of Plates According to the Flow Theory

P. P. Bijlaard
Cornell University, Ithaca, N.Y.
September 5, 1950

In this Journal of July, 1950, Dr. Pearson[1] calculates the plastic buckling stress of a compressed plate that is simply supported at both unloaded sides, assuming plastic flow. He also assumes that during buckling the entire plate deforms plastically in analogy with the tangent modulus theory (Engesser load) for columns. In contrast, in a previous paper, Handelman and Prager[2] had assumed that unloading occurs in part of the plate in analogy with the reduced modulus theory (von Kármán load) for columns.

Handelman and Prager's assumption led to disagreement with tests,[3] as is shown in Fig. 1, where the plastic buckling stress σ_{cr} is plotted against σ_E/E (σ_E is the elastic buckling stress and E is the elastic modulus). The circles refer to the experiments by Pride and Heimerl.[3] In his paper, however, Dr. Pearson tries to show that, if the entire plate is assumed to remain plastic, a fair agreement with the tests is obtained, as is shown in his Fig. 10 and also in Fig. 1 of this item. In Fig. 1 the curve according to the present writer's theory[4, 5] is also given, as calculated by Pride and Heimerl.[3]

Dr. Pearson's paper is misleading in several respects. In the first place, the same case of plastic flow (Prandtl-Reuss body) and of the fully plastic plate was already considered in reference 4 by the present writer. In Fig. 11 of that reference, the second dashed curve from the left (Case 2, $e = 0$, pl.) refers to this case. This curve is, however, fairly close to the curve farthest to the left (Case 2, $e = 0$, el. + pl.), which was obtained by assuming partly elastic behavior. Both of these curves are in practically the same marked disagreement with Kollbrunner's tests.

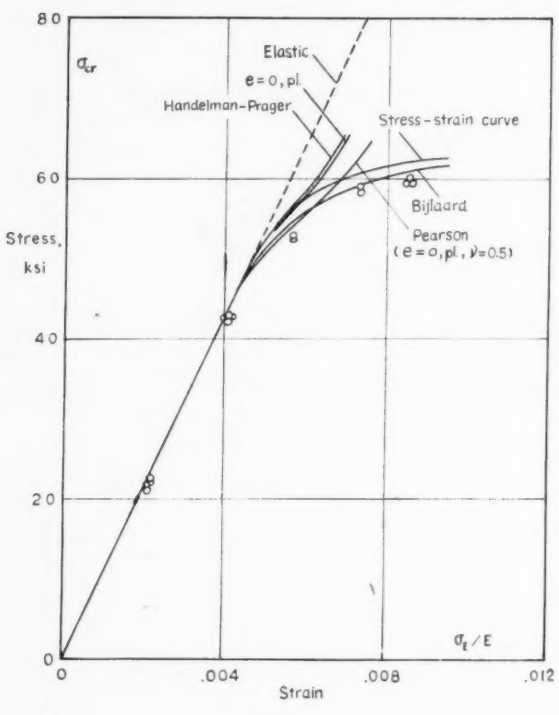

Fig. 1

For the material used in Pride and Heimerl's tests, the curve for plastic flow and fully plastic plate is given here in Fig. 1 by the curve denoted by ($e = 0$, pl.). It follows directly from Eq. (53) of the writer's 1938 paper,[5] or from Table 5 of reference 4, according to which

$$\eta = \sigma_{cr}/\sigma_E = 0.455\,(\sqrt{AD} + B + 2F) \tag{1}$$

if in reference 4, in Eqs. (21) or (21a) for A, B, D, and F, the ratio $\beta = \rho_2/\rho_1$ between the principal compressive stresses is equated to zero. Furthermore, for plastic flow, in these equations $e = (E/E_s) - 1$ has to be equated to zero (E_s is the secant modulus). Here, too, the curve ($e = 0$, pl.) thus obtained for the flow theory is practically in the same disagreement with the Pride and Heimerl tests as is the Handelman-Prager curve (Fig. 1).

Why is the curve obtained by Dr. Pearson for the same case in better agreement with the tests? The reason is that he assumes Poisson's ratio ν for the elastic deformations equal to 0.5, instead of the more accurate value $\nu = 0.3$ used by the present writer. With $\nu = 0.5$ in Eq. (1), the first factor to the right, representing $0.5\,(1 - \nu^2)$, becomes 0.375 and the expression in parentheses follows from the above-mentioned equations of reference 4 with $\nu = 0.5$. This yields indeed the curve obtained by Dr. Pearson.

Although it would appear from Dr. Pearson's paper that the better agreement with the tests is obtained by assuming the entire plate as plastic, about 85 per cent of this improvement is actually obtained by the arbitrary and incorrect assumption $\nu = 0.5$. As stated on page 423 of Dr. Pearson's paper, he made this assumption "for simplicity of algebra."

It is obvious that, if Dr. Pearson wanted to show the improved agreement of his approach with tests, it is not permissible to introduce an arbitrary, simplifying assumption that accounts for 85 per cent of the apparent improvement. From a scientific point of view it is important to state that, actually, the assumption of plastic flow and fully plastic plate leads to practically the same amount of disagreement with experiments as that of plastic flow and partly elastic plate.

Dr. Pearson states, furthermore, that all treatments using deformation theories are open to objection, for which he refers to a 1942 paper by Handelman, Lin, and Prager (actually published 1947). He says that the problem of plastic plate buckling has been most rigorously treated by Handelman and Prager,[2] using the flow theory and that his paper is based on their results.

In his 1938 papers, the present writer developed the general theory of plastic buckling of plates, including both the case of a Hencky body (later referred to by other authors by the confusing name of "plastic deformation") and that of a Prandtl-Reuss body (plastic flow). He showed that, in general, a complete behavior as a Hencky body is not possible, since in extreme cases the external work done with plastic deformation would be negative[5] or the work done during the total (elastic + plastic) deviatoric deformation would be zero.[4] This objection is more convincing than that given by the above-mentioned authors, who state that discontinuities in the plastic strain would occur. Such discontinuities also occur in other cases of plasticity. In reference 4, it was explained why, in the special case of concentric buckling, the material will nevertheless behave in accordance with the deformation theory.

Furthermore, the writer showed in reference 4 that all later treatments are special cases of his earlier general theory. The treatment by Handelman and Prager is only rigorous as far as their results are identical with those derived by the present writer in 1938—i.e., as far as their excess stress-strain relations are concerned, which, for plastic flow, follow from his formulas by equating his value e to zero. He considered this case of a Prandtl-Reuss body explicitly in his 1938 papers[5] but concluded that it yielded unsafe values as compared with the then available test results. The newer investigations since then have confirmed this conclusion.

REFERENCES

[1] Pearson, C. E., *Bifurcation Criterion and Plastic Buckling of Plates and Columns*, Journal of the Aeronautical Sciences, Vol. 17, No. 7, p. 417, July, 1950.

[2] Handelman, G. H., and Prager, W., *Plastic Buckling of a Rectangular Plate Under Edge Thrusts*, N.A.C.A. T.N. No. 1530, 1948.

[3] Pride, R. A., and Heimerl, G. H., *Plastic Buckling of Simply Supported Compressed Plates*, N.A.C.A. T.N. No. 1817, 1949.

[4] Bijlaard, P. P., *Theory and Tests on the Plastic Stability of Plates and Shells*, Journal of the Aeronautical Sciences, Vol. 16, No. 9, p. 529, 1949.

[5] Bijlaard, P. P., *A Theory of Plastic Stability and Its Application to Thin Plates of Structural Steel*, Koninklijke Nederlandsche Akad. v. Wetenschappen, Proc., Vol. XLI, No. 7, p. 731, 1938.

Note on Desirability of Completely Expanded Nozzles

C. B. Cohen and P. J. Evans, Jr.
Lewis Flight Propulsion Laboratory, N.A.C.A., Cleveland

September 8, 1950

IN REFERENCE 1, the effect of velocity coefficient upon the relative merit, in terms of thrust, of sonic nozzles, and completely expanded nozzles, is investigated. The conclusion is reached that, for overall pressure ratios less than approximately 6, more thrust will be obtained with the sonic exit than with the completely expanded exit. There, for simplicity, it is arbitrarily assumed that $\phi_c = \phi_s$, where ϕ is the ratio of actual exit velocity to the velocity corresponding to an isentropic expansion from the initial conditions to the actual exit pressure. The subscripts s and c refer to the sonic exit and to the completely expanded exit, respectively. If there are no losses in the diverging section, ϕ_c will be greater than ϕ_s. This statement follows from the physical meaning of ϕ. The quantity ϕ^2 is the ratio of actual to ideal kinetic energy. For the completely expanded nozzle, the ideal kinetic energy is greater than for the sonic nozzle. Therefore, for the same value of ϕ the losses will be greater in the completely expanded nozzle. Thus, for a given ϕ_s, ϕ_c can be greater than, equal to, or less than ϕ_s, depending on the losses. In general, it appears that the losses in the diverging section will be excessive from the standpoint of good design if it be required that ϕ_c be as low as ϕ_s. For example, Fig. 2, reference 1, shows that for a ϕ of 0.95 the pressure ratio for equal thrust is about 5.75. In order for ϕ_c and ϕ_s to both equal 0.95, the total pressure loss in the diverging section would have to be about 12.6 per cent; but calculations (explained later in this letter) for this pressure ratio, for a diverging section having reasonably high losses, indicate a total pressure loss of only about 5.6 per cent. Thus, the assumption of equal ϕ does not appear justified in general. It appears that a more correct procedure would replace Fig 2, reference 1, by a family of curves of P_1/p_0 versus ϕ_c, where ϕ_s is constant on each curve. Here P and p refer to total and static pressures, respectively. These curves would be obtained directly from curves similar to Fig. 1, reference 1. However, to draw definite conclusions, ϕ_s must be known, as well as reasonable values of the ϕ_c corresponding to ϕ_s.

An analysis starting from the sonic section and considering only the losses downstream of this section does not require this information. A velocity coefficient, ψ, is defined as the ratio of the actual exit velocity to that obtained by expanding isentropically from the actual sonic section (station 2) to the actual exit pressure. Then for each pressure ratio, P_2/p_0, the thrusts for sonic and complete-expansion exits can be equated and a value for ψ explicitly determined. The result of this procedure is shown as the equal-thrust curve of Fig. 1.

In order to estimate on which side of the equal-thrust curve an actual nozzle will lie, a series of calculations were made for conical diverging exits having constant friction coefficient, f.

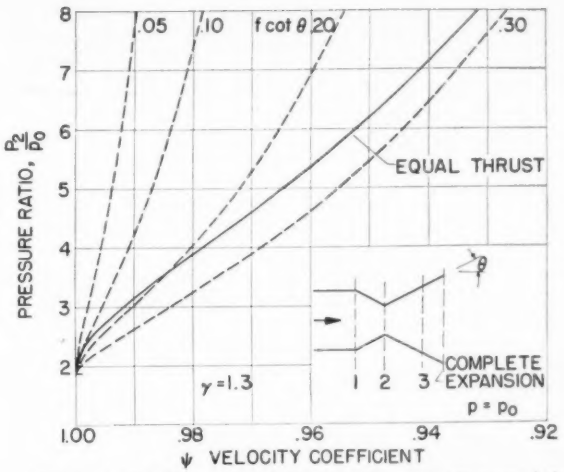

FIG. 1. Equal-thrust curve for sonic and completely expanded nozzles showing relation between the pressure ratio, P_2/p_0, and velocity coefficient.

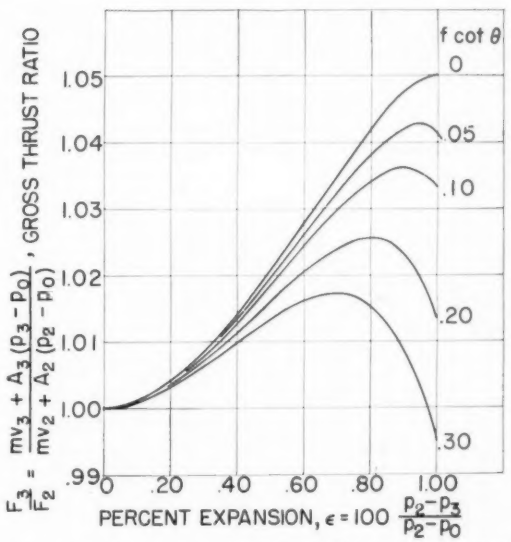

FIG. 2. Variation of gross thrust ratio with per cent expansion $P_2/p_0 = 6$, $\gamma = 1.3$.

For the conical nozzle the effect of friction is introduced only through the one-dimensional equation relating areas and Mach Numbers:

$$\frac{A_3}{A_2} = \frac{M_2}{M_3}\left[\frac{1 - (\gamma M_2^2/2) f \cot\theta}{1 - (\gamma M_3^2/2) f \cot\theta}\right]^{\alpha}\left[\frac{(t/T)_2}{(t/T)_3}\right]^{\beta}$$

where

$$\alpha = \frac{1 - (\gamma/2) f \cot\theta}{(\gamma - 1)\{(1 + [\gamma/(\gamma - 1)] f \cot\theta\}}$$

$$\beta = \frac{(1/2)[(\gamma + 1)/(\gamma - 1)]}{1 - [\gamma/(\gamma - 1)] f \cot\theta}$$

t = static temperature
T = total temperature
γ = ratio of specific heats
θ = cone half angle

This results in curves of P_2/p_0 versus ψ for constant values of $f \cot\theta$ as shown in Fig. 1. Since a friction coefficient of 0.005

is higher than generally obtained in practice and a divergence half-angle θ of about 3° is as low as seems practical, the combination will yield an approximate maximum value of $f \cot \theta$ of 0.10. This value was used in calculating the total pressure losses of 5.6 per cent discussed in the first paragraph. The 0.10 curve shows that the completely expanded nozzle produces more thrust for values of P_2/p_0 greater than 2.3. The contradiction between this value of 2.3 and the value of 6 arrived at in reference 1 can be attributed to the excessive losses in the diverging section which are implicit in the assumption that $\phi_c = \phi_a$.

There is a point that has not been considered—namely, the possibility of the existence of a maximum thrust at intermediate degrees of expansion. Therefore, calculations of thrust were made for conical nozzles having constant friction coefficient. Fig. 2, for a pressure ratio, P_2/p_0, of 6, is a typical result. It shows the variation of gross thrust ratio, F_3/F_2, with ϵ, the per cent expansion, defined by

$$\epsilon = 100\ [(p_2 - p_3)/(p_2 - p_0)]$$

As one might expect, the maximum thrust occurs for nearly complete expansion for all reasonable values of $f \cot \theta$. From other similar plots, it has been observed that the optimum per cent expansion increases as P_2/p_0 increases. Thus, if maximum thrust is desired, the relative merit of sonic and complete expansion is more an academic question than a practical one, since the maximum occurs somewhere between sonic and complete expansion.

Reference

[1] Durham, F. P., *Increased Jet Thrust from Pressure Forces*, Journal of the Aeronautical Sciences, Vol. 17, No. 7, p. 425, July, 1950.

Note on Base Pressure Measurements

Dean R. Chapman
Ames Aeronautical Laboratory, N.A.C.A. Moffett Field, Calif.
September 5, 1950

SEVERAL APPARENT INCONSISTENCIES in the existing base pressure data on bodies of revolution have not as yet been pointed out and adequately explained in these columns. Moreover, in the recent communications of Gabeaud,[1, 2] wherein his analysis is compared with the free-flight experiments of Hill and Alpher,[3] one essential consideration seems to have been overlooked. The present note attempts to point out and offer explanations of these discrepancies. This note was prompted by the declassification of some N.A.C.A. measurements of base pressure[4] and by an excellent set of experiments recently reported by Kurzweg which did not become available early enough to permit comparison with the most recent unclassified N.A.C.A. measurements given in *T.N. No. 2137*.[6] Before discussing the apparent inconsistencies, a few statements about some general characteristics of base pressure, and the basis for such statements, are presented, since it is felt that inconsistencies have arisen in the past and can easily arise in the future by overlooking some of these characteristics.

(1) *Changes in type of boundary-layer flow can produce large changes in base drag; the effects of variation in Reynolds Number are large in the laminar and transitional region but are small in the turbulent region.* Measurements at low Reynolds Numbers (less than 2×10^6 based on body length) of the effect on base pressure of changes in Reynolds Number have shown that, with laminar flow approaching the base, the base drag easily can vary by a factor of 2 or greater. In this laminar region an increase in Reynolds Number results in an increase in base drag. The transition to turbulent flow, in the cases measured thus far, is accompanied by marked changes in the trailing shock configuration and a decrease in base drag—the decrease being greater for greater angles of boat-tailing. In fact, for large angles of boat-tailing, transition in certain cases[4] has resulted in a small net thrust acting on the base. For completely turbulent boundary-layer flow, however, a different situation exists with regard to the variation of base pressure with Reynolds Numbers. The measurements of reference 6, using different kinds of artificial roughness, show no appreciable effect on base pressure of variations in Reynolds Number between 2×10^6 and 1.6×10^7. Likewise, the measurements of Faro[5] and of Hill and Alpher show no effect of Reynolds Number in the region between 5×10^6 and 1×10^8.

(2) *Large changes in surface temperature can significantly alter the base pressure.* The effect of surface temperature variations from approximately −40° to 350°F., as observed by Kurzweg, resulted in changes in base drag amounting to as much as 45 per cent at $M = 2.87$. This effect would have a bearing on the estimation of base pressure shortly after combustion terminates in a rocket-propelled missile. Changes in surface temperature and in heat transfer can be looked upon as additional methods of changing the boundary-layer flow approaching the base.

(3) *The effect of body shape is large for length-diameter ratios less than about 4 but is small for length-diameter ratios greater than about 6.* At low and moderate supersonic Mach Numbers, the departure of flow conditions along the body surface from corresponding free-stream conditions results in a lower pressure and higher Mach Number approaching the base. This results in much larger base drag for a short body of revolution than for a long one. A set of measurements at $M = 2.46$ showing large effects of body shape for length-diameter ratios less than unity is presented by Kurzweg. Some information is also available from German wind-tunnel measurements[7] and from the Aberdeen firings of Charters and Turetsky.[8] Large differences in base drag for different body shapes, all having length-diameter ratios less than 4, are indicated in reference 6, where the observed differences amounted to several hundred per cent in a few cases. For length-diameter ratios greater than about 6, however, no important effect of changes in the profile of a body of revolution has been found either in the N.A.C.A. measurements, the N.O.L. measurements, the Aberdeen measurements, or the APL/JHU measurements.

(4) *The presence of tail fins can considerably change the base drag.* The effect of tail fins can perhaps best be illustrated by reference to Fig. 1, which shows four independent sets of base

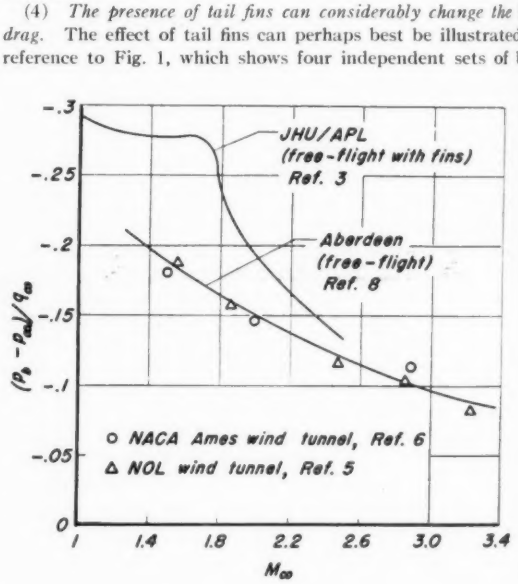

Figure 1.– Comparison of experimental base pressure data for turbulent boundary-layer flow on bodies of revolution without boat tailing.

drag measurements presented in pressure coefficient form. All of these data are representative of the case of turbulent boundary-layer flow approaching the base of relatively slender bodies of revolution having no boat-tailing. The APL/JHU data, indicating the greatest base drag, were taken on bodies having fins. The large difference is not attributable to Reynolds Number effects in view of 1; nor, as shown in reference 6, is it attributable to interference in the wind-tunnel tests from supports or reflected bow waves. Moreover, the approximate similarity of surface temperature conditions in the two flight investigations, and also in the two wind-tunnel investigations, would eliminate temperature effects as the source of trouble in this case. In addition, the free-flight firings of Hill and Alpher at two different rates of deceleration indicate that deceleration rate is not responsible for the large difference. Partly on this basis of elimination of other sources of discrepancy, it has been concluded[6] that the observed difference is due to the presence of tail fins on the APL/JHU missiles. These fins were 10 per cent thick, biconvex airfoil sections, of chord length equal to 1.5 body diameters. Simple calculations of the approximate average decrease in pressure over the rear surfaces of the tail fins show that the order of magnitude of this interference effect in the region of interest is ample to account for the difference. Subsequent wind-tunnel measurements of base pressure at $M = 1.5$ and $M = 2.0$ with and without these particular fins have confirmed this. It may be noted that significant effects of tail fins, only on a different configuration, are also evident in the measurements of reference 5.

Turning now to the inconsistencies mentioned earlier, it is clear that the often-discussed discrepancy between various German wind-tunnel and flight measurements of base pressure[7, 8] can be attributed to the differences in Reynolds Number and type of boundary-layer flow. A second point to be mentioned concerns an observation of Faro,[9] who noted that the measured base pressure behind a hemisphere at $M = 1.7$ agreed very well with the free-flight data on the APL/JHU missile. This good agreement clearly is of no significance to the discrepancy between various base pressure measurements for the following reason: The hemisphere, being quite short, has considerably greater base drag than a slender body; also, the APL/JHU body with fins has considerably greater base drag than a slender body without fins. Base drag on the hemisphere and the missile with fins, therefore, might be expected to agree approximately with each other.

With regard to the comparison between Gabeaud's most recent theory[2] and the measurements of Hill and Alpher, it appears that this good agreement is fortuitous—that is, unless Gabeaud's theory (the details of which are unavailable at present in this country) somehow accounts for the effect of four 10 per cent thick, biconvex tail fins. Similarly, the observed "knee" in the APL/JHU base pressure curve and the particular values of the parameters f and λ introduced by Hill[10] to match the APL/JHU data appear to be more characteristic of the particular tail geometry used rather than of some intrinsic behavior of base pressure in the range of Mach Numbers between 1.5 and 2.0.

References

[1] Gabeaud, *Base Pressures at Supersonic Velocities*, Readers' Forum, Journal of the Aeronautical Sciences, Vol. 16, No. 10, p. 638, October, 1949.

[2] Gabeaud, *Base Pressures at Supersonic Velocities*, Readers' Forum, Journal of the Aeronautical Sciences, Vol. 17, No. 8, p. 525, August, 1950.

[3] Hill and Alpher, *Base Pressures at Supersonic Velocities*, Journal of the Aeronautical Sciences, Vol. 16, No. 3, p. 153, March, 1949.

[4] Chapman and Perkins, *Experimental Investigation of the Effects of Viscosity on the Drag of Bodies of Revolution at a Mach Number of 1.5*, N.A.C.A. RM A7A31a, 1947.

[5] Kurzweg, *New Experimental Investigations on Base Pressure in the NOL Supersonic Wind Tunnels at Mach Numbers 1.2 to 4.24*, NOLM 10113, January, 1950.

[6] Chapman, *An Analysis of Base Pressure at Supersonic Velocities and Comparison with Experiment*, N.A.C.A. T.N. No. 2137, July, 1950.

[7] Lehnert, *Systematische Messungen an neun einfachen Geschossformen un Vergleich zu Messungen der AVA-Gottingen*, Lilienthal-Gesellschaft für Luftfahrtforschung, Bericht 139, Teil 2, 1941.

[8] Charters and Turetsky, *Determination of Base Pressure from Free-Flight Data*, Aberdeen Ballistic Research Laboratory Report 653, March, 1948.

[9] Faro, *Experimental Determination of Base Pressures at Supersonic Velocities*, Bumblebee Report 106, November, 1949.

[10] Hill, *Base Pressures at Supersonic Velocities*, Readers' Forum, Journal of the Aeronautical Sciences, Vol. 17, No. 3, p. 185, March, 1950.

The Reflection of "Rectilinear" Waves in One-Dimensional Gas Flows*

Lorenzo Poggi
University of Pisa, Italy

September 11, 1950

In a recent paper on pulse-jets,[1] I described a method for studying one-dimensional nonsteady flows. This treatment was based on the use of particular solutions of the general equations which govern such phenomena. One of these solutions (denoted in that investigation as the C-type solution) is of especial interest, inasmuch as it provides, to close approximation, a means for representing what happens when a "rectilinear" wave is reflected at a wall. The present note is confined, in particular, to an illustration of such a solution and to its application in the case of a reflection process.

As is well known, the flow of a gas in a one-dimensional duct under the hypothesis that the processes are adiabatic may be summarized by the set of equations[2]

$$\left.\begin{aligned} &\textit{Equation of Motion}\\ &\frac{\partial u}{\partial t} + u\frac{\partial u}{\partial x} = -\frac{2}{\gamma - 1}\,a\cdot\frac{\partial a}{\partial x}\\ &\textit{Equation of Continuity}\\ &\frac{\partial a}{\partial t} + u\frac{\partial a}{\partial x} = -\frac{\gamma - 1}{2}\,a\cdot\frac{\partial u}{\partial x} \end{aligned}\right\} \tag{1}$$

wherein the following notation applies:

x = distance along duct
t = time
u = local flow velocity
a = local velocity of sound
γ = ratio of the specific heats

This system of equations is obviously satisfied if we take as solution

$$\left.\begin{aligned} u &= u_0 t\\ a &= a_0 \end{aligned}\right\} \tag{A}$$

that is, flow and state parameters that are uniform throughout the duct and constant with respect to time.

Another well-known solution is

$$\left.\begin{aligned} u &= \frac{2}{\gamma + 1}\cdot\frac{x \mp a_0 t}{t + t_0}\\ a &= a_0 \pm [(\gamma - 1)/2]u \end{aligned}\right\} \tag{B}$$

where a_0 and t_0 are constant. Solution (B) represents what may be called a "rectilinear wave" because of the linearity of u and a with respect to x.

Solutions of the two types can join up at their end points to produce complex wave setups such as, e.g., the one represented in Fig. 1, which shows an expansion wave (B) between two A-type regions, one of quiescent fluid on the left and one of uniform mo-

* The author wishes to express his thanks to Dr. J. V. Foa, of Cornell Aeronautical Laboratory, Inc., for his interest in the translation and presentation of this note and to Mr. Kramer, of the same Laboratory, for his careful translation.

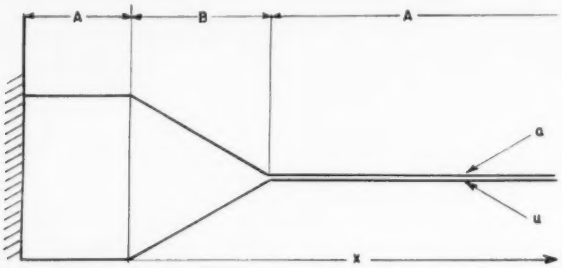

FIG. 1. Typical complex configuration made up of two A-type uniform waves and a B-type expansion wave, before reflection is initiated.

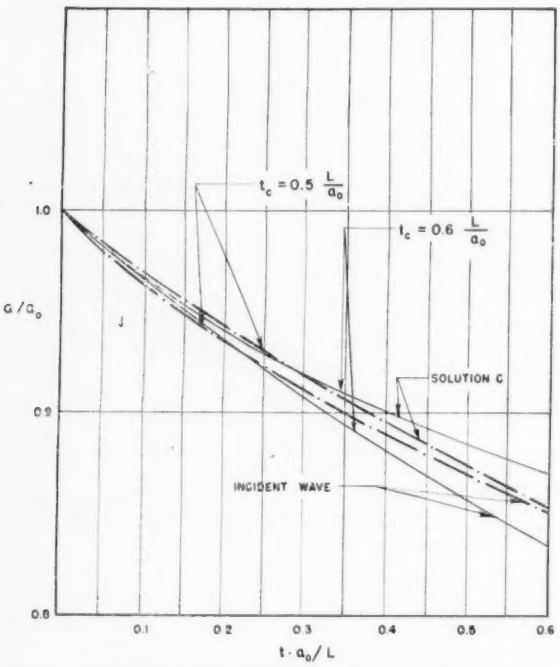

FIG. 2. Approximate and tangent solutions for reflection of a B-type wave against the closed end of a duct.

FIG. 3. Configuration created in the duct during reflection at the closed end.

tion on the right. The expansion wave remains rectilinear but changes its slope with time because of the different speeds with which its end points are propagated toward the left. This speed, as well as the speed of the intermediate points, is always equal to $u - a$.

When the left-hand end point of the wave reaches the closed end of the duct, there begins the process of reflection which forms the object of consideration in this note.

The premise is made that, during this process of reflection, the state of the fluid is almost constant with respect to x (i.e., $\partial u / \partial x = 0$) throughout a region adjacent to the wall. Substantiation for this premise is obtained by analysis with graphical-numerical methods, such as that of reference 3. Furthermore, the velocity is obviously zero at the wall. Thus, one is led to look for a solution of the set of Eqs. (1) for which just these properties are exhibited. Such a search has led me to the third-type solution.

$$\left.\begin{aligned} u &= x/(t + t_c) \\ a &= a_c[1 + (t/t_c)]^{(1-\gamma)/2} \end{aligned}\right\} \qquad (C)$$

where a_c and t_c denote appropriate constants.

Although this solution is not a rigorous mathematical facsimile of what takes place at reflection [even though it is an exact solution of the Eqs. (1)], nonetheless it furnishes a sufficiently approximate description of the phenomenon. For the representation to be rigorously exact, it would be necessary that the solution under consideration join up precisely with the arriving rectilinear wave and that at each instant there should exist a point of intersection between the two solutions (the a-values and u-values of the B-type solution equaling those of the C-type).

This state of affairs does not come about in an exact way, but the constants can be so selected that the C-type solution is "tangent" to the actual solution at the initial point of the reflection process, thereby establishing the above-described condition not only when the incident wave just reaches the closed end but also an infinitesimal time interval later.

More generally, it is possible to select the constants in such a way that the above-mentioned condition is satisfied for two different time values.

Thus, letting $t = 0$ at the initial instant of the reflection, the "tangency" requirement may be realized by assigning to the constant a_c the value a_0 of the originally quiescent fluid, and to the constant t_c the value

$$t = [(\gamma + 1)/4]\,(L/a_0) \qquad (2)$$

The symbol L denotes a characteristic length of the incident wave—namely, the distance from the closed end to that point of the wave where the propagation velocity is zero.

The degree of approximation of such a configuration is depicted in Fig. 2, wherein the values of a that correspond to the incident wave and to the C-type configuration are represented by solid lines; the representation is made for those values of x at which the respective u-values coincide. As may be seen, the two curves are tangent at $t = 0$.

In this same figure, an analogous comparison (using dashed curves) is then carried out for the case in which the constant t_c is assigned the value $0.5L/a_0$ instead of $0.6L/a_0$ [as would be obtained from Eq. (2) with $\gamma = 1.4$]. The closeness of the curves is better on the average over the extensive time interval shown when the value $0.5L/a_0$ is used, even though near the origin they are less satisfactorily close. In practice, depending on the amplitude of the range of values throughout which one desires to approximate the solution, as happens in many similar approximation problems, one or the other (or intermediate) values may be selected for the constant.

Within such limits of approximation, immediately after the wave has reached the closed end, one finds, as shown in Fig. 3, three regions of the flow, one of type (C), one of type (B), and one of type (A) (constant flow velocity). This situation continues until the intersection of the C-type and B-type solutions reaches the intersection of the B-type and A-type ones, which is the right end of the incident wave, traveling in the opposite direction from the former.

From this moment on (as graphical calculations carried out by means of the usual procedure[3] have confirmed), a true and proper reflected wave is established. The intersection between this reflected wave and the C-type wave (again calculable in an approximate manner) moves toward the wall until it finally reaches it, thereby eliminating the C-type configuration, which is then

replaced by a new region of zero velocity (A-type wave), completing the reflection process.

REFERENCES

[1] Poggi, L., *Contributo allo studio della pulsoreazione*, L'Aerotecnica, Vol. XXIX, No. 5, November 15, 1949; Vol. XXIX, No. 6, December 15, 1949. (Now being translated at the Cornell Aeronautical Laboratory under the title, "On pulsejet propulsion.")

[2] Pfriem, H., *Ebene ungedämpfte Druckwelle grosser Schwingungweite*, Forschung auf dem Gebiete des Ingenieurwesen, January–February, 1941.

[3] de Haller, P., *Méthode graphique pour la résolution de quelques problèmes de dynamique des gaz*, Revue Technique Sulzer, No. 1, pp. 6–24, 1945. (Available as R.T.P. Translation No. 2555, entitled, "On a Graphical Method of Gas Dynamics.")

Determination of Deflections in Redundant Structures

H. L. Cox and D. G. Sopwith

Engineering Division, National Physical Laboratory, England

September 11, 1950

THE POINT MADE BY B. A. Boley and R. H. Moore (Readers' Forum, JOURNAL OF THE AERONAUTICAL SCIENCES, Vol. 17, No. 8, p. 526, August, 1950) seems not quite clear. For the determination of deflections in redundant structures, it has been *our* normal practice to include the dummy loads P' with the actual loading P and the redundancies F at the outset, to set up the expression for the strain energy U in terms of all three classes of load, and then to write

$$\partial U/\partial F = 0, \quad \delta = \partial U/\partial P'$$

when $P' = 0$. This we believe to be the normal procedure in England.

In computing $\partial U/\partial P'$, the redundancies F, as well as the applied loads P, are regarded as constants, and in the derived formula for δ the values of F are substituted from the results of equating $\partial U/\partial F$ to zero.

By this procedure the computation of the strain energy is carried out wholly for a simply stiff structure, the actual applied loads, the redundancies, and the dummy loads all being regarded as external loading.

It seems that the normal procedure to which Messrs. Boley and Moore refer must be in some way different, but we cannot agree that the procedure outlined above is missing from the standard texts.

On the Equations of Longitudinal Stability

John W. Miles

Associate Professor of Engineering, University of California at Los Angeles

September 18, 1950

RECENTLY, THERE HAS BEEN some speculation as to which of the unsteady flow terms arising in the calculation of aerodynamic forces on an oscillating aircraft should be retained. The classical procedure[1] includes, in addition to the "quasi-stationary" terms, only that term arising from the effect of wing downwash on the tail. Nevertheless, it has been demonstrated that the calculation of pitch (or yaw) damping on a quasi-stationary basis may lead to serious errors,[2] and Statler has shown that unsteady flow effects may be important in other respects.[3] However, an order analysis of the problem in terms of its (dimensionless) characteristic parameters seems never to have been set forth, and it is to that end that the following is submitted.

Let x, y, z be a set of right-handed axes *fixed in direction* and with origin at the center of gravity of the aircraft, being positive in the direction of undisturbed flight, to starboard and down, respectively; Uu and Uw, perturbation velocities (U is the flight velocity) along x and z and θ a rotation about y; m, the total mass; B, the centroidal moment of inertia in pitch; and δX, δZ, δM the perturbation forces due to the deviations u, w, θ. The equations of motion are

$$m(\partial/\partial t)(Uu) = \delta X \tag{1a}$$
$$m(\partial/\partial t)(Uw) = \delta Z \tag{1b}$$
$$B(\partial^2/\partial t^2)\theta = \delta M \tag{1c}$$

Then, introducing the notation of Durand (reference 1, pp. 130–135; however, Durand uses axes fixed in the body), we have the following dimensionless notation:

$$\mu = m/(\rho S l) \tag{2}$$
$$k_B = B/(\mu\rho S l^3) = B/(ml^2) \tag{3}$$
$$\lambda = (\mu l/U)(\partial/\partial t) \tag{4}$$
$$\delta X = -\rho U^2 S x \tag{5a}$$
$$\delta Z = -\rho U^2 S z \tag{5b}$$
$$\delta M = -\rho U^2 S l k_B m \tag{5c}$$

$$\boldsymbol{x} = (1/2)\delta C_D = [x_{u_0} + (\lambda/\mu)x_{u_1}]u + [x_{w_0} + (\lambda/\mu)x_{w_1}]w + [x_{\theta_0} + (\lambda/\mu)x_{\theta_1}]\theta \tag{6a}$$

$$\boldsymbol{z} = (1/2)\delta C_L = [z_{u_0} + (\lambda/\mu)z_{u_1}]u + [z_{w_0} + (\lambda/\mu)z_{w_1}]w + [z_{\theta_0} + (\lambda/\mu)z_{\theta_1}]\theta \tag{6b}$$

$$\boldsymbol{m} = -(1/2)(\delta C_M/k_B) = [m_{u_0} + (\lambda/\mu)m_{u_1}]u + [m_{w_0} + (\lambda/\mu)m_{w_1}]w + [m_{\theta_0} + (\lambda/\mu)m_{\theta_1}]\theta \tag{6c}$$

where l is a characteristic length. Eqs. (1a)–(1c) then read

$$\lambda u + x = 0 \tag{7a}$$
$$\lambda w + z = 0 \tag{7b}$$
$$\lambda^2\theta + \mu m = 0 \tag{7c}$$

To obtain the stability quartic, we require the determinant, $F(\lambda, \mu)$, of Eqs. (7a)–(7c) to vanish. Arranging this determinant in powers of λ and μ, we have terms of order $\mu^{1,\ 0,\ -1,\ -2}$ and $\lambda^{4,\ 3,\ 2,\ 1,\ 0}$. Now the order of magnitude considerations that distinguish dynamic stability from flutter, where such distinction is possible, require μ to be large and λ to be of order one. (In this connection, we remark that, for harmonic motion, $\lambda = \mu k$, where k is the reduced frequency introduced in flutter work.) Thus, if μ is sufficiently large to justify the original neglect of terms of order $(\lambda/\mu)^2$ in Eqs. (6a)–(6c), which would have contributed terms of order μ^{-1} to the end result, we may consistently retain only terms of order μ^1 and μ^0 in the determinant of Eqs. (7a)–(7c), whence we obtain

$$F(\lambda, \mu) = A\lambda^4 + B\lambda^3 + C\lambda^2 + D\lambda + E \tag{8}$$
$$A = 1 + 0(\mu^{-1}) \tag{9a}$$
$$B = (x_{u_0} + z_{w_0} + m_{\theta_1}) + 0(\mu^{-1}) \tag{9b}$$

$$C = \mu m_{\theta_0} + \left[\begin{pmatrix} x & z \\ u_0 & w_0 \end{pmatrix} + \begin{pmatrix} z & m \\ w_0 & \theta_1 \end{pmatrix} + \begin{pmatrix} z & m \\ w_1 & \theta_0 \end{pmatrix} + \begin{pmatrix} x & m \\ u_0 & \theta_1 \end{pmatrix} + \begin{pmatrix} x & m \\ u_1 & \theta_0 \end{pmatrix}\right] + 0(\mu^{-1}) \tag{9c}$$

$$D = \mu\left[\begin{pmatrix} x & m \\ u_0 & \theta_0 \end{pmatrix} + \begin{pmatrix} z & m \\ w_0 & \theta_0 \end{pmatrix}\right] + \left[\begin{pmatrix} x & z & m \\ u_0 & w_0 & \theta_1 \end{pmatrix} + \begin{pmatrix} x & z & m \\ u_0 & w_1 & \theta_0 \end{pmatrix} + \begin{pmatrix} x & z & m \\ u_1 & w_0 & \theta_0 \end{pmatrix}\right] \tag{9d}$$

$$E = \mu\begin{pmatrix} x & z & m \\ u_0 & w_0 & \theta_0 \end{pmatrix} \tag{9e}$$

where the parenthetic sets of four and six variables denote Jacobians; e.g.,

$$\begin{pmatrix} x & z & m \\ u_0 & w_0 & \theta_0 \end{pmatrix} = \begin{vmatrix} x_{u_0} & x_{w_0} & x_{\theta_0} \\ z_{u_0} & z_{w_0} & z_{\theta_0} \\ m_{u_0} & m_{w_0} & m_{\theta_0} \end{vmatrix} \tag{10}$$

Eqs. (9a)–(9e) simplify considerably for the case of free (power-off, no autopilot) flight at small angles of attack (α), in which case (due to our choice of axes fixed in direction)

$$(\partial/\partial w)_0 = (\partial/\partial\theta)_0 = (\partial/\partial\alpha) \tag{11}$$

Also, we may prove that

$$(\partial/\partial\theta)_1 = (\partial/\partial q) + (\partial/\partial\dot{\alpha}) \tag{12}$$

$$(\partial/\partial w)_1 = (\partial/\partial\dot{\alpha}) \tag{13}$$

where $(\partial/\partial q)$ implies steady flight at constant angular velocity (e.g., along a curved flight path, as in a pull out) and $\dot{\alpha}$ denotes a vertical acceleration, positive down. In view of the assumption of small angle of attack, we also may neglect drag terms relative to lift and moment terms, and Eqs. (9a)–(9e) reduce to

$$A = 1 \tag{14a}$$

$$B = (z_\alpha + m_q + m_{\dot{\alpha}}) \tag{14b}$$

$$C = \mu m_\alpha + \begin{pmatrix} z & m \\ \alpha & q \end{pmatrix} \tag{14c}$$

$$D = \mu \begin{pmatrix} x & m \\ u_0 & \alpha \end{pmatrix} + \begin{pmatrix} x & z & m \\ u_0 & \alpha & q \end{pmatrix} \tag{14d}$$

$$E = 0 \tag{14e}$$

It follows that, in this case at least, the only unsteady flow term of importance is $m_{\dot{\alpha}}$.

We should expect this last conclusion to be equally valid, insofar as aerodynamic (as opposed to autopilot) terms alone are concerned, for power-on flight, but the neighborhood of stalled flight may not be included without further investigation. Moreover, in interpreting Eqs. (14a)–(14e), it should be remarked that z_q, $z_{\dot{\alpha}}$, m_q, and $m_{\dot{\alpha}}$, when properly calculated, all include downwash effects of wing on tail.[4]

A similar analysis of the equations of lateral stability could be carried out, although it would be necessary to use axes fixed in the body and to discuss the effects of yawing the wake.

References

[1] Durand, W. F., *Aerodynamic Theory*, Vol. V; Durand Reprinting Committee, Pasadena, Calif., 1943.

[2] Miles, John W., *Unsteady Flow Theory in Dynamic Stability*, Readers' Forum, Journal of the Aeronautical Sciences, Vol. 17, No. 1, p. 62, January, 1950.

[3] Statler, I. C., *Dynamic Stability at High Speeds from Unsteady Flow Theory*, Journal of the Aeronautical Sciences, Vol. 17, No. 4, pp. 232-242, April, 1950.

[4] Miles, John W., *On Downwash Corrections in Unsteady Flow*, Readers' Forum, Journal of the Aeronautical Sciences, Vol. 17, No. 4, p. 253, April, 1950.

The Transient Temperature Distribution in a Wing Flying at Supersonic Speeds

(*Continued from page 807*)

Final Calculation Equations for Two-Dimensional Heat Flow

For the dimensions of the wedge-shaped wing with a thickness ratio of 8 per cent, we get, for the various dimensions and ratios,

$$S_1 = 0.03142 \text{ ft.}$$
$$S_2 = 0.3928 \text{ ft.}$$
$$S_3 = 0.3941 \text{ ft.}$$
$$\tau = 0.08000$$
$$\lambda = 0.9935$$

Substitution of these values results in the following final equations used in the actual calculations of two-dimensional heat flow in the wing:

(*a*) *Typical Internal Station:*

$$T_{H7}' = 0.4986(T_{H6} + T_{H8}) + 0.0032(T_{G7} + T_{I7}) \tag{A-15}$$

(*b*) *Typical Surface Station:*

$$T_{F2}' = 0.03132\,(\bar{h}/k)\,(\bar{T}_{aw} - \bar{T}_{F2}) + 0.9935T_{F3} + 0.0064T_{G2} + 0.0001T_{F2} \tag{A-16}$$

(*c*) *Mid-Chord Station:*

$$T_{H1}' = 0.06264\,(\bar{h}/k)\,(\bar{T}_{aw} - \bar{T}_{H1}) + 1.9871T_{H2} - 0.9871T_{H1} \tag{A-17}$$

Index to Volume 17

Journal of the Aeronautical Sciences

Numbers 1–12, January–December, 1950

No. 1, January, 1950, pages 1–64
No. 2, February, 1950, pages 65–128
No. 3, March, 1950, pages 129–192
No. 4, April, 1950, pages 193–256
No. 5, May, 1950, pages 257–320
No. 6, June, 1950, pages 321–384
No. 7, July, 1950, pages 385–456
No. 8, August, 1950, pages 457–528
No. 9, September, 1950, pages 529–600
No. 10, October, 1950, pages 601–672
No. 11, November, 1950, pages 673–744
No. 12, December, 1950, pages 745–824

Material that has appeared in the above volume has been indexed under a general subject heading and by author and has been further cross-indexed under various subheadings.

ADAMS, MAC C. Remarks on the Interaction Between Parallel Streams of Subsonic and Supersonic Velocities (Readers' Forum) 250

Aerodynamics—

Application of Frequency-Response Analysis to Aircraft-Autopilot Stability, Charles L. Seacord, Jr. 481

Approximate Solution of Compressible Fluid-Flow Problems by Galerkin's Method, Chi-Teh Wang and R. F. Brodsky 660

Base Drag and Thick Trailing Edges, Sighard F. Hoerner. 622

The Calculation of Supersonic Downwash Using Line Vortex Theory, Harold Mirels and Rudolph C. Haefeli 13

Characteristics of the Turbulent Boundary Layer on a Flat Plate in Compressible Flow from Measurements of Friction in Pipes, Hans Ulrich Eckert 573

Comparison of Analytical and High-Speed Mechanical-Calculator Solutions of the Lateral Equations of Motion of an Airplane, Including Product-of-Inertia Terms, M. W. Fossier, R. W. Bratt, and D. G. Dill 271

An Extension of the Theory of the One-Dimensional Shock-Wave Structure, Leonard Meyerhoff 775

The Flow over a Wedge Profile at Mach Number 1, G. Guderley and H. Yoshihara 723

Hypothesis for Skewness of the Probability Density of the Lateral Velocity Fluctuations in Turbulent Shear Flow, Stanley Corrsin 396

The Incompressible Boundary Layer with Pressure Gradient and Suction, Leon Trilling 335

Influence of Acceleration on Aerodynamic Characteristics of Thin Airfoils in Supersonic and Transonic Flight, C. S. Gardner and H. F. Ludloff 47

Investigation of Lateral Dynamic Stability in the XB-47 Airplane, Roland J. White 133

Lateral-Control Devices Suitable for Use with Full-Span Flaps, Francis M. Rogallo, John G. Lowry, and Jack Fischel 629

Leading-Edge Singularities in Thin-Airfoil Theory, Robert T. Jones 307

Lift on Inclined Bodies of Revolution in Hypersonic Flow, G. Grimminger, E. P. Williams, and G. B. W. Young .. 675

Longitudinal Stability of Autopilot-Controlled Aircraft, Andrew Vazsonyi 399

The Longitudinal Stability of Elastic Swept Wings at Supersonic Speed, C. W. Frick and R. S. Chubb 691

A Mechanical Analogy for Hypersonic Flow, H. Reese Ivey 519

A Method of Determining Some Aerodynamic Coefficients from Supersonic Free-Flight Tests of a Rolling Missile, Ray E. Bolz and John D. Nicolaides 609

Note on Free Turbulent Flows, with Special Reference to the Two-Dimensional Wake, G. K. Batchelor 441

A Note on the Approximate Plane Motion During the Burning Period of Rocket-Propelled Missiles Launched at Small Angles of Yaw from Aircraft, Ray E. Bolz 114

On a Family of Oblique Shock Curves, Edward R. C. Miles. 157

On the Thickness of a Steady Shock Wave, R. von Mises ... 551

Periodic Motions of a Rectangular Wing Moving at Supersonic Speed, H. J. Stewart and Ting-Yi Li 529

The Pressure on a Slender Body of Nonuniform Cross-Sectional Shape in Axial Supersonic Flow, Ernest W. Graham 173

The Pulse Method for the Determination of Aircraft Dynamic Performance, R. C. Seamans, Jr., B. P. Blasingame, and G. C. Clementson 22

The Quasi-Steady Air Forces for Use in Low-Frequency Stability Calculations, Martin Goland 601

Readers' Forum

An Analogy Between Open Soap Bubble and Compressible Flow, V. G. Szebehely 809

Another Note on the Velocity of Sound, C. B. Millikan. 252

Application of Biezeno-Koch Method to Compressible Fluid Flow Problems, Chi-Teh Wang and Pei-Chi Chou 599

Approximate Incompressible Flow Solutions for Slender Polygons, E. V. Laitone 375

Base Pressures at Supersonic Velocities, A. Gabeaud .. 525

Base Pressures at Supersonic Velocities, Freeman K. Hill 185

Boundaries of Fluid Mechanics, Keeve M. Siegel 191

The Extension of the Prandtl-Glauert Rule, E. V. Laitone 250

Flow of Nonviscous Elastic Fluids, F. G. Gravalos ... 375

Further Remarks on the Velocity of Sound, Morris Morduchow 180

Lift-Curve Slope for Swept and Unswept Wings, Innes Bouton 185

Note on Base Pressure Measurements, Dean R. Chapman 000

A Note on Boundary-Layer Type Solutions in Applied Mechanics, S. F. Borg 253

A Note on the Calculation of Oblique Shock-Wave Characteristics, M. J. Thompson 744

Note on "Interference Between Wing and Body at Supersonic Speeds," Ray E. Bolz 453

Note on Rotational Gas Flow, James E. Broadwell 123

A Note on the Subsonic Compressible Flow About Airfoils in a Cascade, Henry W. Woolard 379

A Note on the Velocity of Sound, M. V. Morkovin.... 180
An Observation Concerning the Rankine-Hugoniot Relations, Jack Lorell..... 317
On Boundary-Layer Growth in a Compressible Flow Between Radial Walls, J. Conrad Crown..... 667
On the Compressibility Correction for Subsonic Unsteady Flow, John W. Miles..... 181
On Downwash Corrections in Unsteady Flow, John W. Miles..... 253
On the Equations of Longitudinal Stability, John W. Miles..... 815
On the Reduction of Unsteady Supersonic Flow Problems to Steady Flow Problems, John W. Miles..... 64
On Simple Plan Forms in Supersonic Flow, John W. Miles..... 127
On the Stability of the Boundary Layer over a Cone, R. H. Battin and C. C. Lin..... 453
On the Stability for a Certain Degenerate Type of Disturbance of Viscous Fluid Flow Between Parallel Walls, S. I. Pai..... 525
On the Surface Effects of a Compressible Laminar Boundary Layer, Arthur N. Tifford..... 187
On a Variational Principle in Lifting-Line Theory, Alexander H. Flax..... 596
On Virtual Mass and Wave Drag at Subsonic Speeds, John W. Miles..... 667
On the Vorticity of the Flow Behind Curved Shock, S. I. Pai..... 188
On Wing-Body Interference at Supersonic Speeds, George K. Morikawa..... 315
Potential Flow Around a Rotating, Advancing Cylindrical Blade, L. E. Fogarty and W. R. Sears..... 599
Potential Flow Around a Rotating Cylindrical Blade, W. R. Sears..... 183
The Problem of Edges in the Doublet Distribution Method of Obtaining Supersonic Lift, Theodore R. Goodman..... 376
The Reflection of "Rectilinear" Waves in One-Dimensional Gas Flows, Lorenzo Poggi..... 813
Remarks on the Interaction Between Parallel Streams of Subsonic and Supersonic Velocities, Mac C. Adams 250
Remarks on the Velocity of Sound, Max M. Munk.... 376
Roll to Sideslip or Yaw Ratios, Dunstan Graham and Allan McCaskill..... 741
Second-Order Two-Dimensional Supersonic Airfoil Theory, Bruno W. Augenstein..... 126
Some Relations Between Harmonic and Transient Loading of Airfoils, John W. Miles..... 671
Stabilization of Shock Waves in Channel Flow, Arthur Kantrowitz and Stanford E. Neice..... 316
Supersonic Airfoils Simplified, Ralph H. Upson..... 61
The Surface Pressure Coefficient for Approximate Compressible Flow Solutions, E. V. Laitone..... 381
Unsteady Flow Theory in Dynamic Stability, John W. Miles..... 62
Upper and Lower Bounds on Variational Integral in Compressible Flow, G. V. R. Rao..... 182
Second Approximation to Supersonic Conical Flows, Franklin K. Moore..... 328
Some Exact Solutions of the Flow Through Annular Cascade Actuator Discs, Stephen L. Bragg and William R. Hawthorne..... 243
Some Recent Measurements in a Two-Dimensional Turbulent Channel, John Laufer..... 277
Steady Flow of Nonviscous Elastic Fluids in Axially Symmetric Channels, M. H. Vavra..... 149
A Study of the Nonlinear Characteristics of Compressible Flow Equations by Means of Variational Methods, Chi-Teh Wang and G. V. R. Rao..... 343
Supersonic Tests of Conventional Control Surfaces on a Double-Wedge Airfoil, Michael Pindzola..... 20
A Theoretical Investigation of Heat Transfer in the Laminar Flow Regions of Airfoils, Leonard Goland..... 43
The Theoretical Lateral-Stability Derivatives for Wings at Supersonic Speeds, Arthur L. Jones..... 3
Transient Loading of Supersonic Rectangular Airfoils, John W. Miles..... 64
The Transient Temperature Distribution in a Wing Flying at Supersonic Speeds, Joseph Kaye..... 78
Transonic Flow Past Wedge Sections, H. W. Liepmann and A. E. Bryson, Jr..... 74
Turbulent Boundary-Layer Characteristics at Supersonic Speeds—Theory and Experiment, Robert E. Wilson.... 58
Aeroelastic problems, the solution of, by electronic analogue computation..... 38
Airfoil, thin-, theory, leading-edge singularities in..... 30
Airfoils, a theoretical investigation of heat transfer in the laminar flow regions of..... 43
Airfoils, supersonic rectangular, transient loading of..... 64
Airfoils, thin, in supersonic and transonic flight, influence of acceleration on aerodynamic characteristics of..... 4
ALLEN, RALPH W. The Effects of Weight Variation on the Range of Air-Borne Craft (Readers' Forum)..... 52
ANDERSON, JAMES E., AND WALTER W. SOROKA. Electrical Analog Solution for Centrifugally Tuned Pendulum Absorber System..... 34
AUGENSTEIN, BRUNO W. Second-Order Two-Dimensional Supersonic Airfoil Theory (Readers' Forum)..... 12
Automatic Control—
Application of Frequency-Response Analysis to Aircraft-Autopilot Stability, Charles L. Seacord, Jr..... 48
Determination of Frequency Characteristics from Response to Arbitrary Input, E. R. Walters and J. B. Rea..... 44
Longitudinal Stability of Autopilot-Controlled Aircraft, Andrew Vazsonyi..... 39
BAIRD, EUGENE F., AND HENRY J. KELLEY. Formulation of the Flutter Problem for Solution on an Electronic Analog Computer (Readers' Forum)..... 18
BARTON, M. V. Correction for "The Effect of Variation of Mass on the Dynamic Stability of Jet-Propelled Missiles" (Readers' Forum)..... 74
——— The Effect of Variation of Mass on the Dynamic Stability of Jet-Propelled Missiles..... 19
BATCHELOR, G. K. Note on Free Turbulent Flows, with Special Reference to the Two-Dimensional Wake..... 44
BATTIN, R. H., AND C. C. LIN. On the Stability of the Boundary Layer over a Cone (Readers' Forum)..... 45
BIJLAARD, P. P. On the Plastic Buckling of Plates (Readers' Forum)..... 74
——— On the Plastic Buckling of Plates According to the Flow Theory (Readers' Forum)..... 81
——— Stability of Alclad Plates (Readers' Forum)..... 25
——— Stability of Sandwich Plates in Combined Shear and Compression (Readers' Forum)..... 6
BISPLINGHOFF, R. L., G. ISAKSON, AND T. H. H. PIAN. Methods in Transient Stress Analysis..... 25
BLASINGAME, B. P., R. C. SEAMANS, JR., AND G. C. CLEMENTSON. The Pulse Method for the Determination of Aircraft Dynamic Performance..... 2
BOLEY, BRUNO A. The Shearing Rigidity of Buckled Sheet Panels..... 35
——, AND ROLAND H. MOORE. Note on the Calculation of Deflections of Indeterminate Structures (Readers' Forum)..... 52

BOLZ, RAY E. A Note on the Approximate Plane Motion During the Burning Period of Rocket-Propelled Missiles Launched at Small Angles of Yaw from Aircraft 114
——— Note on "Interference Between Wing and Body at Supersonic Speeds" (Readers' Forum) 453
———, AND JOHN D. NICOLAIDES. A Method of Determining Some Aerodynamic Coefficients from Supersonic Free-Flight Tests of a Rolling Missile 609
BORG, S. F. A Note on Boundary-Layer Type Solutions in Applied Mechanics (Readers' Forum) 253
Boundary layer, incompressible, with pressure gradient and suction 335
Boundary layer, turbulent, on a flat plate in compressible flow from measurements of friction in pipes, characteristics of the 573
Boundary-layer characteristics, turbulent, at supersonic speeds—theory and experiment 585
BOUTON, INNES. Lift-Curve Slope for Swept and Unswept Wings (Readers' Forum) 185
BRAGG, STEPHEN L., AND WILLIAM R. HAWTHORNE. Some Exact Solutions of the Flow Through Annular Cascade Actuator Discs 243
BRATT, R. W., M. W. FOSSIER, AND D. G. DILL. Comparison of Analytical and High-Speed Mechanical-Calculator Solutions of the Lateral Equations of Motion of an Airplane, Including Product-of-Inertia Terms 271
BROADWELL, JAMES E. Note on Rotational Gas Flow (Readers' Forum) 123
BRODSKY, R. F., AND CHI-TEH WANG. Approximate Solution of Compressible Fluid-Flow Problems by Galerkin's Method 660
BROERSMA, G. Detonation and Static Electricity in the Tropical Atmosphere (Readers' Forum) 125
BRYSON, A. E., JR., AND H. W. LIEPMANN. Transonic Flow Past Wedge Sections 745
Buckling, inelastic column 159

Cascade actuator discs, annular, some exact solutions of the flow through 243
Channel, a two-dimensional turbulent, some recent measurements in 277
CHAPMAN, DEAN R. Note on Base Pressure Measurements (Readers' Forum) 812
CHOU, PEI-CHI, AND CHI-TEH WANG. Application of Biezeno-Koch Method to Compressible Fluid Flow Problems (Readers' Forum) 599
CHUBB, R. S., AND C. W. FRICK. The Longitudinal Stability of Elastic Swept Wings at Supersonic Speed 691
CICALA, P. Column Buckling in the Elastoplastic Range 508
——— On Plastic Buckling of a Compressed Strip (Readers' Forum) 378
CLEMENTSON, G. C., R. C. SEAMANS, JR., AND B. P. BLASINGAME. The Pulse Method for the Determination of Aircraft Dynamic Performance 22
COHEN, C. B., AND P. J. EVANS, JR. Note on Desirability of Completely Expanded Nozzles (Readers' Forum) 811
Column behavior in the plastic stress range 323
Column buckling in the elastoplastic range 508
Columns, bifurcation criterion and plastic buckling of plates and 417
Compressible flow equations, a study of the nonlinear characteristics of, by means of variational methods 343
Control surfaces, conventional, on a double-wedge airfoil, supersonic tests of 204
CORRSIN, STANLEY. Hypothesis for Skewness of the Probability Density of the Lateral Velocity Fluctuations in Turbulent Shear Flow 396
COX, H. L., AND D. G. SOPWITH. Determination of Deflections in Redundant Structures (Readers' Forum) 815
CROWN, J. CONRAD. On Boundary-Layer Growth in a Compressible Flow Between Radial Walls (Readers' Forum) 667
Cylinders, thin-walled closed, beyond the elastic limit, torsion of 499

DENKE, PAUL H. Analysis and Design of Stiffened Shear Webs 217
DENNIS, P. A., AND D. G. DILL. Application of Simultaneous Equation Machines to Aircraft Structure and Flutter Problems 107
Design—
Development of High-Speed Water-Based Aircraft, Ernest G. Stout 457
The Influence of Design Parameters on the Performance of Subsonic Air Inlets, Howard E. Roberts and B. D. Langtry 429
Some Factors Affecting Large Transport Aeroplanes with Turboprop Engines, A. E. Russell 67, 176
A Study of the Response of an Airplane Landing Gear Using the Differential Analyzer, Walter C. Hurty 756
DILL, D. G., AND P. A. DENNIS. Application of Simultaneous Equation Machines to Aircraft Structure and Flutter Problems 107
———, M. W. FOSSIER, AND R. W. BRATT. Comparison of Analytical and High-Speed Mechanical-Calculator Solutions of the Lateral Equations of Motion of an Airplane, Including Product-of-Inertia Terms 271
DUBERG, JOHN E., AND THOMAS W. WILDER, III. Column Behavior in the Plastic Stress Range 323
DURHAM, F. P. Increased Jet Thrust from Pressure Forces 425

ECKERT, HANS ULRICH. Characteristics of the Turbulent Boundary Layer on a Flat Plate in Compressible Flow from Measurements of Friction in Pipes 573
EVANS, P. J., JR., AND C. B. COHEN. Note on Desirability of Completely Expanded Nozzles (Readers' Forum) 811

FETTIS, HENRY E. A Note on the Evaluation of a Definite Integral (Readers' Forum) 184
FISCHEL, JACK, FRANCIS M. ROGALLO, AND JOHN G. LOWRY. Lateral-Control Devices Suitable for Use with Full-Span Flaps 629
Flaps, full-span, lateral-control devices suitable for use with 629
FLAX, ALEXANDER H. On a Variational Principle in Lifting-Line Theory (Readers' Forum) 596
Flight Propulsion—
Increased Jet Thrust from Pressure Forces, F. P. Durham. 425
The Influence of Design Parameters on the Performance of Subsonic Air Inlets, Howard E. Roberts and B. D. Langtry 429
Readers' Forum
Comment on "Heat Source in a Uniform Flow," B. L. Hicks, W. H. Hebrank, and S. Kravitz 595
Comments on "Heat Transfer in Laminar Compressible Boundary Layer," P. Grootenhuis 595
Heat Addition to a Flowing Gas, Roger Weatherston .. 182
The Mechanism of Unstable Combustion, W. C. Randels 124
Note on Desirability of Completely Expanded Nozzles, C. B. Cohen and P. J. Evans, Jr 811

A Note on the Subsonic Compressible Flow About Airfoils in a Cascade, Henry W. Woolard ... 379
An Observation Concerning the Rankine-Hugoniot Relations, Jack Lorell ... 317
The Reflection of "Rectilinear" Waves in One-Dimensional Gas Flows, Lorenzo Poggi ... 813
Stabilization of Shock Waves in Channel Flow, Arthur Kantrowitz and Stanford E. Neice ... 316
Some Exact Solutions of the Flow Through Annular Cascade Actuator Discs, Stephen L. Bragg and William R. Hawthorne ... 243
Some Factors Affecting Large Transport Aeroplanes with Turboprop Engines, A. E. Russell ... 67, 176
Steady Flow of Nonviscous Elastic Fluids in Axially Symmetric Channels, M. H. Vavra ... 149
FLOMENHOFT, H. I., AND T. H. H. PIAN. Analytical and Experimental Studies on Dynamic Loads in Airplane Structures During Landing ... 765
Fluids, nonviscous elastic, in axially symmetric channels, steady flow of ... 149
FOGARTY, L. E., AND W. R. SEARS. Potential Flow Around a Rotating, Advancing Cylindrical Blade (Readers' Forum) ... 599
FOSSIER, M. W., R. W. BRATT, AND D. G. DILL. Comparison of Analytical and High-Speed Mechanical-Calculator Solutions of the Lateral Equations of Motion of an Airplane, Including Product-of-Inertia Terms ... 271
FRAEYS DE VEUBEKE, B. M. Crankshaft-Propeller Vibration Modes as Influenced by the Torsional Flexibility of the Engine Suspension ... 288
FRICK, C. W., AND R. S. CHUBB. The Longitudinal Stability of Elastic Swept Wings at Supersonic Speed ... 691
FUNG, Y. C., E. E. SECHLER, AND M. L. WILLIAMS. An Initial Approach to the Overall Structural Problems of Swept Wings Under Static Loads ... 639

GABEAUD, A. Base Pressures at Supersonic Velocities (Readers' Forum) ... 525
GARDNER, C. S., AND H. F. LUDLOFF. Influence of Acceleration on Aerodynamic Characteristics of Thin Airfoils in Supersonic and Transonic Flight ... 47
GATEWOOD, B. E. Effect of Wing Parameters on Load Intensity in Wing Skin (Readers' Forum) ... 668
GERARD, GEORGE. Note on Plastic Column Behavior (Readers' Forum) ... 670
GOLAND, LEONARD. A Theoretical Investigation of Heat Transfer in the Laminar Flow Regions of Airfoils ... 436
GOLAND, MARTIN. The Quasi-Steady Air Forces for Use in Low-Frequency Stability Calculations ... 601
GOODMAN, THEODORE R. The Problem of Edges in the Doublet Distribution Method of Obtaining Supersonic Lift (Readers' Forum) ... 376
GRAHAM, DUNSTAN, AND ALLAN MCCASKILL. Roll to Sideslip or Yaw Ratios (Readers' Forum) ... 741
GRAHAM, ERNEST W. The Pressure on a Slender Body of Nonuniform Cross-Sectional Shape in Axial Supersonic Flow ... 173
GRAVALOS, F. G. Flow of Nonviscous Elastic Fluids (Readers' Forum) ... 375
GREIDANUS, J. H., AND A. I. VAN DE VOOREN. Complementary Energy Method in Vibration Analysis (Readers' Forum) ... 454
———— Station Functions in Flutter Analysis (Readers' Forum) ... 178
GRIMMINGER, G., E. P. WILLIAMS, AND G. B. W. YOUNG. Lift on Inclined Bodies of Revolution in Hypersonic Flow ... 675
GROOTENHUIS, P. Comments on "Heat Transfer in Laminar Compressible Boundary Layer" (Readers' Forum) ... 595
GUDERLEY, G., AND H. YOSHIHARA. The Flow over a Wedge Profile at Mach Number 1 ... 723

HAEFELI, RUDOLPH C., AND HAROLD MIRELS. The Calculation of Supersonic Downwash Using Line Vortex Theory ... 13
HANDELMAN, G. H. Torsion of Thin-Walled Closed Cylinders Beyond the Elastic Limit ... 499
HAWTHORNE, WILLIAM R., AND STEPHEN L. BRAGG. Some Exact Solutions of the Flow Through Annular Cascade Actuator Discs ... 243
HEBRANK, W. H., B. L. HICKS, AND S. KRAVITZ. Comment on "Heat Source in a Uniform Flow" (Readers' Forum) ... 595
Helicopters—
A Method for Improving the Inherent Stability and Control Characteristics of Helicopters, R. H. Miller ... 363
A Type of Lifting Rotor with Inherent Stability, Kurt Hohenemser ... 555
HICKS, B. L., W. H. HEBRANK, AND S. KRAVITZ. Comment on "Heat Source in a Uniform Flow" (Readers' Forum) ... 595
HILL, FREEMAN K. Base Pressures at Supersonic Velocities (Readers' Forum) ... 185
HOERNER, SIGHARD F. Base Drag and Thick Trailing Edges ... 622
HOFF, N. J. Plastic Column Behavior (Readers' Forum) ... 743
HOHENEMSER, KURT. A Type of Lifting Rotor with Inherent Stability ... 555
HOUBOLT, JOHN C. A Recurrence Matrix Solution for the Dynamic Response of Elastic Aircraft ... 540
HURTY, WALTER C. A Study of the Response of an Airplane Landing Gear Using the Differential Analyzer ... 756
Hypersonic flow, a mechanical analogy for ... 519
Hypersonic flow, lift on inclined bodies of revolution in ... 675

Inlets, subsonic air, the influence of design parameters on the performance of ... 429
Instruments—
The Hot-Wire Anemometer in Supersonic Flow, Leslie S. G. Kovásznay ... 565
ISAKSON, G., R. L. BISPLINGHOFF, AND T. H. H. PIAN. Methods in Transient Stress Analysis ... 259
————, AND T. F. O'BRIEN. The Influence of Some Parameters in the Flutter Problem (Readers' Forum) ... 318
IVEY, H. REESE. A Mechanical Analogy for Hypersonic Flow ... 519

JONES, ARTHUR L. The Theoretical Lateral-Stability Derivatives for Wings at Supersonic Speeds ... 39
JONES, ROBERT T. Leading-Edge Singularities in Thin-Airfoil Theory ... 307

KANTROWITZ, ARTHUR, AND STANFORD E. NEICE. Stabilization of Shock Waves in Channel Flow (Readers' Forum) ... 316
————, AND ROBERT L. TRIMPI. A Sharp-Focusing Schlieren System ... 311
KAYE, JOSEPH. The Transient Temperature Distribution in a Wing Flying at Supersonic Speeds ... 787

KELLEY, HENRY J., AND EUGENE F. BAIRD. Formulation of the Flutter Problem for Solution on an Electronic Analog Computer (Readers' Forum) ... 189
KORVIN-KROUKOVSKY, B. V. Lift of Planing Surfaces (Readers' Forum) ... 597
KOVÁSZNAY, LESLIE S. G. The Hot-Wire Anemometer in Supersonic Flow ... 565
KRAVITZ, S., B. L. HICKS, AND W. H. HEBRANK. Comment on "Heat Source in a Uniform Flow" (Readers' Forum) ... 595

LAITONE, E. V. Approximate Incompressible Flow Solutions for Slender Polygons (Readers' Forum) ... 375
——— The Extension of the Prandtl-Glauert Rule (Readers' Forum) ... 250
——— The Surface Pressure Coefficient for Approximate Compressible Flow Solutions (Readers' Forum) ... 381
Landing, analytical and experimental studies on dynamic loads in airplane structures during ... 765
Landing gear, a study of the response of an airplane, using the differential analyzer ... 756
LANGTRY, B. D., AND HOWARD E. ROBERTS. The Influence of Design Parameters on the Performance of Subsonic Air Inlets ... 429
LAUFER, JOHN. Some Recent Measurements in a Two-Dimensional Turbulent Channel ... 277
LEWIS, ROBERT C., AND DONALD L. WRISLEY. A System for the Excitation of Pure Natural Modes of Complex Structure ... 705
LI, TING-YI, AND H. J. STEWART. Periodic Motions of a Rectangular Wing Moving at Supersonic Speed ... 529
LIEPMANN, H. W., AND A. E. BRYSON, JR. Transonic Flow Past Wedge Sections ... 745
LIN, C. C., AND R. H. BATTIN. On the Stability of the Boundary Layer over a Cone (Readers' Forum) ... 453
LIN, TUNG-HUA. Inelastic Column Buckling ... 159
LORELL, JACK. An Observation Concerning the Rankine-Hugoniot Relations (Readers' Forum) ... 317
LOWRY, JOHN G., FRANCIS M. ROGALLO, AND JACK FISCHEL. Lateral-Control Devices Suitable for Use with Full-Span Flaps ... 629
LUDLOFF, H. F., AND C. S. GARDNER. Influence of Acceleration on Aerodynamic Characteristics of Thin Airfoils in Supersonic and Transonic Flight ... 47
LUSKIN, HAROLD. Predictions of Supersonic Airplane Performance ... 5

Materials—
Plastic Collapse and Shakedown Theorems for Structures of Strain-Hardening Material, B. G. Neal ... 297
Readers' Forum
Stability of Alclad Plates, P. P. Bijlaard ... 252
McCASKILL, ALLAN, AND DUNSTAN GRAHAM. Roll to Side-slip or Yaw Ratios (Readers' Forum) ... 741
Meteorology—
Readers' Forum
Detonation and Static Electricity in the Tropical Atmosphere, G. Broersma ... 125
MEYERHOFF, LEONARD. An Extension of the Theory of the One-Dimensional Shock-Wave Structure ... 775
MICKS, W. R. Effect of Torsional Stiffness Requirements on Wing Structural Weight ... 736
——— Minimum Weight of Stiffened Cylindrical Shells in Pure Bending ... 211
MIELE, ANGELO. On the Speed of an Airplane in Steady Flight (Readers' Forum) ... 808
MILLER, R. H. A Method for Improving the Inherent Stability and Control Characteristics of Helicopters ... 363
MILES, EDWARD R. C. On a Family of Oblique Shock Curves ... 157
MILES, JOHN W. On the Compressibility Correction for Subsonic Unsteady Flow (Readers' Forum) ... 181
——— On Downwash Corrections in Unsteady Flow (Readers' Forum) ... 253
——— On the Equations of Longitudinal Stability (Readers' Forum) ... 815
——— On the Reduction of Unsteady Supersonic Flow Problems to Steady Flow Problems (Readers' Forum) ... 64
——— On Simple Plan Forms in Supersonic Flow (Readers' Forum) ... 127
——— On Virtual Mass and Wave Drag at Subsonic Speeds (Readers' Forum) ... 667
——— Some Relations Between Harmonic and Transient Loading of Airfoils (Readers' Forum) ... 671
——— Transient Loading of Supersonic Rectangular Airfoils ... 647
——— Unsteady Flow Theory in Dynamic Stability (Readers' Forum) ... 62
MILLIKAN, C. B. Another Note on the Velocity of Sound (Readers' Forum) ... 252
MIRELS, HAROLD, AND RUDOLPH C. HAEFELI. The Calculation of Supersonic Downwash Using Line Vortex Theory ... 13
Missiles—
Base Drag and Thick Trailing Edges, Sighard F. Hoerner ... 622
The Effect of Variation of Mass on the Dynamic Stability of Jet-Propelled Missiles, M. V. Barton ... 197
A Method of Determining Some Aerodynamic Coefficients from Supersonic Free-Flight Tests of a Rolling Missile, Ray E. Bolz and John D. Nicolaides ... 609
A Note on the Approximate Plane Motion During the Burning Period of Rocket-Propelled Missiles Launched at Small Angles of Yaw from Aircraft, Ray E. Bolz ... 114
Readers' Forum
Base Pressures at Supersonic Velocities, A. Gabeaud ... 525
Base Pressures at Supersonic Velocities, Freeman K. Hill ... 185
Correction for "The Effect of Variation of Mass on the Dynamic Stability of Jet-Propelled Missiles," M. V. Barton ... 741
Note on Base Pressure Measurements, Dean R. Chapman ... 812
MOORE, FRANKLIN K. Second Approximation to Supersonic Conical Flows ... 328
MOORE, ROLAND H., AND BRUNO A. BOLEY. Note on the Calculation of Deflections of Indeterminate Structures (Readers' Forum) ... 526
MORDUCHOW, MORRIS. Further Remarks on the Velocity of Sound (Readers' Forum) ... 180
MORIKAWA, GEORGE K. On Wing-Body Interference at Supersonic Speeds (Readers' Forum) ... 315
MORKOVIN, M. V. A Note on the Velocity of Sound (Readers' Forum) ... 180
MUNK, MAX M. Remarks on the Velocity of Sound (Readers' Forum) ... 376

NEAL, B. G. Plastic Collapse and Shakedown Theorems for Structures of Strain-Hardening Material ... 297
NEICE, STANFORD E., AND ARTHUR KANTROWITZ. Stabilization of Shock Waves in Channel Flow (Readers' Forum) ... 316

NICOLAIDES, JOHN D., AND RAY E. BOLZ. A Method of Determining Some Aerodynamic Coefficients from Supersonic Free-Flight Tests of a Rolling Missile..... 609

O'BRIEN, T. F., AND G. ISAKSON. The Influence of Some Parameters in the Flutter Problem (Readers' Forum)... 318

PAI, S. I. On the Stability for a Certain Degenerate Type of Disturbance of Viscous Fluid Flow Between Parallel Walls (Readers' Forum)..... 525

———————— On the Vorticity of the Flow Behind Curved Shock (Readers' Forum)..... 188

Panels, buckled sheet, the shearing rigidity of..... 356

PEARSON, C. E. Bifurcation Criterion and Plastic Buckling of Plates and Columns..... 417

Performance—

Investigation of Lateral Dynamic Stability in the XB-47 Airplane, Roland J. White..... 133

Predictions of Supersonic Airplane Performance, Harold Luskin..... 5

Readers' Forum

The Effects of Weight Variation on the Range of Air-Borne Craft, Ralph W. Allen..... 527

On the Speed of an Airplane in Steady Flight, Angelo Miele..... 808

Performance, aircraft dynamic, the pulse method for the determination of..... 22

PIAN, T. H. H., R. L. BISPLINGHOFF, AND G. ISAKSON. Methods in Transient Stress Analysis..... 259

————————, AND H. I. FLOMENHOFT. Analytical and Experimental Studies on Dynamic Loads in Airplane Structures During Landing..... 765

PINDZOLA, MICHAEL. Supersonic Tests of Conventional Control Surfaces on a Double-Wedge Airfoil..... 204

Plates and columns, bifurcation criterion and plastic buckling of..... 417

POGGI, LORENZO. The Reflection of "Rectilinear" Waves in One-Dimensional Gas Flows (Readers' Forum)..... 813

Prandtl, Ludwig, seventy-fifth anniversary of..... 121

RANDELS, W. C. The Mechanism of Unstable Combustion (Readers' Forum)..... 124

RAO, G. V. R. Upper and Lower Bounds on Variational Integral in Compressible Flow (Readers' Forum)..... 182

————————, AND CHI-TEH WANG. A Study of the Nonlinear Characteristics of Compressible Flow Equations by Means of Variational Methods..... 343

REA, J. B., AND E. R. WALTERS. Determination of Frequency Characteristics from Response to Arbitrary Input..... 446

REISSNER, E. Determination of Flutter Frequencies and Speeds (Readers' Forum)..... 455

ROBERTS, HOWARD E., AND B. D. LANGTRY. The Influence of Design Parameters on the Performance of Subsonic Air Inlets..... 429

Rocket-propelled missiles launched at small angles of yaw from aircraft, a note on the approximate plane motion during the burning period of..... 114

ROGALLO, FRANCIS M., JOHN G. LOWRY, AND JACK FISCHEL. Lateral-Control Devices Suitable for Use with Full-Span Flaps..... 629

RUSSELL, A. E. Some Factors Affecting Large Transport Aeroplanes with Turboprop Engines..... 67, 176

SCANLAN, R. H., AND JOHN C. TRUMAN. The Gyroscopic Effect of a Rigid Rotating Propeller on Engine and Wing Vibration Modes..... 632

SCHAIRER, GEORGE S. Hydrodynamic Longitudinal Stability..... 513

Schlieren system, a sharp-focusing..... 311

SEACORD, CHARLES L., JR. Application of Frequency-Response Analysis to Aircraft-Autopilot Stability..... 481

SEAMANS, R. C., JR., B. P. BLASINGAME, AND G. C. CLEMENTSON. The Pulse Method for the Determination of Aircraft Dynamic Performance..... 22

Seaplanes and Flying Boats—

Development of High-Speed Water-Based Aircraft, Ernest G. Stout..... 457

Hydrodynamic Longitudinal Stability, George S. Schairer. 513

Readers' Forum

Lift of Planing Surfaces, B. V. Korvin-Kroukovsky... 507

SEARS, W. R. Potential Flow Around a Rotating Clyindrical Blade (Readers' Forum)..... 181

————————, AND L. E. FOGARTY. Potential Flow Around a Rotating, Advancing Cylindrical Blade (Readers' Forum)..... 509

SECHLER, E. E., M. L. WILLIAMS, AND Y. C. FUNG. An Initial Approach to the Overall Structural Problems of Swept Wings Under Static Loads..... 639

Shells, stiffened cylindrical, in pure bending, minimum weight of..... 211

Shock curves, oblique, on a family of..... 157

Shock wave, steady, on the thickness of a..... 551

Shock-wave structure, one-dimensional, an extension of the theory of the..... 775

SIEGEL, KEEVE M. Boundaries of Fluid Mechanics (Readers' Forum)..... 191

SOPWITH, D. G., AND H. L. COX. Determination of Deflections in Redundant Structures (Readers' Forum)..... 815

SOROKA, WALTER W., AND JAMES E. ANDERSON. Electrical Analog Solution for Centrifugally Tuned Pendulum Absorber System..... 349

Stability calculations, low-frequency, the quasi-steady air forces for use in..... 601

Stability, dynamic, at high speeds from unsteady flow theory..... 232

tability, dynamic, of jet-propelled missiles, the effect of variation of mass on the..... 197

Stability, lateral dynamic, in the XB-47 airplane, investigation of..... 133

Stability, longitudinal, of autopilot-controlled aircraft..... 399

STATLER, I. C. Dynamic Stability at High Speeds from Unsteady Flow Theory..... 232

STEWART, H. J., AND TING-YI LI. Periodic Motions of a Rectangular Wing Moving at Supersonic Speed..... 529

STOUT, ERNEST G. Development of High-Speed Water-Based Aircraft..... 457

Stress Analysis and Structures—

Analysis and Design of Stiffened Shear Webs, Paul H. Denke..... 217

Analytical and Experimental Studies on Dynamic Loads in Airplane Structures During Landing, T. H. H. Pian and H. I. Flomenhoft..... 765

Application of Simultaneous Equation Machines to Aircraft Structure and Flutter Problems, P. A. Dennis and D. G. Dill..... 107

Bifurcation Criterion and Plastic Buckling of Plates and Columns, C. E. Pearson..... 417

Column Behavior in the Plastic Stress Range, John E. Duberg and Thomas W. Wilder, III..... 323

Column Buckling in the Elastoplastic Range, P. Cicala.... 508
Effect of Torsional Stiffness Requirements on Wing Structural Weight, W. R. Micks..... 736
Inelastic Column Buckling, Tung-Hua Lin..... 159
An Initial Approach to the Overall Structural Problems of Swept Wings Under Static Loads, E. E. Sechler, M. L. Williams, and Y. C. Fung..... 639
Methods in Transient Stress Analysis, R. L. Bisplinghoff, G. Isakson, and T. H. H. Pian..... 259
Minimum Weight of Stiffened Cylindrical Shells in Pure Bending, W. R. Micks..... 211
Readers' Forum
The Basic Theorems in the Plastic Theory of Structures, P. S. Symonds..... 669
Determination of Deflections in Redundant Structures, H. L. Cox and D. G. Sopwith..... 815
Effect of Wing Parameters on Load Intensity in Wing Skin, B. E. Gatewood..... 668
Note on the Calculation of Deflections of Indeterminate Structures, Bruno A. Boley and Roland H. Moore..... 526
Note on Plastic Column Behavior, George Gerard..... 670
On Plastic Buckling of a Compressed Strip, P. Cicala.. 378
On the Plastic Buckling of Plates, P. P. Bijlaard..... 742
On the Plastic Buckling of Plates According to the Flow Theory, P. P. Bijlaard..... 810
Plastic Column Behavior, N. J. Hoff..... 743
Stability of Alclad Plates, P. P. Bijlaard..... 252
Stability of Sandwich Plates in Combined Shear and Compression, P. P. Bijlaard..... 63
The Shearing Rigidity of Buckled Sheet Panels, Bruno A. Boley..... 356
Torsion of Thin-Walled Closed Cylinders Beyond the Elastic Limit, G. H. Handelman..... 499
Structures of strain-hardening material, plastic collapse and shakedown theorems for..... 297
Supersonic airplane performance, predictions of..... 5
Supersonic conical flows, second approximation to..... 328
Supersonic downwash using line vortex theory, the calculation of..... 13
Supersonic flow, axial, the pressure on a slender body of nonuniform cross-sectional shape in..... 173
Supersonic flow, the hot-wire anemometer in..... 565
SYMONDS, P. S. The Basic Theorems in the Plastic Theory of Structures (Readers' Forum)..... 669
SZEBEHELY, V. G. An Analogy Between Open Soap Bubble and Compressible Flow (Readers' Forum)..... 809

THOMPSON, M. J. A Note on the Calculation of Oblique Shock-Wave Characteristics (Readers' Forum)..... 744
TIFFORD, ARTHUR N. On the Surface Effects of a Compressible Laminar Boundary Layer (Readers' Forum)... 187
Transonic flow past wedge sections..... 745
Transport aeroplanes with turboprop engines, some factors affecting large..... 67, 176
TRILLING, LEON. The Incompressible Boundary Layer with Pressure Gradient and Suction..... 335
TRIMPI, ROBERT L., AND ARTHUR KANTROWITZ. A Sharp-Focusing Schlieren System..... 311
TRUMAN, JOHN C., AND R. H. SCANLAN. The Gyroscopic Effect of a Rigid Rotating Propeller on Engine and Wing Vibration Modes..... 653

UPSON, RALPH H. Supersonic Airfoils Simplified (Readers' Forum: Incorrectly attributed to James E. Broadwell).. 61

VAN DE VOOREN, A. I., AND J. H. GREIDANUS. Complementary Energy Method in Vibration Analysis (Readers' Forum)..... 454
———————— Station Functions in Flutter Analysis (Readers' Forum)..... 178
VAVRA, M. H. Steady Flow of Nonviscous Elastic Fluids in Axially Symmetric Channels..... 149
VAZSONYI, ANDREW. Longitudinal Stability of Autopilot-Controlled Aircraft..... 399
Vibration and Flutter—
Application of Simultaneous Equation Machines to Aircraft Structure and Flutter Problems, P. A. Dennis and D. G. Dill..... 107
Crankshaft-Propeller Vibration Modes as Influenced by the Torsional Flexibility of the Engine Suspension, B. M. Fraeys de Veubeke..... 288
Dynamic Stability at High Speeds from Unsteady Flow Theory, I. C. Statler..... 232
Electrical Analog Solution for Centrifugally Tuned Pendulum Absorber System, James E. Anderson and Walter W. Soroka..... 349
The Gyroscopic Effect of a Rigid Rotating Propeller on Engine and Wing Vibration Modes, R. H. Scanlan and John C. Truman..... 653
Periodic Motions of a Rectangular Wing Moving at Supersonic Speed, H. J. Stewart and Ting-Yi Li..... 529
The Quasi-Steady Air Forces for Use in Low-Frequency Stability Calculations, Martin Goland..... 601
Readers' Forum
Complementary Energy Method in Vibration Analysis, A. I. van de Vooren and J. H. Greidanus..... 454
Determination of Flutter Frequencies and Speeds, E. Reissner..... 455
Formulation of the Flutter Problem for Solution on an Electronic Analog Computer, Eugene F. Baird and Henry J. Kelley..... 189
The Influence of Some Parameters in the Flutter Problem, G. Isakson and T. F. O'Brien..... 318
A Note on the Evaluation of a Definite Integral, Henry E. Fettis..... 184
Station Functions in Flutter Analysis, J. H. Greidanus and A. I. van de Vooren..... 178
A Recurrence Matrix Solution for the Dynamic Response of Elastic Aircraft, John C. Houbolt..... 540
The Solution of Aeroelastic Problems by Electronic Analogue Computation, Jonathan Winson..... 385
A System for the Excitation of Pure Natural Modes of Complex Structure, Robert C. Lewis and Donald L. Wrisley..... 705
VON MISES, R. On the Thickness of a Steady Shock Wave. 551

WALTERS, E. R., AND J. B. REA. Determination of Frequency Characteristics from Response to Arbitrary Input..... 446
WANG, CHI-TEH, AND R. F. BRODSKY. Approximate Solution of Compressible Fluid-Flow Problems by Galerkin's Method..... 660
————————, AND PEI-CHI CHOU. Application of Biezeno-Koch Method to Compressible Fluid Flow Problems (Readers' Forum)..... 599
————————, AND G. V. R. RAO. A Study of the Nonlinear Characteristics of Compressible Flow Equations by Means of Variational Methods..... 343
Water-based aircraft, high-speed, development of..... 457
WEATHERSTON, ROGER. Heat Addition to a Flowing Gas (Readers' Forum)..... 182
Webs, stiffened shear, analysis and design of..... 217

WHITE, ROLAND J. Investigation of Lateral Dynamic Stability in the XB-47 Airplane 133
WILDER, THOMAS W., III, AND JOHN E. DUBERG. Column Behavior in the Plastic Stress Range 323
WILLIAMS, E. P., G. GRIMMINGER, AND G. B. W. YOUNG. Lift on Inclined Bodies of Revolution in Hypersonic Flow. 675
WILLIAMS, M. L., E. E. SECHLER, AND Y. C. FUNG. An Initial Approach to the Overall Structural Problems of Swept Wings Under Static Loads 639
WILSON, ROBERT E. Turbulent Boundary-Layer Characteristics at Supersonic Speeds—Theory and Experiment. 585
Wind Tunnels—
A Sharp-Focusing Schlieren System, Arthur Kantrowitz and Robert L. Trimpi 311
Wing flying at supersonic speeds, the transient temperature distribution in a 787
Wing, rectangular, moving at supersonic speed, periodic motions of a 529
Wing structural weight, effect of torsional stiffness requirements on 736
Wings at supersonic speeds, the theoretical lateral-stability derivatives for 39
Wings, elastic swept, at supersonic speed, the longitudinal stability of 691
Wings, swept, under static loads, an initial approach to the overall structural problems of 639
WINSON, JONATHAN. The Solution of Aeroelastic Problems by Electronic Analogue Computation 385
WOOLARD, HENRY W. A Note on the Subsonic Compressible Flow About Airfoils in a Cascade (Readers' Forum). 379
WRISLEY, DONALD L., AND ROBERT C. LEWIS. A System for the Excitation of Pure Natural Modes of Complex Structure 705

YOSHIHARA, H., AND G. GUDERLEY. The Flow over a Wedge Profile at Mach Number 1 723
YOUNG, G. B. W., G. GRIMMINGER, AND E. P. WILLIAMS. Lift on Inclined Bodies of Revolution in Hypersonic Flow. 675

Library Facilities of the

Institute of the Aeronautical Sciences

To serve Institute members and others in the aeronautical industry, the Institute of the Aeronautical Sciences offers the facilities of:

The W. A. M. Burden Library

2 East 64th Street
New York 21, N.Y.

The facilities of this library are available for reference study at the Institute.

The Paul Kollsman Lending Library

2 East 64th Street
New York 21, N.Y.

This library loans books without charge to members and others in the United States over eighteen years of age. Full information will be sent on request.

The Pacific Aeronautical Library

7660 Beverly Boulevard
Los Angeles 36, Calif.

This is a service and reference library for West Coast members and organizations. Full information as to its facilities will be sent on request.

SUGGESTIONS *for* CONTRIBUTORS
to the Publications of the
INSTITUTE *of the* AERONAUTICAL SCIENCES

The Institute of the Aeronautical Sciences invites both members and nonmembers from any country to submit papers for publication in the JOURNAL OF THE AERONAUTICAL SCIENCES and the AERONAUTICAL ENGINEERING REVIEW. The Institute, following the practice of other societies, does not pay for contributions.

The following directions for the preparation of papers, if followed by authors, will save correspondence, avoid the return of papers for changes, minimize the work of preparation for the printer, and save the expense due to the charges made for "author's corrections."

MANUSCRIPTS: The original typewritten copy of the paper desired, double or triple spaced on one side of white paper sheets, consecutively numbered. There should be wide margins to allow for the marking of directions to the printer. Correcting, changing, or adding to papers after they are in type is costly. It is, therefore, imperative that papers submitted be in final form. Typographical errors may be corrected on proofs, but if authors wish to add material, they may do so at their own expense. In mailing, drawings may be rolled, but manuscripts should be sent flat. Send by first-class mail (register, if you wish, for your own protection) to the Editorial Office, Institute of the Aeronautical Sciences, 2 East 64th Street, New York 21, N.Y. All manuscripts will be examined by the Editorial Committee and by the Editor. Authors will be advised as promptly as possible whether the paper is acceptable for publication.

TITLES: The title of the paper should be brief. The name and initials of the author should be written as he prefers. The use of the full name of an author is advocated because of the frequent duplication of initials and surnames which sometimes makes it difficult to establish the identity of the author. This is particularly important for large annual indexing and abstracting services. All titles and degrees or honors are omitted. The name of the organization with which the author is associated should be placed after his name on a separate line. The date on which the paper is received will be inserted by the Editor. The author's title should be indicated in a footnote.

SUMMARIES OR ABSTRACTS: An abstract to be printed at the beginning should accompany each article. It should be adequate as an *index* and as a *summary*. It should contain a statement of major conclusions reached, since summaries in many cases constitute the only source of information used in compiling scientific reference indexes. Abstracts printed in other journals, especially foreign, in most cases, consist of summaries from printed papers. The summary should explain as adequately as possible the major conclusions to a nonspecialist in the subject and should contain from 100 to 300 words, depending on the length of the paper.

SUBHEADINGS: Subheadings should be inserted by the author at frequent intervals. The work of editorial preparation will be simplified by the author providing many subheadings.

MATTER USUALLY DELETED: Photographs or illustrations of little technical interest and not showing advances in general practice. Too detailed tabular matter (general results of such tables may be included in the text). Lengthy descriptions of materials or processes or of preliminary experiments or theories that preceded final results; salient features only are of interest.

REFERENCES AND FOOTNOTES: References should appear as footnotes only, numbered consecutively, grouped together at the end of the manuscript. The arrangement should be as follows: (for books)—[1] Durand, W. F., *Aerodynamic Theory*, 1st Ed., Vol. 1, p. 23; Julius Springer, Berlin, 1934. (For magazines)—[1] Englund, C. R., Crawford, A. B., and Mumford, W. W., *Some Results of a Study of Ultra-Short-Wave Transmission Phenomenon*, Proc. I. R. E., Vol. 20, No. 12, pp. 481–482, March, 1933. Please give author, title, edition, volume, page, publisher, and date of publication as indicated. Omission of one required fact causes much extra editorial work and possible inaccuracies.

ILLUSTRATIONS: Illustrations should accompany manuscripts, and each should always be referred to in the text, by number. Drawings or graphs should not be larger than 12 × 16 inches, and must be made with jet black India Ink on white paper or tracing cloth, the latter being preferred. *Do not use typewriter for lettering.* The smallest lettering on 8- × 10-inch figures should be no less than 1/4 inch high. Cross-section paper (white with black lines) may be used but should not have more than 4 lines per inch. If finer ruled paper is used, the major division lines should be drawn in with black ink, omitting the finer divisions. In the case of finely ruled paper, only blue-lined paper can be accepted. *Tracing paper* and *blueprints* are not acceptable. Lettering and all markings must be large enough to be readable after reduction. Mail rolled or flat, never fold. Drawings that cannot be reproduced (including pencil drawings) will be returned to the author for redrawing, thus delaying publication of the paper. Photographs should be distinct and show clear black and white contrasts. They must be on glossy white paper. Avoid round and oval photographs.

CAPTIONS AND LEGENDS: Legends or captions must accompany each drawing or photograph submitted. If written on the drawing or photograph, they should be placed below and well outside the part to be reproduced. Each table should have a caption such as Table 1, Table 2, Table 3, etc. Captions should be complete in themselves so as to make the data intelligible to the reader without reference to the text. A duplicate list of captions for figures should be included as the last page of the manuscript. Use "Fig. 1" (not Figure 1), Figs. 3 and 4, etc., in both the text and the numbering of illustrations. In the text, "Eq. (1)," or "Eqs. (1) and (2)" are used, not "Equation (1)." In captions and legends, except for "Fig." and "Eq.," and in table headings, write all words in full; do not abbreviate.

MATHEMATICAL WORK: Only the simplest formulas should be typewritten, all others should be carefully written in pen and ink, the writing to be large enough so that ample room is provided to mark mathematical matter for the printer. A considerable space for marking should be allowed above and below all equations. All complicated equations should be repeated on separate sheets with plenty of space left for marking. The solidus should be used for simple fractions appearing within the text. Make all expressions clear to the typesetter. Greek letters used in formulas should be clearly designated by name on the margin of the manuscript. All symbols should be clearly written and carefully checked. The difference between capital and lower-case letters should be clearly distinguished and care taken to avoid confusion between zero (0) and the letter (o), between the numeral (one) and the letter (ell) and the prime (′), between alpha and a, kappa and k, u and mu, v and nu, n and eta. All subscripts and exponents should be clearly marked, and dots and bars over letters or mathematical expressions should be avoided. Avoid complicated exponents and subscripts. When it is necessary to repeat a complicated expression, it should be represented by some convenient symbol.

NOMENCLATURE AND ABBREVIATIONS: Standard abbreviations should be used, and it should be noted that most abbreviations are lower case such as m.p.h., b.m.e.p., i.hp., b.hp., hp., . . . etc.

CORPORATE MEMBERS
OF THE
INSTITUTE OF THE AERONAUTICAL SCIENCES

ACADEMY OF AERONAUTICS, INC.
  CASEY JONES SCHOOL OF AERONAUTICS
ALVIN P. ADAMS AND ASSOCIATES
ADAMS RITE MANUFACTURING COMPANY
AEROJET ENGINEERING CORPORATION
AEROLAB DEVELOPMENT COMPANY
AEROPRODUCTS DIVISION, GENERAL MOTORS CORPORATION
AEROQUIP CORPORATION
AGAWAM AIRCRAFT PRODUCTS, INC.
AIRBORNE ACCESSORIES CORPORATION
AIRBORNE INSTRUMENTS LABORATORY INC.
AIRCRAFT RADIO CORPORATION
AIRESEARCH MANUFACTURING COMPANY, DIVISION OF THE GARRETT CORPORATION
ALLIS-CHALMERS MANUFACTURING COMPANY
ALLISON DIVISION, GENERAL MOTORS CORPORATION
ALUMINUM COMPANY OF AMERICA
AMERICAN AIRLINES SYSTEM
AMERICAN BOSCH CORPORATION
AMERICAN PHENOLIC CORPORATION
AMERICAN STEEL & WIRE COMPANY
ASSOCIATED AVIATION UNDERWRITERS
ATLAS SUPPLY COMPANY
BAKER STEEL & TUBE COMPANY
BEECH AIRCRAFT CORPORATION
BELL AIRCRAFT CORPORATION
BENDIX AVIATION CORPORATION
  BENDIX INTERNATIONAL DIVISION
  BENDIX PRODUCTS DIVISION
  BENDIX RADIO COMMUNICATIONS DIVISION
  ECLIPSE-PIONEER DIVISION
  FRIEZ INSTRUMENT DIVISION
  PACIFIC DIVISION
  SCINTILLA MAGNETO COMPANY
THE BG CORPORATION
BOEING AIRPLANE COMPANY
  SEATTLE DIVISION
  WICHITA DIVISION
BREEZE CORPORATIONS, INC.
  AIRCRAFT STANDARD PARTS COMPANY, INC.
  ALDRICH COMPANY
  ANDERSON STOVE COMPANY, INC.
  FEDERAL LABORATORIES, INC.
  FOUNDRY SERVICE, INC.
BROOKS AND PERKINS, INC.
CAL-AERO TECHNICAL INSTITUTE, A DIVISION OF GRAND CENTRAL AIRCRAFT COMPANY
CALIFORNIA PANEL & VENEER COMPANY
CANADAIR, LTD.
CESSNA AIRCRAFT COMPANY
CHASE AIRCRAFT COMPANY, INC.
CHASE NATIONAL BANK OF THE CITY OF NEW YORK
THE CLEVELAND PNEUMATIC TOOL COMPANY
  AUTOMOTIVE-AIRCRAFT DIVISION
CLIFFORD MANUFACTURING COMPANY, DIVISION OF STANDARD-THOMSON CORPORATION
CONSOLIDATED VULTEE AIRCRAFT CORPORATION
  FORT WORTH DIVISION
  STINSON AIRCRAFT DIVISION
CONTINENTAL MOTORS CORPORATION
CORNELL AERONAUTICAL LABORATORY, INC.
CORNELL UNIVERSITY
CURTISS-WRIGHT CORPORATION
  AIRPLANE DIVISION
  PROPELLER DIVISION
  WRIGHT AERONAUTICAL CORPORATION
DAYTON AIRCRAFT PRODUCTS, INC.
DOAK AIRCRAFT COMPANY, INC.
DOELCAM CORPORATION
DOUGLAS AIRCRAFT COMPANY, INC.
  EL SEGUNDO PLANT
  LONG BEACH PLANT
  SANTA MONICA PLANT
THE DOW CHEMICAL COMPANY
DZUS FASTENER COMPANY, INC.
EASTERN AIR LINES, INC.
EATON MANUFACTURING COMPANY
  DYNAMATIC CORPORATION (SUBSIDIARY)
  EATON-WILCOX RICH LTD. (SUBSIDIARY)
EDO CORPORATION
ELASTIC STOP NUT CORPORATION OF AMERICA
ELECTROL INCORPORATED
ESSO STANDARD OIL COMPANY
ETHYL CORPORATION
FAIRCHILD CAMERA & INSTRUMENT CORPORATION
  FAIRCHILD AERIAL SURVEYS, INC.
FAIRCHILD ENGINE AND AIRPLANE CORPORATION
  AL FIN DIVISION
  FAIRCHILD AIRCRAFT DIVISION
  FAIRCHILD ENGINE DIVISION
  FAIRCHILD GUIDED MISSILES DIVISION
  FAIRCHILD PERSONAL PLANES DIVISION
  NEPA DIVISION
  STRATOS DIVISION
FEDERAL TELEPHONE AND RADIO CORPORATION
  FEDERAL ELECTRIC MANUFACTURING COMPANY LTD.
  FEDERAL TELECOMMUNICATION LABORATORIES, INC. (PARTIAL SUBSIDIARY)
THE FIRESTONE TIRE & RUBBER COMPANY OF CALIFORNIA
FLETCHER AVIATION CORPORATION
FLIGHT SAFETY FOUNDATION
GENERAL ELECTRIC COMPANY
  AIRCRAFT GAS TURBINE DIVISION
  AVIATION DIVISIONS
GLOBE CORPORATION, AIRCRAFT DIVISION
THE B. F. GOODRICH COMPANY
THE GOODYEAR TIRE & RUBBER COMPANY
  GOODYEAR AIRCRAFT CORPORATION
GRUMMAN AIRCRAFT ENGINEERING CORPORATION
W. & L. E. GURLEY
HARVEY MACHINE COMPANY, INC.
INDUSTRIAL SOUND CONTROL
INSURANCE COMPANY OF NORTH AMERICA COMPANIES
  INSURANCE COMPANY OF NORTH AMERICA
  PHILADELPHIA FIRE AND MARINE INSURANCE COMPANY
  INDEMNITY INSURANCE COMPANY OF NORTH AMERICA
THE INTERNATIONAL NICKEL COMPANY, INC.
IRVING AIR CHUTE COMPANY, INC.
JACK & HEINTZ PRECISION INDUSTRIES, INC.
JOHNS-MANVILLE SALES CORPORATION
EARLE M. JORGENSEN COMPANY
WALTER KIDDE & COMPANY, INC.
KOLLSMAN INSTRUMENT DIVISION, SQUARE D COMPANY
LAVELLE AIRCRAFT CORPORATION
LEAR INCORPORATED
THE LIQUIDOMETER CORPORATION
LOCKHEED AIRCRAFT CORPORATION
  AIRQUIPMENT COMPANY (SUBSIDIARY)
  LOCKHEED AIR TERMINAL (SUBSIDIARY)
  LOCKHEED AIRCRAFT OVERSEAS CORPORATION (SUBSIDIARY)
  LOCKHEED AIRCRAFT SERVICE, INC. (SUBSIDIARY)
LONGINES-WITTNAUER WATCH COMPANY, INC.
MARMAN PRODUCTS COMPANY, INC.
THE GLENN L. MARTIN COMPANY
McDONNELL AIRCRAFT CORPORATION
MELETRON CORPORATION
MINNEAPOLIS-HONEYWELL REGULATOR COMPANY
  BROWN INSTRUMENT COMPANY (SUBSIDIARY)
NATIONAL CREDIT OFFICE, INC.
NORTH AMERICAN AVIATION, INC.
  NORTH AMERICAN AVIATION, INC., OF TEXAS
NORTHROP AIRCRAFT, INC.
NORTHWEST AIRLINES, INC.
PAN AMERICAN WORLD AIRWAYS, INC.
THE PARKER APPLIANCE COMPANY
PESCO PRODUCTS DIVISION, BORG-WARNER CORPORATION
PHILLIPS PETROLEUM COMPANY
PIASECKI HELICOPTER CORPORATION
THE PURE OIL COMPANY
RADIOPLANE COMPANY
REPUBLIC AVIATION CORPORATION
E. V. ROBERTS AND ASSOCIATES
A. V. ROE CANADA LIMITED
JOHN A. ROEBLING'S SONS COMPANY
ROHR AIRCRAFT CORPORATION
RYAN AERONAUTICAL COMPANY
SAVAL, INC.
SCHRILLO AERO TOOL ENGINEERING COMPANY
SERVOMECHANISMS, INC.
SHELL OIL COMPANY, INC.
SIMMONDS AEROCESSORIES, INC.
SOCONY-VACUUM OIL COMPANY, INC.
SOLAR AIRCRAFT COMPANY
SPERRY GYROSCOPE COMPANY, DIVISION OF THE SPERRY CORPORATION
SQUARE D COMPANY
STANDARD OIL COMPANY OF CALIFORNIA
STANDARD OIL COMPANY (INDIANA)
THE STEEL PRODUCTS ENGINEERING COMPANY
STURGESS, INC.
SUMMERS GYROSCOPE COMPANY
TELECOMPUTING CORPORATION
THE H. I. THOMPSON COMPANY
THOMPSON PRODUCTS, INC.
TINNERMAN PRODUCTS, INC.
TOOLKO ENGINEERING COMPANY
TRANS WORLD AIRLINES, INC.
UNION CARBIDE AND CARBON CORPORATION
  BAKELITE CORPORATION
  ELECTRO METALLURGICAL DIVISION
  HAYNES STELLITE DIVISION
  THE LINDE AIR PRODUCTS COMPANY
  NATIONAL CARBON DIVISION
UNITED AIR LINES, INC.
UNITED AIRCRAFT CORPORATION
  CHANCE VOUGHT AIRCRAFT DIVISION
  HAMILTON STANDARD DIVISION
  PRATT & WHITNEY AIRCRAFT DIVISION
  SIKORSKY AIRCRAFT DIVISION
  UNITED AIRCRAFT EXPORT CORPORATION
  UNITED AIRCRAFT SERVICE CORPORATION
UNITED STATES AVIATION UNDERWRITERS, INC.
VARD, INC
VICKERS, INC.
WESTERN GEAR WORKS
WESTINGHOUSE ELECTRIC CORPORATION
  AVIATION GAS TURBINE DIVISION
  INDUSTRIAL ELECTRONICS DIVISION
  MARINE & AVIATION SALES DEPARTMENT
  SMALL MOTOR DIVISION, AVIATION SALES
WESTON ELECTRICAL INSTRUMENT CORPORATION
WYMAN-GORDON COMPANY
YOUNG RADIATOR COMPANY